Towards *In situ* extraction of fine chemicals and biorenewable fuels from fermentation broths using Ionic liquids and the Intensification of contacting by the application of Electric Fields

BY

Satya Aravind Gangu,

B.Tech., Chemical Engineering, Osmania University, India, 2003

Submitted to the Department of Chemical and Petroleum Engineering and the Graduate Faculty of the University of Kansas in partial fulfillment of the requirements for the degree of Doctor of Philosophy

Committee Members:

_____

Aaron M. Scurto (Chair)

_____

Laurence R. Weatherley

_____

Bala Subramaniam

_____

Cory J. Berkland

_____

Belinda M. Sturm

Date defended: _____

The Dissertation Committee for Satya Aravind Gangu certifies that this is the approved version of the following dissertation:

Towards *In situ* extraction of fine chemicals and biorenewable fuels from fermentation broths using Ionic liquids and the Intensification of contacting by the application of Electric Fields.

Committee Members:

_____
Aaron M. Scurto (Chair)

_____
Laurence R. Weatherley

_____
Bala Subramaniam

_____
Cory J. Berkland

_____
Belinda M. Sturm

Date approved: _____

ABSTRACT

Cost-effective synthesis of fine chemicals/biorenewable fuels via fermentation invariably hinges upon efficient separations from the dilute broth. Biphasic/*in situ* extraction can positively impact both upstream fermentation and the downstream product separations. For developing environmentally sustainable processes, ionic liquids are touted as greener alternative to organic solvents not only because of their relatively low volatility but also due to the ability to tune their properties and design new ionic liquids for task specific needs. Solvent selection for *in situ* fermentation is depended on high solute partitioning and their biocompatibility with the microorganisms. Such information for these new set of solvents, ionic liquids that comprise of ions is very limited compared to organic solvents. Here, a new methodology to enable successful use of ionic liquids in *in situ* extraction is developed by focusing on two model systems: 1. Fine chemical - (1*R*,2*S*)-1,2-napthalene dihydrodiol (NDHD), produced from the biotransformation of naphthalene by *Escherichia coli* strain JM109(DE3) pDTG141 and 2. Biorenewable fuel - Biobutanol (along with Acetone and Ethanol), produced from the Fermentation of sugars by *Clostridia*.

The partitioning of each of the solutes, NDHD, Acetone, 1-butanol and ethanol between water and ionic liquid has been measured in the range of concentrations typical of actual fermentations. Different cationic classes of ionic liquids including 1-alkyl-3-methylimidazolium ([RMIm]), trialkylmethylammonium ([TRMAm]) and trihexyltetradecylphosphonium ([$P_{6,6,6,14}$]) were investigated along with anions such as halides and hydrophobic bis(trifluoromethylsulfonyl)imide [Tf_2N] and (trifluorotris(perfluoroethyl)phospate [FAP]. The model ionic liquid, [HMIm][Tf_2N] (an IUPAC/IACT standard), demonstrated the highest affinity for NDHD (K_C = 2.8) while phosphonium and ammonium ionic liquids with bulkier alkyl side chains had the lowest extractability (K_C < 0.5). Incorporating polar functional groups by replacing one of three octyl side chains in the trioctylammonium cation with side chains containing functional groups such as carbonyl and cyano increased the partition coefficients (K_C > 2) illustrating the role of molecular design for improvement.

Ternary diagrams for the extraction of ABE solutes from water using model ionic liquid, [HMIm][Tf_2N] were developed. Acetone and 1-butanol solutes were favorably extracted from water with high selectivities while its affinity for ethanol was low. NRTL activity coefficient

model was used to model the ternary data and a regression program was written to obtain the binary interaction parameters for the ternary system. Simulation of 1-butanol extraction using [HMIm][Tf_2N] was conducted using process simulator, Aspen Plus. Energy analysis was performed on an optimized flowsheet and these results along with equipment costs were compared with traditional organic solvent extraction and distillation.

The toxicity of twenty different ionic liquids to the mutant strain of *E. coli* was tested with results varying from biocompatible to antimicrobial evidenced from EC_{50} values of growth rates. Here, the molecular toxicity was measured and EC_{50} refers to concentration of the ionic liquid that reduces cell growth rate by 50% at molecular level; the EC_{50} was compared with water solubilities, to determine if the ionic liquid was toxic at molecular level. As widely known, the increase of alkyl-chain length increased the toxicity. However, even highly alkylated cations may become biocompatible by the choice of anion, for e,g, trioctylmethylammonium bromide was antimicrobial while with [Tf_2N] anion, it was biocompatible. The mechanism of growth inhibition in presence of ionic liquids was studied through imaging and initial explanations of possible inhibition mechanisms includes the effect of dissociation of these ionic liquids on how the cations/anions interact with the cell membrane.

Fermentation broths can be viscous and exhibit non-Newtonian behavior and efficient liquid-liquid contacting is required for higher mass transfer rates and hence faster extractions. Intensification of contacting of non-Newtonian rheology fluids was studied by the application of electric fields. Continuous phase was Mineral oil containing a rheological modifier while aqueous carboxymethylcellulose (CMC) solutions were used as dispersed phase with the apparent viscosities varying between 1 cP to > 1000 cP. Significant reduction in drop size was observed when the applied voltages were varied between 0 to 15 kV; viscosity of the continuous phase resulted in lower terminal velocities while dispersed phase viscosity affected the droplet formation times. Empirical correlations for droplet diameter as a function of physical properties, nozzle dimensions and electric field strength were developed and discussed here.

Keywords: *in situ* extraction, ionic liquids, NDHD, Acetone-Butanol-Ethanol (ABE), toxicology / biocompatibility, phase equilibrium, energy analysis, liquid-liquid contacting, non-Newtonian rheology, charged droplets, DC electric fields

ACKNOWLEDGEMENTS

I would like to express my sincerest gratitude to my advisor Professor Aaron Scurto and Co-advisor Professor Laurence Weatherley for their guidance, motivation, continuous encouragement and patience through the course of my research and thesis writing process. I would like to thank my committee members, Professors Cory Berkland, Bala Subramanian and Belinda Sturm, for their cooperation and for serving on my committee.

I would like to thank Professor Stevin Gehrke, for providing constant access to his lab equipment critical for biocompatibility studies and Professor Michael Detamore & his lab members for being cooperative while conducting these studies. I would like to acknowledge the CPE TORP group for allowing me to use their rheometers to characterize the non-Newtonian fluid rheology and the Microscopy & Analytical Imaging Laboratory for their help with imaging of the bacteria.

I would like to acknowledge the help from the Center for Biocatalysis and Bioprocessing at the University of Iowa; Professor Tonya Peeples and her group members for sharing bacterial strains; Professor Jack Rosazza for arranging for NDHD stock samples; frequent interactions about cell culture techniques with various group members were helpful. I would like to acknowledge Professor Jerzy Petera, University of Lodz, Poland for his interest and interactions along with inputs on the modeling of charged droplet trajectories in non-Newtonian systems.

I would also like to acknowledge the financial support from KU, CEBC and DuPont; members of CEBC, especially Claudia Bode, for her constant encouragement; CPE staff including the lab technicians.

I would like to acknowledge the companionship with various former CPE graduate students: Zheyan Qiu, during process intensification lab setup; Wei Ren, Azita Ahosseini and Sylvia Nwosu during Ionic liquid studies. I would like to acknowledge the work performed by Nameer and Wei Ren on developing overall ternary diagrams for ABE solutes. I would like to acknowledge all my roommates who made my adjustment to graduate student life easier and fun, especially Milind Singh, Sagar Sarsani, and Prakash Manikwar.

Finally, I am indebted to my parents Sastry and Lakshmi for instilling a strong sense of purpose, values and spirituality. I would like thank my in-laws, Murthy, Nirmala and Harish, for their faith in me and constant encouragement. I am ever grateful to my brother Prashanth and

sister-in-law, Jyothi, for their love and support; their children Vikram and Varsha for bringing a smile. Most importantly, I offer special thanks to my wife, Sirisha, for enduring the hardships of a tough graduate life, patiently pushing me to achieve my goals and for her unending love for me.

Title Page

Acceptance Page

Abstract

Acknowledgements

Table of Contents

List of tables

List of figures

Ionic liquids Nomenclature

Ionic liquid cations and anions with their abbreviation

Cations	Abbrev.	Anions	Abbrev.
1-ethyl-3-methyl imidazolium	[EMIm]	chloride	[Cl]
1-butyl-3-methyl imidazolium	[BMIm]	bromide	[Br]
1-hexyl-3-methyl imidazolium	[HMIm]	tetrafluoroborate	[BF_4]
1-octyl-3-methyl imidazolium	[OMIm]	hexafluorophosphate	[PF_6]
1-butyl-3-methyl pyrrolidinium	[BMPl]	tris(pentafluoroethyl) trifluorophosphate	[FAP]
1-hexyl-3-methyl pyrrolidinium	[HMPl]	bis(trifluoromethyl suflonyl)imide	[Tf_2N]
1-butyl-3-methyl pyridinium	[BMPy]	tosylate	[TOS]
1-hexyl-3-methyl pyridinium	[HMPy]	ethylsulfate	[$EtSO_4$]
1-octyl-3-methyl pyridinium	[OMPy]	octylsulfate	[$OcSO_4$]
1-decyl-3-methyl pyridinium	[DMPy]	ethyleneglycol monomethylethersulfate	[$MDEGSO_4$]
PEG-5 Cocomonium	[CABHEM]	methanesulfonate	[$MeSO_3$]
tributyl methyl ammonium	[TBMAm]	dodecylbenzene sulfonate	[$C_{18}H_{29}O_3S$]
trihexyl methyl ammonium	[TBMAm]	diethylphosphate	[Et_2PO_4]
trioctyl methyl ammonium	[TOMAm]	dimethylphosphate	[Me_2PO_4]
dimethylethanolammonium	[DME]	decanoate	[$C_{10}H_{19}O_2$]
2-hydroxyethyl-trimethyl ammonium	[$EtOHNMe_3$]	dicyanamide	[C_2N_3] or [DCN]
didecyldimethyl ammonium	[DDA]	acetate	[Ac]
tributyl-methyl phosphonium	[$P_{1,4,4,4}$]	tetracyanoborate	[TCB]
tributyl-ethyl phosphonium	[$P_{2,4,4,4}$]	dihexylsulfosuccinate	[DHSS]
trihexyl-tetradecyl phosphonium	[$P_{6,6,6,14}$]		
tributyl-tetradecyl phosphonium	[$P_{3,3,3,14}$]		
N,N,N',N'-tetramethyl-N''-	[EWTMG]		

ethylguanidinium	
dioctyl(5-butanenitrile)methyl ammonium	[DOM(5-BuCN)]
dioctyl(5-hexanone)methyl ammonium	[DOM(5-HxOne)]
1-(6-hydroxyhexyl)-3-methylimidazolium	[HOhMIm]
1-(2-hydroxyethyl)-2,3-dimethylimidazolium tetrafluoroborate	[HOEMMIm]
1-(2-hydroxyethyl)-3-methylimidazolium tetrafluoroborate	[HOEMIm]

1. INTRODUCTION

1.1. Overview

1.1.1. Introduction to Biocatalysis

Catalysis, the technique of increasing the rate of a chemical reaction using a catalyst, is involved in the production of 75% of chemicals. A catalyst increases chemical reaction rates by reducing the activation energy without being consumed in the reaction itself. Conventional catalysts are produced through chemical routes, while biocatalysts are produced by microorganisms. Synthesis using biocatalyst (i.e. enzyme) is called biocatalysis or biochemical synthesis.

Biocatalysis is a sustainable ("green") process with low-impact to humans and the environment[5,6] and adheres to the 12 principles of green chemistry and engineering. It is an inherently safer chemistry as it operates in water, at mild conditions and the reactions are rarely exo- or endo-thermic thereby reduces E-factors and possibility for accident prevention. Biocatalysts represent some of the fastest and most selective catalysts (both –regio and –enantio) known. It also results in improved life cycle analysis as renewable feedstocks can be used.

Biocatalysis is important for the chemical industry in many ways. Chemicals from biocatalysis are predicted to increase 5% in 2009[6,7] and beyond with market of $53 billion market by 2017.[8] The US Department of Energy has released a report[9] focusing on the 12 most promising bio-renewable chemical building blocks for the sustainable production of a wide-variety of chemical products from polymers to pharmaceuticals, etc.; the majority of these chemicals are produced from biocatalysis and not chemical processing. While the cost-benefit of producing fuel using biocatalysis is being debated[10], the ability to use renewable cellulose feedstocks to make chemicals and fuels would be very advantageous for sustainability.[7,9,10] The

high (enantio)selectivity of biocatalysts is especially useful in the fine-chemicals sector, in particular in the production of pharmaceutical intermediates and for organic synthesis.[11]

1.1.2. Types of biocatalysis

Enzymes, the biocatalysts, are macromolecules with the ability to bind small molecules and to effect reaction. These are continually produced by microorganisms. Enzymes are classified into six classes depending upon the type of reaction catalyzed: Oxireductases (oxidation), Hydrolases (introduction of hydrogen), Liase, Isomerase, Lyase and Transferase. Of these six classes, three commonly are used: Oxireductases catalyze oxido-reduction reactions (examples include dioxygenases and dehydrogenases); Transferases catalyze the transfer of a functional group (examples include CoA-Transferase); and Lyases catalyze the breaking of various chemical bonds by means other than hydrolysis and oxidation (examples include decarboxylase).

Biocatalysis can be divided into whole-cell biocatalysis, where the enzyme catalyzes the reaction inside the whole-cell, while in enzymatic catalysis, pure enzyme, extracted from the microorganism, is used to catalyze the reactions. Whole-cell are known to have about 10-100 lesser reaction rates and have inherent mass transfer limitations compared to enzymatic catalysis because substrate has diffuse to through the cell and reach the enzyme and the product formed has to diffuse out of the cell. Whole-cell biocatalysis can be further classified into fermentation and biotransformation depending upon the intermediate steps involved. Generally with biotransformations, an enzyme catalyzes the substrate to product in a single step, while multiple steps requiring multiple enzymes are involved in fermentation. Here the substrate undergoes series of intermediate conversions catalyzed by different enzyme classes before product is formed. Because of this, byproducts are also formed frequently in fermentation.[12,13]

Enzymatic and whole-cell biocatalysis have advantages and challenges for both bench-scale and industrial-scale chemistry.[14] Whole-cell systems benefit from various factors: the ability to use low-cost and renewable feedstocks; a large choice of microorganisms either naturally occurring or recombinant ("designer cells"); co-factor addition and regeneration are not necessary; cascades of transformations by different enzymes can be performed consecutively; and reactions are often conducted at near-ambient temperatures. This thesis focuses on whole-cell systems and from now on, unless otherwise indicated, biocatalysis refers to whole-cell biocatalysis.

1.1.3. Downstream processing

The target compound is produced in one stage in most common biocatalysis methods and separated in the second stage, called "downstream". Product removal from biocatalysis mixtures is achieved using a variety of downstream separation processes such as evaporation/distillation, precipitation, gas stripping, membrane separations (micro-/ultra-filtration, pervaporation, etc.), adsorption, liquid chromatography, etc.[15,16,17] These techniques are depended upon the product characteristics and are implemented *ex situ*, i.e., the aqueous product stream from the bioreactor is processed after cells are separated/filtered as shown in the figure.

Despite the potential of biocatalysis, a number of challenges to efficient implementation exist, primarily due to product inhibiting the microorganism. These include production of dilute solution, lower reaction rates, reduced cell growth and lower fermenter productivity.[10] Accumulation of product/substrate above certain concentration limits causes interference with the producing cell at the biochemical level, resulting in cell growth inhibition. In some cases, this accumulation leads to a series of chemical and physical effects such as pH changes,

precipitation, increased viscosity and solvent/detergent-like activities.[18] Further, low substrate availability to cells due to substrate hydrophobicity can limit the yield.

These dilute aqueous solutions require large energy input and high costs for downstream processing.[19] In addition, the environmental impact of large water usage must be considered, especially for those involving downstream separations.[20] Additionally, the solutions involved may be rheologically complex, and may contain significant levels of impurity such as bio-surfactants, cell debris, polynucleotides, and polysaccharides, all of which may complicate efficient separation. Observed examples of inhibition include[21]

- Production of 1-butanol using *Clostridium Acetobutylcium,* where the growth of the microorganism is inhibited above 10-15 g/L of 1-butanol.[13]
- Aromatic compounds like naphthalene, toluene and phenanthrene have very low solubilities in aqueous phase; hence lower amounts of substrate can participate in the biocatalysis.[22]

Figure 1.1: Various steps involved in development of biocatalytic process[3]

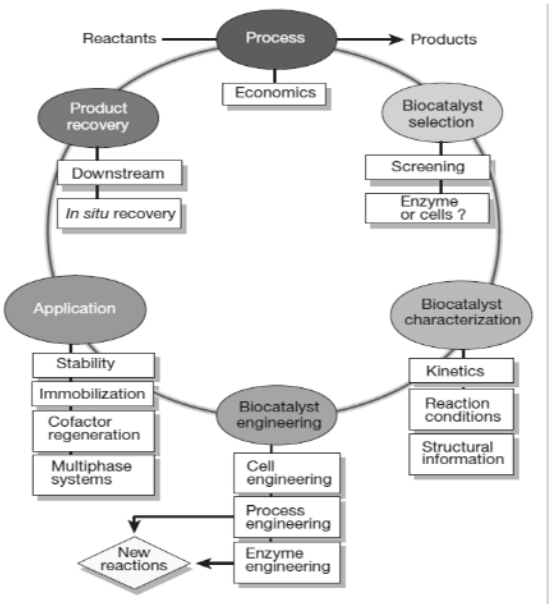

Many strategies have been adopted to overcome these shortcomings as shown in the Figure 1.1. Of these, important ones are strain improvements using recombinant DNA (genetic engineering to modify organisms) / metabolic engineering/screening for new mutants[14] and process engineering techniques such as *in situ* product removal. While strain improvement techniques have been well explored by various researchers improvements of the production system still need to be applied.[18]

1.1.4. *In situ* product removal

1.1.4.1. Overview

In situ product removal involves removing target solute from the cell surface as the product is formed, preventing undesirable effects of product inhibition and leading to higher product yields and more efficient separations. Integration of reaction and separation can reduce the number of downstream processing steps required and thus reduce capital costs.[23] *In situ* method requires less investment in terms of the infrastructure, man power and processing costs.[24] Identifying an *in situ* method for product removal is very much depended on the chemical and biochemical properties of the product. Various *in situ* product removal techniques based on product properties are summarized in figure 1.2 below.

The three most common classes of integrated biocatalysis and product recovery are based on volatility (vacuum or gas stripping), permeation (dialysis, pervaporation, etc.) and extraction.[15] While conceptually elegant, volatility based approaches are applicable for a limited number of solutes. Permeation uses membranes; advances in membrane research have resulted in improved selectivity/flux, and reduced fouling. However, large-scale use of permeation is still limited.

Figure 1.2: In situ product removal techniques for various product characteristics. (+) technique is applicable for selective removal. (++) technique is very useful for selective removal of the product and has shown its effectiveness in several cases.

ISPR Technique	Product categories: Low molecular wt: Hydrophobic – volatile	Low molecular wt: Hydrophobic – nonvolatile	Low molecular wt: Hydrophobic – neutral – volatile	Low molecular wt: Hydrophobic – neutral – nonvolatile	Low molecular wt: Hydrophobic – charged	High molecular wt: Hydrophobic	High molecular wt: Neutral	High molecular wt: Charged	Important examples
Evaporation									
stripping, (vacuum-) distillation, per vaporation, transmembrane distillation	++		++						ethanol
Extraction									
organic solvent (inc. perstraction)	++	++	+	+		+			ethanol, flavors
supercritical fluid	+	++	+	+	+				flavors
reactive (inc. perstraction)	+	+	+	+	++	+	+	+	organic acids, ethanol
aqueous two-phase			+	+	+	+	++	++	enzymes
Permeation									
dialysis			+	+	+				lactic acid,ethanol, ammonium
electrodialysis					++				lactic acid
reverse osmosis, nanofiltration			+	+	+				ethanol
Immobilization									
hydrophobic adsorption	++	++	+	+		+	+	+	butanol, flavors
ion-exchange					++			+	organic acids
affinity adsorption	+	+	+	+	+	++	++	++	proteins
Precipitation					+			+	lactic acid, citric

Extraction using solvents ("Extractive biocatalysis" or "Biphasic biocatalysis") is a feasible option for addressing some of these challenges. The term extractive biocatalysis refers to two-phase biocatalysis employed to overcome the sensitivity of the cells to the substrate or to the metabolite formed in single phase inhibiting the bioconversion. Here the second phase mostly organic acts as a reservoir supplying the substrate to the enzyme once it is consumed in the aqueous broth and also simultaneously extracting the product from the broth, depending upon the partitioning properties of the solvent. Biphasic system can aid the development of larger-scale processes based on biocatalysis. Continuous direct extraction integrated with continuous biocatalysis, allows recovery of intermediate products during multi-stage reactions, thus improving the overall yields of such compounds.

1.1.4.2. Extractive or biphasic biocatalysis

Typically a biphasic system comprises of non-aqueous phase which is selected for its ability to subsequently extract the product from the aqueous phase, thus reducing the inhibition of the biocatalyst by the product. The product is removed into the extract phase, preventing the further cell growth inhibition. This can be valuable for sequential reactions in which an intermediate product is the desired one. Further, product removal can shift the thermodynamic reaction equilibrium and facilitate complete biocatalysis.

In cases where substrate toxicity needs to be overcome, the non-aqueous phase acting as a substrate reservoir which delivers substrate to an aqueous phase which hosts the biocatalyst either as a whole-cell or as an immobilized whole-cell. Thus the apparent solubility of hydrophobic substrate is controlled while at the same time substrate inhibition of the biocatalyst is reduced. This control of partitioning is also beneficial for substrates which are prone to hydrolysis in the aqueous phase. Enantioselectivity can also be enhanced by substrate control, e.g. biotransformation of α-β-carbonyls.[25]

Advantages of extractive biocatalysis include: increased fermenter productivity, concentrated substrate usage, potential to decrease the final cost of the product, higher concentrations of the product, and faster recovery of the product, as the extraction is integrated with the fermentation, making the purification step much simpler.

Disadvantages with this *in situ* method are, higher volumes of the fermenter (pilot scale or industrial scale), high shear rates at the impeller (necessary for the cell growth) might create stable emulsions of the phases and *in situ* method extracts the product mostly from whole broth, unlike the external method where the product can be extracted from whole or purified broth, which might improve the extraction.

Solvent extractability and toxicity to the cells are key factors for designing extractive biocatalysis for a given system. Solvent extractability is understood by measuring partition and selectivity coefficients. Toxicity is understood by studying the biocompatibility of cells and solvent.

1.1.4.3. Solvent extractability

Solvent performance is controlled by the thermodynamic and kinetic properties. To quantify the ability of a solvent to extract solutes selectively from an aqueous system, the partition coefficient, *K*, and selectivity, *S*, are computed. The partition coefficients are the ratio of the composition of the target solute, *i*, in solvent phase over that of the aqueous phase as shown below using mole fraction composition units, *x*.

$$K_{x,i} = \frac{x_i^{IL}}{x_i^{Aq}} \qquad \text{Eqn. 1}$$

The partition coefficient is usually a function of the original loading composition. The higher the value for *K*, the less amount of solvent extractant is necessary to perform a given separation. In any real system, the extractant will also solubilize other components from the aqueous mixture, *j*. Thus a measure of the selectivity of the solvent for a particular solute *i*, over *j* is given as:

$$S_{x:i,j} = \frac{K_{x,i}}{K_{x,j}} = \frac{x_i^{IL} / x_i^{Aq}}{x_j^{IL} / x_j^{Aq}} \qquad \text{Eqn. 2}$$

The number of different selectivity numbers will depend on the number of components extracted. However, selectivity of the target solute over water ($j = H_2O$) often represents the most important co-extraction especially from a process economics point of view. While most phase equilibrium thermodynamics are measured, modeled and discussed in terms of mole

fraction or percent, other composition units such as mass fraction (ω_i), molarity (M), molality, etc. may be more practical for evaluation or design of an *in situ* extraction process.

$$mass:\ K_{\omega,i} = \frac{\omega_i^{IL}}{\omega_i^{Aq}} \qquad molarity:\ K_{C,i} = \frac{C_i^{IL}}{C_i^{Aq}}$$

Hence, optimal solvent from the phase equilibrium thermodynamics should partition the target solute out of the broth, have little loss to the aqueous phase and extract little water so the selectivities should be high.

1.1.4.4. Toxicity

Solvent biocompatibility is one of the basic prerequisites for successful biphasic biocatalysis, though other requirements for solvents vary from process to process. Solvent toxicity to a given microorganism can be divided into toxicity at the molecular level and at phase level. *Molecular toxicity*[26] occurs in a solvent saturated cell culture medium encountered in any biphasic system. The toxicity could be due to enzyme inhibition, protein denaturation or modification of the cell membrane by the solvent. Cells can absorb some of the solvent molecules into their lipid membrane which could cause cell membrane expansion. Membrane modification could be also due to structural disorder or permeability change of the cell membrane. *Phase toxicity* is due to the presence of a solvent phase or interface. Phase toxicity could be present even if the molecular toxicity does not have an effect on the cells. Extraction of important nutrients or organic precursors essential for the growth of the microorganism might inhibit their growth. Emulsion formation, the formation of a solvent coat on the cells might further lead to reduced nutrient access to the cells. Also, extraction of biomass by the solvents like outer components of the cell wall could lead to the cell death. Attraction of the cells to the interface might enhance this process.

1.1.4.5. Solvent selection criteria

The key criteria for selecting solvent include:

- High extractabilities and selectivities for the target product to overcome product toxicities.
- Solvent toxicity (biocompatibility) to the microorganisms
- Higher solubility of the substrates in the solvent in cases where substrate is toxic to the cells.
- Water immiscibility
- Less costly, Readily available,
- Lower vapor pressure, Non-toxic for safe handling and easy disposal.
- Higher density difference, higher interfacial tensions with aqueous phase resulting in faster phase disengagement and easier phase separations.

Some of the *in situ* solvents used are: organic solvents, ionic liquids, supercritical solvents. Organic solvents have been employed as biphasic solvents industrially and their toxicity to microorganisms is well understood. But they are a fixed set of solvents with fixed set of properties, hence limiting the choice of the solvent for a given system. Furthermore, they have measurable vapor pressure (adventitious emissions into environment) which could have significant human and environmental impact and lead to unsustainable processes that are inherently hazardous. Conventional organic solvents used are: saturated hydrocarbons, primary alcohols, cycloalkanes, unsubstituted and substituted aromatics, primary and branched esters. High molecular weight polymer solutions such as polyethylene glycol, cyclodextrin and dextran have also been used as solvents.

Supercritical solvents are the fluids above their critical temperature [27] and pressure (P_c). Some of advantages[28,29] include low residual solvent in the final product, high diffusivity reduces mass transfer limitations and changes in solubility with pressure can result in easy extraction. Main disadvantage is that the technology for superfluid systems lags with the technology for traditional solvents.[28] Further, these fluids have lower substrate/product solubilities compared to liquid solvents. High pressure apparatus is required incurring higher capital costs. Formation of carbonic acids with CO_2 may also problems in relation to extraction chemistry. Biocompatibilities[30] are also difficult to study due to changing pressures and temperatures. There also may be difficulty with operating in the continuous phase mode in the presence of solids in the extractor. Examples of room temperature supercritical fluids used in biocatalysis[28,29,30] are ethylene, ethane and Carbon-di-oxide.

1.1.4.6. Ionic liquids

Ionic liquids are organic salts that are liquids at or near room temperature (with $T_m < 100°C$) and consist of asymmetrical organic cations, and organic and/or inorganic anions. Commonly used cation classes are imidazolium, quaternary ammonium and phosphonium and anions, such as halides, sulfonates, phosphates, carboxylates, etc (Figure 1.3). For example, 1-Hexyl-3-methyl-imidazolium bis(trifluromethylsulfonyl)amide ([HMIm][Tf_2N]) (Figure 1.3b) has been chosen by IUPAC's Working Committee on Ionic Liquids to be a reference IL for worldwide study.[31] As composed of ions, ionic liquids have low to immeasurably small vapor pressure which has led to some of them to be considered as potential "green"/sustainable solvents as they eliminate the most common cause of solvent pollution: evaporation. This is a marked advantage over any other organic solvent. Negligible vapor pressure also results in highly-elevated flash points, which extends safety to the decomposition temperature (>300°C). Current toxicological studies have shown a wide range of human and environmental toxicity ranging from low to high. Ionic liquids are termed as "designer compounds" in that their physical and chemical properties can be adjusted molecularly to the application due to the myriad possibilities in designing them. It has been estimated that nearly 10^{18} ILs are possible[32] (~10^{14} unique cation/anion combinations). Some of the tunable physical properties[33,34] of ionic liquids that are reported in the literature are viscosity, surface tension, solubility, polarity, acidity/basicity, stereochemistry etc. Ionic liquids

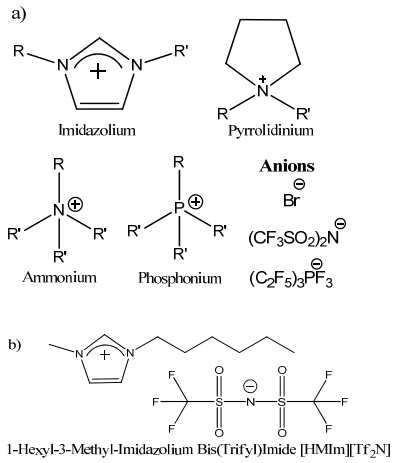

Figure 1.3: a) Structures of common ionic liquids. b) Model ionic liquids [HMIm][Tf_2N]

have been used in many practical applications especially as solvents in extractions[35,36,37,38,39,40], enzymatic biocatalysis.[41,42,43]

1.1.5. Outline of the document

The focus of the thesis is to identify optimal ionic liquids by understanding structure-partitioning and structure-toxicity relationships. The rest of the chapter is organized as follows: in section 1.2, model systems identified for the present study are introduced and literature review of their product separation techniques both *in situ* and *ex situ* are discussed, in section 1.3, ionic liquids are introduced and their current usefulness as bi-phasic solvents in biocatalysis is discussed and in section 1.4, prior efforts to intensify liquid-liquid contacting using electric fields are outlined.

In chapter 2, methodology for experiments conducted relating to toxicity, portioning and electric fields is described in detail. In chapter 3, the results of the toxicity experiments are analyzed and the possible inhibition mechanisms in the presence of ionic liquids are discussed. In chapter 4, results of the ABE partitioning experiments are analyzed, and modeling of 1-butanol extraction and simulation of 1-butanol separation are described. In chapter 5, results of the experimental work to extend electric field contacting from Newtonian to Non-Newtonian systems is described.

Finally, in chapter 6, conclusions derived from this work are summarized and recommendations for future work are presented.

1.2. Review of downstream processing of model biocatalytic systems

In this section, various *in situ* product removal and extraction techniques described in the literature for model systems are discussed with focus on extractive biocatalysis. Two model systems, (+)-*cis*- (1*R*, 2*S*)-dihydroxy-1,2-dihydronaphthalene (NDHD) and Acetone-Butanol-Ethanol (ABE), which were chosen for this study as they represent a full spectrum of chemicals from fine to bulk chemicals respectively. Among ABE solutes, 1-butanol is the primary focus of this thesis. NDHD is a fine chemical whereas ABE are bulk chemicals. NDHD is a chiral aromatic compound produced from a hydrophobic substrate and represents a class of substrates which have low solubility in water. 1-butanol is a straight chained polar alcohol and is produced from water soluble mono saccharides. Both systems suffer from product inhibition.

1.2.1. NDHD model system

1.2.1.1. Overview

This model system involves the production of NDHD by the microbial oxidation of naphthalene[44,45] as shown in Scheme 1. Most common enzymes for microbial oxidation are Monoxygenase and Dioxygenase. These enzymes have broad substrate specificity, and catalyze enantiospecific reactions, useful in preparation of chiral building blocks and pharmaceutical intermediates and fine chemicals. These enzymes fall under the general category of oxidoreductases which catalyze oxidation-reduction reactions and occur by the transfer of electrons when enzymes act on the substrate (both aliphatic and mono/poly-cyclic aromatics). Generally the reactions of Oxidoreductases are considered to be complex because all these are cofactor dependent[46], which makes using just the enzyme without the microbe more difficult.

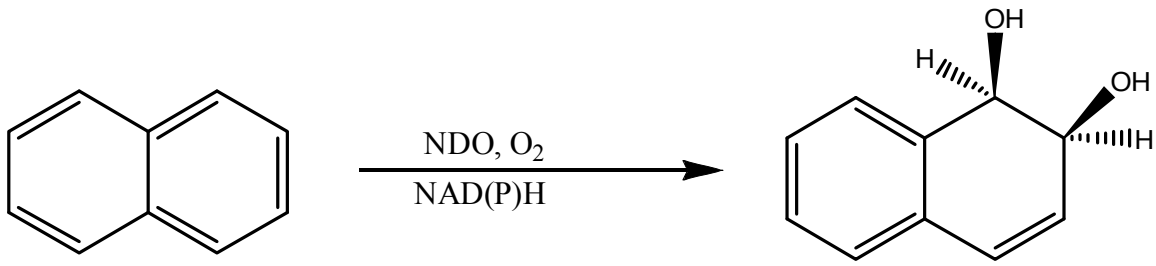

Naphthalene

(+)-cis-(1R,2S)-1,2-napthalene dihydrodiol (NDHD)

Scheme 1. Synthesis of (+)-cis- (1R, 2S)-dihydroxy-1,2-dihydronaphthalene (NDHD) by the enzyme naphthalene dioxygenase (NDO).

Here, the enzyme naphthalene dioxygenase (NDO) (EC 1.14.12.12) is produced in a genetically modified strain of *E. coli.*[47] This microbial oxidation is carried out in presence of oxygen and the cofactor NAD(P)H is regenerated during the cell metabolism. These enzymes introduce two O-atoms derived from molecular oxygen into the substrate (either aliphatic / aromatic) to form cis-diols as the primary metabolite. Recycling of the cofactor is the main disadvantage with dioxygenases. These cofactors are very costly and hence must be regenerated. The use of pure NDO enzyme would have required regeneration of NAD(P)H which often adds to the cost of such a system.[48] This strain of *E. coli* suffers from both substrate (naphthalene) and, especially, product (NDHD) toxicity[22], which limits its titer in a batch configuration. NDHD and other aromatic diols form a pool of chiral synthons that can be used in asymmetric synthesis for example as pharmaceutical intermediates[49] and synthesis of polymers like polyphenylene. These diols have also attracted interest as substrates for further functionalization in efficient synthesis of stereo- and regio-specific biologically active compounds.[50,51]

1.2.1.2. Literature review on NDHD extraction

Low product yields are common in the oxidation of hydrophobic aromatic substrate due to their lower solubility in water and their toxicity to the cells at higher concentrations. In a batch

reaction, the product NDHD is extracted from the broth using volatile organic solvents like ethyl acetate or methanol which are further evaporated to obtain the pure product. Different techniques have been employed to increase the product yields like using organic solvents as the biphasic medium in the reaction, and cell immobilization to reduce contact between the substrate and the cells. Downstream processing techniques like solvent extraction with organic solvents, adsorption using resins, and direct micellar systems have been employed in the literature to obtain product separation. Choice of the downstream technique is important as the NDHD is known to degrade to α-naphthols at acidic pH.

Hsieh *et al.*,[52] developed the kinetic models for the microbial oxidation of naphthalene in pure aqueous media performed in batch and continuous modes by using different particle sizes of naphthalene and proposed two stage fermentation. Optimum sizes of naphthalene particles (16-60 mesh) were identified to ensure the substrate availability to the cells and the product was separated and through solvent extraction using ethyl acetate and purified by evaporation of the solvent.

Cox *et al.*,[53] investigated the biological process of converting naphthalene to NDHD for optimal carbon source for cell growth and studied the addition of naphthalene solubilizing agents. The authors reported the inhibition of the bacteria by NDHD at concentrations of 2 g/L. Emulsified mixtures of naphthalene were created using 0.5% v/v each of non-ionic surfactant (Tergitol NP-14) and anionic surfactant (Shell Neodol 25-3A) and the naphthalene concentration in the mixture was 50 g/L. Addition of surfactants to the cell culture media improved the substrate mass transfer and the production of NDHD was stimulated and the reaction rates doubled. The concentration of NDHD was 8 g/L in these media compared to 2.7 g/L produced in media without any surfactants added.

Harrop *et al.*,[22] studied the effect of addition of organic solvents to a medium containing free cells and immobilized cells to improve substrate availability during the reaction. Solvents with $log\ P > 4$ were found to maintain the enzyme activity and hence not toxic to the cells, while solvents with $log\ P < 3.5$ inhibited the cell growth identified from lower enzyme activity. Immobilization reduced the solvent toxicity to the cells for solvents with *log P* values between 3.5 and 4. Only non-polar solvents like dodecane were identified as non-toxic to the cells which can be expected to have low extractability for the product.

Bosetti *et al.*,[54] studied the cis-dihydroxylation of naphthalene in a stirred bioreactor with resting cells where the substrate concentration was reported not to affect the cell viability due to the mutant strain of the organism used. Productivity and amount of the product produced was similar in the cases of the pure aqueous system and biphasic media with 12% of hexadecane. This was attributed to product inhibiting the biocatalyst. The focus was to overcome the inhibition from product accumulation using membrane ultrafiltration device. Retained cells and insoluble naphthalene were recycled to the reactor while the product in the permeate stream was separated by adsorption using hydrophobic macroreticular resins. Out of the different resins, XAD 1600 and XAD 16 adsorbed the maximum amount of the product. A continuously operated bioconversion process with one step production and separation resulted in three times higher productivity than batch process.

Briganti *et al.*,[55] investigated the *cis*-dihydroxylation of naphthalene using direct or reverse micellar systems, which creates a microheterogeneous environment in the micelles to increase substrate bioavailability. Nonionic surfactants are used instead of the ionic surfactants, which were known to damage cell membranes. Cell viabilities were not maintained in the aqueous phase in reverse micelles. Cell viabilities, upon the addition of different nonionic surfactants (1-

2% (v/v)) to form oil in water emulsions, were tested under stirring and standing conditions. Tween 60 was found to least inhibit the cells, among other surfactants like Tween 20, Triton X100 and Triton X114, as known from the cell count, obtained by plating on Agar plates. The substrate concentration in the presence of nonionic surfactant increased 0.038 mM to 3.8 mM. Further addition of oil, isopropyl palmitate, to the micelles increased the substrate concentration in the media, which greatly increased the conversion rate and improved the productivity. The authors proposed temperature and/or change in oil to break the micelles to achieve fast reagent and product separation and scale up the process.

Randazzo *et al.*,[56] improved the availability and hence the bioconversion of naphthalene by creating biocompatible, stable direct microemulsions using nonionic surfactants like Triton-X (t-octylphenoxypolyethoxyethanol) 1.5% by v/v and oils (0.6% - 1%v/v). Addition of oil improves the substrate naphthalene concentrations and increases its concentration in the medium up to 200 times. The authors had reported 100% product yields at the initial substrates for naphthalene near 10 mM. The oils used were like isopropylpalmitate, ethyl oleate, methyl oleate, and tetradecane lactone. For other aromatic substrates studied like Anthracene and Phenantrene, lower product yields were reported which was attributed to product inhibition at higher concentrations.

McIver *et al.*,[57] studied the microbial oxidation of naphthalene in biphasic media to overcome the substrate toxicity and increase substrate availability. Organic solvents were screened based on their *log P* values. Further screening was done by growing cells in presence of 0.5%, 5% solvents and by measuring and comparing the optical densities with control. Solvents like dodecane, lauryl acetate, decanol, and dioctyl phthalate did not inhibit the cell growth. Dodecane was identified as the optimal organic solvent by measuring the amount of diol

formed from the biotransformation of naphthalene though the solvent phase was reported to extract low amounts of diol. The optimal phase ratio of 20% and substrate loading of 40 g/L gives 5.1 g/L of the product after 24 hours with initial rate. Recycling of cells with biphasic media either in resting state or by immobilization in calcium alginate was studied to improve the process economics. Immobilization of the cells improved the stability of the enzymes though the activity reduced due to mass transfer limitations compared to resting cells.

1.2.2. Introduction to ABE model system

1.2.2.1. Overview

Fossil fuels, which are non-renewable sources of energy, are currently used as the primary fuel for transportation. Supply of fossil fuels is limited and they are the main source of greenhouse gas emissions into the environment, that have been related to global climate change.[58] The US Department of Energy has been actively addressing this by passing laws to reduce the use of fossil fuels and increase the use of renewable fuels for transport.[58] Production of renewable fuels (termed biofuels) in a sustainable and low cost manner is the key to replacing fossil fuels. Biofuels such as ethanol, 1-butanol, have been identified to possess chemical properties similar to gasoline.[59] The current mandate is to produce 136.3×10^6 m^3 per year of biofuels for the U.S. market by 2022. Of this amount, corn-based ethanol is capped at 56.8×10^6 m^3 per year, leaving a gap of 69.5×10^6 m^3 per year that could be potentially filled by bio-butanol.[60]

1.2.2.2. Production of ABE solutes

1-butanol is produced from the fermentation of sugars using bacteria. If the bacteria belong to the genum of gram positive bacteria *Clostridia*, the fermentation is commonly referred to as acetone-butanol-ethanol (ABE) fermentation, where these solutes are produced in 3:6:1 ratio by

weight. Fermentation is carried out under anaerobic conditions at 37°C. These bacteria are referred to as solventogenic *Clostridia* and are considered a slow growing native host. ABE fermentation is one of the oldest large scale industrial fermentation processes developed in early 20th century especially during World War II. However the production declined due to less expensive petrochemical routes.

The main substrates for this fermentation are monosaccharides such as glucose, galactose, cellobioise, mannose, xylose and arabinose. These have been are utilized from various biomass sources: energy crops such as sugar beets, sugar cane, corn grain, liquefied corn starch, wheat and cassava; non-food energy crops such as switch grass and guayule, lignocellulosic biomass, biomass hydrolysates; and agricultural byproducts such as straw and corn stalks.[61] Solventogenic *Clostridia* produces ABE solutes via acidogenesis and solventogenesis as shown in Figure 1.4.[62]

Figure 1.4: Metabolic pathway for production of ABE (highlighted in black box) by the *Clostridium Acetobutylicum*.[62] The byproducts, acetate and butyrate, are highlighted in dotted box. Dotted and solid lines indicate reactions during acidogenesis and solventogenesis phases respectively.

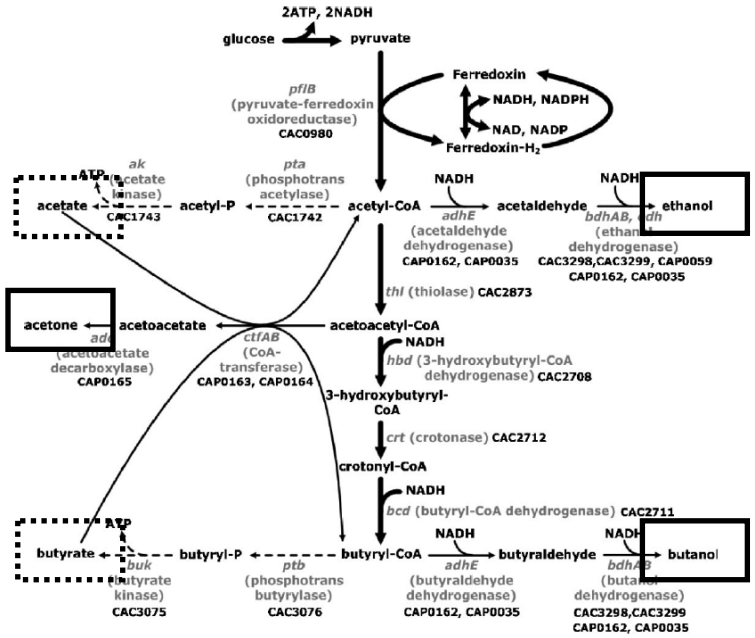

Acidogenesis phase occurs first during the exponential growth phase where metabolic pathways that produce acids are activated resulting in major products such as acetate, butyrate and gases such as CO_2 and H_2. Due to dramatic changes in the gene expression pattern, solventogenesis phase begins during which the acids are converted to the solvents, 1-butanol, acetone and ethanol. This transition is coupled with the onset of sporulation of the bacteria.

1-butanol produced in a typical fermentation using *Clostridium acetobutylicum* is around 10 g/L of 1-butanol or around 2% by wt., while total solutes are around 20 g/L; the product yield from glucose is low around 15% to 25% (w/w). Polar 1-butanol is known to inhibit the fermentation due to its chaotropic effects on the cell membrane[63] and it is the most toxic of three solvents. 7-13 g/L of 1-butanol results in 50% inhibition in growth while 40 g/L acetone and ethanol resulted in 50% inhibition.[13] Currently there are no *Clostridia* species that produce 1-butanol suitable for industrial scale fermentations. The amount of 1-butanol produced from various Clostridia strains are shown in the Table 1.1. The focus in the ABE fermentation area is to genetically engineer bacteria that produce maximum amount of 1-butanol and least amount of ethanol such that the unwanted reactions that produce ethanol are minimized. Other strain of bacteria known to produce 1-butanol include *E. coli* but the bacteria cannot tolerate 1-butanol above 2%[64], while yeast strains such as *Candida*, *Zymomonas*, *Saccharomyces* are shown to produce 1-butanol.

Table 1.1: Amounts of 1-butanol produced from industrial strains of *Clostridia*

Bacteria	1-butanol produced (g/L)	Total solvents produced (g/L)
Clostridium Acetobutylicum ATCC 824 [65]	17.6	27.9
Clostridium Beijerinckii NCIMB 8052 [65]	15.8-19.6	24.2-26.1
Clostridium Saccharoperbutylacetonicum[66]	14	19.2

While ethanol is already widely produced at commercial scale, a few companies such as Butamax (DuPont/BP), Gevo, Cobalt biofuels, Butalco Gmbh, etc., are actively trying to produce 1-butanol at commercial scale. These companies are either focused on strain improvement or on integrating *in situ* product recovery techniques with fermentastion. Another added benefit of ABE fermentation is that the acetone produced can be separated and used to replace acetone produced from traditional chemical engineering route.

Production of 1-butanol through chemical routes

In 1996, the worldwide annual production of 1-butanol and acetone was 2.49×10^9 and 2.10×10^9 kg, respectively. The total production of acetone and 1-butanol was achieved by chemical process using petroleum-based raw materials. Since 1990, production of 1-butanol has been constant in the United States at 2.49×10^9 kg, while worldwide 1-butanol production has fluctuated slightly.

Production of 1-butanol through chemical routes such as the Oxo process, the Reppe process and the Crotonaldehyde hydrogenation is well established.[62] But these processes involve

hydroformylation and hydrogenation of alkenes. High product yields of 92-95% using Rhodium carbonyl catalyst are reported though the operating temperatures and pressures are high at 100-180°C and 7-10 atm respectively. In the Reppe process, propylene in presence of catalyst, water and CO_2 is converted to 1-butanol and isopropanol at low operating temperatures and pressures but the process technology is expensive for commercialization. 1-butanol can also be produced by Crotonoaldehyde hydrogenation[67] involving aldol condensation, dehydration and hydrogenation steps. Ethanol is potential starting material for this process however this process is rarely used. All these processes do not adhere to many of the 12 principles of green chemistry and engineering.[6]

Uses of 1-butanol

1-butanol is traditionally used in the chemical industry as a solvent and plasticizer. It is used as solvent in surface coatings, paints, lacquers, enamel, and for manufacturing vitamins, antibiotics, hormones, camphor and alkaloids.[62] Further, it is used as solubilizer in textile industries, ether and ester derivatives of 1-butanol are used in dental products, resins, plasticizers and as a synthetic fruit flavoring.

In the last decade, 1-butanol has gained recognition as a potential biofuel. It contributes to clean air by reducing emissions and unburned hydrocarbons in the tail pipe exhaust.[68] It is considered a superior fuel than ethanol because it has a higher energy density, blends easily with gasoline or diesel fuel due to longer chain length, lower volatility and polarity [69], does not absorb moisture and does not lead to corrosion. Further, the vapor pressure for pure 1-butanol of 0.63 psi is lower than 2.25 psi for ethanol and the heat of vaporization for 1-butanol of 141.3 kcal kg^{-1}, is lower than that for ethanol of 204.1 kcal kg^{-1}. Also, motor octane numbers of 94 for 1-butanol is better than 92 for ethanol.[70] However, the high boiling point (118.8°C) and lower vapor pressure for 1-butanol may affect cold starting compared to ethanol or gasoline.[68]

1.2.3. Literature review of down-stream processing of 1-butanol from fermentation systems

As discussed in Section 1.1.3, in ABE fermentation, the solutes can be separated *ex situ*, i.e. they are produced in one stage and then separated "downstream". Alternatively, the target solute can be removed in situ from the fermentation reaction directly, eliminating product inhibition of the microorganisms and leading to more efficient separations.

Various methods used for *in situ* and *ex situ* separation[15,16,17] are: a) distillation, b) gas stripping, c) pervaporation, d) membrane separations (micro-/ultra-filtration, etc.), e) adsorption, f) liquid-liquid extraction (LLE).

Most *ex situ* fermentation processes produce dilute solutions, often due to the product inhibiting the microorganism.[10] Removal of 1-butanol from water via distillation methods does not result in complete recovery of 1-butanol as water and 1-butanol form heteroazeotropes (at water mole fraction of 0.76 at 1atm). These dilute aqueous solutions require large energy inputs.[19] In addition, the environmental impact of large water usage must be considered, especially for those involving downstream separations.[20]

In the case of *in situ* separation, continuous direct extraction, integrated with continuous biotransformation, offers the possibility of the recovery of intermediate products during multi-stage reactions thus improving the overall yields of such compounds. Integration of reaction and separation can reduce the number of process steps required and thus reduce capital costs.[23] The continuous removal of product may also enhance those biotransformations which experience product inhibition. However, the key challenge with *in situ* separation is finding a solvent with high extraction efficiency that is also biocompatible with the microorganism.

Product recovery is based on the characteristic property of the solute such as volatility, size selective permeation, evaporation, adsorption and extraction.[15,16,17] While conceptually elegant, volatility based approaches are applicable for few solutes. Membrane research continues to improve selectivity, improve flux, and reduce fouling, but large-scale use is still limited. Use of organic solvents is a feasible option for addressing some of these challenges and thus aids the development of larger-scale processes.

As discussed in Section 1.1.3, LLE is the simplest method to implement extraction of1-butanol from the fermentation broth either *ex situ* or *in situ* to overcome product toxicity. A literature review of solvent extraction is conducted to understand the current state of LLE for ABE fermentation. In this review, the wide range of solvents tested and any inherent drawbacks are highlighted.

1.2.3.1. *Ex situ* solvent extraction

Griffith *et al.*,[71] measured the distribution coefficients (K) of 1-butanol as a function of initial concentration of 1-butanol and water at 20°C. The organic solvents used were halogenated hydrocarbons like chloroform, fatty acids / esters like butyl butyrate, isobutyl palmitate and walnut oil; polyoxyalkylene ethers like polyoxypropylene; aromatics and alcohols. Highest K-values were obtained for hexanol and octanol with $K > 700$. The polyethers also had high partition coefficients around 2.5-3.0. While the fatty acids like isobutyl palmitate had K-values around 2.5. Out of all the solvents tested, based on the viscosity and water solubility, fatty acids were the suitable extractant solvents for 1-butanol.

Mattiasson *et al.*,[72] used a phase system consisting of 6% (w/w) Dextrane T-40 and 25% (w/w) carbowax peg 8000 forming a 6:1 phase ratio with water. They reported partition coefficients of 2.0, 1.9 and 1.9 for ABE solutes.

Traxler *et al.*,[73] measured the distribution coefficient of 1-butanol in solvents like dodecanol, hexadecanol, mineral oil, fuel oil and dodecane in 1.8% aqueous solution of 1-butanol. As found in previous papers, the *K*-values were highest in aliphatic alcohols while the hydrocarbons had values around 0.5.

Ishii *et al.*,[74] measured the partition coefficients of ABE solutes from aqueous mixture containing 0.5% acetone, 1.3% 1-butanol, and 0.1% ethanol at 37°C using organic solvents with carbon number greater than 10. Isostearyl alcohol, C-20 guerbet alcohol (branched-chain alcohol) and oleyl alcohol for 1-butanol had *K*-values greater than 4.5 while the *K*-values of acetone and ethanol were less than 0.5. Acids like oleic acid and isostearic acid also had higher *K*-values for 1-butanol (around 2.3-3.0), while the *K*-values for acetone and ethanol were less than 0.5. All the organic solvents studied extracted1-butanol selectively from an ABE mixture.

Dadgar *et al.*,[75] evaluated the equilibrium distribution coefficients and separation factors for ABE solutes from water using 47 organic solvents. Only the slightly polar solvents like alcohols, esters and ketones had *K*-values greater than 1. The separation factors for these set of solvents were low at lower carbon numbers ($C < 10$), though the numbers improved for $C > 10$. Aliphatic alcohols have high heat of vaporization, while the ketones have solubility in water and are flammable, and the esters have the problem of high reactivity.

Compere *et al.*,[76] studied the extraction of up to 4% w/v 1-butanol from aqueous phase using soybean oil fatty acid ethyl ester at three different temperatures (25°C, 40°C and 55°C). The partition coefficients at these temperatures were >1 and they increased with temperature with a highest value of 2.4 was reported at 55°C. Authors studied the effects of salts such as NaCl, Na_2SO_4, Na_2SO_3, KH_2PO_4 and compounds such as ketones and alcohols such as acetone, ethanol, propanol and pentanol on the partitioning. The salts concentration was varied from 0-

1.5 M. Addition of NaCl did not result in a significant decrease in the partitioning coefficient. However, at the lower 1-butanol concentrations, the partition coefficients were 10% higher. Addition of Na_2SO_4 resulted in increased partition coefficients at all temperatures and pressures. At 40°C and 4% 1-butanol in water, there was 20% increase in the partition coefficient. Addition of Na_2SO_3 resulted in decrease of the partition coefficients, with the higher % decrease at higher temperatures. KH_2PO_4 did not have any effect on the partition coefficients. Similarly, effects of addition of co-solvents between 0 - 4% were studied on the 1-butanol extraction. For acetone, ethanol and 2-propanol, there was no significant effect on partitioning at 25°C, while presence of 1-pentanol increased the partitioning coefficient. For acetone and 2-propanol at 40 and 55°C, the partitioning coefficients decreased by 15%, while for ethanol the change was around 5%. For 1-pentanol, partitioning coefficients increased by 5-10% at the three temperatures.

Malinowski *et al.*,[77] studied the effect of salt addition to ternary system comprising of water, A/B/E solutes and extractants Adol 85NF/Valeraldehyde/cyclopentanol/tert-amylalcohol. Addition of potassium acetate and sodium chloride salts markedly increased the partition coefficients and selectivities. This is attributed to the reduced water activity as the salt addition leads to lower solubility of extractant in the aqueous phase based on the hydration theory. However, below the water activity of 0.92, no effect on the partition coefficient was reported.

Wayman *et al.*,[78] tested extractants such as alcohols, freon, dialkylphthalate for use in extractive fermentations of ABE solvent for their extractability and toxicity. Diethylphthalate and dibutylphthalate had *K*-values >1 though diethylphthalate was toxic. As reported in previous papers, alcohols like 2-ethyl-1-hexanol, 1-octanol, and 1-dodecanol had *K*-values > 3 but were toxic. The *K*-values for extraction of acetone, 1-butanol and ethanol solutes present in 3:6:1 ratio

in the aqueous phase using 1:4 phase ratio of aqueous to dibutylphthalate were 1.39, 0.63 and 0.1 respectively.

Groot *et al.*,[79] evaluated 36 different solvents belonging from a pool consisting of alkanes, alcohols, oils and esters. Alcohols were found to have the highest distribution coefficients (>6), alkanes and oils had the lowest (<0.8), except castor oil with K=2.6, and esters had K-values between 1.5 and 3.6. Eventually castor oil, isopropyl myristate and oleic acid were chosen based on their non-toxicity, high K and S values, and easier availability. The authors also compared LLE with membrane solvent extraction with both polar and non-polar solvents.

1.2.3.2. *In situ* extraction

Honda *et al.*,[80] simulated the effect of solvent selection on ABE fermentation and reported improvement can be obtained with extractive fermentation. Fermenter performance significantly increases when the solvent partition coefficients are higher. Oleyl alcohol which had a partition coefficient of 3.7 gave the highest 1-butanol concentration of 12 g/L with a productivity of 0.54 g/(L. h)

Rofler *et al.*,[81,82,83] studied the process economics for the extractive fermentation of acetone and 1-butanol. Oleyl alcohol was used as the solvent because of its high K-values of 4. The solvent diluted with decane in 1:1 ratio to improve its transport properties. Also, authors report that usage of decane reduces the boiling point of the mixture which helps in regeneration of the solvent. Roffler *et al.*,[84] developed a continuous process for the extraction of acetone and 1-butanol from the ABE fermentation broth using oleyl alcohol as the extracting solvent and reported a 70% increase in volumetric productivity over batch production. A KARR reciprocating plate extraction column was used during the extractive fermentation to eliminate

emulsion formation. The authors also reported easy integration of this continuous system into large scale fermentation processes.

Shukla *et al.*,[85] studied the ABE production using 2-ethyl-1-hexanol in a novel micro-porous hollow-fiber tubular based extractant. This setup allows dispersion free extraction of products. 2-ethyl-1-hexanol was chosen as the extractant from a solvent pool consisting of octanol and esters as it had a high partitioning coefficient of 6.1 and the highest selectivity of 276.7 with 1-butanol compared to the others. Improved overall productivity was reported with this *in situ* technique.

Shah *et al.*,[86] studied the 1-butanol production by simultaneous saccharification followed by extractive fermentation. Here oleyl alcohol was used to continuously remove 1-butanol from the bioreactor resulting in a higher 1-butanol-acetone production ratio (2.6-2.8 instead of 2.0).

Ishizaki *et al.*,[87] compared the performance of methylated crude palm oil with oleyl alcohol as extractant of ABE solutes from fermentation broth. The extraction capacity of CPOE was found to be less than that of oleyl alcohol and about 47% of 1-butanol was extracted. Increased 1-butanol production was reported along with improved concentration of ABE solutes. The authors compared the partition coefficients of ABE solutes in oleyl alcohol with crude palm oil extractant.

Shi *et al.*,[88] mathematically formulated and evaluated the effect of using multiple solvents to extract the ABE solutes while overcoming their inhibitory effect on cell growth. Oleyl alcohol was used to extract 1-butanol selectively while benzyl benzoate was used to extract acetone and ethanol. The solvents were either added sequentially or simultaneously. The predicted results indicated the effectiveness of using multiple extractants on increasing performance.

Barton *et al.*,[89] evaluated 31 solvents to determine their partition coefficient with 1-butanol in fermentation medium. Poly(propelene glycol) 1200 was found to be the most biocompatible solvent with the highest partition coefficient, which further evaluated in an actual fermentation.

Davison *et al.*,[90] studied oleyl alcohol as a 1-butanol extractant for ABE fermentation conducted in a fluidized-bed bioreactor. Amount of 1-butanol produced increased by 50-90% when a 1:4 phase ratio of organic to aqueous medium was used.

Shi *et al.,*[91] investigated the performance of acetone-butanol continuous flash extractive fermentation using oleyl alcohol as the extractant in terms of productivity, energy requirement and product purities. The results showed that performance can be improved by using highly concentrated substrate as feed and dilution of the solvent increases the total productivity while decreasing the energy utilization efficiency. Further, the authors mathematically formulated the production and separation of acetone and 1-butanol in a bi-phasic fermenter. The products accumulated in the solvent phase during fermentation were separated using a partial flash with 2-3 plates for acetone and complete flash for 1-butanol, operated under vacuum (70-150 torr). The authors studied the effect of aqueous and solvent dilution rates on the overall productivity. High solvent dilution rates greater than 1.0 h^{-1} resulted in productivity greater than 10 g/(L.h). Maximum productivity of 30 g/L was reported at 10 h^{-1} and 0.35 h^{-1} solvent and aqueous dilution rates. Energy consumption per unit obtainable product increased as a function of the solvent dilution rate while it decreased with higher substrate feed concentration. The total productivity at a particular energy input increases as the substrate feed concentration increases. However, to reach maximum productivity, higher feed concentration requires more energy compared to that required for lower feed concentration. Energy efficiency, the ratio of product produced to energy consumed, and 1-butanol purity were calculated as a function of acetone purity in the first flash

unit by varying the number of stages. At acetone purity of 0.97 and N=3, energy efficiency of 0.37 and 1-butanol purity of 0.97 were obtained. Optimal reflux ratio of 1-2 was reported.

Li *et al.*,[92] evaluated the ABE fermentation using fatty acid biodiesel as an *in situ* extractant. The idea behind using biodiesel was that ABE solutes enhanced the biodiesel properties and also reduce cost as the energy intensive downstream processing is not required. Authors measured the partition coefficients of acetone, 1-butanol, and ethanol dissolved in a fermentation broth medium using 1:2 phase ratio of the extractant to the broth. The initial concentration of ABE solutes were 1 g, 2 g and 0.5 g in 100 ml, while the broth also other contaminants like acetic acid and butyric acid at 0.02 g/L and 0.05 g/L respectively. *K*-values, measured at 30°C, were highest for 1-butanol and butyric acid at 1.23 and 1.62 respectively while for other solutes it was around 0.2. The biodiesel was reported to increase final 1-butanol production from 42% in an actual in situ ABE fermentation

Adhami *et al.*,[93] used soya derived biodiesel as extractant for 1-butanol. The partition coefficient of 1-butanol in biodiesel was reported to be 0.91, which is less than 1, but the biodiesel is considered as suitable extractant since 1-butanol blends with biodiesel. 60% 1-butanol was extracted at 2:1 biodiesel to water phase ratios.

1.2.3.3. Other methods

Nielsen *et al.*,[94] tested four adsorbents to eliminate the growth inhibition of 1-butanol. In pure system, adsorbents XAD-4 (cross-linked polystyrene resin) and Bonopore (copolymers of divinylbenzene and styrene) adsorbed the highest amounts of 1-butanol 83 and 74 mg/g of adsorbent respectively. In presence of other broth components like butyric acid, reduced the amount of 1-butanol adsorbed to 27 and 23 mg respectively. Further, these adsorbents did not inhibit cell growth while the pH of the medium affected the amount butyric acid adsorbed which

high at *pH*=4. Addition of bonopore adsorbents to an actual fermentation step increased the 1-butanol production from 2-3 g/L to 12 g/L and with low final concentrations of 1-butanol (0.2 g/L) in the broth medium. Using Silicate as adsorbent, concentrated the 1-butanol concentration from 5 to 790 g/L while complete desorption and regeneration by heat treatment were reported. The energy requirements for 1-butanol recovery by adsorption-desorption process is 1948 kcal/kg compared to 2000 kcal/kg for extraction, 5220 kcal/kg for gas stripping and 5800 kcal/kg for steam-stripping distillation.[95] Suitability of resin adsorbent for 1-butanol recovery is depended on its hydrophobicity.[96] Use of Polymeric resin Dowex Optipore SD-2 (Poly(styrene-co-divinylbenzene)) *in situ*, resulted in production of twice the amount 1-butanol compared to titer and the resin did not have toxic to the bacteria.

Afschar *et al.*,[97] improved the productivity of ABE fermentation using cell recycle and studied a two stage reactor cascade to maintain low 1-butanol concentration and obtained long term cultivation under stable conditions.

Gas-stripping, an inexpensive method that does not harm the culture, have been used to remove 1-butanol *in situ* from ABE fermentation in batch, fed batch and continuous operation modes. N_2, CO_2 and H_2 have been used to remove volatile solutes with selectivities in the range of 4-30 while condensation temperatures from -60 to -4°C to separate the gas and solutes are reported with ABE removal rates between 0.1-0.45 g/(L.h). Gas recycle rates of 4.8L/min are optimum rates while optimum gas bubble sizes in the range of 0.5-5 mm are recommended.[98] Up to 10 times higher initial substrate concentration was possible with this method. *Ex situ* gas stripping in a separate packed-bed stripper resulted in low selectivities and possibly clogging at higher gas recycle rate though the removal rate was high. Fluidized bed reactor with immobilized cells using these gases have been also been reported.

1.2.3.4. Economic and energy analysis

Groot *et al.*,[99] evaluated 5 different *in situ* product recovery technologies - stripping, adsorption, LLE, pervaporation, and perstraction (membrane solvent extraction) - to increase the performance of 1-butanol fermentation. LLE and pervaporation were found to have the greatest potential. For LLE, oleyl alcohol and 1:1 phase ratio of oleyl alcohol and decane were used and extraction was conducted in a rotating disk contactor. The estimated total energy required for recovering alcohol is 14 MJ/kg using LLE / perstraction and 9 MJ/kg using pervaporation. The energy requirements for adsorption and stripping were high (around 21 and 33 MJ/kg) due to low selectivities of the processes. The final product purities of these processes are important for energy calculations but were not specified in the paper.

Dadgar *et al.*,[27] developed the process flow sheet and determined the economics of extraction of ABE solutes from fermentation broth using 2-ethyl-1-hexanol. They reported an improved process with over 15% better economics compared to traditional distillation.

Simulation of the production of bio-butanol through ABE fermentation using corn as biosource with goal of estimating potential life-cycle energy and emission effects of bio-butanol as a transportation fuel has been reported.[100, 101] The study was conducted using a well to wheels analysis tool called the Greenhouse Gases, Regulated Emissions and Energy Use in Transportation (GREET) model and the ASPEN simulation software. Further, they evaluated the potential of bio-acetone, a co-product of the ABE fermentation, as replacement for petroleum-based acetone. The authors developed an ASPEN simulation for corn source treatment and downstream processing with final product specification of 99.5% for each of ABE solutes. The solutes were removed from the fermentation broth (operated at 35°C and 1 atm) using *in situ* gas stripping and recovered using molecular sieve adsorption. The products were separated from

residual aqueous phase at required purity using three-stage distillation. The yields of ABE solutes per gram of glucose used are 0.155, 0.303 and 0.007 respectively. The authors used shortcut methods for simulating most of the unit operations and did not examine different distillation component simulation. For a bushel of corn, 69,525 Btu of energy was required to produce 0.868 gallons of acetone, whereas 149,267 Btu of energy was required per bushel of corn to produce 1.50 gallons of 1-butanol. The steam energy requirement in the three distillation columns was 33.1 MW. The steam energy requirement for the gas stripping process and the three distillation columns was 0.38 MW and 32.7 MW respectively.

Qureshi *et al.*,[102] studied the effect of various integrated techniques for extraction of ABE solutes on the production of the 1-butanol in the ABE fermentation with continuous substrate feeding in a 2 L bioreactor. Continuous *ex situ* liquid-liquid extraction using Oleyl alcohol as the solvent resulted in solvent toxicity to cells after 4 recycles. Introducing a membrane (perstraction) to avoid cell-solvent contact prevented emulsion formation and increased the productivity but saturated solvent concentration in the aqueous phase was toxic to cells. Diffusion of mineral salts through the membrane away from the culture medium affected the fermentation. Gas stripping uses gases produced in the reactor CO_2 and H_2, wherein the gases are recirculated back to the rector to facilitate the removal of volatile ABE solutes. This produces more concentrated solutions for distillation though foaming problems need to be addressed. Pervaporation comprises passing the culture medium through a membrane module where the ABE solutes are adsorbed and sweep gas, N_2 is used to remove them. Cell immobilization could modify the membrane's properties. Total substrate consumed increased along with higher total ABE productivities of 0.15 g/(L.h) for LLE, 0.24 g/(L.h) for perstraction,

0.26 g/(L.h) for gas stripping, 0.14 g/(L.h) compared to 0.07 g/(L.h) for control ABE fermentation.

Qureshi *et al.*,[68] presented the economic assessment of 1-butanol production from corn using a hyper-butanol producing strain of bacteria, *Clostridium beijerinckii BA101*, with a yield of 0.42 (g ABE / g glucose). The authors used data from their pilot plant scale studies and assumed ABE productivity of 0.38 – 0.39 g/(L.h) for their batch reactors and reactor productivities of 0.35-0.50 g/(L.h). They reported a total 1-butanol production of 121,596 metric tones (153,000 metric tones of total ABE) when the plant was operated for 350 days a year. For ABE recovery, four distillations columns were used along with four reboilers and four heat exchangers. The costs for major equipment for ABE recovery was $33.47 million. A final 1-butanol cost of $0.34/kg was reported when the raw material corn price was 79.23 $/ton. The cost of the by-product, acetone, was 0.38 $/kg. The total utility cost for the plant was $12.06 million, of which steam and electricity were $6.23 million and $4.66 million respectively. The total capital investment was $110.46 million. The actual energy consumption for the ABE recovery was not reported.

Liu *et al.*,[103] developed cost effective flow sheets for downstream processing of ABE solutes from fermentation broth for different combinations of unit operations. They started by identifying various operating unit designs and developed p-graphs representation. They used graph-theoretic algorithms to analyze various combinations of flow sheets to identify maximal structures with lowest costs. Different unit operations chosen were liquid-liquid extraction, fermentation, distillation, azeotropic distillation, gas stripping and solvent stripping. The capital cost and total operating costs for each flowsheet are based on the type of mixture to be separated. For liquid-liquid extraction, 1-ethyl-2-hexanol was chosen as the extractant. 10 optimal

flowsheets were identified and the systems were found to resemble each other. The optimal flowsheet consists of extractor followed by solvent stripper and two distillation columns with total annual operating cost of $9.416. The cost estimations are based on producing 20 million pounds of 1-butanol per year spanning 325 operating days and final product purities of 99.9% 1-butanol, 99.5% ethanol and 99% acetone. The cost estimation are based either on heuristics or on ASPEN Plus simulator.

Oudshoorn *et al.*,[69] analyzed 9 different water-butanol separation techniques by looking at the thermodynamic and fundamental phase properties. The authors used a shortcut method which only evaluates the internal energy change and calculated the energy requirements of both the amount of 1-butanol recovered and the 1-butanol in the auxiliary phase. The energy requirement was lowest for adsorption and pervaporation (1.3 and 2.0 MW per kg of 1-butanol produced respectively), while the energy requirement for extraction using oleyl alcohol was 7.7 MW per kg of 1-butanol.

Kraemer *et al.*,[104] developed a hybrid *ex situ* extraction-distillation downstream process for the separation of ABE solutes from the fermentation broth. Mesitylene was identified as an optimal organic solvent using a computer-aided molecular design technique. The distribution coefficients of ABE solutes at 25°C in mesitylene were 0.43, 0.76 and 0.03 respectively. The distribution coefficients for 1-butanol were higher with oleyl alcohol (3.8) than with mesitylene but selectivities were higher with mesitylene (1,650) than oleyl alcohol (330). Using rigorous optimization methods, the reboiler duties for mesitylene were reported to be 7.28 MW with a phase ratio of 1:2.3, total 1-butanol production rate of 40,000 tones/annum and initial concentrations of ABE solutes in fermentation broth were 10.5, 8.0 and 5.0 respectively. With shortcut methods, the reboiler duties for mesitylene, oleyl alcohol and pure distillation were

found to be 6.7, 18.5 and 25.6 MW respectively with the initial ABE concentrations of 10.5/8/5, 12/8/5 and 4/8/2 respectively. The energy costs for mesitylene, oleyl alcohol and pure distillation were 2.2, >5.1 and 5.4 M$/annum.

1.3. Application of ionic liquids to whole-cell biocatalysis

A review of available literature shows that application of ionic liquids to whole-cell biocatalysis is still in its nascent stage. In this section, various applications of ionic liquids to whole-cell biocatalysis are reviewed. Further, their toxicity to the microorganisms is summarized.

1.3.1. Literature review of biphasic biocatalysis using ionic liquids

1.3.1.1. Asymmetric reduction reactions

In this section 13 schemes involving reduction of both linear and cyclic ketones using ionic liquids as the biphasic medium are reviewed.

Scheme 2: Asymmetric reduction of 1,3-dicyanobenzene by bacteria *Rhodococcus R31*.

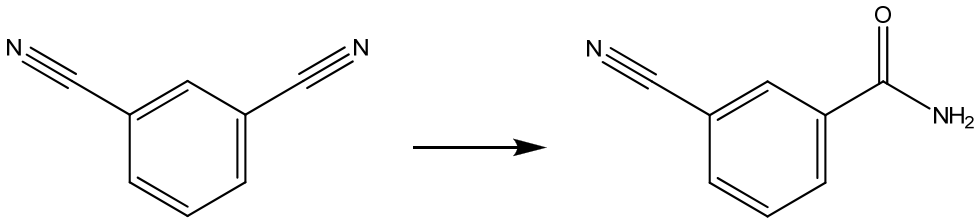

Scheme 1: Asymmetric reduction of 1,3-dicyanobenzene by bacteria Rhodococcus R31.

In the first known study of whole-cell biocatalysis with ionic liquids, Cull *et al.,*[105] optimized the production of 3-cyanobenzamide using a biphasic medium with [BMIm][PF_6] and compared it with a standard organic solvent, toluene (Scheme 2). The substrate, 1,3-dicyanobenzene, has very low aqueous solubility, but a high partition coefficient between the ionic liquid to organic phase of 76.2 (molarity based), while the partition coefficient with toluene is 40. Performance of the ionic liquid in the biphasic system was similar to toluene judging from the product concentrations after 20 minutes. However, different initial rates and long-term rates exist between the two biphasic systems. It is unclear whether the differences are due to reduced

activity of the bacteria in presence of ionic liquid or slower mass transfer of substrate from the more viscous ionic liquid phase to the aqueous phase. Phase separation was slower in aqueous-[BMIm][PF_6] system compared to aqueous-toluene for pure systems however no cell aggregation was found near the interface with [BMIm][PF_6]; this could simplify downstream separations.

Scheme 3: Asymmetric reduction of aliphatic and cyclic ketones to corresponding alcohols by immobilized baker's yeast.

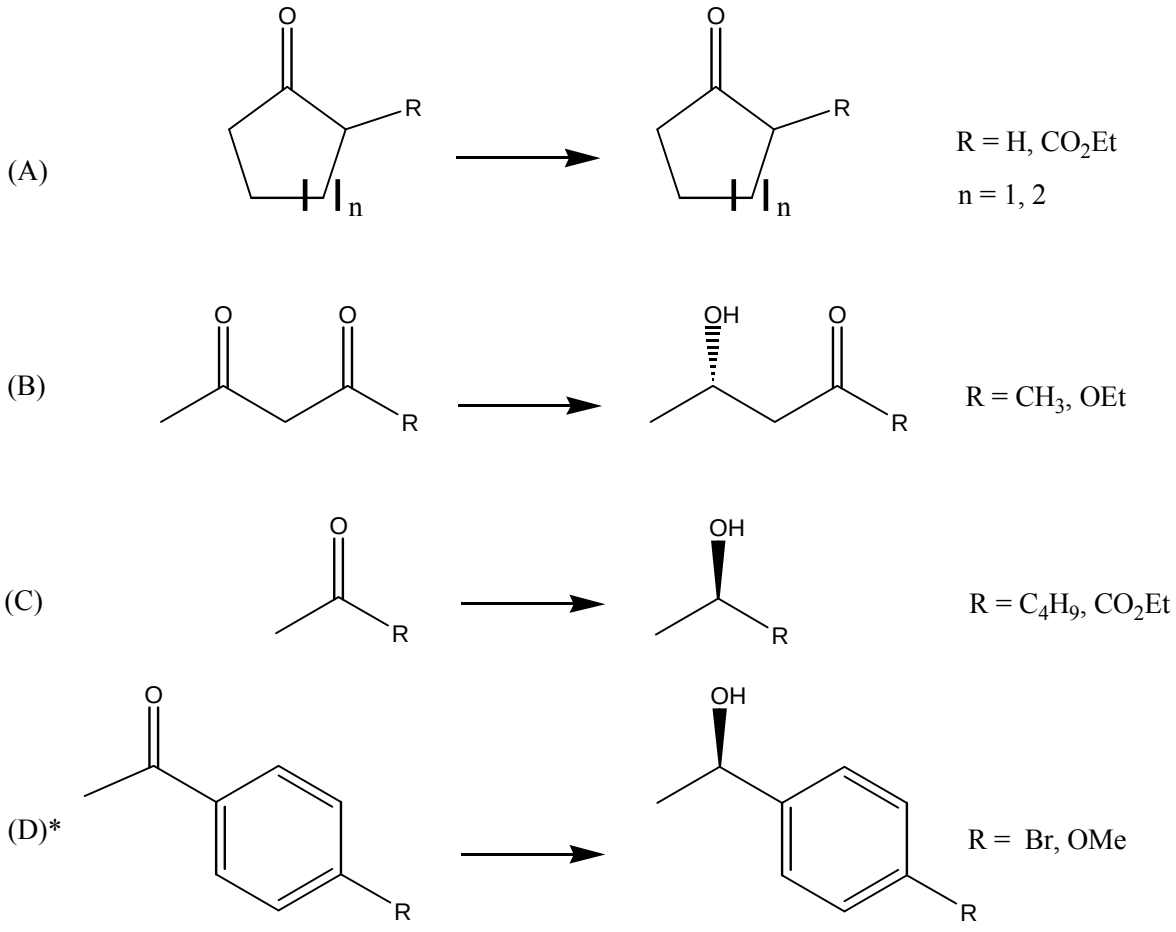

Howarth *et al.,*[35] reported preliminary results with immobilized baker's yeast in a biphasic medium with ionic liquid [BMIm][PF_6] (Scheme 3). A high ionic liquid to water volume ratio of 10:1 was used. The yields and enantiomeric excess (%ee) from the biotransformation in aqueous-ionic liquid media were compared to the results with different organic solvents (hexane, benzene, toluene, petroleum ether and carbon tetrachloride) published in the literature. For some

of the systems, higher yields were obtained with the ionic liquid compared to organic solvents. For instance, the reduction of ethyl acetoacetate (Scheme 2B, R=OCH_3) with ionic liquids increased the yield from 43% using hexane as the solvent to 60%; however the %ee decreased from 91 to 76%. For the reduction of pentane-2,4-dione (Scheme 2B, R=CH_3), the %ee increased from 74% in aqueous medium to 95% in the biphasic ionic liquid media, while the yield decreased from 90 to 22%. The reduction of 4-bromoacetophenone and 4-methoxyacetophenone (Scheme 2D) did not yield any product.

Scheme 4: Asymmetric reduction of 1-(4-chlorophenyl)ethanone) to (*R*)-1-(4-chlorophenyl)ethanol by bacteria *Lactobacillus kefir* DSM20587

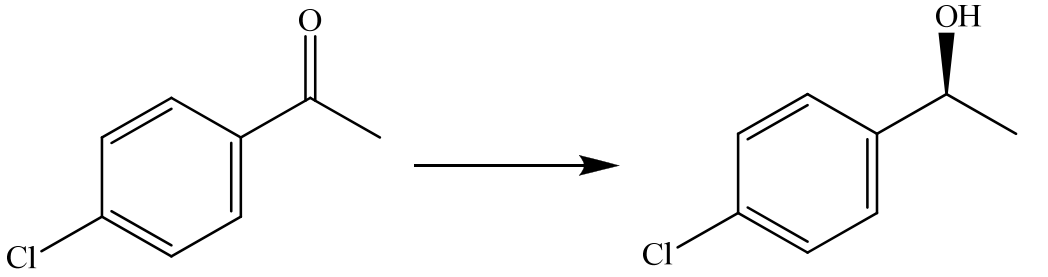

1-(4-chlorophenyl)ethanone (*R*)-1-(4-chlorophenyl)ethanol

Pfruender *et al.,*[36] used hydrophobic ionic liquids such as [BMIm][Tf_2N], [TOMAm][Tf_2N], and [BMIm][PF_6] in the study (Scheme 4), as *Rhodococcus* and immobilized yeast exhibited activity in presence of these ionic liquids.[35,105] [BMIm][Tf_2N] gave higher product yields (92.8%) while the yield was 88.2% with the other ionic liquids. These yields were 2-times higher than those obtained in the monophasic aqueous system which suffers from both substrate and product toxicity. Yields using the organic solvent methyl-*tert*-butyl-ether (MTBE) were very low at 4%, which indicates that cell viability in MTBE was very low. Similar %ee values, 98+%, were obtained in all of the systems.

Aspects of solvent toxicity were directly measured from the cell membrane integrity in presence of 20% by volume of the ionic liquids or organic solvents. Cell membrane integrity

was determined with Live/Dead viability test kit using a fluorometer, wherein live cells and dead cells exhibit different fluorescence intensity depending upon whether the membrane is intact or not. Biphasic medium with ionic liquids performed better than the organic solvents (decane and methyl-*tert*-butyl-ether) and even better than the monophasic aqueous system. Surprisingly with all the three ionic liquids, the % membrane integrity was greater than control at around 125% for [BMIm][Tf_2N], and [BMIm][PF_6], and 175% for [TOMAm][Tf_2N]. These results were compared with those published values in the literature for *Lactobacillus brevis* grown in the presence of a wide range of organic solvents like n-decane, n-octanol, n-decanol, isopropanol, methy tert-butyl ether (MTBE) and di-isopropylether. Solvents with high *log P* (~ 5) among the organic solvents tested, gave highest cell membrane integrity at 52.7%.

Interestingly, these membrane integrity results dramatically decreased with the presence of the substrate, 4-chloroacetophenone, dissolved in the ionic liquid. The percent membrane integrity observed with [BMIm][Tf_2N] was 90% (125% without substrate present) compared to the other two ionic liquids where it was only 30% (125+% without substrate present). However, this was actually an improvement to the substrate dispersed in aqueous phase, where near complete membrane disruption was observed. The partition coefficients for the substrate in each of the ionic liquids is nearly same, thus substrate inhibition alone cannot explain the trends.

Scheme 5: Asymmetric reduction of ketones by bacteria *Lactobacillus kefir, Escherichia coli*K12 (DSM 498) and yeast, *Saccharomyces cerevisiae* FasB His6.

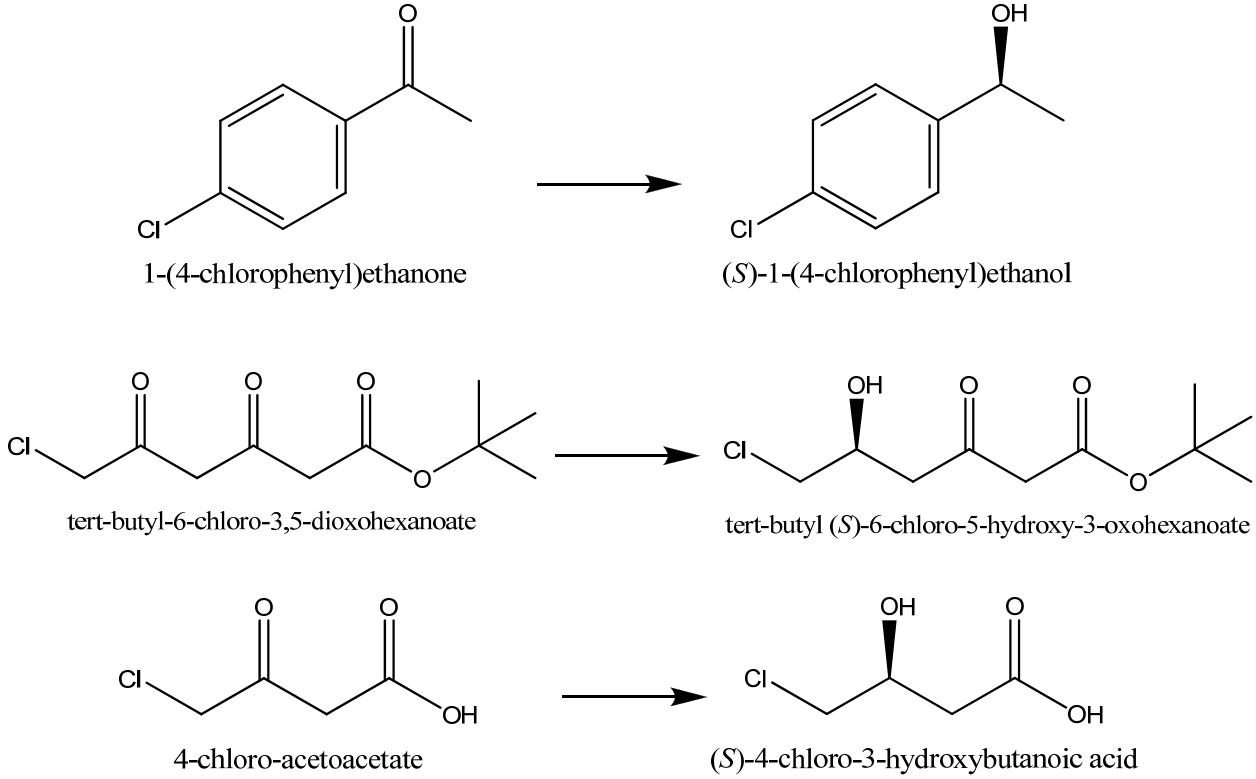

Pfruender *et al.,*[37,106] tested ionic liquids ([BMIm][Tf_2N], [TOMAm][Br], and [BMIm][PF_6]) for their biocompatibility and ability to improve product yields for the biotransformation of ketones to alcohols by gram negative bacterium, *Escherichia coli K12,* gram positive bacteria, *Lactobacillus kefir*, and yeast, *Saccharomyces cerevisiae* (Scheme 5). Product yields from the reduction of 4-chloro acetoacetate were, around 28.7% in [BMIm][PF_6] compared to 16.8% in n-butyl acetate, and 12.4% in [BMIm][Tf_2N]. The toxicity of the product (*S*)-4-chloro-3-hydroxybutanoic acid could play a role as its partition coefficient in the ionic liquids is 0.75 and indicates a slight preference for the aqueous phase. The authors confirmed that higher viscosity of the ionic liquids does not affect the mass transfer as the final product yields of 88% for the synthesis of 1-(4-chlorophenyl)ethanol using *L. kefir,* are higher than those obtained with pure aqueous system around 46.2% over same reaction time. *S. cerevisiae* cells showed high cell

viability (~90%) in 20% by volume of ILs/buffer system while *E. coli* cell viability was lower (60-70%).

Cell viability, in absence of substrate, was measured by adding 20% by volume of ionic liquid organic solvent to buffer containing 20 g/L (based on dry cell weight) of the microorganism. *S. cerevisiae* cells showed high cell viability (~90%) in 20% by volume of ILs/buffer system which was similar to the control medium while *E. coli* cell viability was lower (60-70%). For bacterial cells, cell outer membrane could play a minor role in determining the solvent biocompatibility, as cell viability with gram negative *E. coli*, is lower between 58-70% compared to *L. kefir* where the cell viability was >100%. These observations might change for biocompatibility studies conducted in presence of substrate. Comparing the *E.coli* cell viabilities in presence of organic solvents like n-decane, n-decanol, MTBE, n-octanol and ionic liquids, cells viabilities (60-70%) were similar in ionic liquids and in n-decane (which is hydrophobic and non-polar). For *S. cerevisiae,* cell viability was higher in ionic liquids (90-95%) compared to organic solvents (75-80%). Organic solvents were more biocompatible with *S. cerevisae* than *E. coli.*

Scheme 6: Asymmetric reduction of acetyltrimethylsilane by immobilized yeast *Saccharomyces cerevisiae.*

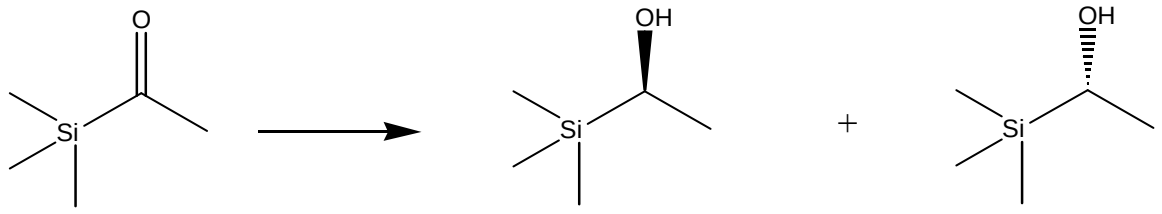

acetyltrimethylsilane (*S*)-1-trimethylsilylethanol (*R*)-1-trimethylsilylethanol

Organosilicon compounds, such as enantiopure organosilyl alcohols, are finding increasing use in the design and development of new pharmaceuticals. Synthesis of these alcohols through

asymmetric reduction of organosilicoketones can be performed using whole-cell biocatalyst to overcome the issue of cofactor regeneration with pure enzymes and to overcome issues with requirement of chiral feedstocks for traditional chemical processes. Lou *et al.,*[107] used immobilized *Saccharomyces cerevisiae*, for the asymmetric reduction of acetyl-trimethylsilane (

Scheme **6**) in an aqueous-IL system. Both hydrophilic ionic liquids, e.g. [BMIm][BF_4] and hydrophobic [BMIm][PF_6] were tested as possible solvents or co-solvents. A simple biocompatibility study performed over a period of 48 hours indicates that the whole-cells (in a suspension) in presence of 3% by volume of the ionic liquids produced slightly higher cell concentration compared to aqueous buffer alone. However, biocompatibility of the cells with the organic solvent hexane was lower than the aqueous buffer.

A comprehensive study for whole-cell biocatalysis with ionic liquids was attempted to optimize the phase ratio, buffer *pH*, reaction temperature, and substrate concentration for both the ionic liquids. Hydrophilic ionic liquids which act as co-solvents were employed as they were previously found to improve enzyme stability and activity.[108] Such effects were not very evident with whole-cells with [BMIm][BF_4] compared to the hydrophobic [BMIm][PF_6], although the initial reaction rates were higher. However, a higher substrate loading was possible with the ionic liquid as either immiscible solvent or co-solvent. Ionic liquids performed better than hexane and a pure aqueous system. Initial reaction rates were 40 times higher than those obtained with hexane and about 14 times higher than aqueous phase. Greater than 99% yields were obtained with both the ionic liquids compared to 97.4% in hexane and only 84% in aqueous buffer. The reaction time in ionic liquids was comparable to aqueous buffer, but 4 times faster when compared to biphasic reactions with hexane. The applicability of ionic liquids as solvents

in stereochemical reactions was highlighted by very high %ee values of (*S*)-enantiomer at 99+% compared to 95% in aqueous medium.

Operational stability of immobilized yeast cells is required for their re-use and recycle. 90% enzyme activity was retained after 6 recycles with the ionic liquids compared to 2 recycles in aqueous buffer and only one recycle in hexane. Thus, the yeast cells are more operationally stable in ionic liquids. Stability was believed to be due to the lower toxicity of ionic liquids, and protection of the cells in the immobilization phase. Scalability of the biphasic system at larger reaction volume (150 ml) furnished high %ee values of 99.9% though the yields reduced to 95%.

Scheme 7: Asymmetric reduction of ketones by *Escherichia coli.*

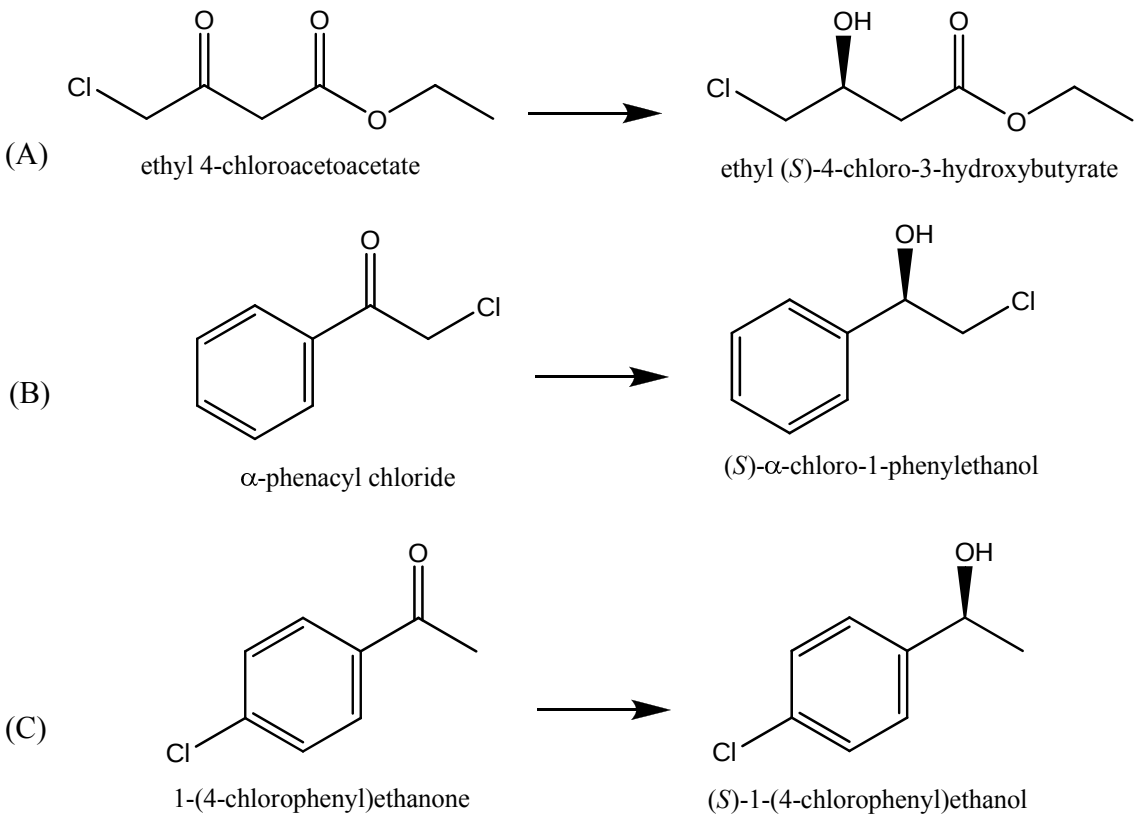

Brautigam *et al,.*[38] conducted an extensive investigation of commonly available ionic liquids to perform biphasic whole-cell biocatalysis. Asymmetric reduction of 4-chloroacetophenone,

ethyl 4-chloroacetate and phenacyl chloride to corresponding enantiomeric alcohols were used as model reactions (Scheme 7). The following water-immiscible ionic liquids [BMIm][PF_6], [HMIm][PF_6], [BMIm][Tf_2N], [HMIm][Tf_2N], [BMPl][Tf_2N], [HMPl][Tf_2N], [BMPl][E_3FAP], [HMIm][E_3FAP], and [EWTMG][E_3FAP] were identified based on their physical properties. These ionic liquids were further evaluated by an approach highlighted in the authors' previous paper.[36] *E. coli* demonstrated 70% cell viability in [PF_6]-based ionic liquids which was higher than the cell viabilities in [Tf_2N] and [E_3FAP] ionic liquids. [E_3FAP]-based ionic liquids showed <5% cell viability. For the same anion [Tf_2N], changing the cations from imidazolium to pyrrolidinium slightly reduced the cell viability.

Product yields, enantiomeric excess and the distribution coefficients (*log D*) were measured after 1 hour of biotransformation in 20% by volume of ionic liquid with the aqueous medium to further evaluate the performance of these ionic liquids. The yields and *log D* values increased as the cation chain-length increased from n-butyl- to n-hexyl for different anions used. Keeping the anion [Tf_2N] constant, yields with the pyrrolidinium-based ionic liquids were higher than imidazolium ionic liquids, which is reverse of cell viability trend. Yields and *log D* values with [PF_6] based ionic liquids compared to [Tf_2N] based ionic liquids did not follow a discernable trend. For Scheme 6A, 6B, and 6C, substrate *log D* values were between 1.8 and 3.1, and product *log D* values were between 1 and 2.4.

The product yield in Scheme 6A in different ionic liquids tested was >95.8% compared to 7.5% in aqueous medium. The enantiomeric excess of the (*S*)-enantiomer was similar in both cases. The yields were highest in [BMPl][Tf_2N] and [HMPl][Tf_2N] ionic liquids (99.3%) with space-time-yield (20 g/L/h) 13-fold higher than in the aqueous system. Higher chemical yields with [BMPl] and [HMPl] were attributed to higher product partition coefficients (*log D*). The

product yield in Scheme 6B was maximum at 89% in [HMIm][PF_6], while the yield in aqueous medium was only 3.3%. The corresponding yields in [HMIm][Tf_2N] and [HMPl][Tf_2N] were 69.8% and 74.2%. While the substrate and product *log D* were higher compared to Scheme 6A, lower product yields were obtained. The product yields in Scheme 7C were between 40-64% for the ionic liquids used, which were much higher than the 8% in the monophasic aqueous system. High *log D* values for the product and 70% cell viability in [HMIm][PF_6] did not result in high product yields here. Enatiomeric excess of the (*S*)-enantiomer in the biphasic medium (99.5%) were slightly higher compared to the aqueous medium (96%).

Further, 21 ionic liquids[109] were chosen based on their hydrophobicity, density > 1.2 g/cm^3, kinematic viscosity < 4 cm^2/s. All ionic liquids tested had *log D* > 2 for both the water-insoluble substrates and products. Further, biphasic biotransformation with 1:4 (v/v) IL:Aq at 1.4 mL scale for 1 hour with 600 mM substrate resulted in yields 10 times larger than the pure aqueous biotransformation and %ee of 99.6 with aqueous were maintained with 90% of the ionic liquids tested. 9 ionic liquids tested gave yields > 60%; [Tf_2N] and [PF_6] anion based ionic liquids performed better than [FAP] anion based ionic liquids for both systems; [(E_2OH)MIm][Tf2N] and [(P_3OH)Pyr][Tf2N] were not suitable for either systems. It was concluded that distribution coefficient values are not a direct indicator for lower or higher yields. With 1:4 (v/v) [HMPl][Tf_2N]: aq at a 200 mL scale and 600 mM substrate, yields of 95%, space-time-yield of 180 g/L/d were reported for asymmetric synthesis of (*R*)-2-octanol compared to only 55% yields with aqueous biotransformation. Similar high yields with [HMPl][Tf_2N] and [BMIm][Tf_2N] for synthesis of (*R*)-1-(4-chlorophenyl)ethanol are reported which are much higher than those with decane as solvent.

Scheme 8: Asymmetric reduction of 6-Br-β-tetralone by yeast strain *trichosporon capitatum* MY1890 and bacteria strain *Rhodococcus erthyropolis* MA7213.

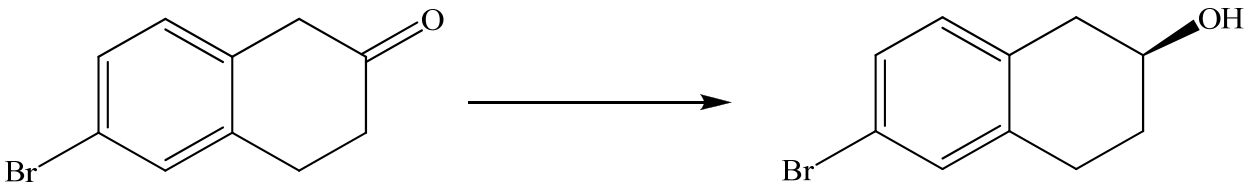

6-Br-β-tetralone (*S*)-6-Br-β-tetralol

Hussain *et al.,*[110] investigated the stereospecific reduction of 6-bromo-β-tetralone to (*S*)-6-bromo-β-tetralol in the presence of ionic liquids using both yeast and bacteria (Scheme 8). They evaluated hydrophilic and hydrophobic ionic liquids, by measuring the cell viabilities, initial rate of product formation and the final substrate conversion, for the stereospecific reduction of 6-bromo-β-tetralone using both yeast and bacteria. The bacterial cell viabilities at a 1:1 (v/v) of ionic liquids to aqueous phase were measured by a plate count method. The hydrophobic ionic liquids ([BMIm][PF_6] and [TOMAm][Tf_2N]) and the hydrophilic ionic liquids ([EMIm][TOS] and [BMIm][BF_4]) showed >80% cell viability; no cell viability was observed with other ionic liquids like [BMIm][$OcSO_4$], [BMIm][$MDEGSO_4$], and [CABHEM][$MeSO_4$]. By changing the anion group from [$OcSO_4$] to [BF_4] with a [BMIm] cation, cell viability was increased. With 20% volume concentration of the ionic liquid [EMIm][TOS], 100% substrate conversion and 88% enantiomeric excess was possible with yeast, while with the bacterium *R. erthyropolis* MA1392, the conversion was around 28%. In presence of the immiscible ionic liquids ([BMIm][PF_6], and [TOMAm][Tf_2N]), and miscible ionic liquid ([BMIm][BF_4]), the substrate conversion by yeast and bacteria were only between 35 – 60% and 7 – 17%. This was attributed to slower mass transfer rate of the substrate from the ionic liquid phase to the aqueous phase (for

the biphasic systems) and also attachment of ionic liquid to cell membrane preventing effective transfer of substrate into cell.

Scheme 9: Asymmetric reduction of 2,5-hexadione and 1-phenyl-2-propanone by *Escherichia coli.*

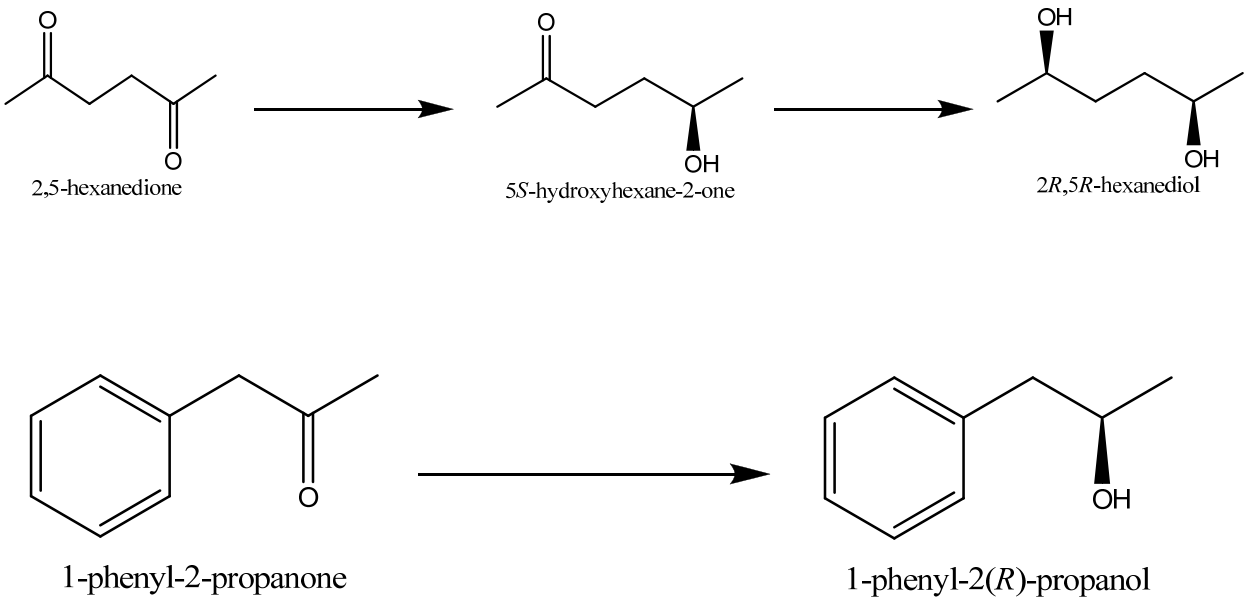

Schroer *et al.,*[111] studied the whole-cell reduction of ketones with substrate coupled cofactor regeneration with recombinant *Escherichia coli*. Here the intracellular cofactor regeneration is achieved by using a co-substrate such as 2-propanol as a redox equivalent as shown in Fig (1). 2-propanol is oxidized to acetone by the enzyme to regenerate the cofactor (nicotinamide adenine dinucleotide phosphate (NADPH)). In this study, *Escherichia coli* expresses alcohol dehydrogenase enzyme that catalyzes both redox reactions. Formation of acetone was mentioned to be a bottleneck for higher yields as thermodynamic equilibrium between the four components and two reactions limits the yields obtained. Also, acetone above certain concentrations can affect the activity and stability of the cells.

Fig (1): Reaction mechanism for the asymmetric reduction of a model ketone with substrate-coupled cofactor regeneration

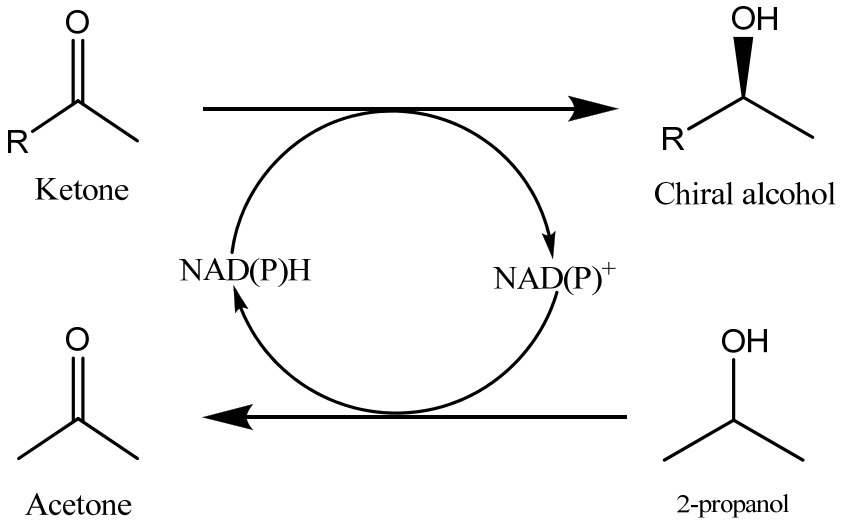

In order to overcome the detrimental effects of acetone build-up, three *in situ* techniques were investigated for its removal: partitioning into an immiscible ionic liquid phase; air sparging (stripping) throughout the reaction mixture, and a pervaporation technique. Scheme 9a and Scheme 9b show the model reactions studied. The partition coefficient of the acetone in the ionic liquid [BMIm][Tf_2N]/buffer medium was higher than in a methyl *tert*-butyl ether (MTBE)/buffer medium. However, the partition coefficient of 2-propanol in the ionic liquid [BMIm][Tf_2N]/buffer medium was slightly lower than in a methyl *tert*-butyl ether (MTBE)/buffer medium. Using the [BMIm][Tf_2N]/buffer medium also improves the substrate availability to the cells. Accordingly, higher yields >95% were obtained with ionic liquids compared to only 24% in MTBE. The relative stability, calculated from the initial catalytic reaction rate, in the IL/aqueous system was higher than the MTBE system and aqueous one-phase system without any acetone removal. From Scheme 9a, yields increased from 54% in the aqueous phase to >95% by air sparging, while pervaporation improved yields to >90%. The

relative stability of the *E. coli* was higher at 82% in pervaporation compared to only 25% relative stability after sparging air. Specific productivity ($g_{product}/g_{(cell\ wet\ weight)}/d$) was higher in pervaporation at 46.3 compared to 2.59 with *in situ* extraction with ionic liquids.

Scheme 10: Asymmetric reduction of nitrobenzene by bacterial anaerobe *Clostridium sporogenes.*

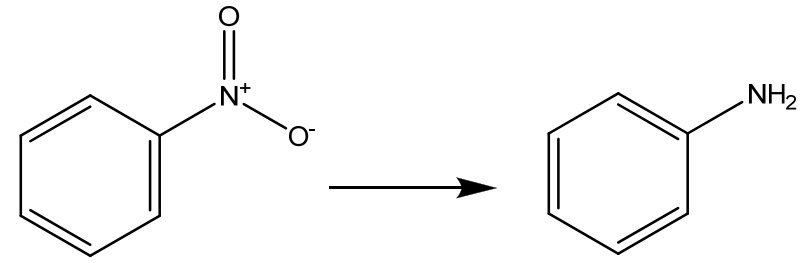

Nitrobenzene Aniline

Stephens's *et al.,*[112] evaluated nitro reduction by *Clostridium sporogenes* in water miscible ionic liquids. Water-miscible ionic liquids were investigated as co-solvents, unlike earlier studies where hydrophobic ionic liquids were investigated for faster phase separation.[113] The effects of the ionic liquids between 0.1 – 2% (w/v) on cell growth and corresponding product yields for the reduction of water-insoluble nitrobenzene (Scheme 10) were studied and compared with the results from using organic solvents like n-heptane and ethanol.

[BMIm][BF_4] was found completely toxic to the cells at 0.5% (w/v). This was attributed to the toxicity HF formation due to the anion degradation as identified by the drop in pH over time. With the ionic liquid AMMOENG 100 (Cocosaklyl pentaethoxy methyl ammonium methylsulfate), complete growth inhibition was observed. This was believed to be related to decrease in nutrient concentration caused by the immediate precipitation of the culture medium even at 0.25% (w/v) of the ionic liquid. With [DME][Ac] and [$EtOHNMe_3$][Me_2PO_4], an increase in cell growth by 17% and 28% respectively was observed. The authors hypothesize

that the presence of these ionic liquids might increase availability of particular nutrients to cells or the ionic liquid salts themselves might act as a nutrient source. [EMIm][$EtSO_4$] inhibited 58% of the cell growth. However at 99+% conversion, a 4% w/v solution of [EMIm][$EtSO_4$] had a 79% yield of aniline compared to 43% yield with heptane and only 8% yield with 4% ethanol. This suggests that the ionic liquid may suppress unproductive substrate conversion, although it could also be inhibiting some of the cell anabolic processes. While the selected ionic liquid, [EMIm][$EtSO_4$], was not the optimized solvent, the results indicate the potential of ionic liquids to tune the biotransformation.

Scheme 11: Asymmetric reduction of aromatic keto ester by baker's yeast, *Saccharomyces cerevisiae.*

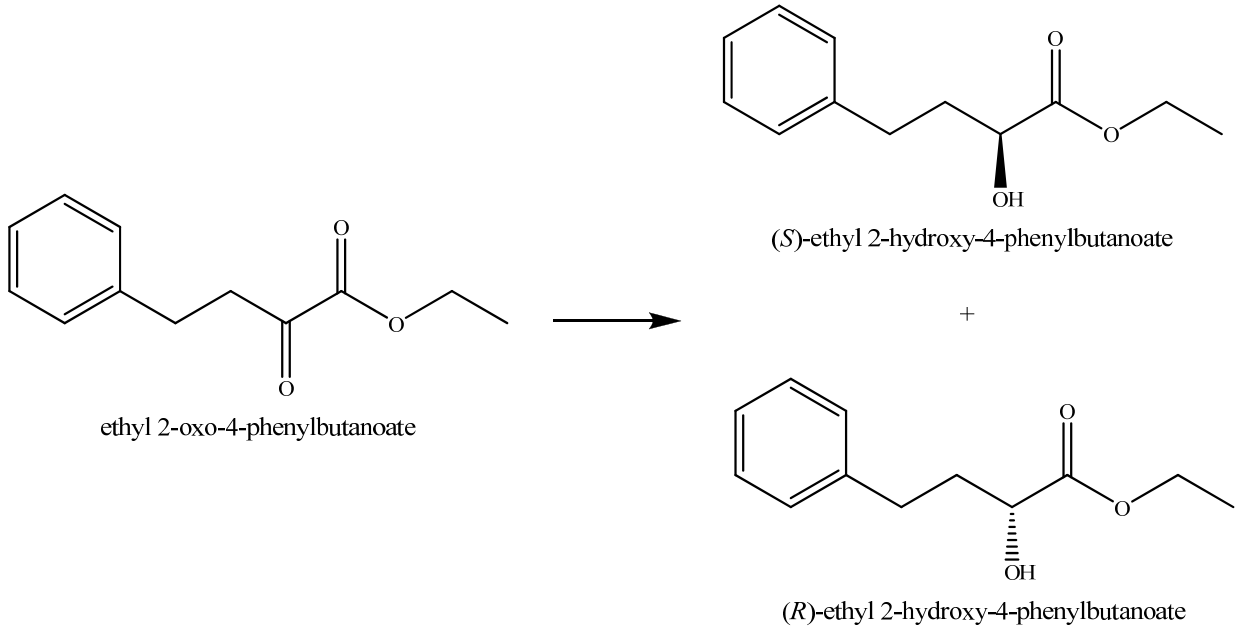

Guan *et al.,*[114] investigated the synthesis of optically active (*R*)-enantiomer of ethyl 2-hydroxy-4-phenylbutanoate by suspensions of *Saccharomyces cerevisiae* in nonaqueous (organic solvent) media. Water as the broth medium was avoided as decomposition of (*R*)-enantiomer was observed. The ionic liquid [BMIm][PF_6] and organic solvents ethyl ether, benzene and

toluene were used as the nonaqueous media. Addition of small amounts of water (1 – 3% (v/v)) to the nonaqueous media resulted in the formation of (*S*)-enantiomer in the ionic liquid medium, while higher enantiomeric excess of (*R*)-enantiomer was observed in benzene (80%) and ethyl ether (70%). But at higher water concentrations the system becomes a biphasic system (1:10 by volume of water in the ionic liquid), enantioselectivity is reversed and only 6.6% ee of (*R*)-enantiomer is formed. Addition of 1% (v/v) of ethanol to the 1:10 (v/v) of water in ionic liquid increased the formation of the (*R*)-enantiomer and enantiomeric excess increased from 6 to 82.5%. Also improved product yields and conversion were also obtained. The increase in the enantiomeric excess and yields is attributed to utilization of ethanol as co-substrate for cofactor regeneration, which was reported in the literature.[115]

Scheme 12: Asymmetric bioreduction of 1-(4-methoxyphenyl)ethanone by immobilized yeast *Rhodotorula sp.* AS2.2241.

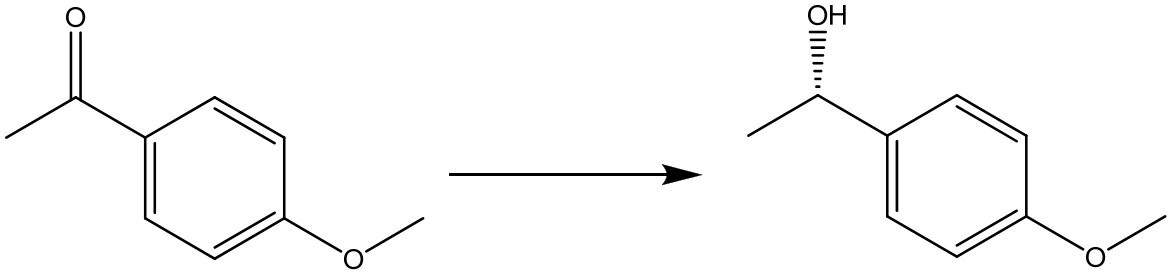

1-(4-methoxyphenyl)ethanone (*S*)-1-(4-methoxyphenyl)ethanol

Lou *et al.,*[116] were successfully able to demonstrate the asymmetric reduction of 4-methoxyacetophenone to enantiopure (*S*)-(1)-(4-methoxyphenyl) ethanol using a new strain of immobilized yeast *Rhodotorula sp.*AS2.2241 (Scheme 12) in a IL/water biphasic system. Earlier, Howarth *et al.,*[35] reported unsuccessful reduction of this substrate by immobilized baker's yeast in biphasic medium with [BMIm][PF_6]. Ionic liquids like [RMIm][PF_6], where R was varied from n-C_4H_{11} to n-C_7H_{15} and [RMIm][Tf_2N], where R was C_2H_5, n-C_4H_{11} were tested initially for their cell viability and substrate conversion. [BMIm][PF_6] was found with lowest

cell inhibition from cell viability studies conducted both in presence and absence of substrate. Cell viabilities with this ionic liquid in presence of substrate were around 90% compared to 60% in pure aqueous medium. This may be due to the reduced substrate toxicity from the high partition coefficient of the substrate into the ionic liquid phase.

For the asymmetric reduction, >99% enantiomeric excess was obtained with 20% by volume of all the ionic liquids, and a maximum substrate conversion of 69.5% with [BMIm][PF_6]. Conversion decreased with increasing carbon number of the imidazolium alkyl chain with either of the anions. For the [BMIm][PF_6]/water biphasic medium, the optimum substrate loading with ionic liquids present was 40 mM, which is about 8 times higher than in aqueous medium. While the initial reaction rates were lower with ionic liquids by one third, the time taken to reach the final conversion was similar. Lower initial reaction rates were attributed to mass transfer limitations associated with the biphasic medium. Operational stability of immobilized yeast in the presence of 20% by volume of ionic liquid was found to be excellent after over 8 recycles and about 5 times higher than the aqueous system.

Scheme 13: Asymmetric reduction of ethyl 3-oxobutanoate by yeast cells, *Pichia membranaefaciens* Hansen ZJPH07.

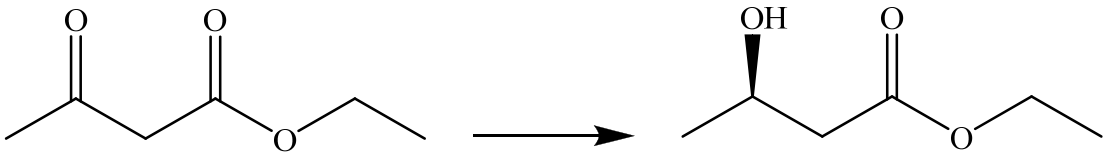

ethyl 3-oxobutanoate ethyl (*R*)-3-hydroxybutyrate

Zu *et al.,*[117] employed [BMIm][BF_4] as the co-solvent for the asymmetric reduction of ethyl 3-oxobutanoate by yeast cells to synthesize optically active ethyl (*R*)-3-hydroxybutyrate, which is a intermediate in the synthesis of β-lactamase inhibitors. Enantiomeric excess increased with the IL-aqueous cosolvent volume percent, but a maximum product yield of 32% was obtained at 2.5% by volume of ionic liquid with 0.35 M of substrate concentration, 30 g/L glucose concentration and 140 g/L cell concentration. Further optimization of the reaction parameters like substrate concentration (0.55 M), cell concentration (240 g/L), and glucose concentration (50 g/L) improved the product yields (77.8%) and enantiomeric excess (73%) with 2.5% by volume of [BMIm][BF_4] in aqueous medium compared to 68.5% and 65.1% obtained with monophasic buffer system.

Scheme 14: Asymmetric reduction of aromatic α-keto esters by *Escherichia coli*

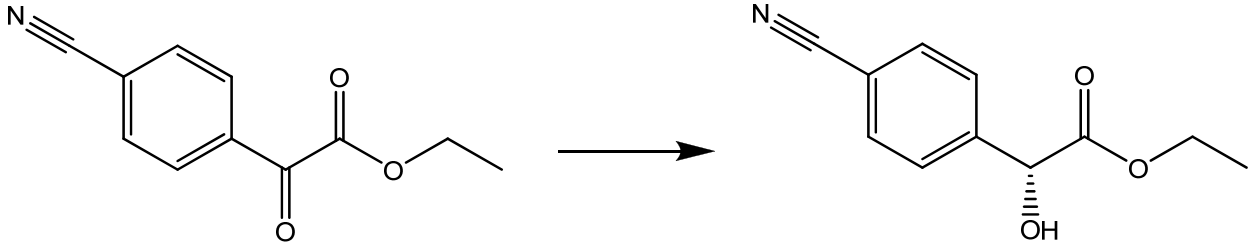

ethyl 4-cyanobenzoylformate ethyl (*R*)-4-cyanomandelate

Kratzer *et al.,*[118] studied the enantioselective bioreduction (Scheme 14) of aromatic α-keto esters to chiral alcohols by developing a new strain of *E. coli* by co-expressing *Candida tenuis* xylose reductase that promotes cofactor dependent reduction and *Candida boidinii* formate dehydrogenase. Performance of the bacteria was compared with the previously investigated yeast, *Saccharomyces cerevisiae*. In the pure aqueous system, 100 mM of substrate and 20 g/L cell concentration resulted in formation of 70 mM of the product with enantiomeric excess of 99.3% and a product yield of 80%. At higher substrate concentrations of 500 mM and 40 g/L cell concentration, the %ee was maintained at 99+%, but the yield was three times lower despite initial rates that were 6-times higher. Low substrate solubility (10 mM) in the aqueous phase and effect of higher substrate concentrations on the cell stability appears to limit its reduction.

[BMIm][PF_6] and organic co-solvents like ethyl acetate, hexane, and n-butyl acetate were investigated to possibly reduce the substrate toxicity and improve product yields. However, [BMIm][PF_6], although better than the other organic solvents, reduced product yields to much less than those obtained in aqueous system. Addition of external cofactor NAD^+ improved the yields from 74 mM to 108 mM, but this addition may not be economically feasible for scale-up.

1.3.1.2. Hydrogenation reactions

Two schemes that use hydrogenation and oxidation are discussed in this section.

Scheme 15: Hydrogenation of sodium caffeate by bacteria *Spormusa termitida* JSN-2.

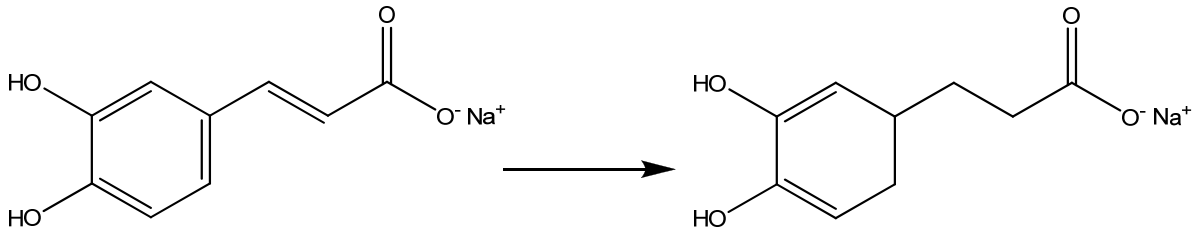

sodium caffeate sodium hydrocaffeate

Stephens *et al.,*[39] focused their study on the direct effect of presence of ionic liquid [BMIm][PF_6] on the performance of the bacterium, *Spormusa termitida* (Scheme 15). A highly water-soluble substrate was chosen to eliminate mass transfer limitations between the immiscible phases which was a possible reason for reduced rates of product formation in earlier study.[105] Substrate reaction rates and the final conversion in aqueous medium and with the solvent, n-tetradecane, and [BMIm][PF_6] were measured throughout the reaction. Overall productivity with a two-phase system using tetradecane as the solvent was similar to the aqueous phase alone. However, the results in presence of 1:5 IL:Aq. phase ratio indicate that [BMIm][PF_6] has a negative effect on the bacteria. The initial reaction rate was around 1120 mmol/kg/h for tetradecane and the reaction was effectively completed after 3 hours with a conversion of 95%. For [BMIm][PF_6], the initial rate was higher 880 mmol $kg^{-1}h$, but the rate dropped by three orders of magnitude after 2 hours with final conversion of 88% after 27 hours. Hence, the reaction time needed for near-completion with [BMIm][PF_6] would be approximately 9 times longer compared with tetradecane. As the initial reaction rate in the presence of the ionic liquid was relatively high, this suggests that the cells did not die instantaneously as would happen in presence of other toxic solvents like 1-butanol. The authors hypothesize that the toxicity of the ionic liquid may be attributed to the known degradation of the [PF_6] anion to form hydrofluoric acid (HF), which would be very toxic to the cells. However, it is unclear if the presence of HF was due to degradation within the timescale of the reaction or from its initial concentration.

Scheme 16: Microbial oxidation of toluene by *Escherichia coli*

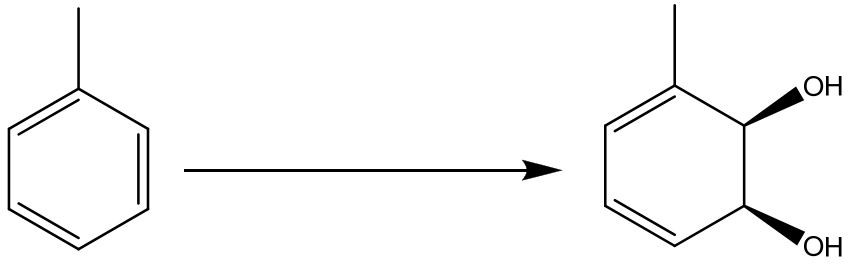

toluene

(1*S*,2*R*)-3-methylcyclohex 3,5-diene-1,2-diol

Stephens *et al.,*[40] were the first group to study the microbial oxidation of aromatic compounds in a biphasic medium with ionic liquids. Ionic liquids can overcome the issue of substrate toxicity along with lower substrate concentrations associated with aromatic compounds by acting as substrate reservoir. *Cis*-dihydroxylation of toluene to (1*S*, 2*R*)-3-methylcyclohexa-3,5-diene-1,2-diol (Scheme 16) by recombinant *E. coli* with a toluene dioxygenase gene was investigated. Suitable ionic liquids were identified by conducting biocompatibility studies with the host strain of *E.coli* without recombinant plasmid.

Cell growth rates in presence and absence of ionic liquids were measured using an immuno-light scattering technique to avoid any possible interference of ionic liquid induced changes in cell morphology with the results from common staining techniques. Hydrophilic ionic liquids such as [OMIm][Cl], [TOMAm][Cl], and $[P_{6,6,6,14}][Cl]$ caused complete growth inhibition at low phase ratios. $[PF_6]$ based ionic liquids were not tested due to their low stability in water. $[EMIm][Tf_2N]$, $[BMIm][Tf_2N]$, and $[DMPy][Tf_2N]$ inhibited growth completely at just 0.25% phase ratios. The results with $[BMIm][Tf_2N]$ are somewhat in contrast to the 24% cell viability of *E. coli* reported by Brautigam *et al.,*[38] with 20% by volume of the ionic liquid in the aqueous phase. Growth rates in absence of solvent phase is 0.357 h^{-1}, compared to 0.276 h^{-1} and 0.219 h^{-1} in presence of 23% by volume of hydrophobic ionic liquids ($[P_{6,6,6,14}][Tf_2N]$ and

[TOMAm][Tf_2N]). Hence these ionic liquids at 23% phase ratio, were shown to inhibit the cell growth by 23% and 39% respectively compared to 5.9% by organic solvent like tetradecane.

The ionic liquids were able to achieve much higher loadings (~ 20×) of the substrate over the aqueous phase solubility. Biotransformation at 50 ml scale with same substrate concentration of 3.76 mM in presence and absence of ionic liquid resulted in same final chemical yields at 87-90%, though the viable cell count were reported to be slightly lower. In [$P_{6,6,6,14}$][Tf_2N]/water and [TOMAm][Tf_2N]/water systems, further growth inhibition was observed during the reaction at 32% and 43% respectively. This was higher than the growth inhibition observed with these systems during ionic liquid biocompatibility studies with no substrate/products present. In the aqueous system, the growth rate is positively affected by the presence of the substrate and an increase of 3.6% was observed. This suggests that enzyme catalyzing the reaction and the cofactor regeneration mechanism are unaffected by ionic liquids, though there is growth inhibition. Possible reasons for this could be due to intensification of growth inhibition by the ionic liquids in substrate, product, presence of recombinant plasmid and inducer. Biotransformation carried out in ionic liquids at optimal substrate concentration of 75.2 mM resulted in 2.5 fold increase in product concentration compared to only 1.2 - 1.4 fold increase obtained with tetradecane.

Lower chemical yield at 27% with ILs/aqueous system compared to 88% with aqueous system, was attributed to limited oxygen supply in the sealed culture vessel. Experiments were performed in a 1.25 L bioreactor, in biphasic medium with [$P_{6,6,6,14}$][Tf_2N] and in aqueous medium, with unlimited oxygen supply to overcome the oxygen limitation. Higher mean product was formed at 55.5 ± 22.5 mM in presence of the ionic liquid compared to 20.7 mM in 50 ml flask culture. Similarly, increase in mean product formed from 8.31 mM to 18.2 ±8.2 mM

was observed with aqueous system. This indicates that the oxygen might be a limiting factor in the 50 ml flask, though the initial concentrations in the flask and bioreactor might be different as higher amounts of liquid toluene were added to the bioreactor. Average final product yields per unit biomass in presence of ionic liquid were 11.7 $mmol/g_{(dry\ weight\ cell)}$ compared to 3.46 $mmol/g_{(dry\ weight\ cell)}$ obtained with aqueous medium.

1.3.1.3. Scale up studies

Prefuender *et al.,*[36] extended the reduction reactions at 2.4 mL scale (Scheme 4) to larger reaction volumes in a 200 ml batch stirred tank reactor to test the scalability of the process. Similar results were obtained as in the 2.8 ml scale of the aforementioned reactions with a 600 mM substrate concentration, and 1:4 (v/v) of [BMIm][Tf_2N]-aqueous medium. Volumetric productivity was reported to be 20.4 g/L/h and the final product concentration was 81.6 g/L, which are in good comparison to industrial biocatalytic processes. Relatively easy phase separation occurred as no emulsification was reported.

Dennewald *et al.,*[119] extended Scheme 7 and the reduction of (*R*)-2-octanol by studying the effect of recycling of most suitable ionic liquid, [HMPl][Tf_2N] on the product yields for scheme. Ionic liquid was separated from the cell broth by centrifugation after 6h of biotransformation and pure ionic liquid was recycled after distillation of the product and unreacted substrate. Over 25 batch cycles, 82.8% ionic liquid was recovered and no ionic liquid degradation was observed. It was predicted that this could reduce the material costs by 70%. The average product purity was 96.8%, average substrate conversion was 98.5% and product %ee were maintained at > 99.5%. A total of 999 g of product (*R*)-2-octanol L_{IL}^{-1} was produced.

Further, the results with 48 miniaturized bioreactors operated in parallel were compared with a 20-fold larger stirred tank reactor (200 ml) to understand if high throughput small volume bioreactors can reduce the time and resource investment for process development with biphasic biotransformation with ionic liquids.[120] The volumetric power consumption and maximum local energy dissipation at different impeller speeds for both the setups were in good agreement. With 1:4 IL:aq, final % substrate conversion with 4 different ionic liquids matched at both scales. % conversions obtained with reactors in parallel decreased compared to the stirred reactor as the phase ratios of [HMPI][Tf_2N] increased from 20 to 70%; the conversion at 70% ionic liquids at lower scale was ~40% compared to ~70% at large scale.

1.3.1.4. Application of Ionic liquids to *Clostridia* fermentation

Nancharaiah *et al.,*[121] studied the effect of various ionic liquids on cell growth, glucose utilization and amount of 1-butanol produced during the glucose fermentation by *Clostridium* sp. Ionic liquid concentration was varied between 0 to 15 g/L and the cell growth was monitored via optical density (OD_{600nm}) for around 150 h. Below 1.5 g/L, the cells exhibited growths at the same level as the control or higher (30 to 40%) while between 2.5 to 5 g/L, lag phase extended up to 96 hours but the final *OD* was close to the control. Between 5 to 7.5 g/L, lag phase was extended and final *OD* was less than the control. At higher concentrations, the growth was completely inhibited and the pH of the medium also increased. Out of the three hydrophilic ionic liquids tested, [EMIm][Ac] performed better than [EMIm][DEP] and [MMIm][DMP] at 96 hours of incubation. At 1.5 g/L, glucose utilization with [EMIm][Ac] and control was 41 mM and 30.6 mM respectively. Corresponding 1-butanol and total solute concentration was 8 g/L and 8.8 g/L compared to 1.7 g/L and 2.9 g/L with the control. This was attributed to hermetic effect which stimulated the fermentation by modulating culture medium pH.

Wang *et al.,*[122] studied the effects of hydrophilic 1-methoxyethyl-3-methylimizadolium cations based ionic liquids on the growth of anaerobic bacterium, *Clostridium sp.* during the fermentation of glucose. The growth was followed by adding ionic liquids in the range of 0 – 1% (v/v) to the culture medium and following the OD_{600nm} over 50 h duration. The trend in growth inhibition by various anions as deduced from the IC_{50} values (from *OD* vs. time plot) is: $[Tf_2N]^- \geq [PF_6]^- > [BF_4]^- > [CF_3COO]^- > [OMS]^-$, with $[Tf_2N]^-$ affecting the growth most. Presence of fluorine in the anion made the ionic liquid more toxic; higher fluorine numbers resulting in more toxic ionic liquids. Further, presence of oxygen in the cation reduced the toxicity of $[MOEMIm][BF_4]$ compared to $[BMIm][BF_4]$. Similar trend was observed with the production of CO_2 and H_2 gases during the fermentation.

Cascon *et al.,*[123] measured the extractability of 1-butanol from aqueous phase and fermentation broths using ionic liquids as extractants. *K*-values for $[P_{6,6,6,14}][Tf_2N]$, $[TOMAm][Tf_2N]$, $[P_{6,6,6,14}][DCN]$ and [THAm][DHSS] were 1.1, 1.4, 8 and 7.5 respectively. Estimation of K-values using group contribution model coupled with linear energy relationship (GC-LSER) was not good. *K*-values using mixed extractants varied between pure extractants K-values. All the ionic liquids extracted 1-butanol from the fermentation broth better than acetone; acetone was better than ethanol due to the solute's decreasing hydrophobicity. $[P_{6,6,6,14}][DCN]$ and [THAm][DHSS] exhibited high partitioning for butyric acid at low pH (3-5). $[TOMAm][Tf_2N]$ and [THAm][DHSS] were toxic to the cells. $[P_{6,6,6,14}][Tf_2N]$ affected the glucose uptake at 1% (by vol) for both *Clostridium acetobutylicum* (ATCC 824) and *Clostridium beijerinckii* (ATCC 51743) while Oleyl alcohol showed total biocompatibility up to 5% (by vol).

1.3.2. Toxicity of Ionic liquids

Many studies on the toxicology of ionic liquids have emerged over the past decade. Most have focused on human cells [124,125], animal cells [126,127], as well as plants and aquatic organisms in the environment (including fish, daphnia, algae, etc.).[128,129] However, very few studies exist for the hydrophobic ionic liquids that would be involved with *in situ* extraction for common fermentation organisms. Solvent biocompatibility is one of the basic prerequisites for successful biphasic biocatalysis, though other requirements for solvents vary from process to process.

Matsumoto *et al.,*[130] studied toxicity on 9 lactic acid-producing bacteria of imidazolium based ionic liquids and organic solvents for *in situ* acid extraction. Toxicity of biphasic mediums of 5% by volume of ionic liquids and 1% by volume of organic solvents were compared by measuring the concentration of lactic acid produced and viable cell count after growing the cells for 48 hours. The ionic liquids ([BMIm][PF_6], [HMIm][PF_6], [OMIm][PF_6]) and 14 different organic solvents were tested for their toxicity. Lactic acid production was found in various degrees by all 9 bacteria in presence of three ionic liquids. Relative activity is defined as the ratio of lactic acid produced in presence to that of the aqueous medium. The relative activity was maximum with *Lactobacillus delbruekii* in presence of [HMIm][PF_6] at > 0.94 and the effect of imidazolium cation carbon chain length on the activity was not very pronounced for this particular bacterium. However, the relative activity in presence of [R-MIm][PF_6], where R is n-butyl, n-hexyl- or n-octyl for the other bacteria varied between 0.2-0.95 and 0.04-0.8.

Baumann *et al.,*[131] explored the possibility of ionic liquids as replacement to organic solvents for xenobiotic degradation in a two-phase partitioning bioreactor (TPPB). TPPB is useful in the destruction of biologically recalcitrant organic pollutants in large volume bioreactors and involves substrates that are water insoluble and cytotoxic. Phenol degradation by three

commonly used bacteria – *Achromobacter xylosoxidans* Y234*, Pseudomonas putida* ATCC 1172*, Sphingomonas aromaticivorans* B0695 was studied as a model system with phosphonium based ionic liquids in 6% by volume systems. Cell viability and metabolism was investigated by measurement of glucose consumption as other common methods like optical density or cell dry weight measurement were problematic. $[P_{6,6,6,14}][Tf_2N]$ was found to be biocompatible with all 3 bacteria, while ionic liquids $[P_{6,6,6,14}][C_{10}H_{19}O_2]$ and $[P_{6,6,6,14}][C_2N_3]$ were biocompatible with only *A. xylosoxidans* and *P. putida*. With $[P_{6,6,6,14}][Cl]$, $[P_{2,4,4,4}][C_4H_{11}O_4P]$, and $[P_{1,4,4,4}][TOS]$, no cell growth was observed with any of the bacteria. This group determined a critical octanol-water partition coefficient value ($log\ P_{crit}$,) to indicate the sensitivity of the cell to solvents; solvents with $log\ P > log\ P_{crit}$ are considered more biocompatible. For example, $log\ P_{crit}$ for *A. xylosoxidans* is 3.1 compared to 4 for *S. aromaticivorans* and indicates that *A. xylosoxidans* is biocompatible with more hydrophilic ionic liquids compared to *S. aromaticivorans.* However, the values of *log P* for ionic liquids have only been measured for several systems.

Ganske *et al.,*[132] investigated the growth of two bacteria *Escherichia coli*, and *Bacillus cereus,* and the yeast *Pichia pastoris,* in ionic liquid/buffer medium. Growth results with $[BMIm][BF_4]$ and $[BMIm][PF_6]$ were compared to those obtained with common organic solvents like methanol, ethanol, and dimethyl sulfoxide. With 0.1% by volume of water-soluble $[BMIm][BF_4]$ in the aqueous medium, there was no growth inhibition, while at concentrations higher than 4%, no growth was observed in either of the species. With *E. coli,* further experimentation conducted at concentrations between 0.1 - 2.5%, shows that growth inhibition occurs between 0.7 - 1%. With a biphasic system with $[BMIm][PF_6]$, complete growth of *P. pastoris* was observed, while the growth inhibition of *B. cereus* was observed under similar

conditions. The microorganisms were found to be more tolerant to organic solvents than the [BMIm][BF_4] and [BMIm][PF_6].

Lee *et al.,*[133] examined the toxicity of 13 room temperature ionic liquids to *Escherichia coli* and compared the toxicity to 8 common organic solvents. Toxicity was measured both on solid agar plates and in suspension media from the early stationary phase of the *E. coli* between concentration ranges of 20 – 50,000 mg/L. Viability and optical density were used as basis to understand toxicity. The EC_{50} values (in mg/L) are defined as the effective concentration of the solvent that inhibits growth of the microorganism by 50%. Hydrophilic ionic liquids like [EMIm][BF_4] showed higher toxicity (lower EC_{50} values) compared to hydrophobic ionic liquids such as [BMIm][PF_6] in solid culture. The trend was opposite in suspension media. This was attributed to differences in diffusivities of the ionic liquid in solid and suspension culture. In solid culture, low diffusivity of hydrophobic ionic liquids results in reduced contact between hydrophobic ionic liquid and the microorganisms. In suspension, the hydrophobic or hydrophilic ionic liquids are mixed well with the culture medium leading to uniform distribution of phases.

Larger alkyl chain length increases the cation hydrophobicity and this lead to increased toxicity. For example, the EC_{50} value for [EMIm][BF_4] was 35,000 mg/L compared to the EC_{50} values for [BMIm][BF_4] at 9000 mg/L. With [BMIm] as the cation, the EC_{50} value for [BF_4] to [PF_6] (hydrophobic) are 9000 mg/L to 4000 mg/L, respectively. This was found to further reduce to 150 mg/L when the anion was [Tf_2N] (very hydrophobic ionic liquids). The *log P* of the ionic liquids studied were compared, and no direct relation to EC_{50} was established. Organic solvents like acetonitrile, ethanol and acetone were found to be less toxic than most of the ionic liquids, while dimethyl sulfoxide was less toxic than all of the ionic liquids tested. But solvents like chloroform, chlorohexane, 1-chlorophenol were more toxic than most of the ionic liquids.

Docherty *et al.,*[134] analyzed the toxicity and antimicrobial properties of imidazolium and pyridinium based ionic liquids to different bacteria and yeast by varying the anions and cations' chain length. Detailed antimicrobial tests of the above ionic liquids were performed with gram negative rods *Escherichia coli*, and *Pseudomonas fluorescens*, a gram positive rod *Bacillus subtilis*, gram positive cocci *Staphylococcus aureus,* and the yeast *Saccharomyces cerevisiae*. Colony forming units (CFU) per ml in presence of 1000 ppm of ionic liquids were measured over a period of 8 hours. Increase in the carbon chain length increased the toxicity. Similar growth inhibition was observed with [OMIm][Br] and [OMPy][Br], while the ionic liquids [BMIm][Br] and [BMPy][Br] did not show any inhibitory effects. The effects of [OMIm][Br] and [OMPy][Br] varied from microorganism to microorganism, as the [OMIm][Br] for instance inhibited growth of gram positive *B. subtilis* completely after 4 hours, while it did not affect growth of another gram positive bacteria *S. aureus*. As found in earlier studies[37], *S. cerevisiae* was least affected by the presence of ionic liquid. The behavior of [BMIm][Br] was the most inconsistent as it was found to have acute and chronic effect to higher organisms like *Daphnia magna* and similar activity to carcinogenic pesticide (1,1'-dimethyl-4,4'-bipyridinium chloride) suggesting that the mechanism might be different in different organisms.

Yang *et al.,*[135] investigated the tolerance of yeast cells immobilized in calcium alginate beads to the general ionic liquids [R-MIm][PF_6]. The relative activity retention was at 70% [BMIm][PF_6] and this retention decreased with increase in carbon chain length on the ionic liquid. The activity retention in corresponding bromides like [BMIm][Br] was around 22%. The decrease in the activity was primarily related to dehydration of the yeast cells in presence of water miscible bromides. Comparing the activity retention of immobilized and free cells, the retention was remarkably higher in immobilized cells due to protection of immobilized cells

from the hydrophobic ionic liquids by hydrophilic calcium alginate beads. Effect of moisture content in ionic liquid was investigated as it plays an important role in non-aqueous biocatalysis. Activity retention was higher in water saturated ionic liquid at 70% compared to anhydrous ionic liquid where the activity was 50%.

Rebros *et al.,*[136] reported the use of simple and rapid Agar diffusion test as a reliable first stage screen to identify toxicity of ionic liquids to *Clostridium butyricum* (DSM 10703). Here, filter disc soaked in ionic liquid was placed in lawn of cells on an Agar plate and the size/diameter of inhibition zone of no growth around the disc indicated the ionic liquid toxicity. Inhibition zone size correlated well with EC_{50} values (between 0.034 M and 0.25 M) obtained from growth rates experiments. Alkylmethlyimidazolium halides were toxic to the bacteria above 0.5 g/L. The toxicity increased with increase in chain length of the alkyl group while iodide seemed more toxic than bromide anion. $[N_{2,4}(C_2OH)_2][C_2OSO_3]$ and $[N_{24}(C_2OH)_2][DCN]$ were biocompatible with cells up to 20 g/L and 10 g/L; while imidazolium and pyrrolidinium cations with these anions were toxic below 5 g/L.

Coleman *et al*.,[137] synthesized novel chiral imidazolium ionic liquids containing amino acid ester and dipeptidyl functional groups. Many of these ionic liquids exhibited low antibacterial activities with minimum inhibitory concentrations > 2 mM. Alkyltrihexyl phosphonium ionic liquids [138] are reported to have different effects on microbial activity compared to the imidazolium class. Increased microbial activity was reported when the halide anion is replaced with more hydrophobic ones like $[BF_4]$ and $[Tf_2N]$. Microbial activity was higher in longer alkyl chains like $C_{14}H_{29}$ and $C_{16}H_{31}$ and concentrations of $[P_{6,6,6,14}][Tf_2N]$ >1 mM caused cell death. Among the long alkyl chain quaternary ammonium salts[139], only $[DDA][Tf_2N]$ ionic liquids did not show antimicrobial activity against any of the microorganism, while the rest of the ionic

liquids showed high antimicrobial activity. Above concentrations of 1 mg/ml, cell death was observed with [DDA][Tf_2N].

Cornmell *et al.,*[113] investigated the possibility of intracellular uptake of ionic liquids in *Escherichia coli* by applying Fourier transform infrared spectroscopy (FT-IR) technique. Ionic liquids were found to give a distinct IR spectrum, without the necessity to label them, compared to the cell components. Hence the technique can be used for high throughput screening of ionic liquids. The intracellular chemical composition after exposure to 23% phase ratio of ionic liquids supposedly biocompatible ionic liquids, [TOMAm][Tf_2N], and [$P_{6,6,6,14}$][Tf_2N], and to toxic ionic liquids [TOMAm][Cl], and [$P_{6,6,6,14}$][Cl]. However, [TOMAm][Cl] was found to be toxic to the bacteria, while [$P_{6,6,6,14}$][Cl] initially retarded the cell growth, but began to recover after 3 hours. The cells were lysed and fractionated into cytoplasmic and membrane fractions. By applying Fourier transform infrared spectroscopy (FT-IR) technique, they were able to identify the ionic liquids primarily in the lipid membranes and possibly caused membrane disruption. The more toxic ionic liquids were found to accumulate faster compared to "biocompatible" ones.

Evans[140] evaluated the direct effect of ionic liquids on *1,2-dielaidoylphosphatidylcholine* bilayers supported on a silica surface. Interactions of cation [$OMIm^+$], present as [OMIm][Cl] and the anion [Tf_2N], present as [$LiTf_2N$], on the bilayers were studied using Quartz crystal microbalance with dissipation and atomic force microscopy. These ions were found to cause membrane defects. The [OMIm] cation was shown to dissolve in the supported bilayers. [Tf_2N] anions were hypothesized to disrupt the bilayer by removing the lipids and forming nanoscale holes with the remaining bilayer unaffected. [BMPy][Tf_2N] was concluded to form an adsorbed film over the supported bilayers without disturbing the bilayer.

1.3.3. Summary

It is unfortunate that most early studies were conducted with imidazolium ionic liquids with the [PF_6] and [BF_4] anions as these have subsequently been shown to degrade over time especially in the presence of water, and the degradation products have a high probability of affecting the biocatalysis. This might explain the different results for similar reactions using similar organisms. Thus, more systematic toxicology and biocatalysis studies are needed avoiding these anions. Yeasts seem to be more tolerant than bacteria to at least imidazolium ionic liquids. An increase in the chain length of the imidazolium cations appears to increase its toxicity to most organisms while the trend can be quite different with quaternary ammonium or phosphonium. Growth inhibition of gram negative and gram positive bacteria by imidazolium ionic liquids seems to be similar. Several reports indicate that the same ionic liquids have often mixed effects even depending on the strain, e.g. *E. coli*. Immiscible solvents are often used in biocatalysis to circumvent issues of low substrate aqueous solubility or substrate/product inhibition. Ionic liquids with their molecular flexibility appear to be a perfect platform for optimizing these solubilities needed for any biocatalytic reaction. However, the sheer number of potential ionic liquids also may make correlation of trends in biocompatibility and biocatalysis to structure difficult without very good experimental data.

1.4. Electric fields

1.4.1. Product separation techniques

There are various unit operations for separating a component from a phase. These unit operations are based either on heat or mass transfer. These include:

- Distillation
- Absorption (e.g., stripping)
- Adsorption (e.g., membrane extraction, chromatography)
- Liquid-liquid ("solvent") extraction

1.4.1.1. Liquid-liquid extraction for bioseparations

Liquid-liquid extraction is an important unit operation and is employed for many separation process techniques in hydrometallurgical, nuclear, pharmaceutical, oil industry, and precious metals industry.[141] For bioseparations, liquid-liquid extraction is one of the most important techniques.[142] Other techniques for bioseparation are discussed in Section 1.2. Microbiological separations or whole broth extraction are limited inherently by slow mass transfer rates involved due to accumulation of cell debris at the liquid interface.[143,144] Liquid-liquid extraction is a simple process for extraction of bio-products from cells or debris that reduces process volume, results in higher purity, process simplification and facilitates further product recovery via absorption or crystallization. Also, this operation is conducted at close to ambient temperature and at ambient pressures. Hence, it has the potential to reduce production costs.[142] Loss of activity (e.g., denaturation) associated with solid membrane barriers or adsorptive phase and bio-product dilution elution or heat intensive processes like distillation can be avoided using liquid extraction. Further, *in situ* biphasic extraction can extract unstable intermediate products formed in a sequential reaction schemes.

1.4.1.1.1. Mixing

Contacting is commonly achieved by mixing the phases to enhance the mass transfer coefficient and the interfacial area. When mixing two immiscible systems, vigorous agitation causes dispersion of one phase into another leading to the formation of small droplets. Due to the mechanical energy required, energy input is significant. Further, phase separation through settling can become time consuming when a diffused layer of small drops at the interface become semi-stable. Mixing even miscible systems where the liquid viscosities are quite different, can pose problems. The energy input increases with the viscosity of the systems involved.[145] With high viscosity systems, the mixing is slow both at microscopic and macroscopic levels due to low diffusivities and poor bulk flow respectively. The flow involving non-Newtonian fluids is mostly laminar. In mixing of non-Newtonian fluids, the momentum is not transferred to the bulk fluid from an impeller even if high speed mixing is used; specially designed impellers are required in narrow diameters columns to achieve momentum transfer. In general viscous drops are known to form larger drops.[146]

1.4.1.1.2. Rheology

A fluid's rheology gives information on its deformation and subsequent flow when subject to an external force and how liquids respond to applied force by flowing. Liquid flow is characterized by viscosity which is a measure of its resistance to applied shearing force. The flow can be classified into two types[147]:

1. Newtonian liquids: In Newtonian flow, the fluid flow is directly proportional to the force applied

Figure 1.5: Shear stress vs. Shear rate responses for Newtonian and Non-Newtonian liquids

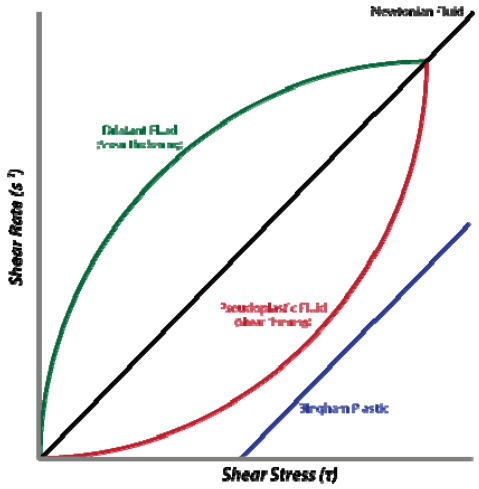

or the resulting flow or shear rate is linear with the strain applied and the viscosity is constant (Figure 1.5). Water is a common Newtonian liquid with low viscosity while glycerol is a high viscosity Newtonian liquid.

2. Non-Newtonian liquids: Complex fluids have non-linear response to applied stress and are referred to as non-Newtonian fluids (Figure 1.5). Common examples are polymer solutions, biological solutions, emulsions, soaps, etc. The viscosity of non-Newtonian solutions is not constant and is a function of shear rate. Pseudoplastic and dilatant fluids are types of non-Newtonian fluids where the viscosity decreases and increases with shear rate respectively. Viscosity of these liquids is reported as apparent viscosity. Other types include: Plastic systems - have a yield point stress, beyond which flow occurs; Viscoelastic fluids - exhibit both non-Newtonian flow and elastic behavior too.

1.4.1.2. Solvent extraction equipment

Solvent extraction can be achieved using various types of equipment. The extraction rate depends upon the mass transfer coefficient, interfacial area and concentration gradient. Efficient contacting between the phases and subsequent phase disengagement for separation purposes is important in liquid-liquid extraction. In whole broth extraction, product recovery is affected by the physical nature of the broths which may exhibit non-Newtonian behavior. Also, presence of broth impurities and biomass solids can significantly affect the partitioning.[148,149] Impurities can be side products from biotransformation, residual components added in the pre-fermentation steps like broth preparation. Some other components added during fermentation include chemical surfactants as anti-foaming agents like de-emulsifiers, lipids, fatty acids, and electrolytes. Further, phase disengagement could become difficult as result of reduction in interfacial tension due to cell debris. Pretreatment of the whole broth significantly increases the

capital cost and maintenance of the filter media.[144] The design of liquid-liquid contacting equipment requires knowledge of drop size and distribution in order to formulate mass transfer and/or reaction rate equations. Drop size is required for calculating interfacial areas, droplet holdup volume and hence the flow rates. Common equipment includes[142]: mixer-settlers, spray columns, gravity settlers, mechanically agitated columns, centrifugal extractors, packed columns and plate columns. Efficiency of contacting can be increased by mechanical or thermal energy, though both are energy intensive.[142] The broth impurities can negatively impact process advantages of direct extraction like the number of stages required as they may slow mass transfer rate and affect the thermodynamics of the solute partitioning.

Spray columns are among the simplest and one of the oldest examples of devices used in solvent extraction processes. The spray column does not require mechanical agitation. Here, a nozzle is used to disperse one phase (referred to as "the dispersed phase") into a second phase ("the continuous phase"). Droplet size and terminal velocity are the key droplet characteristics influencing mass transfer and ultimately the product yield and extraction rate. However, it is difficult to obtain both high mass transfer and low processing times using traditional spray columns: high throughputs due to lack of column internals result in low mass transfer; slower throughputs result in higher processing times. These limitations lead to higher operating and equipment costs. Other problems encountered in spraying include axial dispersion or back mixing in the continuous phase which limits spraying to applications where only one or two continuous stages are required. Additionally spraying is ineffective in viscous systems and in the presence of impurities.[142]

1.4.1.3. Intensification of liquid-liquid contacting

High mass transfer drives product yield and extraction rates. Intensifying liquid-liquid contacting in liquid-liquid extraction is the key to improving mass transfer. Additionally, study of intensification of contacting is also relevant for chemical reactions involving mass transfer between two liquid phases. LLE contacting process can be enhanced if the high interfacial area and shear stress are created by effective mixing. Also, after the LLE operation, effective separation of the phases is also important. Application of electrical energy has been reported to intensify the contacting and also consume small amount of energy compared with other mixing techniques.[141,150,151,152,153]

1.4.2. Background

Interaction of fluids with electric fields is a sub-branch of fluid mechanics termed as electrohydrodynamics. Taylor[154] extended understanding of impact of electric fields on forming droplets suspended in air to drop formation in a non-conducting liquid medium. The drop elongated, assuming a prolate spheroid shape and beyond a critical value of electric field strength became unstable with axial jets reported. Electric fields have primarily been used for breaking aqueous-oil emulsions until 1960's. From early 1960's, their application to extraction process was explored and the focus was on the droplet formation through charged nozzles. Application of electric fields to the spray column has been demonstrated to reduce droplet sizes, increase droplet velocities and to produce fine sprays in some cases. Important quantities for understanding the phenomenon are volumetric charge density, electric field induced forces at the interfaces, charge effects at the interface and discontinuity. The key phenomena associated with the application of electric field are:

- Smaller droplets forming at the nozzle due to decrease in the net interfacial tension at the nozzle. For same volume, the charged droplets generate higher interfacial area than uncharged droplets
- Acceleration of droplets occur after detachment due to the electric field acting on the charged droplet, and the droplet reaches a terminal velocity
- Accelerated droplets increase the interfacial shear stress and the slip velocity, thereby improving the continuous phase mass transfer coefficient
- Oscillations and internal circulation are created in the droplet as the droplet size decreases (onset of oscillation can be predicted from the Weber number and this number must be > 3.3)
- Marangoni flows can develop additionally because of the non-uniform charge distribution on the droplet.

1.4.2.1. Types of electric fields

Three types of electric fields AC, DC and pulsed DC have been used. All are found to promote droplet deformation that alters velocity profile within and around the droplet.[155] DC electric fields are found to disintegrate droplets and also under certain conditions promote droplet coalescence.[156,157] Primarily AC and pulse DC electric fields are used for efficient phase separation as they are shown to promote coalescence and used in de-emulsification.[151,158] In comparing AC and DC fields, higher applied voltages are required when using AC fields to achieve similar levels of drop disintegration. In the case of pulsed DC, applied frequency and amplitude of the electric field can also be varied. Also, using AC electric fields at frequencies of 45 kHz, dispersions of non-conducting oil in water with reduced droplet size, less deformation and low currents have been reported.[159]

Further, applied voltage can be divided into three levels: extra low-voltages are less than 120 V; low voltages are between 120-1500 V and high voltages are greater than 1500 V. Generally, the extra-low to low voltages are applied in applications involving dielectrophoresis, microfluidics, biomaterials synthesis, or DNA restructuring. For achieving either phase separation or drop coalescence enhancing liquid-liquid contacting, high voltages are generally employed.

1.4.2.2. Applications

The advantages of electrostatic dispersion include significant reduction in the drop size, enhancement of mass transfer, and enhanced rates of phase separation. The reduction in drop size can be very large and is one of the principal factors in the intensification of liquid-liquid contacting and hence mass transfer.[160] Using electric fields, short residence times and high extraction efficiencies are possible at relatively low cost. Electric fields have been used to control and enhance formation of liquid dispersions in liquid-liquid contacting and promote coalescence. There is also evidence that electrically enhanced contacting may offer significant advantages in the presence of impurities such as surface-active agents, non-Newtonian rheology, and in the presence of biopolymers.[161] For example viscous biologically active media can be dispersed electrostatically with relative ease and in a manner which gives rise to an unstable dispersion, which is readily coalesced. Earlier studies[162,163,164] have accurately predicted charged droplet motion in Newtonian systems as a function of charge, external geometry and physical properties using novel finite element techniques.[165,166] Electric fields have been used to create emulsions of water in oil and it was shown that less than 1% of energy was used compared to corresponding mechanical agitators to achieve same droplet sizes.[155,167] Electric fields have been used with gas/liquid systems such as paint spraying, crop spraying and surface coating

processes.[141] These applications are referred to as electrohydrodynamic spraying.[168] Further they have been employed in heat transfer where the controlling nucleation rates in boiling heat transfer have resulted in higher heat transfer coefficients. Electric fields have been used in solvent extraction of metals in mineral industry extensively and various scaled processes have been reported in literature.[160,169,170] Further, dry electrostatics has been used in separation of powder mixtures[171,172] and production of ceramic materials in an electric dispersion reactor.[173] With liquid-liquid systems, electric fields have also been used in enhancement of interfacial polymerization reactions[174] and kinetic acceleration of biotransformations in two phase systems. In an entirely different kind of application, pulsed electric fields (PEF)[175] with voltages in range of 40 – 90 kV have been applied at different pulses for microseconds (around 1 – 50 ms) to food products (for example apple and tomato juices) to inactivate/kill the various microorganisms like bacteria, fungi via electroporation. This process is used at commercial scales to sterilize around 6000 L of food products.[176]

1.4.3. Electrostatic spraying

1.4.3.1. Theory

An electric field may be created across a liquid continuous phase along the length of the spray column by inserting two electrodes at the top and bottom of the column. Different electrode geometries have been used in the literature: parallel plates and cylindrical rods.[177] In either case, one electrode, generally the bottom one, is connected to a high tension electrical source, while the other electrode is grounded. Here, the grounded electrode is used as the spray nozzle. Application of electric field results in charge accumulation on the droplet as it is formed at the nozzle because of the contact. As the droplet grows in size at the nozzle tip, charge density on the droplet increases. At one point when excess charge accumulates on the surface of the

droplet, instability is created to negate this excess charge accumulation. Scott *et al.,*[155] found that charges that are initially in the interior of most liquids will in general move quickly through the liquid and seek out the area where there is a discontinuity of electric conductivity and permittivity i.e. at the liquid-liquid interface. The instability results in disintegration of the droplet at the nozzle into smaller drops. The total surface area of the daughter droplets is higher than that of the parent droplet.

Daughter droplets have residual charge as they fall into the continuous phase. Charge acquired by the droplet affects the droplet dynamics. Because of the charge acquired while falling under the influence of the external field, the droplet experiences acceleration and thus increase in velocity. Interfacial forces acting on the droplet decrease with the result that droplets formed exhibit faster movement. Because of the higher droplet velocities and lower interfacial tensions, high degree of internal circulation and shape oscillations are achieved.[150,178,179] This increase in interfacial area or specific area along with increase in droplet dynamics from internal circulation are major reasons for the observed enhancement in mass transfer.[161,180] In mechanically agitated systems, where the dispersed phase breaks into droplets, these advantages are not observed due to the intrinsically static nature of the droplets. Further other destabilizing phenomena like creation of interfacial Marangoni instabilities are a beneficial effect of charged droplets. These are created across the drop surface due to differential interfacial tension changes from concentration gradients, variations in charge density for charged droplets and differences in local field strength at different points on the droplet. Much of the observed increase in mass transfer is from the increase in interfacial area, droplet stability is very important. In many cases, very small drops tend to show rigid sphere behavior where internal mass transfer is dominated by molecular diffusion, the presence of electrical charge on the droplet makes this less so.

In electrically enhanced contactors, there are two stages: droplet formation and the motion of falling droplet after detachment. Each of these stages is driven by the force balance. Formation of the droplet from a nozzle in the absence of electric fields is influenced by three forces on the droplet:

1. Gravitational force resulting from the density difference between the dispersed phase and continuous phase. This helps in detachment of the droplet.
2. Kinetic force experienced by the droplet due to its own velocity resulting from the dispersed phase flow in to the nozzle. This helps in droplet detachment.
3. Interfacial force resulting from interactions between the molecules at the interface of both the phases.

When the electric field is applied, additional electrical force in the downward direction acts on the droplet due to its charge acquisition. Further, additional repulsive electric force develops between the droplet, as it is formed, and the nozzle. In contrast, this force would be minor due to the geometry of the nozzle compared to parallel plates that were used earlier.

In the presence of electric fields, droplet formation can occur in two regimes depending upon the magnitude of the applied voltage:

1. At low applied voltages and dispersed phase flow rates, pendant drops form and these pendant droplets detach sequentially and the droplet volume is governed by the force balance (Figure 1.7 A & B). In the discrete droplet regime there is a net positive interfacial tension, i.e., interfacial tension is stronger than the applied electric field. Also, drop size at detachment is reduced by its acceleration due to charge on the droplet.
2. At higher applied voltages, droplets are formed from the pendant droplet itself. As the E increases, the charge accumulated increases, leading to a non-uniform charge distribution

on the pendant drop, the maximum of this charge is centered near the point of maximum curvature, i.e., on the tip of the pendant drop. The tip of the pendant drop attached to the nozzle elongates into long filament and a steady stream of daughter droplets are ejected from the tip of this elongated pendant drop as spray (Figure 1.7 C & D). This creates non-uniform distribution of the surface forces, which are minimum at the tip.[150] This regime is referred to as the electrostatic dispersion regime; the force created by electric field at the tip is much higher compared to the interfacial tension leads to droplet instability and forms the spray. Electrospraying can result in formation of clouds of droplets (Figure 1.6)

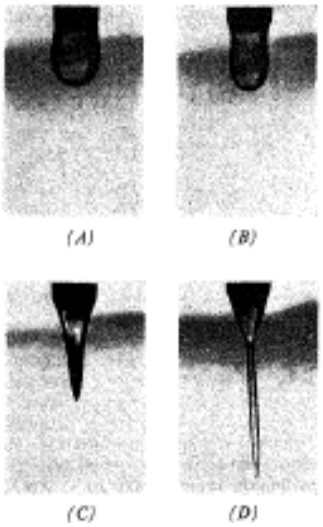

Figure 1.7: Droplet formation under electric fields discrete and spray regime.[1]

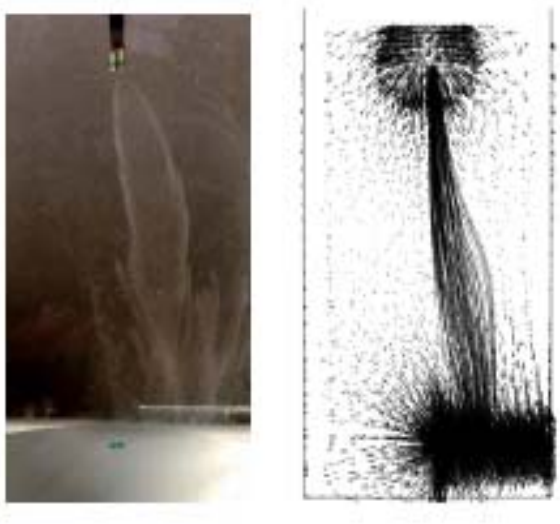

Figure 1.6: Electrostatic Spray of oil-water system in a liquid-liquid contactor.[4]

1.4.3.2. Selection of continuous phase and dispersed phase

The key physical properties of both the phases that affect the onset of electrostatic regime are electrical conductivity, viscosity, permittivity of the continuous phase and the interfacial tension between the phases.

For the choice of solvent in solvent extraction, extractability and selectivity are the important factors apart from others discussed in the previous sections. Incorporating high electric fields imposes additional requirements on the type of solvents that can be used in a contactor. To maintain this high electric field potential applied across the solvent/continuous phase, the continuous phase should have low conductivity. This to ensure that there is no electrical discharge and minimal current flow between the electrodes. Further, the magnitude of the field affects the drop break-up at the nozzle, charged droplet retention of its surface charge during its fall and hence its acceleration.[141,181] Solvents with electrical conductivities lower than 10^{-9} S/m and dielectric constant lesser than four are frequently used as continuous phases.[150] It has been reported that there could be slight increase in conductivity of continuous phase due to dispersed phase holdup and due to transfer of dispersed phase contents especially with whole broth components.[181] This restricts novel solvents such as ionic liquids from being used as the continuous phase in the contactor.[182] In an electrically enhanced contactor, the current flow is in milliamperes but there is a possibility of fire due to static discharge if the flammability of the solvent is high. This is an aspect to keep in mind when looking for solvents.

Some of the solvents that have been frequently used as continuous phase under applied electric fields are: N-decanol, Sunflower oil, Silicone oil, Heavy oil/gas lube oil, Vegetable oil, Mineral oil, D2EHPA or hydroxyoximes in Kerosene diluent, C_5-C_{10} hydrocarbons, Toluene, Carbon tetrachloride, Chloroform, TBP, Amine extractants and Heavy gas oil, Amine extractants.

Electric enhancement is also governed by the properties of the dispersed phase especially electrical conductivity as the droplet has to acquire and retain charge at the nozzle. The

conductivities of dispersed phase must be higher than 10^{-9} S/m and dielectric constant higher than 10.[150]

1.4.3.3. Space charge migration

Stewart *et al.,*[150,183] reported non-linearity in the electric fields at the electrodes primarily due to the ionic impurities in the continuous phase that have electrical conductivity. Application of electric field leads to concentration of these charge carriers at either of the electrodes. These impurities are called space charges and they are generally polar molecules and dissolved gases which are unavoidable in the dielectric liquids. Accumulation of a –ve/+ve space charge at one electrode leads to higher –ve/+ve charge at that electrode and hence higher electric field strength near this electrode. In the same manner, accumulation will occur at the other electrode as the external electric field is constant. This leads to non-linearity near the vicinity of the electrodes though the electric field strength in the bulk continuous phase would be linear. Because of the space charge effects, the applied E (voltage/distance) is not actual the electric field as it assumes that the space charge effect is negligible. The space charge migration under electric fields has been shown to decrease with decrease in conductivity of the continuous phase and the conductivity increases when the electric field is removed indicating mixing of space charges from natural convection.[181]

Carleson[184] developed a model for relating the field strength at the nozzle and in the bulk liquid at high applied voltages as shown below. The equation was developed for parallel plate electrodes and the droplets are dispersed by inserting a nozzle in the top plate/electrode. Uniform charge distribution on the plates is assumed.

$$\frac{E_o}{E_n} = \frac{1}{2}\left(\frac{R}{L} + 1 - \sqrt{\frac{R^2}{L^2}+1}\right)^{-1}\left(2 - \left(\frac{R^2}{L^2}+1\right)^{-0.5}\right)$$

where

R – Plate/electrode dimension

L – Interelectrode distance

E_o – Electric field strength at the nozzle

E_n – Applied Electric field strength

For R/L = 0.75, electric field strength at the nozzle was 20% higher than the applied field, which shows the non-linearity in the field.

With silicone oils as continuous phase, a time dependence of the droplet volume because of space charge effect was reported.[185] Also, change in drop volume with time at an applied voltage was observed which stabilized after 20-25 minutes irrespective of applied E. For low viscosity cyclohexane continuous phase no space charge effect was reported. But the reason seems to be incorrect because the space charge effect is not disturbed by the fall of the drop. The accumulation occurs at the electrode because of the attraction of space charge to respective electrodes.

Petera *et al.,*[2] developed finite element analysis for incorporating the effect of space charge to obtain the actual electric field equation while modeling droplet trajectories in the presence of electric fields. This has been incorporated for predicting droplet trajectories of both discrete drops[162] and for cloud of droplets[4], coalescence and the mixing achieved in presence of electric fields. The inhomogeneity of the field was accounted for by including a pure transport equation for charge concentration along with the force balance equations.

$$\frac{\partial \sigma}{\partial t} + u \cdot \nabla \sigma = 0$$

Where t is the time, u is a velocity field of the continuous field σ, determined by the particles mobility α and the local electric field strength E, $u = \alpha E$

The amount of microscopic electricity carriers is difficult to gauge, so an iterative trial and error procedure was adopted by the authors. Space charge accumulation around the electrodes from the finite element modeling is shown in

Figure 1.8.

Figure 1.8: Final space charge distribution after finite element modeling[2]

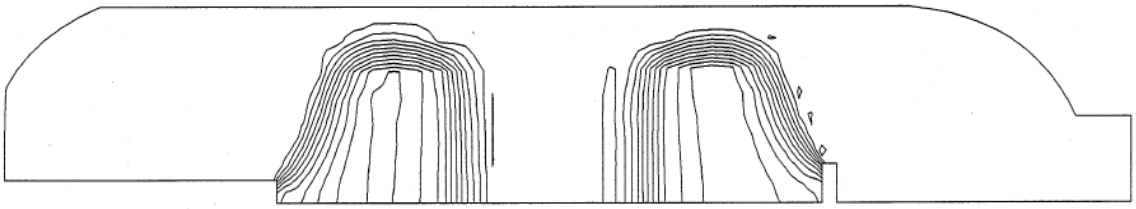

1.4.4. Effect of electric field on key properties

1.4.4.1. Drop charge

The drop acquires charge from conducting nozzle until both attain the same charge. The charge on the droplet can be dependent on the formation time. Charge acquisition and subsequent charge retention during drop fall is a function of relaxation time of dispersed phase and continuous phase respectively. Rate of droplet charge loss is a function of relaxation times and is written as:

$$Q = Q_o \exp\left(-{}^{t}/_{\tau}\right) \quad where, relaxation\ time\ constant\ (\tau)\ is\ \frac{\varepsilon\,\epsilon_o}{K}$$

For complete and quick charge acquisition, dispersed phase relaxation time should be lower than its formation time. For example, the relaxation time constant of charged droplet formed from distilled water is around 1 microsecond.[155] While for the continuous phase, the relaxation time should be very high so that the droplet as it falls through the continuous phase does not lose it charge to experience electrical force. Efficient charge acquisition is function of dispersed

phase throughput at the nozzle. Higher throughput requires higher voltages to achieve electrostatic dispersions.[141] The charge acquired by the droplet at the nozzle depends upon the applied electric field and permittivity of the continuous phase.

Different equations have been proposed for the identifying the electrical force acting on the droplet during its formation and fall. Electrical force is a complex function of drop charge, drop shape and electric field strength near the nozzle which is dependent on nozzle/electrode geometry. For theoretical calculations of droplet charge, diameter and terminal velocities using force balances, electric field is assumed uniform along length of the. To incorporate non-uniformity near the electrodes, empirical relations have been developed which are proportional to square of electric field strength and include constant to account for nozzle geometry. Various forms of drop diameter are included in this expression.[152] Further, electric field distribution has been theoretically established by the introduction of finite element modeling by Petera *et al.,*[2,162] which included the effect of space charge on the distribution.

Yang *et al.,*[178] defined charge density as the charge acquired per surface area of the drop based on its diameter and measured it as a function of applied E for the systems of heptane-water, pentane-water. Charge density acquired by the water droplet dispersed in heptane and pentane at flow rate of 8 µl/sec was similar around $13e^{-10}$ (coulombs/cm^2) at applied electric field strength of 4 kV/cm. There was no effect of nozzle diameter on the charge density but the droplet acquired charge density of $13e^{-10}$ at 3 kV/cm when the flow rate was reduced from 8 to 5 µl/sec. At low electric field strengths, from 0-3 kV/cm, the charge density was linearly correlated with the field strength, i.e. the electric field strength at nozzle and in the bulk is the same. But at higher field strengths, non-linearity appeared as the electric field at the nozzle is non-linear due to space charge migration. Using the Equations (1) and (2), and with R/L = 0.75

and $\gamma = 1.64$ for a non-protruding nozzle, charge density and applied electric field strength were related as $q = 1.97\epsilon E_n \; and \; E_n = 0.8E_n$, while the varied from 1.7 to 2.44 and averaged value was 1.94. The variation in the slope was related to a possible increase in nozzle geometric factor (γ) due to drop elongation during the spray formation.

Takamatsu[186] analytically derived, using the method of images, the theoretical solutions for the charge on the drop at the nozzle. Here, pendant drops are assumed to be perfectly conducting spheres, they are at the same potential as the nozzle and that the charge on protruding nozzle can be neglected. Electric charges on detached and pendant drop are assumed to be same though their volumes are different. $Q = \pi\varepsilon_c\gamma d_e^2 E_o^2$

Where $\beta \; and \; \gamma$ are force and charge coefficients respectively and are approximated from the equations as:

$$\beta = \begin{cases} 1.12 & (\alpha = 1) \\ \alpha + 0.34 & (\alpha > 1) \end{cases}$$

$$\gamma = \alpha + 0.63 \quad (\alpha \geq 1) \; where, \alpha = {}^{(l+r)}/_{r}$$

Here, measured droplet charge increased with increasing voltage but reached a maximum value beyond which the charge acquired reduces. At higher voltages, droplet volume was small correspondingly decrease in charge acquired. Further, the charge acquired in presence of applied voltage increased with protrusion length. For cyclohexane/water system, predicted charge matched well with the experimental values when the nozzle protrusion length was small but at higher lengths, the values were quite different. For silicone oil/water, the match was poor at small protrusion lengths. Also, as the dispersed phase flow rate was increased, the measured charge acquired deceased. The equation predicted charges at low dispersed phase flowrates very

well but at higher flowrates, the predictions were not so accurate. Furthermore, predicted and measured charges were closer when the drop formation times were higher.

Vu *et al.,*[187] measured drop charge at the nozzle for systems consisting of water and glycerol as dispersed phase and pentane, heptane as the continuous phases respectively. Here, gradual increase in drop charge was reported with increase in electric fields along with substantial decrease in drop volumes. But a maximum drop charge in the electrical field range studied was not observed.

Weatherley *et al.,*[141] defined an equation for spherical droplet charge as a combination of free charge and charge induced which is a function of colatitude angle (θ). So, the charge distribution is identified as non-uniform. The equation for charge distribution is: $q = \frac{Q}{\pi d^2} + 3\,\epsilon_c\,\epsilon_0\,E\cos\theta$.

1.4.4.2. Droplet formation and droplet diameters

The study of droplet formation is important as the design of the mixing process is dependent on average droplet size and distribution

Takamatsu *et al.,*[185] studied drop formation in liquid-liquid systems and calculated drop volume and charge. The dispersed phase used was water and the continuous phases used were cyclohexane and silicone oils which had varying viscosities but exhibited Newtonian behavior. They extended the force balance developed by Scheele and Mister[188] for calculating drop volume for uncharged drops to charged drops. Depending upon droplet velocities at the nozzle, drop volume calculations can be divided into those for drops forming below and above the jetting point. Jetting results in formation of jets from which drops are formed and occur above drop velocities of 10 cm/sec. Scheele and Mister proposed two stages for drop formation at low velocities:

a. Force balance on the droplet at nozzle: Buoyancy & kinetic forces acting upward while interfacial tension and drag forces act in downward. For calculation of drag force, the drag coefficient value needs to be determined. The expression for the drag force for solid sphere is used and modified using Harkins-Brown correction factor (F).[189] The drag coefficient for the solid sphere can be calculated as function of Reynolds number. For creeping flow where the Reynolds number < 1, according to Stoke's law, $C_D = \frac{1}{N_{Re}}$

$$F_B + F_K = F_D + F_I$$

$$F_B = g\,\Delta\rho\,V_{FS}$$

$$F_I = \pi\sigma D_N$$

$$F_K = \frac{4}{3}\,\rho_d\,Q_d\,U_N$$

$$F_D = \frac{3\pi\mu_c\,U_F\,D_F}{F^{1/3}}$$

b. Necking process which occurs when the net force on the drop is zero. Before necking starts the volume of the drop may be defined as (V_{FS}). During the necking, additional liquid volume (V_{FN}) flows into droplet increasing its volume. Hence, the total droplet volume is:

$$V_F = V_{FS} + V_{FN}$$

The resulting equation for calculation of droplet volume

$$V_F = F\left[\frac{\pi\sigma D_N}{g\,\Delta\rho} + \frac{20\mu_c Q_d D_N}{d_f^2 g\,\Delta\rho} - \frac{4\,\rho_d Q_d U_N}{3g\,\Delta\rho} + K_n\left(\frac{Q_d^2\rho_d\sigma D_N^2}{(g\,\Delta\rho)^2}\right)^{1/3}\right]$$

In presence of applied electric fields, the droplet experiences electrical force and the resultant force balance would be: $F_B + F_K = F_D + F_I + F_E$

The equation for electrical force experienced by the pendant droplet as developed by Takamatsu is given below. Here, the electrical force acting on the droplet is derived analytically and $F_E = \pi\varepsilon_c\beta d_e^2 E_o^2$. The final equation for droplet volume after detachment from nozzle in presence of electric fields is. The value of necking factor (K_n) for each system studied was calculated from the uncharged droplet cases.

$$\emptyset V_F = \left[\frac{\pi\sigma D_N}{g\,\Delta\rho} + \frac{20\mu_c Q_d D_N}{d_f^2 g\,\Delta\rho} - \frac{4\,\rho_d Q_d U_N}{3g\,\Delta\rho} + K_n\left(\frac{Q_d^2\rho_d\sigma D_N^2}{(g\,\Delta\rho)^2}\right)^{1/3} + \frac{\pi\varepsilon_c\beta d_f^2 E_o^2}{g\,\Delta\rho}\right]$$

The equation predicted the drop volumes well for low viscosity continuous phase such as cyclohexane. For this system, higher protrusion lengths resulted in lower drop volumes at higher E and the equation predicted this well. Increasing the viscosity to viscous silicone oils, the errors increased. But the equation predicted the shape of droplet volume vs. applied electric fields curve correctly. At low dispersed phase flow rates, inertial forces and necking process were negligible. Measured drop volume decreased with increase in Q_d, because of the additional force acting on the droplet at higher Q_d.

Vu *et al.,*[187] assumed drag and kinetic forces experienced by the droplets to be negligible because of low viscosity of the continuous phase used – pentane and heptane. A simple force balance was used to predict droplet diameters: $F_B = F_I + F_E$. The equation used for calculating the electrical force: $F_E = \epsilon_c\epsilon_o\left(\pi d_e^2/4\right)E_o^2$. The equation developed for the droplet volume was a function of the droplet volume under zero electric fields. $V = V_o\left(f/f_o\right) - \frac{\epsilon_c\epsilon_o\,(\pi d_e^2)E_o^2}{4\,g\,\Delta\rho}$

$$where\ \frac{\epsilon_c\epsilon_o\,(\pi d_e^2)E_o^2}{4\,g\,\Delta\rho}\ is\ considered\ as\ charge\ parameter\ group$$

Droplet volume may be plotted as a function of charge parameter group. Experimental droplet volume decreased rapidly with the charge parameter initially but decreases linearly thereafter at higher values. The equation predicts the linear part quite well but does not predict the non-linear region very well. The inability of the equation to accurately predict in the non-linear regions large drop size is related to drop distortion either due to forces from gravity or electric field. Further, the effect of space charge on actual value of electric field is not considered as the reason as similar non-linear was reported with water droplets sprayed in air.

Yang *et al.,*[178] extend the work of Vu and developed an model for predicting droplet volume

$$\left(\frac{V_o - V_d}{V_o}\right)\left(\frac{V_d}{V_o}\right)^{2/3} = K_c \left(\frac{\epsilon_c E_n^2}{g\ \Delta\rho\ d_o}\right)$$

Plotting $\left(\frac{V_o - V_d}{V_o}\right)\left(\frac{V_d}{V_o}\right)^{2/3} vs. \left(\frac{\epsilon_c E_n^2}{g\ \Delta\rho\ d_o}\right)$ resulted in straight lines and experimental and predicted values matched well. Varying the gap between electrodes resulted in different straight lines indicating non-uniform field distribution. This aspect is predicted well by the model.

He *et al.,*[152] developed a fifth order polynomial equation in droplet diameters and solved for the drop diameter for water/mineral oil system. They studied the droplet formation and subsequent motion by varying the angle of the nozzle between 0-90^0. The drop formation was assumed to occur in two stages. Creeping flow around non-circulating spherical drop was assumed and inertial force are ignored. In the first stage, stationary growth occurs when the drop is assumed to remain stationary at nozzle and hence drag force is zero. $F_B + F_e = F_I$

The equation used to define electrical force is:

$$F_e = k_{hb} d^2\ V^2$$

In the second stage of droplet formation, because of inclination of the nozzle (θ), drop movement across the center of nozzle is considered and dynamic force balance is written as:

$$F_B + F_E = F_d + F_I$$

The final equation for droplet diameter in terms of distance between drop center and nozzle tip/edge center (S), inclination angle (θ) and angle of resultant forces is given below. The equation was numerically integrated until: $S = 0.5\,(d + d_N \sin(\theta - \theta'))$

$$\frac{dS}{dd} = \left[\left(\frac{\pi g d^4 \Delta\rho}{36}\right) + \left(\frac{k_{hb}\, d^4\, V^2 \sin\theta}{6}\right)\right] \Big/ (Q\mu_c \sin\theta') - \left[\frac{\pi d_N\, \sigma\, d \cos(\theta - \theta')}{6Q\mu_c}\right]$$

It was observed experimentally there was no effect of the inclination angle on the droplet diameter, though significant effect of θ on the current drawn was observed. The model predicted diameters quite well at voltages > 2 kV but between 0-2 kV prediction was less satisfactory. Dispersed phase flowrate had a strong effect on the droplet diameter. The model accurately predicted the droplet diameters obtained at varying dispersed phase flowrate at voltages >2 kV. At very high voltages, it was deduced from the model that droplet diameter and voltage were related as $d \propto V^{-2/3}$.

The drop velocity just 1-3 cm after its break-off from then nozzle was measured experimentally. Due to the effect of electric field, the droplet detaches rapidly and decelerates away from then nozzle. Further, drop velocity near the nozzle increases with applied voltages though there is sharp decrease in drop diameter. From log-log plots of velocity and diameter, it was observed that droplet velocity varies inversely with the square of the diameter which was confirmed from the force balance equations at high voltages.

1.4.4.3. Droplet velocities – terminal velocities

The forces acting on the droplet as it detaches from the nozzle and during its subsequent fall, irrespective of external applied potential, are gravitational and drag forces. Droplet experiences electrical force depending upon the residual charge on the droplet. Charged droplet experiences

maximum electrical force during the initial fall as it detaches from the nozzle but during its subsequent fall, the residual charge on the droplet is depended upon the relaxation time of the continuous phase (τ_c). If τ_c is high, the droplet holds its charge for a longer time but small τ_c results in droplet losing its charge rapidly. Assuming that the droplet experiences electrical force during its fall, drop velocity can be calculated from the force balance using the following equation:[151]

$$F_G + F_E = F_D$$

$$V\Delta\rho\ g + QE_o = C_D\ \frac{1}{2}\ \rho_c U^2\ \left(\pi\ d^2/_4\right)$$

Ignoring non-linearity of the electric field, drag coefficients under condition of zero applied field were used to obtain the drop velocity. Good agreement between experimental and calculated drop velocities was reported.

Vu *et al.,*[187] demonstrated fairly simple electrostatic model which can predict the effect of electric fields on drop size and velocity for water dispersed in pentane/heptane. They developed the equation for terminal velocity of the droplets based on force balance and used the following electrical force equation.

$$F_E = \epsilon_c\epsilon_o\ \left(\pi d^2/_4\right)E_o^2$$

$$\frac{C_D\pi\rho_c U_t^2 d^2}{8} = \frac{\Delta\rho\pi d^3\ g}{6} + \epsilon_c\epsilon_o\ \left(\pi\ d^2/_4\right)E_o^2$$

A plot $\frac{C_D\pi\rho_c U_t^2}{d}\ vs.\ \frac{\epsilon_c\epsilon_o\ E_o^2}{d\ g\ \Delta\rho}$ resulted in linear increase in the terminal velocity with increase in electric field. The model and experimental values matched with reasonable agreement.

Yang *et al.,*[178] modified the equations developed by Vu to obtain the terminal velocities. The effect of space charge on the distribution of the electric fields as treated in the same way as described previously. The equation used for electric field was the same as used by Vu except the effect of space charge was included.

$$F_E = K_c \epsilon_c d^2 E_n^2$$

From the force balance, the following equation was obtained

$$\frac{C_D \pi \rho_c U_t^2 d^2}{8} = \frac{\Delta\rho \pi d^3 g}{6} + K_c \epsilon_c d^2 E_n^2$$

$$\frac{\rho_c U_t^2}{8\, d\, g\, \Delta\rho} = \frac{1}{6C_D} + \frac{K_c}{C_D}\left(\frac{\epsilon_c E_n^2}{d\, g\, \Delta\rho}\right)$$

A plot between $\frac{\rho_c U_t^2}{8\, d\, g\, \Delta\rho}$ and $\frac{\epsilon_c E_n^2}{d\, g\, \Delta\rho}$ showed linear variation. Drag coefficients were calculated based on Reynolds number from results under no electric fields. Further, a fair agreement between the theory and experimental values was reported. Experimental and predicted values deviated at higher terminal velocities of the droplet. Assuming constant drag when the Reynolds number varied from 750 to 1100 resulted in a linear plot. But when the droplet Reynolds number varied between 750 and 2500, assumption of constant drag did not result in a linear plot and the result was inconsistent with the model.

Petera *et al.,*[2] significantly improved on predicting droplet parameters developed from empirical correlations obtained from force balance equations using a new finite element approach. Here, well-defined equations for distribution of a non-linear electric field in the contactor were developed and solved simultaneously with equations of motion using the model. Accurate experimental particle trajectories were obtained by spraying anionic polymeric ion-exchange beads suspended in silicone oil into a continuous phase of silicone oil in the presence

of DC electric fields in a cylindrical column. Comparisons between experimental and predicted were better at lower voltages (10 and 15 kV) and satisfactory at higher voltages (30 kV).

Electric field was described by the Poisson differential equation as follows.

$$\nabla \cdot \left(\varepsilon_r \nabla \Phi\right) = -\frac{\sigma}{\varepsilon_0}$$

The differential equation is numerically discretized using finite element modeling and the domain is divided into mesh of quadrilateral iso-parametric elements and biquadratic interpolations were used.

With the following boundary conditions:

(a) of the Dirichlet type: $\Phi = 0$ On the earthed electrode,

$\Phi = \Phi_{HV}$ On the charged electrode;

(b) of the Neuman type: $E \cdot n = h$

where E is the electric field strength vector, $E = -\nabla\Phi$ and n is the outward unit vector normal to the boundary, on which a function (of the position) h is given.

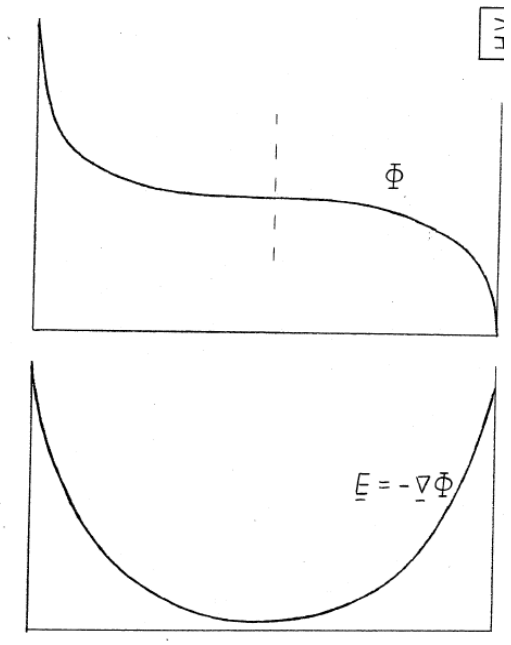

Figure 1.9: Electric field distribution along the contactor from finite element analysis

The resulting profile of electrical field in a liquid-liquid contactor taking into the effect of space charge is shown in the Figure 1.9. As can be seen from the figure, the electric field is linear in away from the electrodes, while closer to the electrodes the distribution is non-linear due to the space charge accumulation.

Using the electric field distribution obtained, motion of a charged particle in the column was obtained from the force balance: $\boldsymbol{F_I = F_G + F_E + F_D}$

$$F_E = Eq \qquad where\ q = q_o e^{(-t/\tau)}\ and\ \tau = {\varepsilon_o \varepsilon_c}/{K}$$

$$F_D = 3\pi\mu_c D_F v \qquad -\ \text{(according to Stokes law)}$$

$$F_B = \frac{\pi D_F^{\,3}}{6}(\rho_S - \rho_c)g$$

$$F_I = \frac{\pi D_F^{\,3}}{6}\rho_S \frac{dv}{dt}$$

These equations can be rearranged to give the dynamical equation as shown below:

$$\frac{dv}{dt} = \frac{6\,E\,Q}{\pi D_F^3\,\rho_s} + \frac{18\,\mu_c}{D_F^2\,\rho_s}v + \left(1 - \frac{\rho_c}{\rho_s}\right)g$$

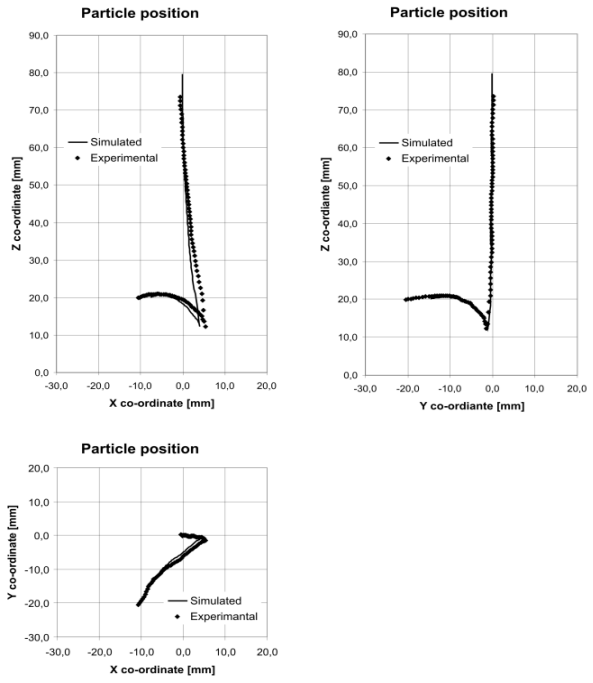

Figure 1.10: Simulated droplet trajectories for discrete droplets[2]

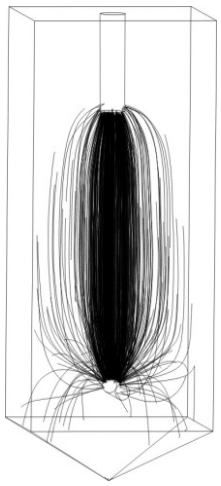

Figure 1.11: Simulated droplet trajectories in electrostatic spray regime

This can be solved numerically to obtain particle position and particle velocity. Here, particle velocity is defined in terms of position as below: $v = \frac{dx}{dt}$ (x is the position vector). Figure 1.10

and Figure 1.11 show the simulated droplet trajectories in discrete and swarming droplets system.

1.4.5. Literature review

A literature review of the enhancement effects of applied electric fields shows that the systems studied have been limited mainly to Newtonian continuous phases, and non-Newtonian and Newtonian dispersed phases. The charge accumulation, droplet formation and droplet size reduction in the presence of applied electric fields was found to be a function of the physical properties of the continuous phase across which the electric fields are applied.[185] Various studies have been looked at the effect of electric fields on the extraction efficiency.

Hume *et al.,*[162,165] measured and predicted one-dimensional trajectories of single droplets in a newtonian liquid systems in the presence of electric fields in a rectangular column. Dispersed phase was water while different continuous phases were used. These included n-decanol, sunflower oil and silicone oil of varying viscosities, 11 cP, 48.3 cP and 48.6 cP. Interfacial tension of the n-decanol/water was lowest at 9.4 mN/m while that of sunflower oil/water had the highest at 44.6 mN/m. Early onset of electrospray was observed at low voltages due to the low interfacial tension for n-decanol/water system. Prediction was done using a quantitative finite element model developed as described in equation section 1.4.4.3. Similar space charge and non-uniform electric field distribution, as obtained with for cylindrical geometry[2] was reported. Good agreement was reported between experimental and predicted ones for different systems studied, under different applied voltages, flow rate and geometry, by adjusting the relaxation time of the continuous phase. For silicone/water, with high relaxation times (~6 sec), the experimental and predicted values matched. However, for the n-decanol system, the relaxation time calculated from literature varied from the predicted values though it was indicated this

would not have much effect on the trajectory as the electrical force acting on the drop after detachment is negligible due to low relaxation times. Further, the model was able to predict the trajectory after their repulsive interaction with the bottom electrode.

Further, for the sunflower oil/water system, good agreement was reported between predicted and experimental trajectories when the model was extended to different contactor sizes (Largest volume - 1.7 L; smallest volume - 0.2 L).[165] This shows the usefulness of the model for potential scale-up design. Larger column gave large drop sizes compared to smaller column though the trajectory and velocity profile were similar. This behavior was similar to reducing the inter-electrode distances. Terminal velocities in the y-direction decreased with increase in electric field and the drop size decreased with increase in the dispersed phase flow rate and electric fields with decrease of 73% when the applied voltage was +15 kV. Smaller drop sizes resulted with positive polarity compared to negative polarity, which led drops under –ve polarity travel faster in the y-direction. Petera *et al.,*[4] extended the 2D trajectory modeling to a more robust 3D modeling using a cloud model for swarming droplets (1-100 μm) produced at the onset of electrostatic spray incorporating various phenomena associated with electric fields. This model was shown to be promising for optimal shape design.

1.4.5.1. Presence of broth components

Terminal velocities of the untreated mycelial (using *Pencillium chrysogenum*) culture broth[164] were lower than those of filtered broth dispersed into 30%tributylphohphate (dissolved in a heavy distillate) and hence result in lower mass transfer and contactor performance when using whole broth. Interfacial tension and viscosity of the whole broth solutions were higher by 60% and 500% over the pure system though change in density was low (4%). The droplets behavior was similar to rigid sphere and the role of biomass solids and surface-active impurities is related

to this behavior and subsequent lack of internal circulation and oscillations. Poor fit of correlation models to terminal velocities of whole drops was reported. Homogenized and treated broths are suggested for consistent drop dynamics.

Weatherley *et al.,*[143] compared the sizes of single drops of aqueous solutions and fermented malt liquor (using *Saccharomyces cerevisiae*) containing 10% by wt. of ethanol dispersed into n-decanol solvent under the influence of electric fields. Theoretical predictions for drop volume[186] correlated well with experimental values ($R^2 > 0.95$) for both solutions. Broth components do not seem have any effect on the sizes as pure and broth had similar drop sizes. Further, it was indicated that the nature of biomass like mycelium, pellets, flocculation and cells could affect the elasticity and shapes of drops during formation. The cell viability of yeast cell culture medium sprayed into n-decanol phase in presence the applied electric fields[180] up to 25 kV did not change and subsequent ethanol produced was unaffected.

1.4.5.2. Mixing related

For feasibility of commercial scale operations, knowledge of residence time distributions and axial mixing is important to determine the performance of the extraction equipment. Characterization of mechanically agitated columns or spray contactors is well documented but the application of electric fields produces electrostatic dispersions, the motion of which is complex and could influence the hydrodynamics including that of continuous phase. In absence of electric fields, mixing is due to diffusion but application of electric fields sets in convection due to acceleration and recirculation of the drops.[166,190] In the initial studies, variation in the solute concentrations along the contactor was attributed to poor mixing[181] during the extraction of penicillin-G from aqueous sample using dichloromethane in presence of electric fields.

Jones *et al.,*[190] studied the mixing behavior and residence time distribution of continuous phase (silicone oil) in co-currently operated liquid-liquid contactor in presence of electric fields. Mean holding times are equal to mean residence times at 0 kV. At 5 kV, the mean residence times decreased and increased 15 kV but were still lower than the holding times. This could mean existence of dead zones and possible bypassing or channeling. Increase in mean residence times with increase in E could be due to flow recirculation in the bulk and also those reflected from charge induced repulsions at the vicinity of the bottom electrode, which suggests enhanced mixing and reduced plug flow behavior. Tanks-in-series model fitted well only at high electric fields while plug-flow/continuous stirred reactor with by-pass flow and advection-dispersion models fitted data well.

Petera *et al.,*[166] accurately modeled the mixing using finite element approach with the system of sunflower oil and water. Important phenomena that enhance mixing like droplet interactions with bottom electrode and coalescence were modeled. It was observed presence of different vortices, single global vortex at 25 kV and distinct vortices at 40 kV with most active one near the nozzle. From tracer response studies, at 25 kV, tracer moved gradually down while at 40 kV due to intensive mixing at the top, slow initial tracer transport to bottom of the column was observed. So at low applied voltages, the residence times become shorter but increase at higher voltages.

1.4.5.3. Mass transfer

Significantly narrower range and substantial reduction in final capsule size of nylon-610 produced from polymerization carried in electric fields was reported.[174] Here, aqueous reactant phase was sprayed into a second phase dissolved in an organic phase in a contactor and reduction was attributed to electrostatic breakup of the dispersed phase before the polymerization.

Stewart *et al.,* studied the effect of electric field on the mass transfer of furfuraldehyde into heptane in both the discrete droplet regime with single droplets[150] and multidrop nozzle.[183] A mean dispersed phase film mass transfer coefficient (based on charged droplets) was calculated that accounts for overall solute transfer. Here, mass transfer is one direction where heptane transfers in to the furfuraldehyde as the heptane phase is saturated with furfuraldehyde. Little variation in the droplet surface area was observed along the length of the column with single droplets. A plot of k_{do} vs E showed significant increase in the mass transfer coefficient with increase in applied voltage. k_{do} increased from 1.8 m/s to 2.1 m/s when the applied voltage was increased from 0 to 12 kV, i.e. using only 2 watts of power. The increase was attributed to smaller droplets that result in higher oscillation frequency which aid in improved mass transfer. Similar percentage increase in no. of transfer units for the dispersed phase (NTU) was reported. Due to different drop sizes possible, mechanisms for mass transfer include molecular diffusion for small drops and eddy diffusion for larger drops. Authors reported droplet oscillation and the frequency of oscillations increasing with applied E. Reduced interfacial tension leads to higher Weber's number and Reynolds' number. A critical applied voltage is indicated beyond which the oscillations were observed.

The studies with multidroplets were conducted by using multinozzle and in a steady-state counter-current manner. Mass transfer coefficient (k_{do}) followed similar to single droplet possibly due to the large droplet sizes compared to discrete drops. Further, at higher applied voltages, higher inter-electrode distance (10, 12 cm) resulted in smaller drop diameters, higher drop velocities and hence higher NTU's. A direct correlation between drop velocity and drop diameter was obtained. Additionally, droplet shape oscillated from sphere to oblate spheroidal. Low droplet phase in the contactor is important to minimize hindered settling effects.

Thornton and Brown reported 200-300% increase in extraction rates of benzoic acid from water into toluene. Processing of 0.75 L/h flow rate of water required 0.1 W of electrical power and scaled-up contactor with flow rates of 50 gal/h consumed 20 W of power for similar enhancement.[191] Yang *et al.,*[178] measured mass transfer efficiencies with different systems of involving low viscosity systems for the transfer of methanol from water into toluene and heptane into furfural. They extended the mass transfer coefficients measurement from overall to calculating the individual mass transfer coefficients: at the drop formation, falling drop and drop coalescence.

Weatherley *et al.,*[161,192] measured the effect of electric field on the extraction of ethanol from pure water, filtered and whole broth using n-decanol and 30% tributylphosphate (TBP) in a hydrocarbon diluent as solvents. The nature of the broth did not have an observable change in the viscosity but partition coefficients for ethanol at low concentrations in whole broth with n-decanol decreased by 30-40% compared to pure system while with 30% TBP they did not change. Applied electric fields increased the overall mass transfer product linearly for both pure and whole broth with both of the solvents in semi-batch mode operation. With 30% TBP as solvent, 80% enhancement in mass transfer product at 27.5 kV/m with whole broth and 170% enhancement at 52 kV/m were reported with pure system. Continuous mode operation resulted in exponential increase in the mass transfer product for the broth system compared to linear increase in pure system as applied electric fields is varied from 0 to 39 kV/m. Length of the column did not have any effect on the mass transfer product.

Five-fold increase in overall mass transfer rates for the extraction of penicillin G from pure aqueous solutions and from untreated mycelial culture broths using an dichloromethane as the extraction solvent was demonstrated by the application of electric fields (4-10 kV) in a liquid-

liquid contactor.[144] Onset of electrostatic spraying increased the extraction rates exponentially and at a pH of 4 for optimal extraction. While the extraction rates with mixing were not included, equilibrium was reached within 20 minutes after application of electric fields and increase in electric field strength increased in the extraction rate at higher concentrations. Here, increase in conductivity of continuous phase was observed after passing single batch of penicillin solution 3 times. There was corresponding increase in the percent mass transfer of penicillin-G.[181]

Hydrolysis of vegetable oil by creation of micro dispersion of aqueous solutions of lipase (produced from *Candida Rugosa*) in an electrically enhanced is reported to be higher than the stirred systems.[193] With 3.5% by wt. of lipase solution, ~85% hydrolysis rate in the presence of electric fields compared to 40% with stirred system after 10 hours of operation is reported. Further, only 10% loss in activity of the enzyme after single pass and no emulsion formation were observed. 40% less power consumption than stirred system is mentioned.

Similarly enzymatic hydrolysis of high oleate sunflower oil in presence of electric fields was demonstrated in an electrostatic dispersion reactor.[194,195] Initial rate of hydrolysis, drop size and rate of approach to equilibrium conversion increased with electric field strength (-500 V/mm) when operated in batch. This attributed to electric wind effects. But onset of coalescence and its rate were observed at lower electric fields (-100 V/mm). Due to lower initial dispersion volumes possible with spraying, the rate was low compared with mixing but adjusted rate of hydrolysis, taking into consideration of initial dispersion volumes, gave higher rates than mixing.

Tsouris *et al.,*[196] evaluated the possibility of integrating DC electric fields in a distillation column with vapor-liquid binary system of water and 2-propanol. Here, the electric field was applied across a tray section where the vapor enters from below through orifices while

condensed liquid enters from top. Size of the vapor phase bubbles decreased from 4.4 mm to 0.8 mm and the plate efficiency increased from 0.74 to 0.78 as the applied voltage is increased from 0 to 30 kV. This led to increase in distillate (2-propanol) mole fraction from 0.738 to 0.754. The increase in the distillation column performance was due to increased mass- and heat transfer rates under the applied electric field between the vapor and liquid phases along with the facilitated transport of vapor by electrospraying through the orifice. However, no such effect was observed with the binary system of 2-butanol and toluene.

To understand the effect of electric fields on the mass transfer rate via modeling, it is important to integrate droplet motion with mass transfer calculations. Petera *et al.,*[163] successfully extended finite element modeling approach to model the mass transfer from discrete falling droplets of aqueous ethanol solutions into n-decanol though without the application of electric fields. Mass transfer efficiencies calculated from modeling were closer to the experimental values compared to the theoretical values. Perturbations due to instabilities at the interface due to mass transfer, changes in interfacial tension and density were accounted. The authors predicted extending to mass transfer from pendant droplet and deforming droplet in presence of electric fields.

1.4.5.4. Droplet coalescence

As important it is to improve mass transfer rate, faster phase separation is also a bottleneck for industrial processes. Apart from increasing the interfacial area in liquid-liquid contacting, the effect of electric fields to do the opposite, that is, to increase the drop size by inducing droplet coalescence for faster phase separation has also been studied. These kinds of situations are encountered primarily when immiscible phases that include emulsions or dispersions of oil in water or separation of phases after extraction, etc. Faster phases separations can reduce the

downstream equipment sizes and hence reduce the capital and operating costs. Coalescence is important in phase separations as it results in increased drop size which leads to faster separation by minimization of total surface area and surface energy occurs during coalescence.[197] This is characterized by the average rest-time and energy balance at the interface. Various internal factors influence the coalescence such as higher viscosity of the oil phase could increase coalescence time for Newtonian liquids.

External factors like electric fields were found to reduce the rest-times by increasing the attractive forces between a drop and it's interface, decreases the drop stability and making coalescence a single staged process. This process is called electrocoalescence. Collision between droplets also leads to coalescence. This promoted is droplets motion back and forth between electrodes without touching the electrode. Charge exchange between drop and electrode at the electrodes plays an important role in coalescence as was observed for water in kerosene emulsion.[198] Field strength at the interface rather than the induced charge on the aqueous drop was found to promote coalescence. Effect of alternating currents on the coalescence was found to be minimal. Another observation during a droplet coalescence is that secondary drops are produced which undergo subsequent drop coalescences. This phenomenon was not observed with electric fields above a critical magnitude below which secondary droplets were observed though the number of partial coalescence stages was less.

Eow *et al.,*[170] tested two systems of water in oil systems like water in sunflower oil and water in heptane. For these, the electric field applied across the two phases and the effect of height of the organic and water layer on the droplet coalescence were studied. Electric current measured was indicative of the effect of electric field on the liquid-liquid interface. For coalescence of 3.9 mm droplet a voltage of < 5 kV that corresponded to 3.9 nA of current was applied. As the

organic layer height was increased, higher voltage was required. Further coalescence of higher drop size larger required higher applied electric potential required. A turning point characterized as Taylor cone, where the electric current increases rapidly above certain electric field strength. Formation of Taylor cone leads to formation of tiny drops which is not required. Formation of these cones depended upon the height of the layers. Turning point voltage was 5 kV, 10 kV and ~22.5 kV when the height of the organic layer was 10 mm, 25 mm and 50 mm respectively. Here water layer height was 30 mm.

Eow *et al.,*[199] reported single droplet deformation in presence of applied voltage into finer droplets. Drop deformation depends on the properties of the continuous phase such as electric al conductivity, permittivity, viscosity and interfacial tension. Further, continuous phase with high electrical conductivity and permittivity tends to cause quicker drop deformation because of higher induced electrical stress at the interface. Also, droplets in a continuous phase with higher interfacial tension do not deform easily. Similarly, smaller droplets tend to deform less easily than larger droplets. Onset of disintegration was found to be dependent on the shape of the droplet i.e., when the ratio of major axis to minor axis is 1.9.[200] Droplet deformation were observed like drop prolongation on one end leading to disintegration into finer droplets. A dimensionless electrostatic weber number was developed from the force balance from which a critical Weber number of 0.47 for droplet deformation was identified. Further a similar droplet which came in contact with one of electrodes became charged and as a result had translational velocities between the electrodes.

A critical electrical field strength was identified by Ristenpart *et al.,*[197] beyond which oppositely charged droplets do not coalesce. Above this, they bounce off each other but below

they tend to coalesce. This bouncing is attributed to transient bridge meniscus formation between drops which is unstable above critical electric fields.

1.4.6. Design and Scale-up of electrical enhanced contactors

Designs for electrically enhanced contactors include multi-nozzle system or single nozzle modular units operated in parallel.[141] Electric fields were created between consecutive sets of sieve plates, with perforations (multi-nozzle), which were stacked vertically in a counter-current contactor with column diameters of around 15 cm.[191] Drop dispersion and drop coalescence on top of grounded sieve plate was observed in the stage-wise contactor. A multi-electrode assembly with electrodes placed perpendicularly along length of counter-current contactor provided good mass transfer.[201] This was attributed to cyclic process of drop break-up and coalescence across each electrode set along with electro-convective motion of continuous phase. Another version of multi-electrode assembly was to arrange optimum number of electrode rods along the circumference of the contactor, depending upon the contactor size, to promote drop break-up.[202] Efficient drop breakup and increase in mass transfer rate was achieved by passing falling drops through horizontally arranged parallel electrodes in a column contactor.[177] Lower end was tapered to promote drop coalescence.

Though research has established the potential of electric fields for process intensification of liquid-liquid contacting, there has not been scaled up applications or industrially employed use of this technique in the open literature. Commercial applications have been constrained due to the safety issues from using high DC voltages in presence of low flash point organics and formation of static discharges in presence of flammable organic vapors. Further, design of the nozzles to handle commercial throughputs of dispersed phase ensuring efficient drop dispersion is another bottleneck. Integration with existing equipment is difficult for example fluid handling systems

designed for organic dispersed phases but not for aqueous phases. Also, design of a contactor with both applied electric fields and mechanically agitation would be difficult because of constraints with electrostatics such as materials of construction.[141] Proper safety testing and evaluation of electrically enhanced systems are required prior to commercial development. AC electric fields are used at commercial scale in electrostatic precipitators, and electrostatic dehydrators and desalters.[203] In mining industries, scaled electrostatic coalescers for the separation of aqueous dispersions during the solvent extraction of uranium have been demonstrated.[169] These were operated at high feed rates of 8 L/s about 6 times higher than conventional mixers-settlers.

Millar *et al.,*[204] extended the extraction of ethanol from pure system and whole broth using 30% TBP to scaled up volumes by designing a compact assembly wherein the whole broth is sprayed from a vertically placed in-line nozzle at a flowrate of 100 ml/min into a horizontal continuously circulating stream of organic phase at a flow rate of 1.62 L/min. Small diameters of the chamber are used for faster throughput and with pure system electrostatic spray is observed at 3 kV though it was indicated prevention of such spray with the whole broth. Such a system can address potential safety concerns with using low flash points organics with electric fields. Velocity of the dispersed phase from the nozzle was found to be predominant compared to effect electric field on the mass transfer product though application of electric field resulted in 100% equilibrium compared to 70% with no electric field after 120 minutes of settling time. Increased dispersed phase flowrate offset the charge acquisition by the drop at the nozzle. Use of multi-drop nozzle and centrifugal mixer is indicated as other options for scaling up electrical enhanced extractions.

1.5. References

(1) Thornton, J. D. Electrically Enhanced Liquid-Liquid Extraction. *Birmingham University Chemical Engineer Journal* **1976**, *27*, 6.
(2) Petera, J.; Rooney, D.; Weatherley, L. R. Particle and droplet trajectories in a non-linear electrical field. *Chemical Engineering Science* **1998**, *53*.
(3) Schmid, A.; Dordick, J. S.; Hauer, B.; Kiener, A.; Wubbolts, M.; Witholt, B. Industrial biocatalysis today and tomorrow. *Nature* **2001**, *409*, 258.
(4) Petera, J.; Weatherley, L. R.; Hume, A. P.; Gawrysiak, T. A finite element algorithm for particle/droplet trajectory tracking, tested in a liquid–liquid system in the presence of an external electric field. *Computers & Chemical Engineering* **2007**, *31*, 1369.
(5) Anastas, P.; Warner, J. C. *Green Chemistry: Theory and Practice*; Oxford University Press: New York, 1998.
(6) Anastas, P.; Zimmerman, J. Through the 12 Principles of Green Engineering. *Environ. Sci. Tech.* **2003**, *37*, 95A.
(7) staff *Report 1921: Fermentation Chemicals to 2009*, Freedonia, Inc. , 2009 http://www.freedoniagroup.com/DocumentDetails.aspx?ReferrerId=FG-01&studyid=1921.
(8) *Fermentation Chemicals: A Global Strategic Business Report*, 2012.
(9) Werpy, T.; Petersen, G. *Report: Top Value Added Chemicals From Biomass: Volume 1*, Department of Energy, 2004.
(10) Stephanopoulos, G. Challenges in Engineering Microbes for Biofuels Production. *Science* **2007**, *315*, 801.
(11) Lye, G. J.; Dalby, P. A.; Woodley, J. M. Better Biocatalytic Processes Faster: New Tools for the Implementation of Biocatalysis in Organic Synthesis. *Organic Process Research and Development* **2002**, *6*, 434.
(12) Vane, L. M. Separation technologies for the recovery and dehydration of alcohols from fermentation broths. *Biofuels, Bioprod. Bioref.* **2008**, *2*, 553.
(13) Jones, D. T.; Woods, D. R. Acetone–butanol fermentation revisited. *Microbiological Reviews* **1986**, *50*, 484.
(14) Bommarius, A. S. R., B.R. *Biocatalysis: Fundamentals and Applications*; Wiley-VCH: Weinheim, 2004.
(15) Daugulis, A. J. Integrated Reaction and Product Recovery in Bioreactor Systems. *Biotech. Prog.* **1988**, *4*, 113.
(16) Gu, T. In *Handbook of Bioseparations*; Ahuja, A., Ed.; Academic Press: New York, 2000; Vol. 2, p 329.
(17) Liddell, J. M. In *Engineering Processes for Bioseparations*; Weatherley, L. W., Ed.; Butterworth-Heinemann: Oxford, 1994, p 5.
(18) Stark, D. v. S., U. In situ product removal (ISPR) in whole cell biotechnology during the last twenty years. *Advances in Biochemical Engineering/Biotechnology* **2003**, *80*, 149.
(19) Matsumura, M. K., H.; Sueki, M.; Araki, K Energy saving effect of pervaporation using oleyl alcohol liquid memberane. *Bioprocess. Eng.* **1988**, *3*, 93.
(20) Keeney, D.; Muller, M. *Water Use by Ethanol Plants: Potential Challenges*, Institute for Agriculture and Trade Policy (iatp.org), 2006.
(21) S R Rofler, C. R. W., H W Blanch Design And Mathematical Description Of Differential Contactors Used In Extractive Fermentation. *Biotechnology and Bioengineering* **1988**, *32*, 192.
(22) Harrop, A. J.; Woodley, J. M.; Lilly, M. D. Production of Naphthalene cis-Glycol by Pseudomonas Putida in the Presence of Organic Solvents. *Enzyme and Microbial Technology* **1992**, *14*, 725.
(23) Lye, G. J.; Woodley, J. M. Application of in-situ product removal techniques to biocatalytic processes. *Trends in Biotechnology* **1999**, *17*, 395.
(24) Banik, R. M. S., A.; Kanari, B.; Sabrinath Technological aspects of two-phase extractive fermentations. *World Journal of Microbiology and Biotechnology* **2003**, *19*, 337.
(25) D-Arrigo, P.; Fuganti, C.; Fantoni, G. P.; Servi, S. Extractive Biocatalysis: a powerful tool in selectivity control in extractive biotransformations. *Tetrahedron Letters* **1998**, *54*, 15017.
(26) Bar, R. In *Biocatalysis in Organic media*; Laane, C., Tramper, J., Lilly, M. D., Eds.; Elsevier Science: The Netherlands, 1986, p 147.
(27) Dadgar, A. M.; Foutch, G. L. Improving the Acetone-Butonol Fermentation Process With Liquid-Liquid Extraction. *Biotechnology progress* **1988**, *4*, 36.
(28) Randolph, T. W. Supercritical fluid extractions in biotechnology. *Trends in Biotechnology* **1990**, *8*, 78.

(29) Lozano, P.; Diego, T.; Vaultier, M.; Iborra, J. L. Continuous green biocatalytic processes using ionic liquids and supercritical carbon dioxide. *Chemical Communications* **2002**, 692.
(30) Bothun, G. D.; Knutson, B. L.; Strobe, H. J.; Nokes, S. E. Molecular and Phase Toxicity of Compressed and Supercritical Fluids in Biphasic Continuous Cultures of Clostridium thermocellum. *Biotechnology and Bioengineering* **2005**, *89*, 34.
(31) Anon. Thermodynamics of Ionic Liquids, Ionic Liquid Mixtures, and the Development of Standardized Systems. *Chem. Int.* **2005**, *27*, 22.
(32) Holbrey, J. D.; Seddon, K. R. Ionic Liquids. *Clean Prod. Proc.* **1999**, *1*, 223.
(33) Han, D.; Row, K. H. Recent Applications of Ionic Liquids in Separation Technology. *Molecules* **2010**, *15*, 2405.
(34) Edward, W. C.; James, F. W. Spotlight on ionic liquids. *The Journal of Chemical Physics* **2010**, *132*, 120901.
(35) Howarth, J.; James, P. D., J.; Immobilized baker's yeast reduction of ketones in an ionic liquid, [bmim]PF6 and water mix. *Tetrahedron Letters* **2001**, *42*, 7517.
(36) Pfruender, H.; Amidjojo, M.; Kragl, U.; Weuster-Botz, D. Efficient whole-cell biotransformation in a biphasic ionic liquid/water system. *Angew. Chem. Int. Ed.* **2004**, *43*, 4529.
(37) Pfruender, H.; Jones, R.; Weuster-Botz, D. Water immiscible ionic liquids as solvents for whole cell biocatalysis. *Journal of Biotechnology* **2006**, *124*, 182.
(38) Brautigam, S.; Bringer-Meyerb, S. W.-B., D.; Asymmetric whole cell biotransformations in biphasic ionic liquid/water-systems by use of recombinant Escherichia coli with intracellular cofactor regeneration. *Tetrahedron: Asymmetry* **2007**, *18*, 1883.
(39) Lenourry, A.; Gardiner, J. M.; Stephens, G. Hydrogenation of C–C double bonds in an ionic liquid reaction system using the obligate anaerobe, Sporomusa termitida. *Biotechnology Letters* **2005**, *27*, 161.
(40) Cornmell, R. J. W., C.L.; Schuler, S.; Goodacre, R.; Gill Stephens, G.; Using a biphasic ionic liquid/water reaction system to improve oxygenase-catalysed biotransformation with whole cells. *Green Chemistry* **2008**, *10*, 685
(41) Gorke, J.; Srienc, F.; Kazlauskas, R. Toward advanced ionic liquids. Polar, enzyme-friendly solvents for biocatalysis. *Biotechnology and Bioprocess Engineering* **2010**, *15*, 40.
(42) Zhen, Y. Hofmeister effects: an explanation for the impact of ionic liquids on biocatalysis. *Journal of Biotechnology* **2009**, *144*, 12.
(43) Manthiriyappan, S.; Lee, C.-K. Biocatalytic reactions in hydrophobic ionic liquids. *Journal of Molecular Catalysis B: Enzymatic* **2009**, *60*, 1.
(44) Jerina, D. M.; Daly, J. W.; Jeffrey, A. M.; Gibson, D. T. cis-1,2-Dihydroxy-1,2-dihydronaphthalene-bacterial metabolite from naphthalene. *Arch. Biochem. Biophys.* **1971**, *142*, 394.
(45) Ensley, B. D.; Gibson, D. T.; Laborde, A. L. Oxidation of naphthalene by a multicomponent enzyme-system from Pseudomonas sp. strain Ncib9816. *Journal of Bacteriology* **1982**, *149*, 948.
(46) Liese, A. S., K.; Wandrey, C. *Industrial biotransformations*; 2nd ed.; Wiley-WCH, 2006.
(47) Yu, C.-L.; Parales, R. E.; Gibson, D. T. Multiple mutations at the active site of naphthalene dioxygenase affect regioselectivity and enantioselectivity. *Journal of Industrial Microbiology & Biotechnology* **2001**, *27*, 94.
(48) van Beilen, J. B.; Duetz, W. A.; Schmid, A.; Witholt, B. Practical issues in the application of oxygenases. *Trends in Biotechnology* **2003**, *21*, 170.
(49) Eaton, R. W.; Chapman, P. J. Bacterial Metabolism of Naphthalene: Construction and Use of Recombinant Bacteria To Study Ring Cleavage of 1,2-Dihydroxynaphthalene and Subsequent Reactions. *Journal of Bacteriology* **1992**, *174*, 7542.
(50) Raschke, H.; Meier, M.; Burken, J. G.; Hany, R.; Muller, M.; Meer, J. R. V. D.; Kohler, H.-P. E. Biotransformation of Various Substituted Aromatic Compounds to Chiral Dihydrodihydroxy Derivatives. *Appl. Environ. Microbiol.* **2001**, *67*, 3333.
(51) Bestetti, G.; Bianchi, D.; Bosetti, A.; Di Gennaro, P.; Galli, E.; Leoni, B.; Pelizonni, F.; Sello, G. Bioconversion of subsituted naphthalenes to the corresponding 1,2-dihydro-1,2-dihydroxy derivatives. Determination of the regio- and stereochemistry of the oxidation reactions. *Appl. Microbiol. Biotechnol.* **1995**, *44*, 306.
(52) Hsieh, J. H.; Wang, S. S. Microbial Cooxidation of Naphthalene for the Production of 1,2-dihydroxy-1,2-dihydronaphthalene. *Enzyme and Microbial Technology* **1980**, *2*, 299.
(53) Cox, D. P.; Williams, A. L. Biological Process for Converting Naphthalene to cis-1,2-Dihydroxy-1,2-Dihydronaphthalene. *Appl. and Environ. Microbiol.* **1980**, *39*, 320.

(54) Bosetti, A.; Bianchi, D.; Andriollo, N.; Cidaria, D.; Cesti, P.; Sello, G.; Gennaro, P. D. Microbial Oxidation of Naphthalene to cis-1,2-Dihydroxy-1,2-dihydronaphthalene in a Membrane Bioreactor. *Journal of Chemical Technology and Biotechnology* **1996**, *66*, 375.
(55) Briganti, F.; Randazzo, D.; Scozzafava, A.; Berti, D.; Baglioni, P.; Gennaro, P. D.; Galli, E.; Bestetti, G. Characterization of the biological conversion of naphthalene to (+)-*cis*-(1R,2S)-dihydroxy-1,2-dihydronaphthalene in direct micellar systems. *Journal of Molecular Catalysis B: Enzymatic* **1999**, *7*, 263.
(56) Randazzo, D.; Berti, D.; Briganti, F.; Baglioni, P.; Scozzafava, A.; Gennaro, P. D.; Galli, E.; Bestetti, G. Efficient Polycyclic Aromatic Hydrocarbons Dihydroxylation in Direct Micellar Systems. *Biotechnology and Bioengineering* **2001**, *74*, 240.
(57) McIver, A. M.; Garikipati, S. V. B. J.; Bankole, K. S.; Gyamerah, M.; Peeples, T. L. Microbial Oxidation of Naphthalene to cis-1,2-Naphthalene Dihydrodiol Using Naphthalene Dioxygenase in Biphasic Media. *Biotechnol. Prog.* **2008**, *24*, 593.
(58) Bernstein, L. *An Assessment of the Intergovernmental Panel on Climate Change;* , IPCC 2007.
(59) Liu, J.; Fan, L. T.; Seib, P.; Friedler, F.; Bertok, B. Downstream Process Synthesis for Biochemical Producation of Butanol, Ethanol and Acetone from Grains: Generation of Optimal and Near-Optimal Flowsheets with conventional Operating Units. *Biotechnical.Prog.* **2004**, *20*, 1518.
(60) Beckman, J. H., T.; , Taheripour, F.; Tyner, W. Structural change in the biofuels era. *European review of agricultural economics* **2012**, *39*, 137.
(61) Qureshi, N. B., H. P. In *Food Biotechnology, Second Edition*; CRC Press: 2005.
(62) Lee, S. Y.; Park, J. H.; Jang, S. H.; Nielsen, L. K.; Kim, J.; Jung, K. S. Fermentative Butanol Production by Clostridia. *Biotechnology and Bioengineering* **2008**, *101*, 209.
(63) Ezeji, T. M., C.; Price. N. D.; Blaschek, H. P.; Achievements and perspectives to overcome the poor solvent resistance in acetone and butanol-producing microorganisms. *Appiled Microbiology and Biotechnology* **2010**, *85*, 1697.
(64) Knoshaug, E. P.; Zhang, M. Butanol tolerance in a selection of microorganisms. *Appiled Biochemistry and Biotechnology* **2009**, *153*, 13.
(65) Green, W. M. Fermentative production of butanol- the industrial perspective. *Current Opinion in Biotechnology* **2011**, *22*, 337.
(66) Tashiro, Y.; Takeda, K.; Kobayashi, G.; Sonomoto, K.; Ishizaki, A.; Yoshino, S. High Butanol Production by Clostridium saccharoperbutylacetonicum N1-4 in Fed-Batch Culture with pH-Stat Continuous Butyric Acid and Glucose Feeding Method. *Journal of Bioscience and Bioengineering* **2004**, *98*, 263.
(67) Bochman, M.; Cotton, F. A.; Murillo, C. A.; Wilkinson, G. *Advanced inorganic chemistry*; John Wiley & Sons, Inc., 1999.
(68) Qureshi, N.; Blaschek, H. P. ABE production from corn: a recent economic evaluation. *Journal of Industrial Microbiology & Biotechnology* **2001**, *27*, 292.
(69) Oudshoorn, A.; van der Wielen, L. A. M.; Straathof, A. J. J. Assessment of options for selective 1-Butanol recovery from aqueous solution. *Industrial Engineering and Chemistry Research* **2009**, *48*, 7325.
(70) Ladisch, M. R. Fermentation-derived butanol and scenarios for its uses in energy-related applications. *Enzyme and Microbial Technology* **1991**, *13*, 280.
(71) Griffith, W. L.; Compere, A. L.; Googin, J. M. Novel neutral solvents fermentations. *Developments in Industrial Microbiology* **1983**, *24*, 347.
(72) Mattiasson, B.; Suominen, M.; Andersson, E.; Haggstrom, L.; Albertsson, P.-A.; Hahn-Hagerdal, B. Solvent production by clostridium acetobutylicum in aqueous two-phase systems. *Enzyme Engineering* **1982**, *6*, 153.
(73) Traxler, R. W.; Wood, E. M.; Mayer, J.; Wilson Jr, M. P. Extractive fermentation for the production of butanol. *Developments in Industrial Microbiology* **1985**, *26*, 519.
(74) Ishii, S.; Taya, M.; Kobayashi, T. Production of butanol by Clostridium Acetobutylicum in extractive fermentation system. *Journal of Chemical Engineering of Japan* **1985**, *18*, 126.
(75) Dadgar, A. M.; Foutch, G. L. Evaluation of solvents for the recovery of Clostridium fermentation products by liquid-liquid extraction. *Biotechnology and Bioengineering Symposium* **1986**, *15*, 611.
(76) Compere, A. L.; Googin, J. M.; Griffith, W. L. Effect of possible interferences on the extraction of 1-butanol from aqueous solution by the ethyl ester of soybean oil fatty acids. *Separation Science and Technology* **1987**, *22*, 373.
(77) Malinowski, J. J.; Daugulis, A. J. Salt Effects in Extraction of Ethanol, 1-butanol, and acetone from aqueous solutions. *AIChE* **1994**, *40*, 1459.
(78) Wayman, M.; Parekh, R. Production of Acetone-Butanol by extractive fermentation using dibutylphthalate as extractant. *Journal of Fermentation Technology* **1987**, *65*, 295.

(79) Groot, W. J.; Soedjak, H. S.; Donck, P. B.; van der Lans, R. G. J. M.; Luyben, K. C. A. M.; Timmer, J. M. K. Butanol recovery from fermentations by liquid-liquid extraction and membrane solvent extraction. *Bioprocess Engineering* **1990**, *5*, 203.
(80) Honda, H.; Mato, T.; Taya, M.; Shimizu, K.; Matsubara, M.; Kobayashi, T. A general framework for the assessment of extractive fermentations. *Chemical Engineering Science* **1987**, *42*, 493.
(81) Roffler, S. In situ recovery of butanol during fermentation Part 1: Batch extractive fermentation. *Bioprocess Engineering* **1987**, *2*, 1.
(82) Roffler, S. In situ recovery of butanol during fermentation Part 2: Fed-batch extractive fermentation. *Bioprocess Engineering* **1987**, *2*, 181.
(83) Roffler, S.; Blanch, H. W.; Wilke, C. R. Extractive fermentation of acetone and butanol: Process design and economic evaluation. *Biotechnology progress* **1987**, *3*, 131.
(84) Roffler, S.; Blanch, H. W.; Wilke, C. R. In situ extractive fermentation of Acetone and Butanol. *Biotechnology and Bioengineering* **1988**, *31*, 135.
(85) Shukla, R.; Kang, W.; Sirkar, K. K. Acetone-Butanol-Ethanol (ABE) production in a hollow fiber fermentor-extractor. *Biotechnology and Bioengineering* **1989**, *34*, 1158.
(86) Shah, M. M.; Lee, Y. Y. Process improvement in Acetone-Butanol production from Hardwood by simultaneous saccharification and extractive fermentation. *Appiled Biochemistry and Biotechnology* **1994**, *45-46*, 585.
(87) Ishizaki, A.; Michiwaki, S.; Crabbe, E.; Kobayashi, G.; Sonomoto, K.; Yoshino, S. Extractive Acetone-Butanol-Ethanol Fermentation using Methylated crude palm oil as extractant in batch culture of Clostridium saccharoperbutylacetonicum N1-4 (ATCC 13564). *Journal of Bioscience and Bioengineering* **1999**, *87*, 352.
(88) Shi, Z.; Shimizu, K.; Iijima, S.; Morisue, T.; Kobayashi, T. Theoretical development and performance evaluation of extractive fermentation using multiple extractants. *Biotechnology and Bioengineering* **1990**, *36*, 520.
(89) Barton, E. W.; Daugulis, A. J. Evaluation of solvents for extractive butanol fermentation with Clostridium acetobutylicum and the use of poly(propylene glycol) 120. *Applied Microbiology and Biotechnology* **1992**, *36*, 632.
(90) Davison, B. H.; Thompson, D. W. Continuous direct solvent extraction of butanol in a fermenting fluidized-bed bioreactor with immobilized *Clostridium acetobutylicum*. *Applied Biochemistry and Biotechnology* **1993**, *39-40*, 415.
(91) Shi, Z.; Zhang, C.; Chen, J.; Mao, Z. Performance evaluation of acetone–butanol continuous flash extractive fermentation process. *Bioprocess Biosystems Engineering* **2005**, *27*, 175.
(92) Li, Q.; Cai, H.; Hao, B.; Zhang, C.; Yu, Z.; Zhou, S.; Chenjuan, L. Enhancing Clostridial Acetone-Butanol-Ethanol (ABE) Production and Improving Fuel Properties of ABE-enriched Biodiesel by Extractive Fermentation with Biodiesel. *Applied Biochemistry and Biotechnology* **2010**, *162*, 2381.
(93) Adhami, L.; Griggs, B.; Himebrook, P.; Taconi, K. Liquid–Liquid extraction of butanol from dilute aqueous solutions using Soybean-derived biodiesel. *Journal of the American Oil Chemist' Society* **2009**, *86*, 1123.
(94) Nielsen, L. K.; Larsson, M.; Holst, O.; Mattiasson, B. Adsorbents for extractive bioconversion to the acetone-butanol fermentation. *Applied Microbiology and Biotechnology* **1988**, *28*, 335.
(95) Qureshi, N.; Hughes, S.; Maddox, I. S.; Cotta, M. A. Energy-efficient recovery of butanol from model solution and fermentation broth by adsoprtion. *Bioprocess and Biosystems Engineering* **2005**, *27*, 215.
(96) Nielsen, D. R.; Prather, K. L. In situ product recovery of n-butanol using polymeric resins. *Biotechnology and Bioengineering* **2008**, *102*, 811.
(97) Afschar, A. S.; Biebl, H.; Schaller, K.; Schugerl, K. Production of acetone and butanol by *Clostridium Acetobutylicum* in continuous culture with cell recycle. *Applied Microbiology and Biotechnology* **1985**, *22*, 394.
(98) Ezeji, T. K., P. M.; Qureshi, N.; Blaschek, H. P.; Improving performance of a gas stripping-based recovery system to remove butanol from *Clostridium beijerinckii* fermentation. *Bioprocess Biosystems Engineering* **2005**, *27*, 207.
(99) Groot, W. J.; van der Lans, R. G. J. M.; Luyben, K. C. A. M. Technologies for butanol recovery integrated with fermentations. *Process Biochemistry* **1992**, *27*, 61.
(100) Wu, M.; Wang, M.; Liu, J.; Huo, H.; Energy Systems Division, A. N. L., Ed. 2007, p 59.
(101) Liu, J.; Wu, M.; Wang, M. Simulation of the Process for Producing Butanol From Corn Fermentation *Ind.Eng.Chem.Res.* **2009**, *48*, 5551.
(102) Qureshi, N.; Maddox, I. S.; Fried, A. Application of continuous substrate feeding to the ABE fermentation: Relief of product inhibtion using extraction, perstraction, stripping and pervaporation. *Biotechnology progress* **1992**, *8*, 382.

(103) Liu, J.; Fan, L. T.; Seib, P.; Friedler, F.; Bertok, B. Downstream Process Synthesis for Biochemical Production of Butanol, Ethanol, and Acetone from Grains: Generation of Optimal and Near-Optimal Flowsheets with Conventional Operating Units. *Biotechnology progress* **2004**, *20*, 1518.
(104) Kraemer, K.; Harwardt, A.; Bronneberg, B.; Marquardt, W. In *20th European Symposium on Computer Aided Process Engineering – ESCAPE20*

Pierucci, S., Ferraris, G. B., Eds.; Elsevier: 2010.
(105) Cull, S. G.; Holbrey, J. D. V.-M., V.; Seddon, K.R.; Lye, G.J.; Room-temperature ionic liquids as replacements for organic solvents in multiphase bioprocess operations. **2000**, *69*, 227.
(106) Weuster-Botz, D. Process intensification of whole-cell biocatalysis with ionic liquids. *The Chemical Record* **2007**, *7*, 334
(107) Lou, W.-Y.; Zong, M.-H. S., J.T.; Use of ionic liquids to improve whole-cell biocatalytic asymmetric reduction of acetyltrimethylsilane for efficient synthesis of enantiopure (S)-1-trimethylsilylethanol. *Green Chemistry* **2006**, *8*, 147.
(108) Lou, W.-Y.; Zong, M.-H.; Wu, H.; Xu, R.; Fang, W.-J. Markedly improving lipase-mediated asymmetric ammonolysis of D,L-p-hydroxyphenylglycine methyl ester by using an ionic liquid as the reaction medium. *Green Chemistry* **2005**, *7*, 500.
(109) Brautigam, S.; Dennewald, D.; Schurman, M.; Lutje-Spelberg, J.; Pitner, W.-R.; Weuster-Botz, D. Whole-cell biocatalysis: Evaluation of new hydrophobic ionic liquids for efficient asymmetric reduction of prochiral ketones. *Enzyme and Microbial Technology* **2009**, *45*, 310.
(110) Hussain, W.; Pollard, D. J. L., G.J.; The bioreduction of a .beta.-tetralone to its corresponding alcohol by the yeast Trichosporon capitatum MY1890 and bacterium Rhodococcus erythropolis MA7213 in a range of ionic liquids. *Biocatalysis and Biotransformation* **2007**, *25*, 443.
(111) Schroer, K.; Tacha, E.; Lutz, S. Process Intensification For Substrate-Coupled Whole Cell Ketone Reduction by In Situ Acetone Removal. *Organic Process Research and Development* **2007**, *11*, 836.
(112) Dipeolu, O.; Green, E.; Stephens, G. Effects of water-miscible ionic liquids on cell growth and nitro reduction using *Clostridium sporogenes*. *Green Chemistry* **2008**, *11*.
(113) Cornmell, R. J.; Winder, C. L. T., J.T.G.; Goodacre, R.; Stephens, G.; Accumulation of ionic liquids in Escherichia coli cells. *Green Chemistry* **2008**, *10*, 836
(114) Shi, Y. G. F., Y.; Ren, Y.P.; Wu, H.P.; Guan, H.L.; Effect of ionic liquid [BMIM][PF6] on asymmetric reduction of ethyl 2-oxo-4-phenylbutyrate by Saccharomyces cerevisiae. *Industrial Microbiology and Biotechnology* **2008**, *35*, 1419.
(115) Dahl, A. C.; Fjelderg, M.; Madsen, J. Baker's yeast: improving the D-stereoselectivity in reduction of 3-oxo esters. *Tetrahedron: Asymmetry* **1999**, *10*, 551.
(116) Wang, W.; Zong, M.-H.; Lou, W.-Y. Use of ionic liquids to improve asymmetric reduction of 4'-methoxyacetophenone catalyzed by immobilized Rhodotorula sp. AS2.2241 cells. *Journal of Molecular Catalysis B: Enzymatic* **2009**, *56*, 70.
(117) He, J.-Y.; Zhou, L.-M.; Wang, P.; Zu, L. Microbial reduction of ethyl acetoacetate to ethyl (R)-3-hydroxybutyrate in an ionic liquid containing system. *Proc. Biochem.* **2009**, *44*, 316.
(118) Kratzer, R. P., M.; Egger, S.; Nidetzky, B.; Whole-cell bioreduction of aromatic α-keto esters using Candida tenuis xylose reductase and Candida boidinii formate dehydrogenase co-expressed in Escherichia coli. *Microbial Cell Factories* **2008**, *7*, 37.
(119) Dennewald, D.; Pitner, W.-R.; Weuster-Botz, D. Recycling of the ionic liquid phase in process integrated biphasic whole-cell biocatalysis. *Process Biochemistry* **2011**, *46*, 1132.
(120) Dennewald, D.; Hortsch, R.; Weuster-Botz, D. Evaluation of parallel milliliter-scale stirred-tank bioreactors for the study of biphasic whole-cell biocatalysis with ionic liquids. *Journal of Biotechnology* **2012**, *157*.
(121) Nancharaiah, Y. V.; Francis, A. J. Alkyl-methylimidazolium ionic liquids affect the growth and fermentative metabolism of *Clostridium* sp. *Bioresource Technology* **2011**, *102*, 6573.
(122) Wang, H.; Malhotra, S. V.; Francis, A. J. Toxicity of various anions associated with methoxyethyl methyl imidazolium-based ionic liquids on Clostridium sp. *Chemosphere* **2011**, *82*, 1597.
(123) Cascon, H. R.; Choudhari, S. K.; Nisola, G. M.; Vivas, E. L.; Lee, D.-J.; Chung, W.-J. Partitioning of butanol and other fermentation broth components in phosphonium and ammonium-based ionic liquids and their toxicity to solventogenic clostridia. *Separation and Purification Technology* **2011**, *78*, 164.
(124) Stepnowski, P.; Skladanowski, A.; Ludwiczak, A.; Laczynska, E. Evaluating the cytotoxicity of ionic liquids using human cell line HeLa. *HUM EXP TOXICOL* **2004**, *23*, 513.

(125) Wang, X.; Ohlin, C. A.; Lu, Q.; Fei, Z.; Hu, J.; Dyson, P. J. Cytotoxicity of ionic liquids and precursor compounds towards human cell line HeLa. *Green Chemistry* **2007**, *9*, 1191.
(126) Sipes, I. G.; Knudsen, G. A.; Kuester, R. K. The effects of dose and route on the toxicokinetics and disposition of 1-butyl-3-methylimidazolium chloride in male F-344 rats and female B6C3F1 mice. *Drug Metabolism and Disposition* **2008**, *36*, 284.
(127) Landry, T. D.; Brooks, K.; Poche, D.; Woolhiser, M. Acute toxicity profile of 1-butyl-3-methylimidazolium chloride. *Bull. Env. Cont. Tox.* **2005**, *74*, 559.
(128) Cho, C.-W.; Jeon, Y.-C.; Pham, T. P. T.; Vijayaraghavan, K.; Yun, Y.-S. The ecotoxicity of ionic liquids and traditional organic solvents on microalga *Selenastrum capricornutum*. *Ecotoxicology and Environmental Safety* **2008**, *71*, 166.
(129) Pham, T. P. T.; Cho, C.-T.; Min, J.; Yun, Y.-S. Alkyl-chain length effects of imidazolium and pyridinium ionic liquids on photosynthetic response of *Pseudokirchneriella subcapitata*. *Journal of Bioscience and Bioengineering* **2008**, *105*, 425.
(130) Matsumoto, M.; Mochiduki, K.; Kondo, K. Toxicity of Ionic Liquids and Organic Solvents to Lactic Acid-Producing Bacteria. *Journal of Bioscience and Bioengineering* **2004**, *98*, 344.
(131) Baumann, M. D.; Daugulis, A. J.; Jessop, P. G. Phosphonium ionic liquids for degradation of phenol in a two-phase partitioning bioreactor. *Appl. Microbiol. Biotechnol.* **2005**, *67*, 131.
(132) Ganske, F.; Bornscheuer, U. T. Growth of Escherichia coli, Pichia pastoris and Bacillus cereus in the Presence of the Ionic Liquids [BMIM][BF_4] and [BMIM][PF_6] and Organic Solvents. *Biotechnology Letters* **2006**, *28*, 465.
(133) Lee, S.-M.; Chang, W.-J.; Choi, A.-R.; Koo, Y.-M. Influence of ionic liquids on the growth of Escherichia coli. *Korean Journal of Chemical Engineering* **2005**, *22*, 687.
(134) Docherty, K. M.; Kulpa, C. F. Toxicity and antimicrobial activity of imidazolium and pyridinium ionic liquids. *Green Chemistry* **2005**, *7*, 185.
(135) Yang, Z.-H.; Zeng, R. W., Y.;; Li, X.-K.; Lv, Z.-S. L., B.;; Yang, S.-Q. L., J-G.; Tolerance of Immobilized Yeast Cells in Imidazolium-Based Ionic Liquids. *Food Technol. Biotechnol.* **2009**, *47*, 62.
(136) Rebros, M.; Gunaratne, H. Q. N.; Ferguson, J.; Seddon, K. R.; Stephens, G. A high throughput screen to test the biocompatibility of water-miscible ionic liquids. *Green Chemistry* **2009**, *11*, 402.
(137) Coleman, D.; Spulak, M.; Garcia, M. T.; Gathergood, N. Antimicrobial toxicity studies of ionic liquids leading to a 'hit' MRSA selective antibacterial imidazolium salt. *Green Chemistry* **2012**, *14*, 1350.
(138) Cieniecka-Roslonkiewicz, A.; Pernak, J. K.-F., J.; Ramani, A.; Robertsond, A.J.; Seddon, K.R.; Synthesis, anti-microbial activities and anti-electrostatic properties of phosphonium-based ionic liquids. *Green Chemistry* **2005**, *7*, 855.
(139) Pernak, J.; Smiglak, M. G., S.T.; Hough, W.L.; Wilson, T.B.; Anna Pernak, A.; Zabielska-Matejuk, J.; Fojutowski, A.; Kitad, K.; Rogers, R.D.; Long alkyl chain quaternary ammonium-based ionic liquids and potential applications. *Green Chemistry* **2006**, *8*, 798.
(140) Evans, K. O. Supported Phospholipid Bilayer Interaction with Components Found in Typical Room-Temperature Ionic Liquids – a QCM-D and AFM Study. *International Journal of Molecular Sciences* **2008**, *9*, 498.
(141) Weatherley, L. R. Electrically Enhanced Mass Transfer. *Heat Recovery Systems & CHP* **1993**, *13*, 515.
(142) Seader, J. D.; Henley, E. J.; Roper, D. K. *Separation Process Principles: Chemical and Biochemical Operations*; 3rd ed.; John Wiley & Sons, Inc., 2011.
(143) Weatherley, L. R. Relationship between Drop-size and Field Strength in Enhanced Whole-broth Liquid Liquid Extraction. *Speculations in Science and Technology* **1991**, *15*, 91.
(144) Weatherley, L. R.; Campbell, I.; Kirton, D.; Slaughter, J. C. Electrically enhanced extraction of Penicillin G into dichloromethane. *Journal of Chemical Technology and Biotechnology* **1990**, *48*, 427.
(145) Grace, H. P. Dispersion phenomena in high viscosity immiscible fluids systems and application of static mixers as dispersion devices in such systems. *Chemical Engineering Communications* **1982**, *14*, 225.
(146) Richardson, J. F.; Harker, J. H.; Backhurst, J. R. *Particle Technology and Separation Processes*; 5th ed.; Butterworth-Heinemann, Elsevier, 2002; Vol. 2.
(147) Bird, R. B.; Stewart, W. E.; Lightfoot, E. N. *Transport Phenomena*; 2nd ed.; John Wiley & Sons, 2002.
(148) Carolan, N.; Weatherley, L. R. The effect of additives and impurities on the partition of ethanol into n-decvanol from aqueous solutions. *Developments in Chemical Engineering and Mineral Process* **2000**, *8*, 551.
(149) Carolan, N.; Weatherley, L. R. The effect of protein and broth impurities on the partition of citric acid into n-butanol from aqueous solutions. *Developments in Chemical Engineering and Mineral Process* **2003**, *11*, 223.
(150) Stewart, G.; Thornton, J. D. In *IChemE Symposium series* 1967; Vol. 26, p 29.
(151) Bailes, P. J. Solvent Extraction in an Electrostatic Field. *Ind. Eng. Chem. Process Des. Dev.* **1981**, *20*, 564.

(152) He, W.; Baird, M. H. I.; S.;, C. J. The effect of electric field on droplet formation and motion in a viscous liquid. *The Canadian Journal of Chemical Engineering* **1991**, *69*.
(153) Tsouris, C.; Neal, S. H.; Shah, V. M.; Spurrier, M. A.; Lee, M. K. Comparison of liquid-liquid dispersions formed by a stirred tank and electrostatic spraying. . *Chemical Engineering Communications* **1997**, *160*.
(154) Taylor, G. I. Disintegration of water droplets in an electric field. *Proceedings of Royal Society of London. A* **1964**, *280*, 383.
(155) Scott, T. C. Use of Electric Fields in Sovlent Extraction: A Review and Prospectus. *Seperation and Purification Methods* **1989**, *18*, 65.
(156) Ghadiri, M.; Eow, J. S. The behaviour of liquid-liquid interface and drop-interface coalescence under the influence of an electric field. *Colloids and Surfaces A: Physicochem. Eng. Aspects* **2003**, *215*, 101.
(157) Allan, R. S.; Mason, S. G. Effects of electric fields on Coalescence in Liquid-Liquid systems. *Transactions of Faraday Society* **1961**, *57*, 2027.
(158) Bailes, P. J.; Larkai, S. K. L. Liquid Phase Separation in Pulsed D.C. Fields. *Transactions of Institution of Chemical Engineers* **1982**, *60*, 115.
(159) Gneist, G.; Bart, H.-J. Electrostatic drop formation in liquid/liquid systems. *Chemical Engineering and Technology* **2002**, *25*, 899.
(160) Briggs, M. K.; Cheng, C. Y.; Ibana, D. C. An electrostatic solvent extraction contactor for nickel-cobalt recovery. *Minerals Engineering* **2000**, *13*.
(161) Laughland, G. J.; Miller, M. K.; Weatherley, L. R. In *Extraction '87 IChem E Symposium Series No 103* 1987, p 263.
(162) Hume, A. P.; Weatherley, L. R.; Petera, J. Trajectories of charged drops in a liquid-liquid system. *Chemical Engineering Journal* **2003**, *95*.
(163) Petera, J.; Weatherley, L. R. Modeling of mass transfer from falling droplets. . *Chemical Engineering Science* **2001**, *56*.
(164) Weatherley, L. R.; Turmel, C. Terminal Velocity Studies of Whole Broth Single Drops in a Liquid-Liquid System. *Industrial Engineering and Chemistry Research* **1992**, *31*, 1739.
(165) Hume, A. P.; Petera, J.; Weatherley, L. R. Trajectories of charged drops in a liquid-liquid system: The effect of geometrical scale-up. *Industrial Engineering and Chemistry Research* **2004**, *43*, 2264.
(166) Petera, J.; Strzelecki, W.; Agrawal, D.; Weatherley, L. R. Charged Droplet and Particle-mixing Studies in Liquid-liquid systems in the presence of Non-linear Eletrical Fields. *Chemical Engineering Science* **2005**, *60*, 135.
(167) Scott, T. C. Dimensional analysis of continuous high-capacity electrodispersion of aqueous based liquids in an organic continuous phase. *Separation Science and Technology* **1990**, *25*, 1709.
(168) Cloupeau, M.; Prunet-Foch, B. Electrohydrodynamic spraying functioning modes: a critical review. *Journal of Aerosol Science* **1994**, *25*, 1021.
(169) Prestridge, F. L.; Johnson, B. C.; Sublette, K. L. Electrostatic coalescence in a solvent extraction process. *Society of Mining Engineers of AIME Transactions* **1983**, *274*, 1959.
(170) Eow, J. S.; Ghadiri, M.; Sharif, A. O. Electrostatic and hydrodyamic separation of aqueous drops in a flowing viscous oil. *Chemical Engineering and Processing* **2002**, *41*, 649.
(171) Kelly, E. G.; Spottiwood, D. J. The theory of electrostatic separations: A review part II. Particle charging. *Minerals Engineering* **1989**, *2* 193.
(172) Gupta, R.; Gidaspow, D.; Wasan, D. T. Electrostatic separation of powder mixtures based on the work functions of its constituents. *Powder Technology* **1993**, *75*, 79.
(173) Harris, M. T.; Scott, T. C.; Byers, C. H. The synthesis of metal hydrous oxide particles by multiphase electrodispersion. *Materials Science and Engineering* **1993**, *168*, 125.
(174) Weatherley, L. R.; Etuk, B.; Murray, K. R. Formation of nylon 610 capsules by interfacial polymerization in a high-voltage electric field. *Powder Technology* **1991**, *65*, 227.
(175) Takhistov, P. Dimensionless Analysis Of The Electric Field-Based Food Processes For Scale-Up And Validation. *Journal of Food Engineering* **2007**, *78*, 746.
(176) Clark, P. J. Pulsed Electric Field processing. *Food Technology* **2006**, *60*, 66.
(177) Scott, T. C.; Wham, R. M. United States, 1988; Vol. 4767515.
(178) Yang, W.; Carleson, T. E. Several effects of electric fields on liquid extraction. *IEEE Transactions on Industry Applications* **1990**, *26*, 366.
(179) Taylor, G. Studies in Electrohydrodynamics. I. The Circulation Produced in a Drop by Electrical Field. *Proceedings of Royal Society of London. A* **1966**, *291*, 159.
(180) Weatherley, L. R.; Martin, R.; Slaughter, J. C. The effect of high electric fields on the subsequent fermentation performance of cells on Saccharomyces Cerevisiae. *Biotechnology Techniques* **1990**, *4*, 79.

(181) Arnott, I. A.; Weatherley, L. R. The importance of the electrical properties of the continuous phase in electrically enhanced liquid-liquid extraction. *Food and bioproducts processing :Transactions of the Institution of Chemical Engineers, Part C.* **1992**, *70*, 219.
(182) Leys, J.; Wübbenhorst, M.; Menon, C. P.; Rajesh, R.; Thoen, J.; Glorieux, C.; Nockemann, P.; Thijs, B.; Binnemans, K.; Longuemart, S. Temperature dependence of the electrical conductivity of imidazolium ionic liquids. *Journal of Chemical Physics* **2008**, *128*, 064509.
(183) Stewart, G.; Thornton, J. D. In *IChemE Symposium series* 1967; Vol. 26, p 37.
(184) Carleson, T. E., University of Washington, 1982.
(185) Takamatsu, T.; Yamaguchi, M.; Katayama, T. Formation of single charged drops in liquid media under a uniform electric field. *Journal of Chemical Engineering of Japan* **1982**, *15*, 349.
(186) Takamatsu, T.; Hashimoto, Y.; Yamaguchi, M.; KAtayamna, T. Theoretical and experimental studies of charge drop formation in a uniform electric field. *Journal of Chemical Engineering of Japan* **1981**, *14*, 172.
(187) Vu, N.; Carleson, T. E. Electric Field Effects on Drop Size and Terminal Velocity in Liquid-Liquid Systems. *AIChE* **1986**, *32*, 1739.
(188) Scheele, G. F.; Mesiter, B. J. Drop formation at low velocities in Liquid-Liquid Systems: Part 1: Prediction of drop volume. *AIChE* **1968**, *14*, 9.
(189) Harkins, W. D.; Brown, F. E. the determination of surface tension and the weight of falling drops: The surface tension of water and benzene by the capillary height method. *Journal of American Chemical Society* **1919**, *41*, 499.
(190) Jones, E.; Petera, J.; Ting, S. C.; Weatherley, L. R. Residence time distributions in a co-current electrically enhanced liquid-liquid contactor. *Chemical Engineering Research and Design* **2003**, *81*, 601.
(191) Thornton, J. D.; Brown, B. A. United Kindgom, 1966; Vol. 1205562.
(192) Weatherley, L. R.; Campbell, I.; Slaughter, J. C.; Sutherland, K. M. In *Separations for biotechnology*; Verrall, M. S., Ed.; Horwood: Chichester, UK, 1987, p 341.
(193) Slaughter, J. C.; Weatherley, L. R.; Wilkinson, A. Electrically enhanced enzymic hydrolysis of vegetable oils using lipase from *Candida Rugosa*. *Enzyme and Microbial Technology* **1993**, *15*, 293.
(194) Weatherley, L. R.; Rooney, D. W.; Niekerk, M. V. Interfacial charge effects during natural oil hydrolysis. *Global Environmental Biotechnology* **1997**, *66*, 107.
(195) Niekerk, M. V.; Weatherley, L. R. Electrostatically enhanced enzymic hydrolysis of vegetable oil. *Food and bioproducts processing: Transactions of the Institution of Chemical Engineers, Part C.* **1996**, *74*, 22.
(196) Tsouris, C.; Blankenship, K. D.; Dong, J.; DePaoli, D. W. Enhancement of Distillation Efficiency by Application of an Electric Field. *Industrial Engineering and Chemistry Research* **2001**, *40*, 3843.
(197) Ristenpart, W. D.; Bird, J. C.; Belmonte, A.; Dollar, F.; Stone, H. A. Non-coalescence of oppositely charged drops. *Nature* **2009**, *461*.
(198) Hendricks, C. D.; Sadek, S. Electric field enhanced coalescence of drops in liquid emulsions. *IEEE Transactions on Industry Applications* **1977**, *13*, 489.
(199) Eow, J. S.; Ghadiri, M.; Sharif, A. O. Experimental studies of deformation and break-up of aqueous drops in high electric fields. *Colloids and Surfaces A: Physicochem. Eng. Aspects* **2003**, *225*, 193.
(200) Eow, J. S.; Ghadiri, M. Motion, deformation and break-up of aqueous drops in oils under high electric fields. *Chemical Engineering and Processing* **2003**, *42*, 259.
(201) Martin, L.; Vignet, P. Electrical field contactor for solvent extraction. *Separation Science and Technology* **1983**, *18*, 145501471.
(202) Kowalski, W.; Ziolkowski, Z. Increase in mass transfer in elextraction columns by means of electric field. *International Journal of Chemical Engineering* **1981**, *21*, 323.
(203) Sams, G. W.; Zaouk, M. Emulsion Resolution in Electrostatic Processes. *Energy & Fuels* **2000**, *14*, 31.
(204) Millar, M. K.; Weatherley, L. R. Whole broth extraction in an electrically enhanced liquid-liquid contact system. *Transactions of Institution of Chemical Engineers* **1989**, *67*, 227.

2. EXPERIMENTAL DETAILS

2.1. Synthesis of ionic liquids

2.1.1. Synthesis of Imidazolium based ionic liquids

1-Alkyl-3-methylimidazolium bromides [RMIm][Br] were synthesized through a quaternization reaction between 1-methylimidazole and 1-bromoalkane. Excess moles of the 1-bromoalkane were added and the reaction was conducted in an acetonitrile solvent at 40°C under an argon atmosphere with stirring for three days. The solvent was removed on a rotary evaporator under reduced pressure at 40°C and further purified under high vacuum ($<10^{-4}$ torr) at 50°C for at least two days to obtain pure ionic liquid. For the present study, three ionic liquids: [EMIm][Br], [HMIm][Br], [DMIm][Br] were synthesized. These ionic liquids were characterized using ^{1}H NMR spectra. ^{1}H NMR chemical shifts (relative to TMS internal standard) and coupling constants J/Hz for [EMIm][Br]: δ = 1.54 (t, 3H, *J*=7.4), 3.93 (s, 3H), 4.24 (q, 2H, *J*=7.36), 7.42 (d, 2H, *J*=10.3), 8.59 (s, 1H). ^{1}H NMR chemical shifts (relative to TMS internal standard) and coupling constants J/Hz for [HMIm][Br]: δ(*ppm*) = 0.87 (t, J = 6.82, 3H), 1.33 (m, 6H), 1.95 (q, J = 7.05, 2H), 4.16 (s, 3H), 4.37 (t, J = 7.41, 2H), 7.69 (s, 1H), 7.85 (s, 1H), 10.28 (s, 1H). ^{1}H NMR chemical shifts (relative to TMS internal standard) and coupling constants J/Hz for [DMIm][Br]: δ(*ppm*) = 0.75 (t, J = 6.8, 3H), 1.18 (m, 9H), 1.91 (q, 2H), 3.99 (s, 3H), 4.19 (t, J= 7.4, 2H), 7.37 (s, 1H), 7.5 (s, 1H), 10.09 (s, 1H).

Hydrophobic imidazolium ionic liquids are synthesized via anion exchange reaction between [RMIm][Br] synthesized above and lithium bis(trifluoromethylsulfonyl)amide (Li[Tf_2N]) in deionized water. The precursors are soluble in water but the resulting ionic liquid is immiscible and forms a separate liquid layer. Excess moles of the salt are added and the reaction is conducted at room temperature for around one day and formation of the ionic liquid is identified

from the formation of two phases. Denser hydrophobic ionic liquid is decanted and washed with water vigorously 6-8 times to remove any unreacted salts and dried under high vacuum (<0.013pa). Here it must be ensured that the contaminants, especially bromide are adequately removed as they may interact with the cell cultures. For the present study, [EMIm][Tf_2N] and [HMIm][Tf_2N] were synthesized. For [EMIm][Tf_2N], the ^{1}H NMR chemical shifts (relative to TMS internal standard) and coupling constants J/Hz: δ = 8.59 (s, 1H), 7.42 (d, 2H, *J*=10.3), 4.24 (q, 2H, *J*=7.36), 3.93 (s, 3H), 1.54 (t, 3H, *J*=7.4). For [HMIm][Tf_2N], the ^{1}H NMR chemical shifts (relative to TMS internal standard) and coupling constants J/Hz: δ = 8.65 (s, 1H), 7.39 (d, 2H, *J*=4.19), 4.17 (q, 2H, *J*=7.4), 3.93(s, 3H), 1.87(m, 4H), 1.32(m, 6H) 0.87(t, 3H, *J*=6.53). Water content was measured using a Mettler Toledo DL32 Karl-Fisher Coulometer and the bromide concentration was measured by a Cole Parmer Bromide electrode (27502-05) read with ana Oakton Ion 510 series meter. Water and Bromide content in [EMIm][Tf_2N] and [HMIm][Tf_2N] are less than 24 ppm & 36 ppm, and 125 ppm & 8 ppm respectively.

2.1.2. Synthesis of Ammonium based ionic liquids

Trihexylmethylammonium bromide [THMAm][Br] was synthesized by methylating trihexylamine with bromomethane. The methylation addition reaction was conducted at below room temperature around 15°C to ensure that the volatile bromomethane stays in the reaction medium which consisted of solvents methyl-tert butyl ether and acetone. Excess moles of bromomethane were added and this relatively fast addition reaction was conducted for 2 days. Excess solvent and bromomethane was removed under reduced pressure at 40°C and further dried at 100°C under high vacuum for 48 hrs. The product [THMAm][Br] was characterized using its ^{1}H NMR chemical shifts (relative to TMS internal standard): δ *(in ppm)* = 0.9 (t; 9 H; J = 7), 1.36 (m; 18H), 1.68 (m; 6H), 3.38 (s; 3H), 3.42 (m; 6H).

Dioctyl(5-cyanobutane)methylammonium bromide [DO(5-BuCN)MAm][Br] was synthesized by the addition reaction of 5-chlorovaleronitrile with N-Methyldioctylamine. The addition reaction was conducted at 95-100°C under solvent reflux to ensure that there is no loss of 5-chlorovaleronitrile in the reaction medium which consisted of acetonitrile as the solvent. Excess moles of 5-chlorovaleronitrile were added and this relatively longer addition reaction was conducted for >3 weeks. Excess solvent was removed under reduced pressure at 40°C. The reaction mixture consisting of the unconverted reactants and product were centrifuged at 15000 RPM for 25 mins to obtain clear separation of the phases. The bottom ionic liquid phase was further dried at 120°C under high vacuum for 72 hrs to remove traces of unconverted reactants. ^{1}H NMR chemical shifts (relative to TMS internal standard) for [DO(5-BuCN)MAm][Br]: δ *(ppm)* = 0.85 (t, 9H), 1.27 (m, 24H), 1.65 (m, 4H), 2.39 (m, 2H), 3.3 (s, 3H), 3.57 (m, 6H).

Dioctyl(5-hexanone)methylammonium bromide [DO(5-HxOne)MAm][Br] was synthesized in a similar manner to Dioctyl(5-cyanobutane)methylammonium bromide where the addition of 6-chloro-2-hexanone to N-Methyldioctylamine was conducted at 80-85°C under solvent reflux in a reaction medium consisting of acetone and acetonitrile as solvents. ^{1}H NMR chemical shifts (relative to TMS internal standard) for [DO(5-HxOne)MAm][Br]: δ *(ppm)* = 0.87 (t, 9H), 1.29 (m, 24H), 1.7 (m, 4H), 2.41 (m, 3H), 3.34 (s, 3H), 3.4 (m, 6H), 3.61 (d, 2H).

Tributylmethylammonium bis(trifluoromethylsuflonly)amide [TBMAm][Tf_2N] was similar to the [HMIm][Tf_2N] as described above. Here, tributylmethylammonium chloride salt was used. The ^{1}H NMR chemicals shifts (relative to TMS internal standard): δ *(ppm)* = 0.98 (t, *J*=7, 9H), 1.41 (m, 6H), 1.64 (m, 6H), 2.97 (s, 3H), 3.2 (m, 6H). The chloride concentration was measured by a Cole Parmer Chloride electrode (EW-27502-13) read with a Oakton Ion 510

series meter. The water and chloride content after purification were less than 100 ppm and 30 ppm respectively.

Trihexylmethylammonium bis(trifluoromethylsuflonly)amide [THMAm][Tf_2N] was synthesized from [THMAm][Br] similar to the [HMIm][Tf_2N]. Here acetone and water were used as solvents as [THMAm][Br] has low solubility in water. The ^{1}H NMR chemicals shifts (relative to TMS internal standard): δ *(ppm)* = 0.91 (t, *J*=6.9, 9H), 1.31 (m, 18H), 1.65 (m, 6H), 3.01 (s, 3H), 3.2 (m, 6H). The water and bromide content after purification were less than 110 ppm and 20 ppm respectively.

Trioctylmethylammonium bis(trifluromethylsuflonyl)amide [TOMAm][Tf_2N] was similar to the [HMIm][Tf_2N]. Here acetone and water were used as the reaction solvent as [TOMAm][Cl] has very low water solubility. The ^{1}H NMR chemicals shifts (relative to TMS internal standard): δ *(ppm)* = 0.91 (t, *J*=6.6, 9H), 1.3 (m, 30H), 1.67 (m, 6H), 3 (s, 3H), 3.2 (m, 6H). The water and chloride content after purification were less than 100 ppm and 17 ppm respectively.

Dioctyl(5-cyanobutane)methylammonium bis(trifluromethylsuflonyl)amide [DO(5-BuCN)MAm][Tf_2N] and Dioctyl(5-Hexanone)methylammonium bis(trifluromethylsuflonyl)amide [DO(5-HxOne)MAm][Tf_2N] were synthesized from [DO(5-BuCN)MAm][Br] and [DO(5-HxOne)MAm][Br] respectively similar to the [HMIm][Tf_2N] as described above. Here acetone and water were used as solvents instead of only water as the chloride salts had low solubility in water. The water and chloride content were less than 150 ppm and 20 ppm respectively in both of these ionic liquids. ^{1}H NMR chemical shifts (relative to TMS internal standard) for [DO(5-BuCN)MAm][Br]: δ *(ppm)* = 0.82 (t, 9H), 1.23 (m, 24H), 1.77 (m, 4H), 2.36 (m, 2H), 2.94 (s, 3H), 3.52 (m, 6H). ^{1}H NMR chemical shifts (relative to TMS

internal standard) for [DO(5-HxOne)MAm][Tf_2N]: δ *(ppm)* = 0.87 (t, 9H), 1.29 (m, 24H), 1.7 (m, 4H), 2.41 (m, 3H), 3.34 (s, 3H), 3.4 (m, 6H), 3.61 (d, 2H).

2.2. Toxicology studies

2.2.1. Bacterial cell culturing

The *Escherichia coli JM109(DE3)* strain that contains a plasmid, pDTG141, that codes for naphthalene dioxygenase (NDO), was developed and obtained from Prof. David T. Gibson at the University of Iowa. Plasmid pDTG141 carries four genes that encode NDO under the control of the T7 promoter of pT7-5.[36] Initial cell culture stock was prepared by growing bacterial colonies on a Luria-Bertani (LB) agar plate at 37°C in an incubator. A bacterial colony is transferred into 25 ml LB broth media supplemented with ampicillin (100 mg/ml) and the media is grown at 37°C and 200 RPM for 8 hours. Then 3 ml of this media is transferred into 30 ml MSB media supplemented with glucose, ampicillin, and thiamine until the OD reaches 1. The preparation of MSB is described elsewhere.[48] This cell culture is mixed with 1:1 by volume of glycerol, transferred into small vials and stored at -80°C. Fresh stock cultures from stored stocks are prepared approximately every 3 months.

Prior to the inhibition studies, all the glassware was autoclaved and transferred aseptically into a UV hood and LB medium was autoclaved for 15 mins. 400 ml of Sterilized LB medium is transferred aseptically into 1L Erlenmeyer flask. A filter-sterilized Ampicillin solution (10 mg/ml) was added to this medium to obtain a final concentration of 100 μg/ml. The refrigerated cell stock culture described above (~1 - 1.5 ml), is thawed by placing at -20°C for few minutes and then at room temperature. Thawed stock culture is added to the above medium. The flask is transferred to an orbital shaker and incubated at 37°C and 200 RPM and the cell growth is

followed by measuring the optical density (*OD*) at 660 nm. Optical density is measured in a 3ml cuvette by diluting the cell culture sample and the absorbance is measured using a UV spectrophotometer. 20 ml of cell culture is transferred aseptically in to 125 ml Erlenmeyer flasks once the exponential growth phase is reached after 6-7 hrs. Different volumes of the ionic liquid were added to these flasks such that the concentrations are below the ionic liquid aqueous solubilities. Ionic liquid solutions in acetone or water are used for easier handling and dosing. When acetone is used, the final concentration is maintained orders of magnitude below its own EC_{50} concentration. *OD* measurements are taken every 1.5 hrs for the first 6 hrs and every 6 hrs for next 18 hrs. For each ionic liquid concentration, growth is measured in at least three flasks and the *OD* reading is reported as the average with standard deviation.

An external agent added to a growing cell culture medium can affect the cell growth either temporarily (bacteriostat) or permanently (bactericide). The inhibition studies conducted by measuring the optical density only indicate whether the ionic liquid inhibits the cell growth, but it does not indicate if this inhibition is reversible or not. Here, ionic liquids whose EC_{50} are less than their aqueous solubility values were further investigated. Stock ionic liquid samples are added and the growth is followed via optical density. Stock ionic liquid concentrations chosen are similar where no cell growth is observed during the inhibition studies. Once the exponential phase is reached after 5-6 hours, the contents of the each of the control flasks along with the flasks containing ionic liquid were aseptically transferred to 50 ml centrifuge tubes and the cell culture medium is centrifuged at 3000 g for 8 mins such that the solid cell mass settles at the bottom and the supernatant liquid is clear. The solid cell mass collected at the bottom is washed using DI water after draining out the supernatant solution and the contents are centrifuged and washed again. This sequence of washing and centrifugation are repeated with DI water for three

times and with LB broth medium the final time. These washed cells are made up to initial volume using LB medium after adding ampicillin and the contents are transferred to 125 ml flasks. The flasks are placed on the orbital shaker and incubated at 37°C and 200 RPM and the growth is followed via optical density. Here the control flask is diluted so that the cell density is the same in all the flasks.

2.2.2. EC_{50} calculations

The half maximal effective concentration (EC_{50}) is commonly used to compare the toxicological effect of an external substance to the cell culture medium. This is defined as the effective concentration of the substance added that inhibits the growth rate of the cells by 50% compared that of the control. From the optical density (OD) measurements at 660 nm, a measure of cell mass is obtained. From a plot of ln(OD) with time, the specific growth rate (μ) which is the slope of the initial linear portion of the growth curve was obtained. The results were tabulated with the concentrations of the ionic liquid (C) and their corresponding μ values and compared to the control growth rate, μ_o. A number called growth inhibition index (H_o) at each concentration of the particular ionic liquid is calculated using the equation $H_o = (\mu_o - \mu) / \mu_o$. A new plot is generated by plotting the H_o with concentration and the slope of this line is β. The EC_{50} value is obtained by setting $\mu = \mu_o/2$ *and hence* $EC_{50}=\beta/2$. The EC_{50} values are reported with 95% confidence.

2.2.3. SEM microscopy

After growing the bacteria in presence of different concentrations of ionic liquids, the cell culture was prepared for SEM imaging using the following protocol. The culture was centrifuged for 5 mins at 5000 RPM to pellet the cell mass and the supernatant was removed. The cells were washed twice with DI Water. A few drops of 4% by volume of osmium tetroxide

solution were added to the pellet to stain the cells and the solution was allowed to stand for 30 mins. The solution was centrifuged and the supernatant was removed. The cell pellets were washed with 100% ethanol and centrifuged to remove the supernatant. This process was repeated twice. The cell pellets were dried using critical point drying in ethanol solvent. Here the cell pellet was placed on a plastic holding cup fitted with 0.2 μM filter to ensure cells were not lost during the drying. After the critical point drying, the dried cells were transferred on to an aluminum stub and this stub was further coated with gold particles using Sputter Coater operated at 5 mA for 3 minutes. The stubs were loaded into Leo 1550 Field emission scanning electron microscope and imaged at a field voltage of 10 kV.

2.3. Partition studies

2.3.1. Equilibrium/Partitioning

The 3-phase mixture was prepared by dissolving known about of the solute in water and the partitioning is started by addition of equal amounts of ionic liquid in air-tight vial at room temperature of 22°C. Partitioning is enhanced by mixing the contents using a magnetic bar on a stirrer plate by ensuring tiny droplets of the two phases are formed. Phase equilibrium is assumed to have been reached after 12 hrs and phase disengagement was achieved by allowing the mixture to stand for another 12 hrs. After phase engagement was observed, samples were prepared with required dilution using appropriate solvents. Solute concentrations were measured with GC-FID, while the ionic liquid concentration was measured using ICP-OES and the water concentration using Karl Fischer coulometer.

2.3.2. Solute concentration measurement using HPLC

The equilibrium partitioning of NDHD was measured in a static liquid-liquid equilibrium cell consisting of known concentration of NDHD dissolved in aqueous phase to which an equal volume of ionic liquid was added. The mixture was stirred with a magnetic stirrer and thermostated at 22°C. After 6-8 hrs of mixing, the liquid-liquid mixture was centrifuged at 8000 RPM for 10 mins to coalesce the droplets. No evidence of emulsions was observed visually or under UV-vis spectroscopy. Samples of the aqueous and ionic liquid phases (50-100 μL) were withdrawn using a calibrated pipettor and then dissolved in a small quantity of acetonitrile (1-2 ml) to ensure dissolution of all components at room temperature.

The concentration of NDHD in either of the phases of two-phase mixture was obtained using a Varian HPLC (High Pressure Liquid Chromatography) equipped with gradient pumps and UV-Vis detector. The samples are filtered with a 1 ml filter-syringe, and approximately 200 μL of the samples are injected into the HPLC injector with 20 μL injector loop. The HPLC was equipped with a SUPELCOSIL C_{18} LC-PAH column (Sigma Aldrich, # 58229; 250 mm x 4.6 mm ID, particle size 5 μm, pore size of 120 Å). Two mobile phases are used: solvent *A* is acetonitrile and solvent *B* is the DI water with 0.2% (v/v) glacial acetic acid added. The following method based on volume % was used to obtain good peak resolution: 1. 35% A for 4 minutes; 2. linear gradient from 35% A to 100% A for 2 minutes; 3. gradient 100% A to 35% A for 4 minutes; 4. 35% A for 3 minutes. Total flow rate was 1 ml/minute and the detection wavelength of aromatic NDHD is 262 nm. Prior to start of the sample analysis, the injectors, tubing, the column and the detector were washed with acetonitrile solvent to remove contaminants, after which the column was equilibrated with 35% A. The retention time for NDHD was at ~4.2 minutes. The chromatogram was analyzed using the Varian Star data system

and the peak areas were obtained by using forced peak integration. A calibration curve (R^2 = 0.9999) was prepared in the linear concentration range prior to the sample analysis. The conversion factor from this curve was used to obtain the actual concentration of NDHD in the sample analyzed. Each sample preparation and analysis was repeated at least twice and the %RSD was < 3%.

2.3.3. Solute concentration measurement using GC

For the equilibrium studies, concentrations of solutes in both ionic liquid and aqueous phases have to be measured. For the analysis of the solutes: Acetone, 1-butanol, and Ethanol, gas chromatography was used. HPLC was not used here because of the high volatility and low wavelengths of detection using the UV detector of the solutes, and low accuracies with Refractive Index detector. With GC (Gas Chromatrography), selection of the appropriate injector type is pivotal as the ionic liquids are known for their non-volatility. Finite amounts of ionic liquid are present in the injection samples prepared from either of the phases and can contaminate the injector or the column as the ionic liquid could interact with the surfaces. This problem arises mainly with split-splitless or on-column injector. Headspace gas chromatography is another technique that could be used here for measuring concentrations of volatile solutes in viscous solutions, but the technique is laborious and the results can be erroneous.

A GC equipped with direct injector was used to overcome the problem of ionic liquid contamination. In this technique, glass wool (deactivated wool, part no. 24324) placed in the path of injected sample in the injector traps the ionic liquid, without any loss of the solutes to be analyzed. The carrier gas, Helium, maintained at 10 psia, carries the vaporized solutes and solvent into the column while the ionic liquid gets absorbed into the wool. The injector consists of silanized metal liner (Restek Corp., Part # 21702) with a small aperture for carrier gas and the

vaporized solutes flow into the column. The glass wool is placed in this metal tube such that the syringe deposits the sample directly on the wool. Volatile solutes are vaporized leaving the ionic liquid on the wool. The glass wool is replaced when the peak shape of analytes starts to tail.

A packed column was used to separate the solute and solvent peaks and the FID detector was used to detect and analyze the peaks. A packed column was used instead of a capillary one because of the type of direct injector used and packed columns provides flexibility in higher loading of the solutes. Here the flame was formed using hydrogen and air gases maintained at 20psi and 5psi respectively. The sample was prepared using 200 uL pipettor with a 1:10 dilution rate. Software by 'PeakSimple' was used to integrate the peaks from the chromatogram by using baseline integration. The packed column used in the analysis was an Equity 5 column (catalog#: 28264-U) with the following properties: material - fused silica, d_f - 1.0 μm, L x I.D. - 30 m x 0.53 mm, matrix active group: bonded and poly(5% diphenyl / 95% dimethyl siloxane) phase. The following parameters were obtained through method development for 1-butanol, acetone and ethanol as listed in the below Table 2.1, Table 2.2 and Table 2.3 respectively.

Table 2.1: GC parameters used for 1-butanol analysis	
Solvent used	Acetone
Retention time	7.7 – 8.0 min
Oven temperature program	30°C for 2 mins; 30°C to 150°C for 8 mins
FID temperature	225°C
Injector temperature	70°C

Table 2.2: GC parameters used for Acetone analysis	
Solvent used	1-butanol
Retention time	3.5 – 3.9 min
Oven temperature program	30°C for 2 mins; 30°C to 150°C for 8 mins
FID temperature	225°C
Injector temperature	130°C

Table 2.3: GC parameters used for Ethanol analysis	
Solvent used	1-butanol
Retention time	3.1 – 3.3 min
Oven temperature program	30°C for 2 mins; 30°C to 150°C for 8 mins
FID temperature	225°C
Injector temperature	130°C

2.3.4. Ionic liquid concentration measurement

2.3.4.1. ICP-OES

The solubility of the ionic liquids in water was measured with a Varian UV-Vis spectrometer (BIO300) and using a Jobin-Yvon Inductively coupled plasma optical emission spectrometer (ICP-OES, JY 2000). ICP is a high sensitivity method to detect the concentration of the ionic liquids that contain sulfur, phosphorus, and halides, etc. This allows the measurement at trace concentrations that would be difficult to obtain with NMR, HPLC, etc. For the Ionic liquids that contain sulfur or boron in the anion, the concentrations in the aqueous medium were measured at the primary wavelengths of 181.978 nm and 249.773 nm respectively. Calibration curves were

prepared using ammonium sulfate and ammonium tetrafluoroborate as the calibration standards and R^2 values between 0.995-0.999 were obtained. Equal volumes of ionic liquid and water are allowed to equilibrate, and the centrifuged aqueous phase sample is diluted further with DI water. This diluted solution was analyzed using the ICP and the actual aqueous solubility concentrations of the ILs were obtained. Each sample preparation was repeated twice and a standard deviation of 2-3% reported. The ICP parameters used in the analysis of the aqueous solutions are listed in the Table 2.4 below.

Table 2.4: ICP-OES operating parameters

Pump power	1000 W
Speed	20 RPM
Concentric glass nebulizer flow rate	0.02 L/min
Concentric glass nebulizer pressure	2.4 bar
Plasma argon pressure	620.5 kPa
Nebulizer argon pressure	620.5 kPa
Plasma gas flowrate	12 L/min
Sheath gas flowrate	0.2 L/min
Auxiliary gas flowrate	0 L/min
Sample handling:	
- Rinsing	10 s
- sample transfer	10 s
- stabilization	5 s

2.3.4.2. UV-Vis spectrophotometer

For measuring molecular toxicity, aqueous solubility of each ionic liquid is required to obtain the saturation concentration, as only concentrations lower than the saturation concentration are considered for these studies. This is the maximum amount of IL that partitions into aqueous phase at equilibrium. In this work, Varian Cary 300 Bio UV-Vis spectrophotometer was used to measure the maximum solubility of imidazolium based ionic liquids in water. Methanol was used as the dilution solvent. Initially, the characteristic absorbance peak for an IL was identified by dissolving a small known volume (50-100 μL) of IL in a 3 ml cuvette containing methanol and scanned over the 190-800 nm range to see where an absorbance peak of the IL exists (usually between 205-230 nm). Once the characteristic wavelength was obtained from peak scan, calibration curve was developed by dissolving a known amount of IL in methanol while ensuring that the resulting absorbance vs. concentration is a linear plot and hence follows the Beer's law. From the plot, the slope is obtained and the R^2 value indicates the errors. For the ionic liquids investigated, a R^2 value > 0.995 has been obtained. For obtaining the saturation concentration, equal volumes of ionic liquids in water were added to 10 ml vial and mixed on a magnetic stirrer for one day. The solutions were separated into two phases in a Eppendorf Centrifuge (5451C) for 10 minutes at 8,000 RPM. Aqueous samples were diluted accordingly and average absorbance over three measurements obtained. The standard deviation was ±0.0005. Actual ionic liquid concentration in the aqueous phase was obtained from the calibration.

2.3.5. Karl-Fischer coulometer

The water content in the centrifuged ionic liquid bulk phase was measured using Mettler-Toledo DL 32 Karl-Fischer coulometer. The vessel is rinsed with water, then acetone and

hexane or ethanol as needed to remove organics. Then the interior of the vessel was coated with 65% nitric acid and rinsed off with water. Finally, the vessel was rinsed with methanol and dried. The electrode used was cleaned by dipping it in 65% nitric acid and slowly spun to burn off organics. Then it was rinsed with water and finally with methanol. The voltage probe was rinsed with methanol. The dried vessel was filled with AQUASTAR Combicoulomat Firtless reagent. The electrode and the probe are placed in the vessel and to ensure no moisture inside the vessel, the connections were greased. Drierite was placed above the electrode in a tube to eliminate moisture. The electrical connections were made and the instrument pre-titrated and calibrated using standard solutions of 100 and 1,000 ppm. For the IL sample, around 300 mg of sample was injected to obtain the water concentration in ppm. The following parameters were used in the Karl-Fischer coulometer: speed – 40%, mixing time - 20 sec, current - 2 μA, end point - 100 mV and drift speed - 5 μg/min.

2.4. DC Electric fields

2.4.1. Synthesis of non-Newtonian continuous and dispersed phases

2.4.1.1. Preparation of Continuous phase

The initial focus of the work was to identify a continuous phase which exhibited non-Newtonian rheology. Here the approach taken was to first choose a Newtonian continuous phase whose physical properties allow the application of electric fields across its volume and then modify its rheology by the addition of a modifier. Commonly reported solvents used in the electric field applications are oils such as sunflower, vegetable, silicone, and mineral oil, tributylphosphate (TBP) and alcohols such as n-decanol. Simpler solvents like n-decanol and mineral oil were chosen and different modifiers were added to modify their rheology. Rheology

of the resulting solutions was measured using a viscometer. Modifiers used included Polyisobutylene (PIB) polymer, paraffin wax, isobutylene, methyl methacrylate etc. Addition of different rheological modifiers to n-decanol did not change its rheology. While small amounts of the Polyisobutylene, commercially available as Oppanol® B100, were found to modify the rheology of mineral oil significantly. The resulting solution has apparent viscosity 5-20 times higher than the pure mineral oil and exhibited a shear thinning rheology with power law index less than 1.

For the preparation of the solution, a weighted quantity of the solid polymer was first dissolved using solvent hexane in a 4L Pyrex beaker. To this solution, mineral oil is slowly added while ensuring the contents are stirred vigorously. The above mixture was further stirred under high heat in a fume hood for 3 days to form a uniform solution and to simultaneously evaporate the hexane solvent. Before using the newly synthesized continuous phase, a simple flame test was conducted to check the flammability of the solution. This was done as there is a potential for formation of sparks with application of electric field and this could cause safety hazard if solvent hexane is present in the mixture. This test was conducted by trying to ignite a solution sample for and it was concluded that the solution was not flammable as the sample did not catch fire. Around 2.7 litres of mineral oil phase modified by adding 1% and 3% of Oppanol (by weight) were prepared and used for tracking of the trajectories of the charged droplets.

2.4.1.2. Preparation of Dispersed phase

Enhanced dispersion of aqueous media in an organic continuous phase is the most common applications of electric fields. The enhancement is attributed to high charge accumulation on the aqueous droplet which is a result of higher electrical conductivity of the aqueous phase.

Aqueous solutions of Carboxymethylcellulose (CMC) were used as the dispersed phases. Addition of CMC modifier increases viscosity and electrical conductivity of the aqueous medium. Different weight by volume concentrations of CMC in water were prepared by dissolving known weights of CMC in water followed by occasionally heating and stirring. CMC solutions were prepared freshly as the CMC starts to settle at the bottom of the beaker upon storage, which could change its physical properties.

2.4.1.3. Equilibration of phases

Pure phases were equilibrated by stirring and the phases were separated by centrifugation. Due to the highly viscous nature of some of the non-Newtonian phases studied, equilibration of the phases through mixing followed by phase separation was not practically feasible. Each dispersed phase was equilibrated with corresponding continuous phase in the column manually by adding the dispersed phase in to the continuous phase and drawing the dispersed phase from the bottom after allowing sufficient time for mass transfer to occur. This was process was repeated 5-6 times before starting the experiments.

2.4.2. Experimental setup

2.4.2.1. Contacting column configuration and geometry

The dispersed and the continuous phases were contacted in a rectangular-shaped contacting column made from glass and PVC. Here glass was used instead of plastic for unhindered recording of particle motion, easy cleaning and less susceptibility to sticking. A rectangular cross-section was chosen instead of an easy-to-use quick fit cylindrical geometry to reduce optical distortion / parallax errors present from the curvature of the column. This becomes even more important when three dimensional data is collected, which was the case in these experiments. Columns used in previous lab studies were used here. The column was fabricated

by gluing 4 transparent glass slabs each of thickness 1" to a PVC block at the base as shown in the Figure 2.1. The inner side of the PVC block is conical shaped to ensure that the dispersed phase droplets settle quickly at the bottom and the outside of the PVC block is flat so that the column can be held vertically. A hole was drilled at the bottom of the PVC to withdraw the dispersed phase from the column. To prevent the electric charge discharge, it must be ensured that the dispersed phase does not come in contact with the bottom electrode and that the bottom electrode is immersed in the continuous phase. For this a peristaltic pump was used to control the level of the dispersed phase collected at the bottom. The column was stabilized by placing it on a heavy slab made from wood. This column setup was placed in a rectangular aluminum framework to ensure safety and reduce any electrical contact. A safety switch was installed at the door of this framework which ensures any unexpected access to the setup would result in switching off the high voltage electric field. The column geometry, shown in Figure 2.1 below, was selected by evaluating 4 columns readily available based on the ease of tracking of droplet trajectory. The data for the particular column geometry used are listed in the table below. The dimensions of the rectangular part are 22cm x 10cm x 10cm. Of the dimensions listed in Figure 2.1, I and E were varied during the experimental runs. Different PVC lids that fit on to the column top were fabricated and used to hold nozzles of different dimensions. Additionally, these lids had a hole to insert the thermocouple probe.

Figure 2.1: Column geometry

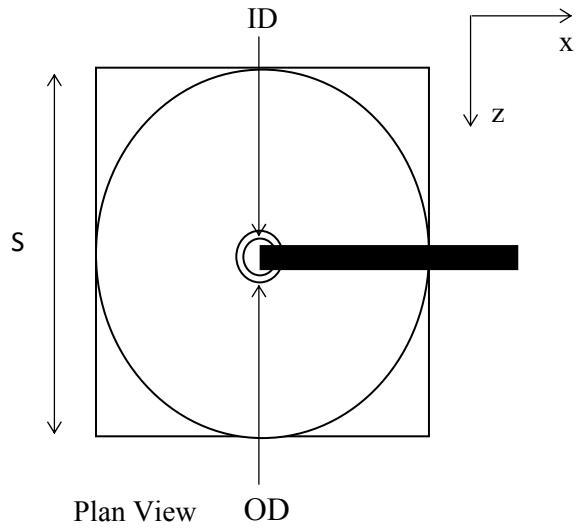

COLUMN GEOMETRY DATA		
B	Distance between the charged electrode and top of the inverted cone	20 mm
D	Electrode insertion depth	8.78 mm
E	Exposed Electrode length (no insulation)	3.71 mm
I	Inter-electrode Distance	193.6 mm
ID	Earthed Electrode Inside Diameter	2.49 mm
OD	Earthed Electrode Outside Diameter	3.25 mm
S	Square column side length	100.45 mm

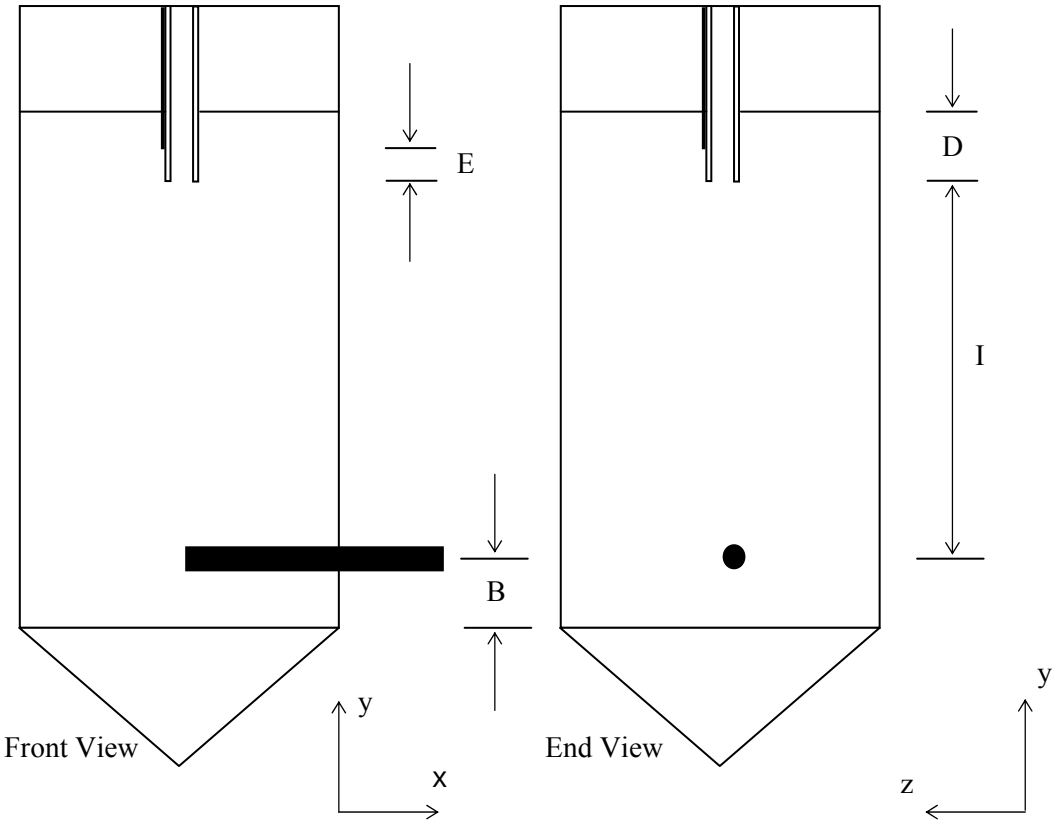

2.4.2.2. High voltage electric field

The electric field was generated by using high voltage equipment (Glassman, catalog # EK60R10). This equipment is used to generate an applied voltage of up to 60 kV with maximum power usage of 600 watts. The applied voltage across the column was generated by connecting the high voltage cable to the top electrode or the nozzle and by earthing the bottom electrode. The applied electric voltage across the column causes heat generation due to joule heating. Safety precautions: This equipment has current monitoring switch, which turns off the voltage if there is any current flow across the continuous phase. For the current work, the auto switch off current was varied between 0.5-1 milliamps. All the metal parts involved with this experimental setup are earthed to prevent any electric shocks. Applied voltages above 25 kV were not used because of electric discharge that occurs at the bottom electrode to which the high voltage is applied. This electrode is exposed to surrounding to air which leads to a discharge.

2.4.2.3. Electrodes

The electric field was applied across the continuous phase through two electrodes, the bottom and the top electrode. The bottom electrode or the fixed electrode is a 1/8" stainless rod covered with an insulating material like Teflon except for the ends. This electrode was placed in the column horizontally by drilling a hole through the PVC block such that the tip of this electrode and the top electrode are in a straight line. The top electrode or the replaceable electrode is a hypodermic needle which also serves the dual purpose of a nozzle for the dispersion of the droplets. This is also insulated with heat shrink tubing except for the ends. Immersion depth of the top electrode in the continuous phase is controlled by holding the electrode using a PVC lid where the lid is held tightly at the top of the column. The column was placed on a heavy wooden

block which acts as a sturdy base and also an insulator of electricity in case of any unexpected leakage.

For obtaining clear images around 12 x 60 W bulbs were used instead of high beam lighting to prevent heat generation. The small amount of heat generated from using the bulbs and from the applied electric field near the column was reduced by placing a fan near the setup. A thermocouple based digital temperature meter with a 12" long probe was used to track the temperature at different levels inside the column.

Electric field losses through the front wall of the column were measured, using a non-contact PCS-715 Static Locator, at an interval of 30 minutes for over a period of 2 hours. At an applied voltage of -7.5 kV, the average field loss across the length of the front wall was almost unchanged, though it appeared the loss at the charged bottom electrode were marginally higher. The average field loss was -300 V. At higher applied voltages the losses increased, with the losses decreasing from the charged electrode to earthed electrode. At an applied voltage of -10 kV, the average field loss was -375 V.

2.4.2.4. Perfusor calibration

A Perfusor syringe pump VI was used to pump a known volume of dispersed phase into the column at a constant volumetric flow rate. For calibrating the pump, dispersed phase is filled into in a 30 ml or 60 ml plastic syringe after rinsing the syringe with the dispersed phase and it is ensured that no air bubbles are present, while silicone tubing transfers the contents of the syringe to the nozzle. The volumetric flow rate for each knob setting of the pump

Table 2.5: Calibration of the Pump

Knob setting	*Flow rate (ml/hr)*
7	30.4
8	71.4
9	180.2
10	360.4

was calibrated by measuring the volume of distilled water collected in a given amount of time. This was repeated three times and the volumetric flow rate is reported as an average value as given in Table 2.5. The syringe pump was placed at the top of the framework and the pump was also grounded to avoid short circuiting from the charge transfer through the tubing carrying the dispersed phase. Two pumps were used to control flow rate of dispersed phase: one to pump dispersed phase into the nozzle and the other to remove the dispersed phase from the column and avoid any excess accumulation at bottom electrode.

2.4.2.5. Imaging

Time dependent three-dimensional trajectories of the drops were recorded using a digital camera DSC-f828 (30 frames/sec) from a distance of 3 to 4 feet. A plane mirror placed at an angle of 45° to the glass column facilitated recording of Y-Z trajectories of the droplets (Figure 2.2). Transparent sheets with grids printed on them were attached to the rear sides of the column. A white background was created to obtain clear images which is crucial for image analysis to obtain actual droplet trajectory data. Additionally, droplets were photographed and droplet formation recorded by using a zoom-in lens from closer distances to obtain high resolution images. This setup is shown in the figure 2.2. Recorded videos and photographs were digitized and the droplet trajectory data were obtained using image analysis software 'IMAGEJ'.

The accuracy of the imaging setup was analyzed as follows. A steel ball of known diameter was suspended in a setup similar to the actual experimental setup and images taken and analyzed to obtain the average droplet size. The error between experimental and actual dimensions was calculated to determine the accuracy of the setup. This error was found to be less than 3%, validating the imaging technique and analysis used.

Figure 2.2: Experimental set-up for droplet trajectory tracking

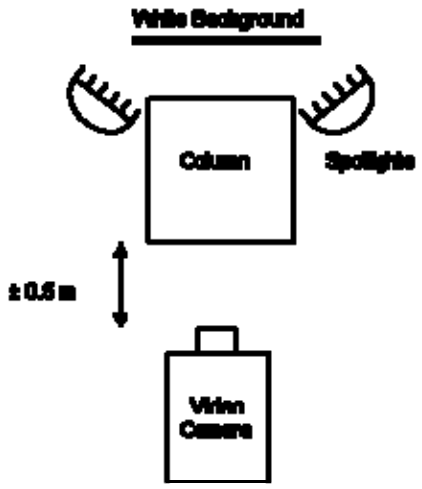

2.4.2.6. Image analysis software

IMAGEJ is a free java based open architecture software and is used for image processing. This software was developed at National Institute of Health (NIH). The software has regularly updated plug-ins, some of which can used to select circular or elliptical shapes, obtain respective diameters, position of the drop from a reference point, track the drop motion, and measure horizontal and vertical distances.

2.4.2.7. Droplet trajectory

The analysis is started first by splitting the video into images at equal time intervals based on a known number of frames. This helps in keeping track of the time for each image. All these images are sequentially loaded into the software using 'image sequence' command. To the get the droplet trajectories, the following numbers are first calculated

a. Scaling factor.

b. Co-ordinates of the center of the nozzle tip (taken as the origin).

c. Co-ordinates of the droplet in the loaded image sequence.

Averaging the distances in pixels between major grids and dividing this number by the actual measured distance between the grids gives the scaling factor. Co-ordinates of the nozzle tip are obtained by finding the mid-point of the straight line drawn along the diameter of the nozzle. Position of a particular droplet during its trajectory is measured by drawing a circle around the droplet and the center of the droplet gives the co-ordinates at that instant. Using the scaling factor and the nozzle co-ordinates, the actual droplet co-ordinates (in centimeter) are calculated. Co-ordinates of tracked drop along with the corresponding time are tabulated in a excel sheet. These steps are repeated to get the Y-Z trajectory from the same set of images. Finite difference approximated velocities of the droplets can also be calculated from the trajectory data.

2.4.2.8. Droplet diameter

First, scaling factor was calculated for the high-resolution image similar to the method adopted while calculating the droplet trajectory. Here, mostly dimensions of the nozzle that are known already were used as the reference scale. Droplets were sometimes spherical or ellipsoidal in shape depending upon the phases used and the applied electric field. The eccentricity of the droplet can be known along with the diameter of either the spherical droplet or the minor and major axis diameters for the elliptical droplet. Droplet diameter was hence calculated by drawing a circle around the droplet circumference and measuring area of the circle. Due to the blurredness inherent with the measurement technique, an average area is obtained by repeatedly drawing circles. Corresponding average droplet diameter is obtained from the averaged area. Some of the videos and photo recorded were taken at improper angles, hence were corrected during the image analysis by rotating the images to make them vertical.

2.4.3. Physical property measurement

For the studies involving dispersion of droplets in presence of electric fields, measurement of physical properties of both phases gives important information on understanding how the droplets behave, developing correlations and simulating droplet trajectories. Consequently, important physical properties of the continuous and the dispersed phases such as interfacial tension, density, viscosity, electrical conductivity, and dielectric constant were measured. This section provides details on the measurement of the physical properties. Though the dispersion of the droplets was performed under zero heat and mass transfer conditions, there were fluctuations in the room temperature and around ±3°C change in temperature along the length of the column during an experimental run. To address this issue, physical properties were measured as a function of temperature wherever it is possible.

2.4.3.1. Density

For the studies involving liquid-liquid contacting, the separation of phases under gravity was based on the density difference between the two phases. Densities of both the phases were directly measured using a densitometer (Model# Anton Paar DMA 4500) instrument. The accuracy of the instrument is ±0.00005 g/cm^3. Table 2.6 and Table 2.7 show the temperature dependence of density for continuous and dispersed phases (measured between 20 - 40°C).

Table 2.6: Temperature dependence of density for continuous phases

Continuous Phase	*Temperature dependence (ρ in gm/cm^3) (T in °C)*
Mineral Oil	-0.0006*T + 0.8686
1% PIB in Mineral Oil (by w/w)	-0.0006*T + 0.8684

3% PIB in Mineral Oil (by w/w)	-0.0006*T + 0.8704

Table 2.7: Temperature dependence of density for dispersed phases

Dispersed Phases	*Temperature dependence (ρ in gm/cm^3) (T in °C)*
Water	-0.0003*T + 1.0035
3% Aq. CMC used with Mineral Oil	-0.0003*T + 1.0196
3% Aq. CMC used with 1% PIB in Mineral Oil	-0.0003*T + 1.0183
3% Aq. CMC	-0.0003*T + 1.0179
5% Aq. CMC	-0.0003*T + 1.0275
7% Aq. CMC	-0.0003*T + 1.0397

2.4.3.2. Interfacial tension

For the dispersion of a liquid phase into a second phase (either liquid/gas), the interfacial tension data for the system provides crucial information relating to droplet size. Interfacial tension is defined as the attractive force between two molecules of the two phases at their interface. Interfacial tension data for different sets of continuous and dispersed phases were measured using a EasyDyne Tensiometer (manufactured by Kruss, catalog# K20) employing an accurate Du Nouy ring method. Accurate temperature dependency of the interfacial tension was obtained as the instrument was equipped with a jacketed vessel along with a temperature probe. In these measurements it was ensured that both the phases are pure as presence of any

contaminants could make the readings random. To overcome the difficulties in equilibrating and separating the viscous phases, pure systems were used. Attempts to equilibrate the phases resulted in formation of stable emulsions. Table 2.8 below shows the results obtained with 5 different systems.

Table 2.8: Interfacial tension data as a function of temperature

Phase	*Average temperature dependence over 24-30°C (in mN/m), (T is in °C)*
Mineral Oil and Water	50.15
Mineral Oil and 3% Aq. CMC	46.50 ± 5 %
1% PIB in Mineral Oil and Water	38.75 ± 5 %
1% PIB in Mineral Oil and 3% Aq. CMC	34.85 ± 4 %
1% PIB in Mineral Oil and 7% Aq. CMC*	-
3% PIB in Mineral Oil and Water	23.03 ± 3 %
3% PIB in Mineral Oil and 3% Aq. CMC	20.00 ± 3 %
3% PIB in Mineral Oil and 5% Aq. CMC	19.90 ± 3 %
3% PIB in Mineral Oil and 7% Aq. CMC*	-

* As the phases were very viscous, it was difficult to handle the solutions and measure the interfacial tension.

2.4.3.3. Rheology

Rheology and apparent viscosities of the continuous and dispersed phases provide an understanding of mixing effects, reduction of droplet size, formation of fine dispersion, and hence any effect on mass transfer between the phases. The viscosity of the phases was measured using two different instruments: (1) Bohlin CS-10 rheometer (Malvern Instruments, Malvern, England) which uses the 40 mm/4° cone-and-plate geometry for high viscosity shear stress vs. shear strain measurements and (2) A Brookfield DV-III Ultra Rheometer which uses the cone/plate method (model no:, LVDV-IIIU) for measurement of low viscosity Newtonian systems. Temperature dependence of the viscosity was measured as both the instruments are fitted with temperature controlled jackets. From the viscosity measurements, it can be seen that Oppanol (PIB) acts as rheology modifier of mineral oil as shown in the Table 2.9 (measured between 20 – 35°C). The resulting 1% and 3% by wt. solutions exhibited shear thinning behavior with power law indices of 0.99 and 0.85. The 3% solution becomes very viscous with apparent viscosity of 2,000 cP. Addition of CMC modifies the viscosity of the aqueous medium significantly with the 7% CMC exhibiting a viscosity 2,000 times more than pure water.

Table 2.9: Rheology of continuous and dispersed phases as a function of temperature

Phase	*Temperature dependence (μ in CentiPoise, τ in N/m^2, γ in s^{-1})*
Mineral Oil equilibrated with Water	$\mu_c = \exp\left[\frac{4510.2}{T} - 11.419\right]$
Mineral Oil equilibrated with 3% Aq. CMC	$\mu_c = \exp\left[\frac{4674.2}{T} - 11.94\right]$

Table 2.9: Rheology of continuous and dispersed phases as a function of temperature	
Phase	*Temperature dependence (μ in CentiPoise, τ in N/m^2, γ in s^{-1})*
1% PIB in MO (by w/w)	**T = 303.15 K, $\tau_c = 76.78\ \gamma_c^{0.9898}$** **T = 301.15 K, $\tau_c = 83.54\ \gamma_c^{0.9865}$** **T = 300.15 K, $\tau_c = 87.76\ \gamma_c^{0.9915}$**
Water	$\mu_d = \exp\left[\frac{2014.5}{T} - 6.8717\right]$
3% PIB in MO	**T = 297.15 K, $\tau_c = 2120\ \gamma_c^{0.8473}$** **T = 300.15 K, $\tau_c = 1851\ \gamma_c^{0.8566}$** **T = 303.15 K, $\tau_c = 1568\ \gamma_c^{0.8671}$**
3% Aq. CMC	**T = 297.15 K, $\tau_d = 43.82\ \gamma_d^{0.9786}$** **T = 300.15 K, $\tau_d = 36.49\ \gamma_d^{0.9809}$** **T = 303.15 K, $\tau_d = 30.88\ \gamma_d^{0.9817}$**
5% Aq. CMC	**T = 297.15 K, $\tau_d = 384.2\ \gamma_d^{0.8782}$** **T = 300.15 K, $\tau_d = 430.5\ \gamma_d^{0.8627}$** **T = 303.15 K, $\tau_d = 440.6\ \gamma_d^{0.8541}$**
7% Aq. CMC	**T = 297.15 K, $\tau_d = 1919\ \gamma_d^{0.7881}$** **T = 298.65 K, $\tau_d = 2227\ \gamma_d^{0.7671}$**

2.4.3.4. Electrical conductivity

For experiments that involve application of electric fields, knowledge of electrical conductivity of both phases provides information on charge transfer. For the continuous phase, the electrical conductivity must be $<10^{-12}$ S/cm so that electrical discharge does not occur during

an experimental run. For the dispersed phase, the electrical conductivity must be higher so that the droplet during its formation accumulates charge near the nozzle. The electrical conductivity for the aqueous dispersed phases was measured using a Thermo conductivity meter (Thermoscientific, Catalog# 1217000-WA) at different temperatures using a 50 ml jacketed beaker (ChemGlass, Catalog # CG1103-01). Electrical conductivity as a function of temperature is shown in the Table 2.10 below. The temperature was controlled using a Fisher Scientific temperature bath. However for the continuous phase, electrical conductivity measurement was not possible due to its very low electrical conductivity. Values reported in the literature for both the mineral oil and the rheological modifier were used.

Table 2.10: Electrical conductivity of dispersed phase as a function of temperature

Phase	*Temperature dependence*
Water	EC = -0.0306*T + 10.77 (in μS/cm)
3% Aq. CMC used with Pure Mineral Oil and 1% PIB in pure Mineral Oil	5.23 mS/cm
Pure 3% Aq. CMC	5.23 mS/cm
Pure 5% Aq. CMC	EC = 0.0247*T + 7.5348 (in mS/cm)
Pure 7% Aq. CMC	EC = 0.0175*T + 10.2 (in mS/cm)

2.4.3.5. Dielectric constant

Initial dielectric constant measurements were attempted using parallel plate capacitor and LCR meter but this proved unsuccessful. Dielectric constant data for mineral oil of 2.1 was sourced from literature and used for the study. Similarly dielectric constant data for PIB of 2.2

was sourced from the manufacturer's (BASF's) technical specifications. Dielectric constant of 2.1-2.2 was used for 1% PIB in mineral oil and 3% PIB in mineral oil, because of low weight percentages of PIB in mineral oil. Table 2.11 gives a summary of range of dielectric constant values.

Table 2.11: Dielectric constant

Phase	*Temperature dependence*
Mineral Oil	2.1
PIB	2.2
1% PIB in MO (by w/w)	2.1-2.2
3% PIB in MO (by w/w)	2.1-2.2

2.4.4. Description of a sample experimental run

To conduct an experimental run, continuous phase, dispersed phase, pump knob setting, nozzle dimensions, various parameters like B, E, I, OD and ID are chosen. The column was filled up with the continuous phase and checked for any possible leaks. The dispersed phase was equilibrated with the continuous phase in the column prior to actual experimental run. The dispersed phase was collected in a syringe and the tubing from the pump connected to the nozzle. Before the experiments with electric fields were performed, a voltage of ±15 kV was applied across the column for at least 2 hrs to allow for the space charge migration near the electrodes. During this time the lighting bulbs and fan were also switched on. The temperature was measured using a thermocouple for each set of experiments before the start and at the end of the experiment to measure the change in temperature of the column; an average temperature is reported.

An experimental run was started by selecting a knob setting on the pump and adjusting the peristaltic pump speed at the bottom to withdraw the dispersed phase simultaneously such that upper level of the continuous phase in the column does not change. Simultaneously, the required voltage is set. This set up was allowed to reach steady state for 1-2 minutes and then the video recording of the falling droplets conducted for one minute. Simultaneously the zoom-in images of the falling droplets were recorded for the purpose of measurement of the droplet diameter. The applied voltage was changed and the capture of the droplet trajectories repeated. Each experimental run usually lasted for one hour. The temperature of the organic phase was noted at 3 levels – top, bottom and middle at the beginning and at the end of each experimental run. For a given combination of continuous phase and dispersed phase, the knob settings, and other column parameters were changed and the video recording repeated. Table 2.12 gives an overview of the different experiments conducted.

Table 2.12: Summary of the dispersed and continuous phases studied along with their rheology

Continuous phases	*Dispersed phases*	*Rheology*
Mineral oil	Water	Newtonian vs. Newtonian
Mineral oil	3% CMC	Newtonian vs. Non-Newtonian****
1% PIB*** in Mineral Oil*	Water	Non-Newtonian vs. Newtonian
1% PIB in Mineral Oil*	3% CMC 7% CMC**	Non-Newtonian vs. Non-Newtonian
3% PIB in Mineral Oil*	Water	Non-Newtonian vs. Newtonian
3% PIB in Mineral Oil*	3% Aq. CMC 5% Aq. CMC	Non-Newtonian vs. Non-Newtonian

	7% Aq. CMC	

* All the phases used were prepared based on w/w basis.

** CMC – Refers to Carboxymethyl cellulose

*** PIB – Refers to Polyisobutylene or Oppanol B100

2.4.5. Obtaining time dependent xyz data and droplet diameters

The time dependent xyz data and droplet diameters were obtained in four steps: a) capture 3D videos and images of the droplets, b) convert the videos into images, c) extract time dependent data from the images and d) measure droplet diameters

a. 3D images: The 3D images were captured using a type of FS30 camera fitted with a zoom-in lens and mounted on a tripod. To improve the quality of the imaging, 10 60W bulbs were used to lighten the column instead of high beam lighting. Low heat bulbs are used instead of the high beam lights which raise the temperature of the setup very rapidly thereby potentially introducing other modes of momentum transfer like heat transfer. The image quality is improved by making the background uniform using white foam sheets. A 3D perspective of the experiment was captured by placing a plane mirror alongside one face of the column, such that XY and YZ planes are captured next to each other on the camera.
b. Discrete images of the experiment were obtained from the videos using Video Charge, a video imaging software.
c. From each image, a droplet trajectory point is extracted and the time dependent xyz data was tabulated from a set of images for an experimental run. In all of these images, the

nozzle tip was used as the reference point and the droplet positions tracked in reference to this point. For converting the pixel data into real trajectory data, a grid was used to two sides of the column. The vertical and horizontal grid length was measured before the experiments and the pixel grid length is compared to the real grid length and a scaling number is obtained. Finally, the droplet pixel co-ordinates are converted to real time data using this scaling factor.

d. Droplet diameters were obtained from close up images of the falling droplets. Image processing software Image J was used to measure the droplet diameters digitally.

2.4.6. Experimental parameters studied

Table 2.13 and Table 2.14 gives a summary of the different column parameters, along with the combination of continuous and dispersed phase and the range and polarity of the electric fields studied.

Table 2.13: First set of experiments

1ST SET OF EXPERIMENTS

Nozzle Type	***SMALL NOZZLE***			***SMALL NOZZLE with higher THICKNESS***			***MEDIUM NOZZLE***			***MEDIUM NOZZLE with INSERTION***			***BIG NOZZLE***		
Knob Setting	8	9	10	8	9	10	8	9	10	8	9	10	8	9	10
MINERAL OIL – WATER	-	-	-	-	-	-	1,2,**5**,8,**10**	-	1,2.5,8, **10,** 12,14,16, 18,20, **22**,25,27,28	-	-	-	-	-	-
MINERAL OIL -- 3% aq. CMC	-	-	-	-	-	-	0,1,2,8,9, 10,**11**,	-	1,2,5,7,8, **11**	-	-	-	-	-	-
1% PIB IN MINERAL OIL – WATER	-	-	-	-	-	-	10,**12.5**, 17.5	10, 17.5	7.5, 10, **12.5**, 15, **17.5**	-	-	-	**13.5**	13.5	**17.5**,20,21.5,**24**
1% PIB IN MINERAL OIL -- 3% aq. CMC	**10**	**15**	**12.5**	**10**	**10,** 12.5	**12.5**	**12.5**	15	17.5, 15	**12.5**	12.5	15, **17.5**	**12.5**	12.5	10, 12.5, 15
1% PIB IN MINERAL OIL -- 7% aq. CMC	10, 12.5	12.5	-	-	-	-	15. 17.5	17.5, 22.5	5, 12.5	-	-	-	12.5	15	12.5

Note: All the electric field voltages in the first set of experiments are of negative polarity.

Table 2.14: Second set of experiments

Nozzle Type	SMALL NOZZLE			SMALL NOZZLE with higher THICKNESS			MEDIUM NOZZLE			BIG NOZZLE			BIG NOZZLE with Large Insulation length			Medium Nozzle with Insertion Depth		
usor Knob Setting	8	9	10	8	9	10	8	9	10	8	9	10	8	9	10	8	9	10
PIB IN MINERAL OIL -- WATER	-	-	-	-	-	-	2,6,10,15, 20	10, 15, **20**, 23	10, 15, **20**	**-15, -13.5**	-15, -13.5	**-15, -17.5, -13.5**	-	-	-	-	-	-
PIB IN MINERAL L -- 2% aq. CMC	-15, -20	-15, -20, -22	-15, -20	-	-	-	-15, -20	-15, -20	-15, -20	-15, -20	-15, -20, -22, -25	-20, -25	-	-	-	-	-	-
PIB IN MINERAL L -- 3% aq. CMC	-15, -20	**-20**	-20	-15, -20	-15, **-20**	-	-5, -10, -15, -20, +10, +15, +20	-15, **-20**, +15, +20	-20	-15, -20	**-15, -20, +15**	-20	-15, -20, -24	-15, **-20**	-20	-15, -20	-15, **-20**	-20
PIB IN MINERAL L -- 5% aq. CMC	-	**-20**, +20	-20, -25, +20, +25	-	-	-	-	**-20, +20**	-20, +20	-15, -20, -25, +15, +20	-20, +20	+20, **-20,** -25	-20	0, -20	**-20**	-	-20	-20
PIB IN MINERAL -- 7% aq. CMC**	-10, -15, +10, +15	-15, +15, **- 20**	-	-	-	-	-15, +15	**-15,** -20, +15	-15, -20, +15	0, -10, -15, **-20**, +10, +15	0, -10, -15, **-20,** +15, +20	0, -5, +5	-	-	-	-	-	-
PIB IN MINERAL L -- Aq Xanthan Gum**	-15, -20	-15, **-20**	-15, **-20**	-	-	-	-15, -20	-15, **-20**	-	0, -10. -5, -20	0, -15, **-20,**	0, **-15,** -20	-	-	-		-	-

Note: The numbers in **bold** denote the experiments where the droplet trajectory are digitized**.**

2.5. Materials

1-Methylimidazole, (CAS 616-47-7, 99+%), lithium bis(trifluoromethylsulfonyl)amide (CAS 90076-65-6, 99.95%), 1-butanol, acetone, ethanol, were purchased from Sigma Aldrich. 1-Bromohexane (CAS 111-25-1, 99+%), were purchased from Acros. KF coulometer solutions and standards from EMD chemicals.

LB broth was purchased from Difco labs (Catalog# 244620). $[P_{6,6,6,14}][Br]$ (CAS 258864-54-9, assay >97%) and $[P_{6,6,6,14}][Tf_2N]$ (CAS 460092-03-9, assay > 99%) were obtained as a gift from CYTEC industries. [HMIm][FAP] (CAS 713512-19-7, assay >99+%) and $[P_{6,6,6,14}][FAP]$ (assay >99+%) were obtained as a gift from EMD Chemicals Inc., USA. 1-Methylimidazole, (CAS 616-47-7, 99+%), lithium bis(trifluoromethylsulfonyl)amide (CAS 90076-65-6, 99.95%) and %), trihexylamine (CAS 102-86-3, 96%), bromomethane (CAS 74-83-9, 2.0M in tert-butyl methylether solution), acetonitrile (CAS 75-05-8, 99.9%), NDHD (CAS 51268-88-3, 98%), naphthalene (CAS 91-20-3, 99%), ammonium sulfate (CAS 7783-20-2, 99%), ammonium tetrafluoroborate (CAS 13826-83-0, 99.99%), methyltrioctylammonium bromide (CAS 35675-

80-0, 97%), methyltributylammonium bromide (CAS# 37026-88-3, 98%), and 1-butyl-1-methylpyrrolidinium bis(trifluoromethylsulfonyl)amide (CAS 223437-11-4, 98%) were purchased from Sigma Aldrich. 1-Bromoethane (CAS 74-96-4, 99+%), bromobutane (CAS 109-65-9, 99%), bromohexane (CAS 111-25-1, 99+%), bromodecane (CAS 112-29-8, 98%.), tetrabutylammonium bromide (CAS 1643-19-2, 99%), N-Methyldioctylamine (CAS 4455-26-9, 98%) and methyltributylammonium chloride (CAS 56375-79-2, 98%) were purchased from Acros. Ampicillin (69-52-3, >95%), glacial acetic acid (CAS 64-19-7, 95%) and glycerol (CAS 56-81-5, 99.5%) were purchased from fisher. Methyltrioctylammonium chloride (CAS 5137-55-3, 95%), 6-chloro-2-hexanone (CAS 10226- 30-9, 97%) and 5-chlorovaleronitrile (6280-87-1, 95%) were purchased from TCI America.

Fisher Scientific Catalog no's: Mineral oil (CAS 8042-47-5, 99%), hexanes (CAS 110-54-3, >95%) were purchased from Fisher Scientific. Sodium salt of Carboxymethyl cellulose (CAS 9004-32-4). Low molecular weight Oppanol B100 was obtained courtesy of BASF.

3. TOWARDS *IN SITU* EXTRACTION OF FINE CHEMICALS USING IONIC LIQUIDS

A broader aim of this work is to look at how novel solvents ionic liquids (added as a second phase to the cell medium) can improve the *in situ* extraction of solutes like fine chemicals and biofuels produced by fermentation. This chapter looks closely at the fine chemicals model system: production of NDHD from the microbial oxidation of naphthalene by the gram negative *Escherichia coli* bacteria. The focus is on gaining biological perspective on identifying *in situ* solvents along with understanding thermodynamics of NDHD partitioning. Though the emphasis is on evaluating ionic liquids for *in situ* extraction, preliminary extraction results using traditional organic solvents and using adsorption are also presented.

3.1. Evaluation of *In situ* extraction and fermentation techniques

As described in the introduction chapter, there are potentially many techniques that can be implemented for *in situ* extraction of the solutes which depend upon favorable physical properties of the solute such as volatility, extraction, adsorption, etc. For the present system, the adsorption and solvent extraction were found to be relevant and employed. Both techniques were evaluated, but solvent extraction was employed for the main study as it is relatively simpler technique for *in situ* solute extraction. In this section, the results from solvent extraction using traditional organic solvents and using resins as adsorbents are described.

3.1.1. NDHD extraction using Organic solvents

With the organic solvents, evaluating their extractability for solute of interest was the primary focus. For these solvents, biocompatibility is well understood: octanol-water partition coefficient or *log P* values are good indicators of biocompatibility. Generally, more hydrophobic solvents are less toxic to the cells. The threshold value of *log P* beyond which solvents are not

toxic varies from organism to organism. The *log P* range of organic solvents, which are used as biphasic media in the hydroxylation of naphthalene by *Pseudomonas Putida,* was used as the basis for organic solvent selection. Organic solvents with *log P* >4 do not affect the activity of enzymes.[1] Two classes of solvents, alcohols and alkanes, were selected based on their water solubility for initial screening and their partition coefficients were measured. Aqueous and organic phases were mixed at 1:1 volume ratio.

Table 3.1 below shows the partition coefficients obtained with various organic solvents. Of the two classes studied, alcohols - octanol and dodecanol, which are the most polar and hence less hydrophobic solvents, extract NDHD favorably out of the aqueous phase. This can be attributed to primarily to high interactions between NDHD and the functional group '-O' atom and potentially to hydrogen bonding as well. C10 and C12 solvents - decane and dodecane - which are highly non-polar extract very little solute from the aqueous phase. In these two classes, irrespective of the number of carbon atoms, presence of a polar '-O' dramatically increases the extractability of the solute. This indicates that the solute, NDHD, which is polar, requires solvents that are polar, yet hydrophobic, in nature for better extraction. Though, more polar a solvent is, the more difficult it would be to separate the resulting aqueous – solvent mixture. *Log P* values of the alcohols - dodecanol and octanol - are closer to the uncertainty range of solvents that affects the cell growth. While the nonpolar solvents with *log P* values greater 4, have lower aqueous solubility and are more biocompatible with the bacteria, they do not extract the solute from the aqueous phase. Here, though the C10 and C12 alkanes have low extractability for NDHD, they are known to have very high solubility for the substrate[1] and low toxicity to the cells. Hence, they have the potential to improve NDHD yield during biotransformation as *in situ* solvents. The lower extractability of dodecane can be overcome by

adding a second solvent to create a mixture. Here, dodecanol was used as the second solvent and the extractability of 1:1 by volume of dodecanol and dodecane was measured. As the partition coefficient is greater than 1, addition of dodecanol to dodecane makes the mixture a potential solvent for the extraction of NDHD from water. Other aspects of the potential solvent mixture for *in situ* extraction like biocompatibility and phase separation need to be evaluated. An approximate *log P* value for 1:1 mixture of dodecanol and dodecane can be calculated from individual *log P* values; although dodecanol with its higher solubility in water would likely be toxic to the cells even at its reduced final concentration. Further, ease of phase separation of the three phase mixture needs to be studied. In conclusion, the suitability of organic solvents for a given *in situ* extractive fermentation system is limited by their number and by their fixed set of properties. These shortcomings can be addressed by studying novel designer solvents - ionic liquids.

Table 3.1: Partitioning of NDHD from aqueous phase using organic solvents conducted at 22°C.

Solvents	Partition Coefficients (based on concentration)
Octanol	4.33
Dodecanol	3.17
Decane	0.018
Dodecane	0.007
Dodecane + Dodecanol (1:1 by volume)	1.21

3.1.2. In situ fermentation using a biocompatible organic solvents

From the partitioning studies using organic solvents, dodecane was found to be the best choice solvent for performing *in situ* biphasic biotransformation primarily because of its low toxicity and low mutual solubility with water. Though its extractability of the solute is low, dodecane's high solubility for the substrate improves the availability of the hydrophobic substrate to the cells which could increase yield of the product during the biotransformation. Higher final concentrations of product could reduce the energy required and make the biotransformation more efficient. In this study, the effect of presence of dodecane on the amount of NDHD produced during the biotransformation was measured.

In this study, the cells were grown in the MSB medium to a particular optical density and then the solvent, dodecane, was added. Here, *E. coli* strain that expresses toluene dioxygenase (TDO) enzyme catalyzes the reaction. Before adding the solvent, the optical density at 660 nm was measured and noted. The substrate, naphthalene, was dissolved in the solvent and its initial concentration was 40 g/L.[1,2] Phase ratio of the solvent added was 19.4% which is considered as the optimum phase ratio for biphasic biotransformations.[2,3] The broth samples were collected for every 3 hours initially and then every 6 hrs for 24 hrs. The samples were centrifuged and filtered to remove the cells and diluted to required concentration using acetonitrile solvent and analyzed on HPLC (method discussed in Chapter 2, Section 2.3.2.). Since NDHD does not partition in to the organic phase, only the aqueous phase was analyzed. The amount of NDHD produced is plotted as a function of time as shown in figure 3.1 below. The maximum amount of NDHD produced after 24 hrs is around 7 g/L when the OD at the beginning is 2.15. The final NDHD concentration obtained with single aqueous biotransformation for this system as reported in the literature is 0.2 g/L.[1,2] The final amount of NDHD produced in biphasic biotransformation when

compared to its production in a pure aqueous phase is 35 times higher. The final NDHD concentration is dependent on the initial OD. Higher the initial OD, the more is the availability of active cells to oxidize readily available naphthalene from dodecane and hence higher is the final product concentration. From the figure, it can be observed that the maximum amount of NDHD is produced in the first 6 hrs. For lower initial OD's of 0.4 and 0.7, after 12 hrs, minimum amount of NDHD is produced and the rate of conversion is almost zero. But at OD = 2.15, from 12 to 24 hrs, there is conversion of naphthalene to NDHD and the rate of production of NDHD is finite. Here, it can be seen that even after 24 hrs there could be still some more NDHD produced before the conversion becomes zero. The amount of NDHD produced in this biotransformation compared well with those reported in the literature. Harrop *et al.,*[1] reported production of NDHD as 6 g/(g. of dry cell wt.) after 6 hrs of biphasic biotransformation of naphthalene by *Pseudomonas Putida*. Here, the initial concentration of naphthalene was 40 g/L in dodecane and the phase ratio was 50%. Angela *et al.*,[2] reported ~2 g/L of NDHD production after 6 hrs when the initial concentration of 40 g/L naphthalene and dodecane phase ratio was 20% and the starting at OD_{660nm} was 1. Here, mutant *E. coli* strain that expresses naphthalene dioxygenase [4] enzyme was used.

Figure 3.1: Microbial oxidation of naphthalene in a biphasic medium with dodecane solvent by mutant strain that expresses for toluene dioxygenase enzyme

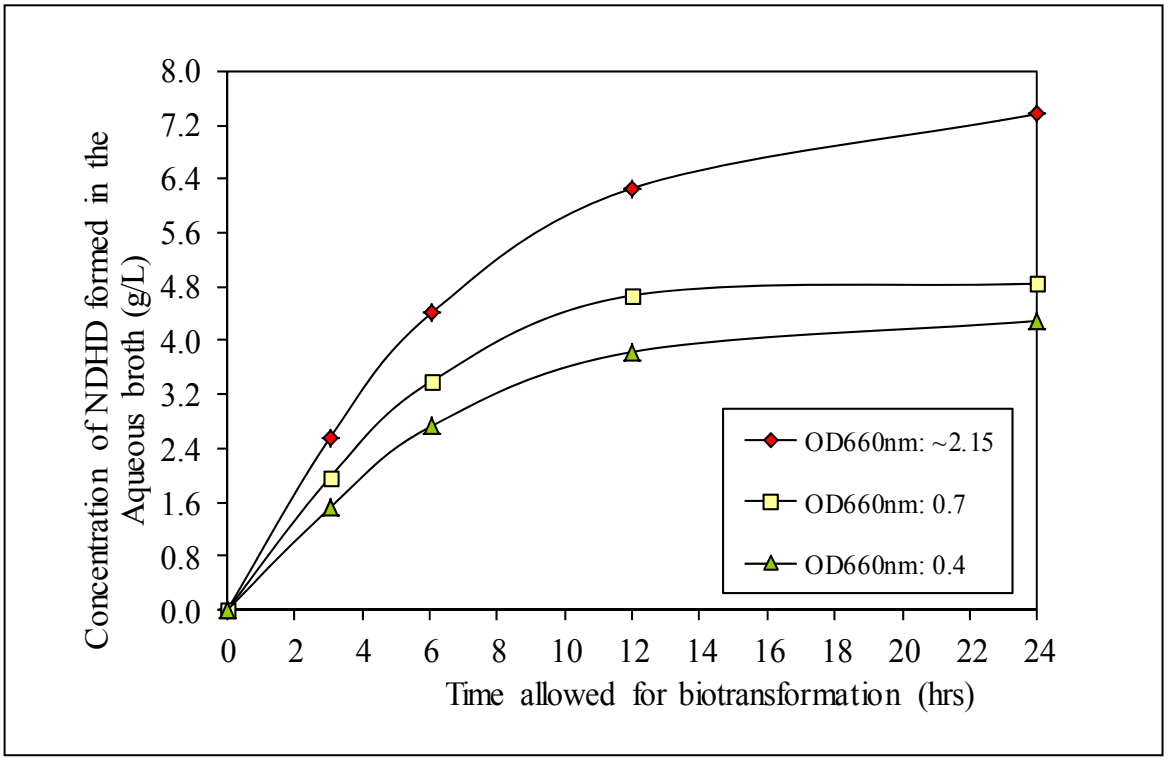

3.1.3. NDHD extraction via Adsorption

The applicability of other technique, adsorption, for *in situ* extraction was evaluated. A hydrophobic XAD-16 resin was used [Styrene-divinylbenzene matrix, 20-60 mesh, 560-710 μm, 200 Å mean pore size]. Initially a sample run was done to test whether the resin selected was appropriate for the present study. Here small amount of pretreated resin was added to stock sample of NDHD solution. A sample collected after one day was found to adsorb around 97% NDHD and here it was observed higher stirrer speeds would break the particles. Further results from adsorption studies using XAD-16 resin and 4 different concentrations of NDHD solutions are summarized in Figure 3.2 and Figure 3.3.

Figure 3.2 shows the time it takes for adsorption of NDHD, from aqueous solution to the resin particles, to reach equilibrium. For the initial aqueous concentrations of NDHD of 0.47, 1.9 and 3.3 g/ml, the adsorption reaches equilibrium around 24 hrs. But at initial higher concentration of 4.7 g/ml, the equilibrium was not observed even after 32 hrs. These results need to be repeated to validate the data. It can also be observed from Figure 3.2 that the rate of adsorption was high for initial few hours and then the rate drops and levels off to zero. In addition to the time taken to reach equilibrium, the amount of NDHD adsorbed on to the resin decreases with increase in the initial concentration of NDHD in the aqueous solution. For example, the percentage of NDHD adsorbed drops to 82% from 97% when the initial NDHD concentration is increased from 0.5 mg/ml to 4.7 mg/ml.

Figure 3.2: Adsorption equilibrium of NDHD from aqueous solutions using different concentrations of XAD-16 resin as a function of time and initial aqueous concentration of NDHD.

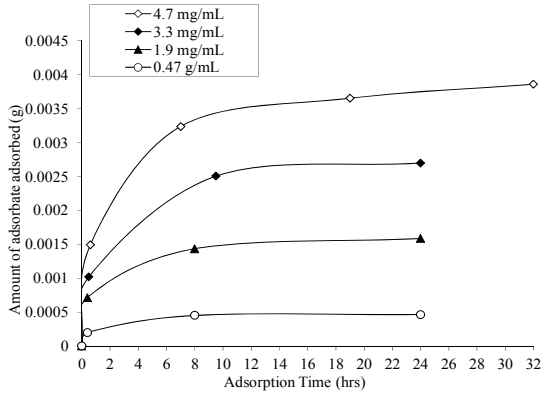

Figure 3.3 shows an incomplete adsorption isotherm with ratio of total amount of adsorbate (NDHD extracted by the resin) to amount of adsorbent added on y-axis to the initial concentration of adsorbate in the aqueous phase on the x-axis. Total amount of adsorbate was obtained by assuming adsorption equilibrium has been reached after 32 hrs. Further adsorption studies have to be conducted at higher concentrations of NDHD in water to get a complete Langmuir isotherm, but these measurements could be limited by low solubility of the NDHD in water. Also, NDHD produced during biphasic microbial oxidation of naphthalene is around 5 g/L which suggests that the above four adsorption runs are sufficient to note that the XAD-16 resins are suitable as polymeric adsorbents for adsorption of NDHD from aqueous phase.

The resin particles can be added to the biotransformation culture directly to adsorb the NDHD as it is formed in the bioreactor. But there could be problems with the particles being broken because of the high speed stirring in the bioreactor. Also, the adsorption rate and amount adsorbed could be affected because of the other components in the broth. Further studies that are necessary to study the effect of following parameters on the performance of resin before it can be used in the extractive fermentation are:

- Presence of biphasic medium with organic phase with and without emulsion separated (during test runs performed, it was observed that the dodecane a suitable organic phase did not dissolve the resin over a period of time).
- Presence of resins on the substrate availability to the cells. This is important as the substrate naphthalene, which is hydrophobic, could be easily adsorbed by the resins, reducing the substrate availability to the cells.
- Presence of biotransformation broth, filtered broth and centrifuged broth on the adsorption.

– Efficiency of the adsorption in a continuous flow setup with regeneration and recycle of the resins.
– Optimum amount of adsorbent to be used and effect of scale up of aqueous solution to be processed.

Some of the disadvantages with this technique as observed with the addition of organic solvent or cell broth medium include:

– Decreased resin surface area that leads to lower adsorption of the solute.
– Breakdown of the resins in the bioreactor.
– Extraction of solute from the adsorbed resin and reuse of the resin particles.

Figure 3.3: Adsorption of NDHD from aqueous solutions with XAD-16 resin as a function of initial NDHD concentration.

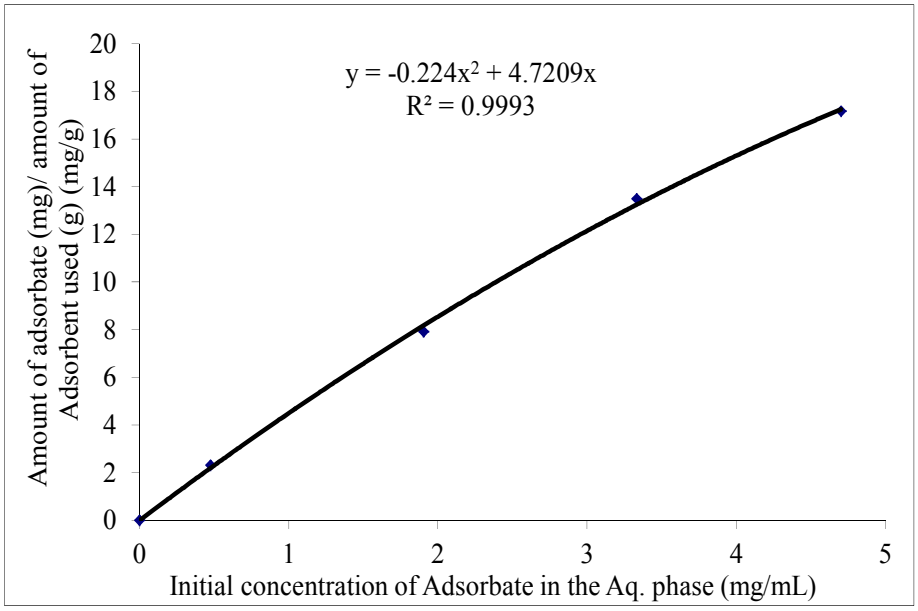

3.2. Ionic liquid as a potential *in situ* extractant

From section 3.1, organic solvents apart from being fixed set of solvents with fixed properties are also volatile organic ompounds. Ionic liquids which are greener because of negligible emissions are potential replacements to organic solvents for biphasic biotransformation.

3.2.1. Relevance of partitioning data

Applicability of *in situ* fermentation/extraction to a given system is reliant upon the fact that the external solvent added can extract the product from the aqueous cell medium and also increase substrate availability to the cells. Additionally, for efficient downstream processing of this biphasic mixture to purify the product, information on the selectivity data of the solute over water is very crucial.

3.2.2. Relevance of toxicology

For conducting an *in situ* fermentation (biphasic biocatalysis/biotransformation), solvent in this case ionic liquid, which is the external medium added to the growing cells, could interfere with normal cell activity and thereby affect the yield of the product. These possible solvent - microorganism interactions should occur at the minimum for a feasible *in situ* fermentation and play a direct role in the selection of the solvent as the second medium. A potential solvent should be least toxic to micro-organism both at molecular and phase levels for it to perform its role of reducing product/substrate and/or increase product yields.

3.2.3. Problem statement

The objective of this work is to provide a general methodology for the optimization of ionic liquids for the *in situ* extraction of fermentation systems. To illustrate this methodology, we will focus on a model system of the oxidation of naphthalene by using a modified *E. coli* strain. We

will first measure the phase equilibrium thermodynamics (partitioning) of the target solute into various ionic liquids are investigated. Then the toxicology of various ionic liquids and preliminary studies into the inhibition mechanism will be discussed. .

3.3. Partitioning

3.3.1. NDHD

The equilibrium partitioning of NDHD between the model ionic liquid [HMIm][Tf_2N] and water was measured at 22°C at various initial aqueous concentrations (loadings) of NDHD. The saturated solubility of NDHD in the aqueous phase is 0.8 g/L (9×10^{-5} mole fraction) at 22°C, while in an actual fermentation system, significant product inhibition starts at approximately 0.5 g/L.[27] The solubility of NDHD in pure [HMIm][Tf_2N] is 2.42 g/L (0.0049 mole fraction) From the binary system of [HMIm][Tf_2N] and water at 22°C, the solubility of the [HMIm][Tf_2N] in water in mole fraction is 8.5×10^{-5} (0.0021 weight fraction; 2.1 mg/ml). For comparison, Brennecke and coworkers have measured the solubility of [HMIm][Tf_2N] in water at 23.5°C and found a weight fraction of 0.0023.[28] The solubility of water in [HMIm][Tf_2N] is 0.164 mole fraction. This dissolution of water appears to be substantial on a mole fraction basis, but as the molecular weight of the IL is much greater than water, the corresponding quantities in weight fraction and mg/ml are 0.0078 and 10.8 mg/ml, respectively. Values of the water solubility in [HMIm][Tf_2N] vary from mole fraction of 0.1978 at 20°C to 0.2556 at 45°C.[29] In a ternary system, the presence of a third component usually changes these mutual solubility numbers. However, due to the relatively low concentrations of NDHD, these solubilities change negligibly in the ternary system.

The results for the ternary system are reported as partition coefficients and selectivities over water from Eqn 1 and 2 in section 1.1.4.3. Partition coefficient yield information on how much of the solute partitions into the ionic liquid compared to that remaining in the aqueous phase. Selectivity yields an indication of how selective is the IL extractant for the desired solute compared with the co-extraction of water. For the ionic liquids to be considered suitable extractants, the partition coefficients and selectivity should be as high as possible (*>1*). Equilibrium studies with the model ionic liquid, [HMIm][Tf_2N], were conducted with initial mole % of NDHD in the aqueous phase between 0.01 to 0.09% (0.5 to 3 mg/ml). The selectivities and partition coefficients, calculated based on mole fraction, as a function of the initial substrate loading are plotted in Figure 3.4. The partition coefficients and selectivity to NDHD increase with increasing initial concentration of NDHD followed by a slight decrease at the highest concentrations investigated near the saturation limit of NDHD. Thus, these values are at least a small function of initial concentration. The average partition coefficient over the entire concentration range investigated is 43.5 ± 5.0 (Table 3.2). Similarly, very high selectivities greater than 200 were obtained due to very low solubility of water in the ionic liquid. The maximum selectivity of 300 is obtained at the substrate loading of 0.05 mole %. These are very encouraging data as they indicate that the loading of the ionic liquid need not be very high to achieve efficient separation of NDHD. While these equilibria data are reported in thermodynamically relevant units of mole fraction, those based on mass fraction, molarity, etc. are often more practical. From Table 3.2, the average partition coefficient and selectivity in units of mass fraction are 2.19 and 288 and in the units of molarity are 2.86 and 264.8 respectively. Thus, these units decrease the partition coefficient by an order of magnitude, but are at least greater than 1. The selectivities are still significantly high.

Figure 3.4: Partition coefficient and selectivity of NDHD (mole% based) as a function of initial aqueous concentration of NDHD.

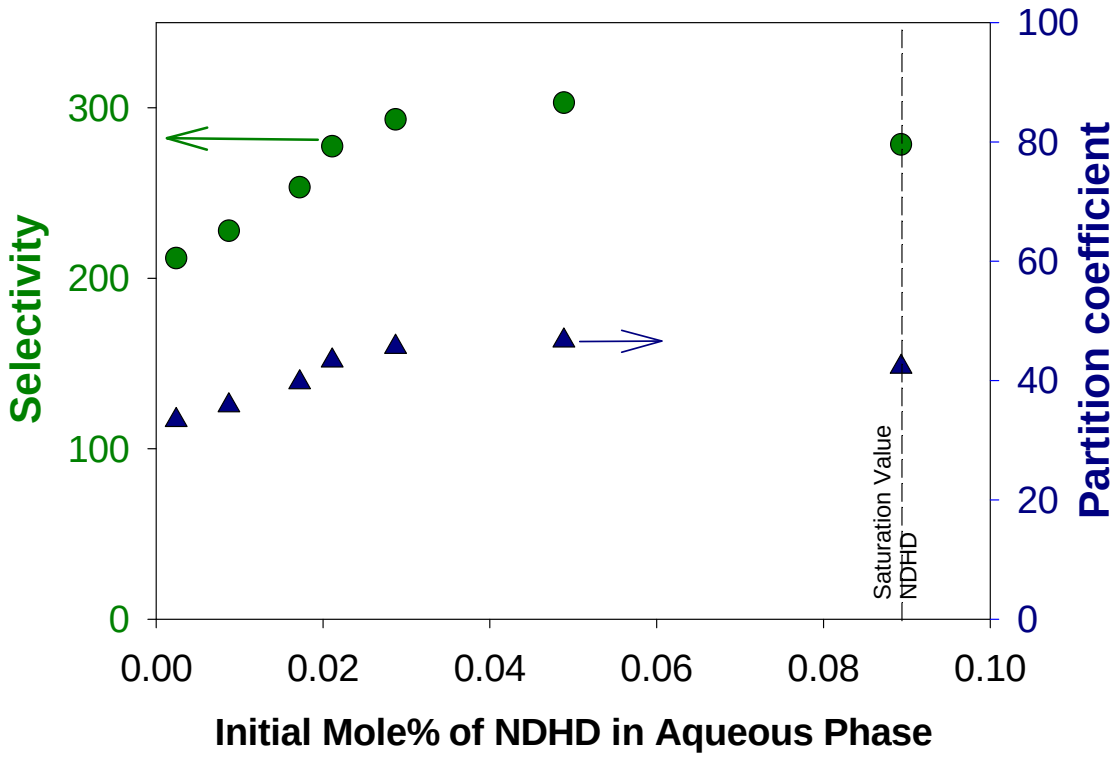

In addition to the extraction studies with the model ionic liquid, [HMIm][Tf_2N], other hydrophobic ionic liquids were investigated to gain an understanding of effect of structure of different cations or anions on the partitioning. Here, ten ionic liquids were investigated with other common cationic classes such as phosphonium and ammonium in combination with hydrophobic anionic groups like trifluoro-tris(perfluoroethyl) phosphate ([FAP]) and [Tf_2N]. Here the average partition coefficients and selectivities measured over the initial NDHD concentrations range of 0.3-3 mg/ml in various units are reported in Table 3.2. These average *K* and *S* are from at least two initial NDHD concentrations at approximately 0.5 and 3 mg/ml. The results show that the structure of both cation and anion can affect the partitioning and these effects will be discussed in the following sub-sections.

Table 3.2: Partition coefficient and selectivity of NDHD in various ionic liquids bases in units of mole fraction, mass fraction, and molarity.

Ionic Liquid	K_x	S_x	K_ω	S_ω	K_C	S_C
[HMIm][Tf_2N]	43.5±5	288±19	2.14±0.10	288±15	2.86±0.34	265±20
[HMIm][FAP]	7.9±0.8	128±13	0.23±0.02	120±12	0.37±0.04	120±12
[DMIm][TCB]	169±18	449±47	9.1±0.96	298±32	8.8±0.93	289±31
[TBMAm][Tf_2N]	15±0.4	153±4	0.57±0.01	140±3.5	0.72±0.01	141±3
[THMAm][Tf_2N]	19.9±0.6	220±6	0.64±0.02	204±7	0.76±0.03	204±7
[TOMAm][Tf_2N]	16.2±2.1	192±25	0.46±0.06	179±22	0.51±0.06	179±23
[$P_{6,6,6,14}$][Tf_2N]	15.9±4.1	86±22	0.38±0.10	72±19	0.41±0.11	72±19
[$P_{6,6,6,14}$][FAP]	3.4±0.5	99±16	0.07±0.01	96±16	0.08±0.01	96±16
[DOM(5Bu-CN)][Tf_2N]	67.8±1.4	287±5	2.00±0.03	222±3	2.31±0.03	221±3
[DOM(5-HxOne][Tf_2N]	78±1.6	288±7	2.2±0.06	213±6	2.51±0.07	212±5
x = mole fraction based; *ω= mass fraction based; C = concentration/molarity based;* ± based upon standard deviation of the values from at least two different concentrations.						

3.3.2. Effect cations on the partitioning

The cation effect on the partitioning was studied by using imidazolium, ammonium, and phosphonium based ionic liquids paired with similar anions. From Table 3.2, the highest partitioning coefficient was obtained with [HMIm][Tf_2N]. The imidazolium cation is planar and partially aromatic. The approximate polarity of [HMIm][Tf_2N] using solvatochromic probes is similar in many respects to propanol.[30] NDHD has one aromatic ring and one aliphatic ring with two hydroxyl groups. The combination of aromaticity and moderate polarity of both solute and IL results in high partitioning into the IL phase. When the aromatic imidazolium cationic group is replaced with more aliphatic ammonium (or phosphonium) cations, the partitioning decreases

irrespective of the length of alkyl side chains. While the charged ammonium group could have favorable enthalpic interactions between the hydroxyl groups of NDHD, the long alkyl- chains sterically hinder this interaction. The same argument may hold true for different aliphatic ammonium based ionic liquids tested wherein increasing the alkyl side chain length from butyl- to hexyl- to octyl- slightly reduces the partition coefficient. The partition coefficients are relatively small due to the longer trihexyl- and tetradecyl- side chains. In general, aliphatic ammonium and phosphonium ionic liquids seem to have low extractability for the aromatic NDHD metabolite. However, as they have very low solubility of water, the selectivities remain relatively high. Incorporating functional groups like ketone, hydroxyl-, ether, nitrile, etc. groups were envisioned to improve the extractability due to their ability to more strongly interact with the diol and two new ILs were synthesized. With trioctylmethylammonium [Tf_2N] as a basis, one of the octyl groups was replaced with a 5-cyano- or 5-hexanone- group to produce [DO(5-BuCN)MAm][Tf_2N] and [DO(5-HxOne)MAm][Tf_2N] respectively. These newly created ILs, yielded the highest partition coefficients and selectivities of all ILs investigated. K_C values for these ionic liquids are 2.31 and 2.51 respectively which are much higher than any of the nonpolar [TRMAm][Tf_2N] (R = n-butyl, n-hexyl, n-octyl-) tested and other ILs. Thus some level of rational design of ionic liquids for highly selective extractions is indeed possible.

3.3.3. Effect of anions on the partitioning

Replacing [Tf_2N] anion with trifluoro-tris(pentafluoroethyl) phosphate ([FAP]), irrespective of the cation present, reduces the concentration based partition coefficients of NDHD by a factor of 7 and 4 respectively. This suggests that the choice of the anion has an important role in partitioning apart from improving the ionic liquid's hydrophobicity. This decrease in the partition coefficients by changing the anions may be attributed to weaker intermolecular forces

between NDHD and the anion or reduced interactions of the aromatic NDHD with the cation. The [FAP] anion contains bulkier fluorinated ethyl groups on the anion with the phosphorus inaccessible to the solute and solvent environment. The [Tf_2N] anion has sulfonyl groups which may form hydrogen bonds with the hydroxyl groups of the NDHD. In addition, depending on the preferred position of the [FAP] anion relative to the cation, the bulky anion may hinder the NDHD access to either the imidazolium cation or the positively charged nitrogen or phosphorus atoms. Replacing the anion on [RMIm][Tf_2N] with tetracyanoborate [TCB] gives higher partitioning coefficients. From molecular simulation studies, the anion appears to orient itself primarily near the C-H group bridging the two nitrogens in the imidazolium ring.[31] [32,33] Larger anions would block this area of highly delocalized electrons (aromatic). If the association between the cation and [FAP] is increased over [Tf_2N], then this region would remain blocked for longer times reducing the NDHD interaction with the cation.

3.4. Toxicology

Toxicity studies were conducted to understand the influence of ionic liquids on the growing cells if an *in situ* extraction were to be carried out. Here the molecular toxicity was measured. In the beginning, the focus was to develop the structure-toxicity relationships on the *E. coli* used in the biotransformation. Both hydrophilic and hydrophobic ionic liquids were synthesized and the toxicity of each ionic liquid was reported as EC_{50} values.

3.4.1. Cell growth plot: Time vs. Optical Density (*OD*)

Figure 3.5 illustrates the change in *E. coli* growth rate by changes in relative optical density with time for various concentrations of 1-butyl-1-methylpyrrolodinium bis(trifluoromethylsulfonyl)amide [BMPy][Tf_2N]. As shown, the growth rate decreases with increasing concentration of [BMPy][Tf_2N] compared to the control. The time $t = 0$ represents

when the different concentrations of the ionic liquid are added to the culture flasks. Time, $t = 0$, also approximately represents the time when the lag phase in the growth cycle ends and the exponential phase has begun. The effective concentration that inhibits the growth by 50% (EC_{50} value) is calculated from this data (method described in chapter 2, section - 2.2.2.) as 7.0 mM and is reported with 95% confidence. This particular ionic liquid significantly inhibits the growth of the cells at relatively low concentrations and hence it is not biocompatible with the cells. The growth rate becomes zero at a concentration of approximately 6.8 mM beyond which a negative rate is observed. This indicates that eventually the ionic liquid must either inhibited the cell metabolism, cell death, or both must have occurred.

Figure 3.5: Growth of *E. coli* with time after addition of different concentrations of the IL, [BMPy][Tf_2N] versus a control. Lines are smoothed data. Intermediate concentrations omitted for clarity.

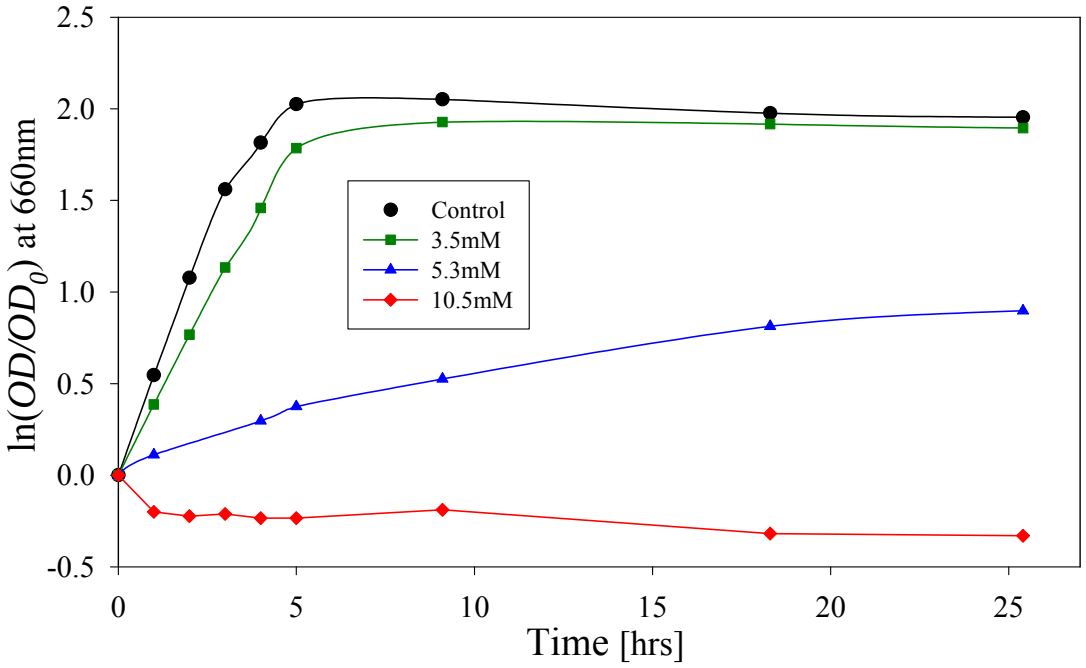

3.4.2. Toxicology results

3.4.2.1. EC_{50} values

In a similar manner, the EC_{50} values of the other ionic liquids are listed in Table 3.3. The corresponding aqueous solubilities are also listed for hydrophobic ionic liquids. From this table, ionic liquids suitable for *in situ* extraction can be identified when the EC_{50} values are higher than their aqueous solubilities, which imply that it is impossible to obtain a 50% reduction in growth rate. If the EC_{50} values are less than the aqueous solubilities, then a biphasic system would not be practical. The trends in the EC_{50} values for different ionic liquids studied are helpful in beginning to understand the structure-toxicity relationships. From these EC_{50} values, it can be inferred that the cation and anion, both separately and as a particular pair, influence the toxicity. The effect of different cations and anions on the toxicity was studied using cations like imidazolium, pyrrolidinium, ammonium and phosphonium in combination with one or more of the anions like bromide, [Tf_2N] and [FAP]. For comparison, the organic solvent, acetone, was also measured and has one of the highest EC_{50} values (lowest toxicity) of 238 mM. However, acetone is miscible with water and could not be used for *in situ* extraction. Potential biological mechanisms are discussed in the last section.

Table 3.3: EC_{50} and aqueous solubility values.

Ionic Liquids/Solids (s)	EC_{50} [mM]	Aqueous Solubility at 22°C [mM]
[EMIm][Br] (s)	44 ±2	4900
[HMIm][Br]	9.5±0.2	Miscible

Ionic Liquids/Solids (s)	EC_{50} [mM]	Aqueous Solubility at 22°C [mM]
[DMIm][Br]	0.31±0.03	Miscible
[EMIm][Tf_2N]	3.5±0.3	46.8
[HMIm][Tf_2N]	0.73±0.02	4.7±0.1
[HMIm][FAP]	35±6	2.85±0.04
[DMIm][TCB]	0.22±0.01	1.7±0.04
[TBMAm][Br] (s)	12±1	357[a]
[TBAm][Br] (s)	22±2	1860[a]
[THMAm][Br] (s)	1.7±0.2	>2.8
[TOMAm][Br] (s)	0.006±0.001	>0.022
[TBMAm][Tf_2N]	6.8±0.2	1.62±0.05
[THMAm][Tf_2N]	1.68±0.08	0.8±0.1
[TOMAm][Tf_2N]	>10±0.06	0.060±0.001
[DO(5-BuCN)MAm][Tf_2N]	0.24±0.02	1.30±0.06
[DO(5-HxOne)MAm][Tf_2N]	0.09±0.01	0.13±0.02
[BMPyrl][Tf_2N]	7.0±0.02	13.2±0.4
[$P_{6,6,6,14}$][Br]	0.056±0.001	<0.94 [5]
[$P_{6,6,6,14}$][Tf_2N]	10.3±0.2	0.220±0.004
[$P_{6,6,6,14}$][FAP]	>17.6±5	<0.22
Acetone	392.3±32.5	miscible
Li [Tf_2N] (s)	11.1±0.3	34.8[a]

Ionic Liquids/Solids (s)	EC_{50} [mM]	Aqueous Solubility at 22°C [mM]
Naphthalene	0.42±0.02	0.27 [6]
NDHD	0.32±0.01	4.94±0.05
[a] solubility data has been obtained from the manufacturer's data sheet		

3.4.2.2. Effect of cation on toxicology

Various "R-" groups are found within each cation class that allow a large number of potential ionic liquids to be created. If the R- group is a linear alkyl chain, then as carbon number increases, the toxicity of the ionic liquid (or solid) increases (decreasing EC_{50}). This is a long-standing trend in the literature.[7,8] Among the 1-alkyl-3-methylimidazolium bromides ([R-MIm][Br]), toxicity increases in the usual order of [EMIm][Br]<[HMIm][Br]<[DMIm][Br] (C_2-, C_6-, C_{10}- respectively). The EC_{50} values for [EMIm][Br] (C_2) and [DMIm][Br] (C_{10}) are 44.0 mM and 0.3 mM respectively. Among, the trialkyl-methylammonium bromides ([R-MAm][Br]), the toxicity increases in the order of [TBMAm][Br] (tributyl-) < [THMAm][Br] (trihexyl-) < [TOMAm][Br] (trioctyl-). The relatively hydrophobic trioctylmethylammonium bromide ([TOMAm][Br]) was the most toxic IL to *E. coli* investigated, while the tributyl analogue had moderate toxicity. The EC_{50} value reduces by a factor of 2000 from tri- butyl to tri-octyl.

For the 1-alkyl-3-metylimidazolium ILs with [Tf_2N] anion ([R-MIm][Tf_2N]), the toxicity increases with increasing alkyl-chain length, however not to the same extent as the ILs with bromide as the anion. The inorganic salt, Li[Tf_2N], has moderate toxicity itself (EC_{50} = 11.1). With an ethyl- group, [EMIm][Tf_2N] has increased toxicity (EC_{50} = 3.5) over the lithium salt and [HMIm][Tf_2N] with hexyl group has a much greater toxicity (EC_{50} = 0.73). The lithium salt

is highly soluble in water, whereas the other two imidazolium ILs are hydrophobic. Despite being hydrophobic, their EC_{50} values are lower than their aqueous solubility values indicating that, in a two-phase system, *E. coli* would not be able to survive for long lengths of time. [HMIm][Tf_2N] is the IUPAC model ionic liquid and from these results would not be able to be used in an *in situ* extraction system. However, due to its excellent extraction properties it may be able to be used for different types of downstream processing after the fermentation is complete.

For the trialkyl-methylammonium ILs with [Tf_2N] anion ([TR-MAm][Tf_2N]), the trend in toxicity is not as clear. In general, these ([TR-MAm][Tf_2N] are slightly less toxic to *E. coli* than the corresponding imidazolium ILs ([R-MIm][Tf_2N]). [TBMAm][Tf_2N] is less toxic than [THMAm][Tf_2N], but a further increase in alkyl-chain length ([TOMAm][Tf_2N]) results in decreased toxicity. For [TOMAm][Tf_2N], the EC_{50} value was very difficult to quantify due to its extremely low solubility in water. A lower limit is therefore reported and, compared to the aqueous solubility, it is quite biocompatible. This is in direct contrast to the [Br] IL, which was found to be one of the most incompatible ILs. Pyrrolidinium ILs are a subset of alkyl-quaternary ammonium cations where the central nitrogen is part of a 5-membered heterocycle with two further alkyl-substituents. In this study, 1-butyl-1-methylpyrrolidinium cation with the corresponding [Tf_2N] anion ([BMPyrl][Tf_2N]) was investigated. This ionic liquid inhibits cell growth as the EC_{50} (7mM) is less than its solubility in water. Its toxicity is similar to its trialkyl-methyl ammonium counterpart, [TBMAm][Tf_2N].

However, one inconsistency to the general trend that longer alkyl-chains increase toxicity is found comparing tributylmethylammonium bromide ([TBMAm][Br]) and tetrabutylammonium bromide ([TBAm][Br]). Here, the smaller methyl group in [TBMAm][Br] is replaced with another n-butyl group to form [TBAm][Br], which results in a higher EC_{50} value (less toxic)

despite the larger alkyl group. The difference in EC_{50} values is beyond the confidence interval of the data and, thus, statistically relevant. This phenomena could be due to the presence of four butyl side chains which would better shield the positive charge for Mg or Ca displacement (more below), but whose alkyl groups are not long enough to significantly interact with the interior of the membrane.

In the literature, biocompatibility studies with hydrophobic ionic liquids have been reported primarily at the phase level. Pfruender *et al.*,[9] reported high *E. coli* membrane integrity of about 85% - 95% in the presence of [BMIM][Tf_2N] and [OMIM][Tf_2N]. However, Brautigam *et al.*,[10] reported that using a recombinant strain of *E. coli* resulted in lower membrane integrities of around 30% with [HMIm][Tf_2N] and about 10% with [HMIm][FAP]. Stephens *et al.*,[11,12], reported no cell growth with a recombinant strain of *E. coli* (which expresses toluene dioxygenase) in the presence of [HMIm][Tf_2N], while the cell growth was inhibited by 39% and 23% respectively in presence of [TOMAm][Tf_2N] and [$P_{6,6,6,14}$][Tf_2N].

Among the different classes of cations with similar anions, several small trends emerge. Among the bromides, the order of increasing biocompatibility was: [TOMAm][Br] < [$P_{6,6,6,14}$][Br] < [DMIm][Br] < [THMAm][Br] << [HMIm][Br] < [TBMAm][Br] < [TBAm][Br] << [EMIm][Br]. Among all of the ILs with [Tf_2N] anions, the order of increasing biocompatibility was: [HMIm][Tf_2N] < [THMAm][Tf_2N] < [EMIm][Tf_2N] < [BMPyrl][Tf_2N] < [TBMAm][Tf_2N] < Li [Tf_2N] < [$P_{6,6,6,14}$][Tf_2N] < [TOMAm][Tf_2N]. Among the two ILs with [FAP] anion, [$P_{6,6,6,14}$][FAP] and [HMIm][FAP] were some of the least toxic ILs studied. Some of these studies represent rather peculiar trends. For instance, the [TOMAm] and [$P_{6,6,6,14}$][Br] are some of the most toxic ILs to *E. coli*. However, with the [Tf_2N] and [FAP] anions they

become some of the least toxic ILs. Even the [HMIm] cation, which is moderately to highly toxic with [Br] or [Tf_2N] anions, becomes one of the least toxic with the [FAP] anion.

3.4.2.3. Effect of anion

The anion seems to play a more significant role in the toxicity of the IL to *E. coli*. For ionic liquids with the [HMIm] cation, the order of increasing biocompatibility is: [HMIm][Tf_2N] << [HMIm][Br] << [HMIm][FAP], i.e. [Tf_2N]<<[Br]<<[FAP]. For ionic liquids with the [$P_{6,6,6,14}$] cation, the order of increasing biocompatibility is: [$P_{6,6,6,14}$][Br] << [$P_{6,6,6,14}$][Tf_2N] << [$P_{6,6,6,14}$][FAP] ([Br] << [Tf_2N] <<[FAP]). Thus, only the ILs with the [FAP] anion are consistently the least toxic. For the trialkylmethylammonium ILs, few trends exist for comparison of cations with [Br] or [Tf_2N] anion. For instance [TBMAm][Tf_2N] is slightly more toxic than [TBMAm][Br]; [THMAm][Tf_2N] is almost equally toxic as [THMAm][Br]; and [TOMAm][Tf_2N] is significantly less toxic than [TOMAm][Br]. Thus, for the smallest cations, the [Br] is least toxic; for [THMAm] cation the anions are approximately equally toxic. However, for the largest cation, [TOMAm], the [Br] IL is more toxic than the [Tf_2N].

3.4.2.4. Discussion on how the structure of the cation or anion affects the toxicity – membrane effects

The mechanism of toxicity of many antimicrobial cationic surfactants is well documented in the literature.[13-18] Classic examples of cationic surfactants are quaternary ammonium chlorides (QAC) like methyltrialkylammonium bromides, benzoalkonium chloride, dialkylmethylammonium halides and dialkylbenzyl ammonium halides with alkyl chain lengths between 8 and 18. Similar antimicrobial behavior is exhibited by phosphonium based bromides as alkyltrimethylphosphonium and dialkyldimethylphosphonium.[4,19] The toxicity of these

surfactants is attributed to their interactions with the cell membrane, at multiple target sites, that result in change in the structure of the membrane leading to loss in its fluidity or even lysis.[20]

Gram-negative bacteria, such as *E. coli*, possess both an outer and inner (cytoplasmic) membrane with a thin peptidoglycan layer present between these two.[21,22] The outer membrane is only semi-impermeable as it contains porins (β-barrel proteins), which allow molecules with a molecular weight less than approximately 1500 daltons to penetrate.[23,24] Thus, all of ionic liquids investigated would most probably diffuse past the outer membrane to some extent. The cytoplasm membrane is more selective and regulates the flow of solute and metabolites in and out of the cell, and is associated with important enzymes required for cell metabolism. Damage to the cytoplasmic membrane can be either due to its physical disruption, membrane related enzyme activity inhibition, and dissipation of the proton motive force.[20] Cationic surfactants carrying a positive charge, especially single positive charge bind to the negatively charged cell membrane by displacing divalent calcium or magnesium (Ca^{2+}, Mg^{2+}) ions that stabilize the negatively charged surface.[13] This cation exchange creates electronic and structural perturbations near these sites and subsequent cell disruption is depended upon the nature of interaction between the membrane proteins and lipid bilayer, and the cations.[13] Ionic liquids, with strongly bound cation and anion (low dissociation), may have difficulty participating in this exchange of the membrane calcium or magnesium. Another mechanism of the surfactants and potentially some of the ionic liquids involves interaction of the hydrophobic portion of the cation interdigitating into the hydrophobic membrane core of the lipid bilayer.[20]

Both mechanisms occur with long-chain cationic surfactants and potentially with the longer chain ionic liquids studied. The aliphatic ammonium bromides are expected to be in dissociated form in the presence of water as the bromide affinity for the alkyl enrobed cation is lower and

water readily solvates the relatively high charge density bromide ion. The positive charged cation could have direct interactions with the negatively charged outer cell membrane possibly through the displacement of the calcium or magnesium ions.[13,20] Further, the compounds with longer hydrophobic alkyl chains on the cation penetrate in to the lipid bi-layer, thereby disturbing the fluidity of cell membrane. As the length of the side chain increases, the cation is expected to have increased interactions with the membrane. However, all of the ammonium/phosphonium ILs with the [Tf_2N] anion appears to be relatively biocompatible with *E. coli*. Although the EC_{50} values decrease slightly as the alkyl-chain length increases, the EC_{50} values are higher than the ionic liquid's aqueous solubilities. Thus, the combination of aliphatic ammonium cations and [Tf_2N] anion may be markedly less toxic due to potentially lower dissociation and Ca/Mg exchange and perhaps some level of reorientation of the hydrophobic side chains which inhibits interdegitation into the lipid bilayer.

The visually observed membrane damage with [$P_{6,6,6,14}$][Br] at small concentrations may indicate that this IL readily participates in both mechanisms. Small hydrophilic cations, such as [EMIm] ($^{1+}$) probably could only participate in cation exchange at the membrane surface. It is currently unclear if this would be enough to disrupt proper membrane or if the mechanism for this cation involves transmembrane penetration and interactions in the cytoplasm. The longer chain [HMIm] and [DMIm] cations may be able to participate through both mechanisms. However, as the results of [HMIm][Tf_2N] show only small % of membrane damage even at relatively large concentrations occurs, as the main mechanism of cell death with this IL is perhaps different. There has been only one study known to the authors done to understand the mechanism of bacterial growth inhibition of ionic liquids where it was shown that one type of ionic liquid, [$P_{6,6,6,14}$][Tf_2N] , accumulated in the cell membrane.[12]

At higher concentrations, the QAC form micellar aggregates that solubilize the membrane components and release the cell components. Cetyltrimethyammonium bromide is further known to discharge membrane potential.[15] Cationic surfactant like dodecylguanidine monoacetate causes rapid degradation by rapidly crossing the membranes and combining with phospholipids and proteins.[20] The potential of micellization of any of the ionic liquids at high concentrations in this study has not been thoroughly investigated but it believed to be improbable for the lower-alkyl chain ILs.

3.4.3. SEM microscopy – images

To begin to elucidate the mechanism of the toxicity of some ionic liquids, preliminary studies of the morphology of the *E. coli* cells were initiated. Figure 3.6 illustrates a SEM micrograph of the cells in a control study of no exposure to ionic liquids. The cells' surface (outer membrane) appears smooth and continuous.

Figure 3.6: SEM micrographs of *E coli* cells without addition of any IL

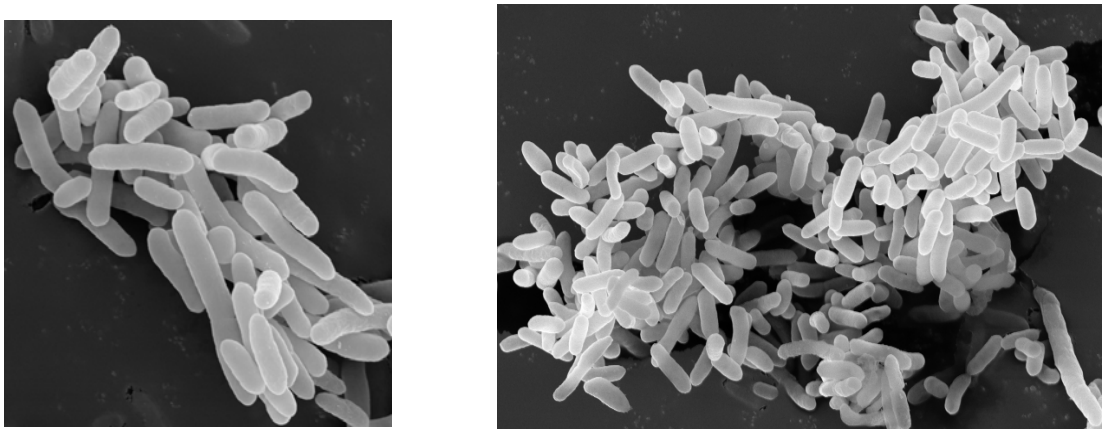

Figure 3.7: SEM micrographs of *E coli* cells incubated with 4.4 mM [HMIm][Br]

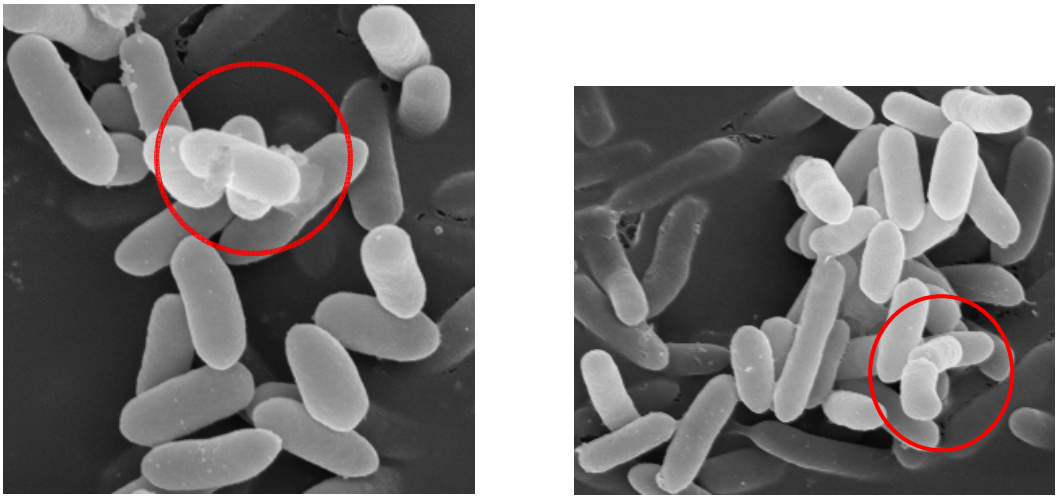

Figure 3.7 illustrates cells that have been incubated in 4.4 mM [HMIm][Br] broth; this concentration is at its EC_{50} value. As shown, there are few cells whose outer membranes

disrupted as highlighted by the circle. However, from a number of additional micrographs of different samples, it can be concluded that the vast majority of cells appear to be intact. This is despite being at a concentration that retards growth by 50%. Careful SEM sample preparation/drying must be performed as the cells may become perforated to yield a false positive. However, poor sample preparation results in circular holes in the membrane and appear much different than shown. Only when the cells are incubated in much higher concentrations of [HMIm][Br] (17 mM), is significant cell membrane disruption observed as shown below.

Figure 3.8: SEM micrographs of *E coli* cells incubated with 17 mM [HMIm][Br]

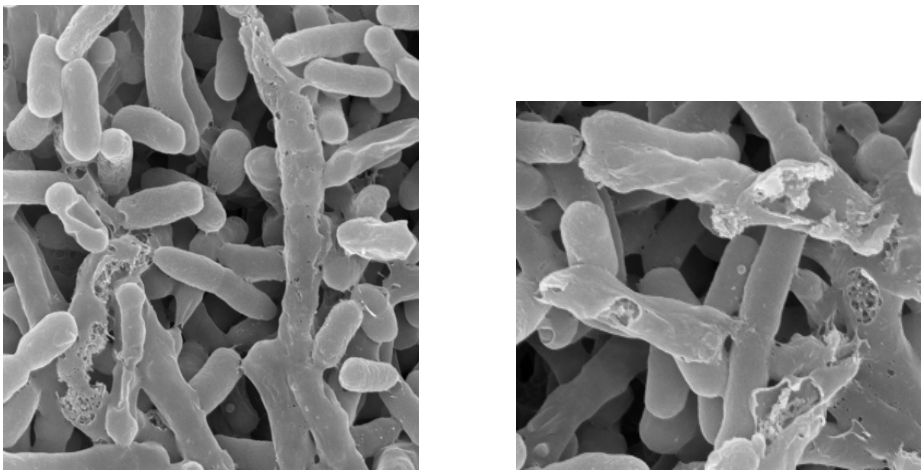

Figure 3.8 illustrates the cell that have been incubated in 17 mM [HMIm][Br] broth. [HMIm][Br] is hydrophilic and completely soluble in water. As shown, several cells now have portions of their outer membranes disrupted. At this high concentration, the effect of IL-cell interactions, specifically $[HMIm]^+$ and the outer membrane seem to be more evident.

Figure 3.9: SEM micrographs of *E coli* cells incubated with 0.73 mM [HMIm][Tf_2N]

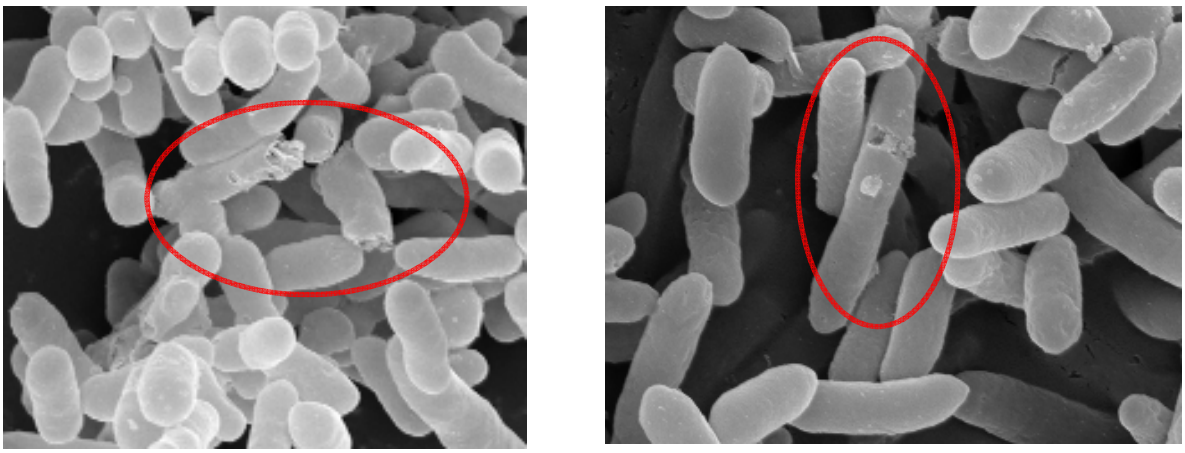

Figure 3.9 illustrates cells that have been incubated in 0.73 mM [HMIm][Tf_2N] broth; this concentration is at its EC_{50} value. As shown, several cells now have portions of their outer membranes disrupted. However, from a number of additional micrographs of different samples, it can be concluded that the vast majority of cells appear to be intact. This is despite being at a concentration that retards growth by 50%. Careful SEM sample preparation/drying must be performed as the cells may become perforated to yield a false positive. However, poor sample preparation results in circular holes in the membrane and appear much different than shown. Only when the cells are incubated in much higher concentrations of [HMIm][Tf_2N] (6.6 mM), is significant cell membrane disruption observed.

Figure 3.10: SEM micrographs of *E coli* cells incubated with 6.6 mM [HMIm][Tf_2N]

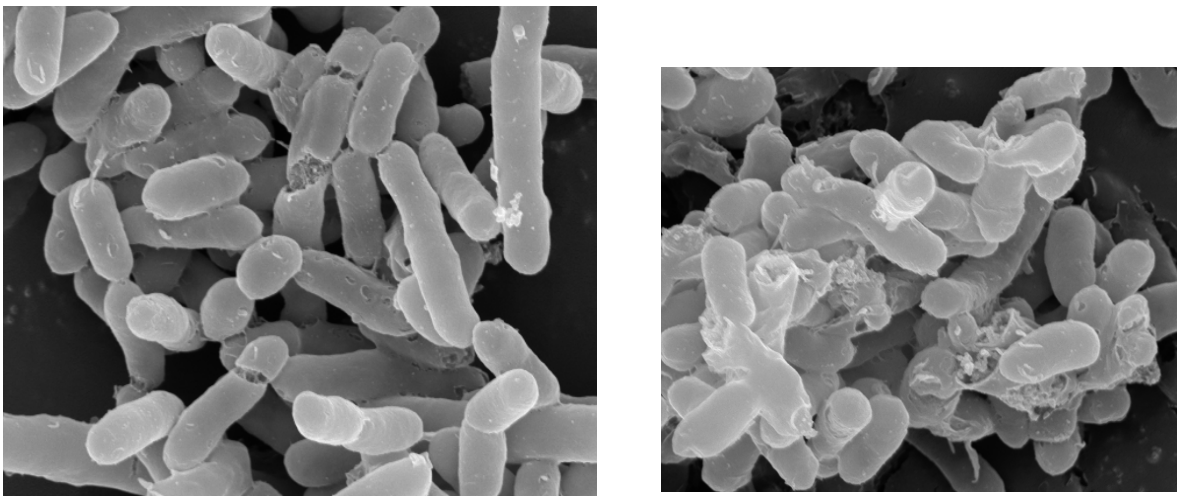

Figure 3.10 illustrates cells after they are exposed to 6.6 mM [HMIm][Tf_2N]. At this concentration, the growth rate would be completely inhibited. However, this percent reduction seems to be significantly less than the percentage of cells with disrupted or lysed membranes. However, this trend appears to be specific to each ionic liquid.

Figure 3.11: SEM micrographs of *E coli* cells incubated with 26 μM [$P_{6,6,6,14}$][Br].

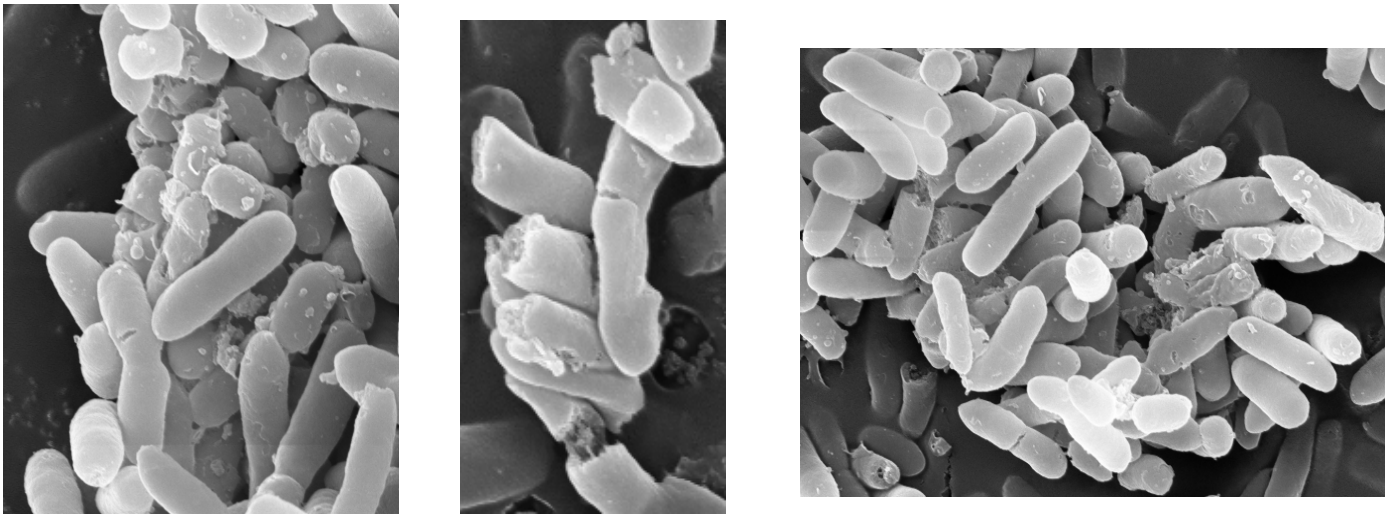

Figure 3.11 illustrates cells incubated in just 26 μM of [$P_{6,6,6,14}$][Br]. As shown, cell disruption seems to affect a higher percent of the cells, despite the concentration of this

phosphonium IL being approximately several orders of magnitude less than the studies with [HMIm][Tf_2N]. The [$P_{6,6,6,14}$] cation is relatively large and contains four long alkyl groups (C_6 and C_{14}) compared with a single hexyl- group on the imidazolium in [HMIm]. These results suggest that different classes of ionic liquids may induce different mechanisms of toxicity.

Figure 3.12: SEM micrographs of *E coli* cells incubated with 40 μM [$P_{6,6,6,14}$][Br]

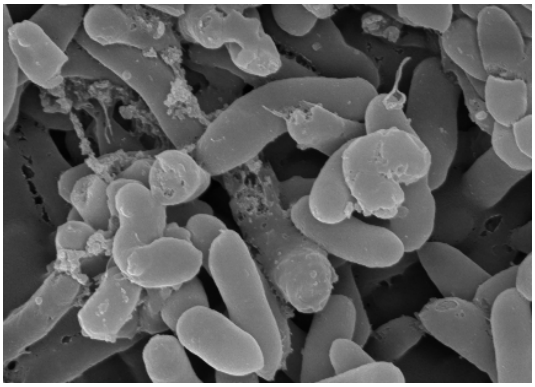

Figure 3.12 illustrates cells incubated in a higher concentration of [$P_{6,6,6,14}$][Br] of 40 μM. As shown, the cell disruption is more prominent and seems to affect a higher percent of the cells as the concentration increases to 40 μM from 26 μM. The cell death was found to be instantaneous upon the addition of the [$P_{6,6,6,14}$][Br] and these long alkyl chain compounds like the quaternary ammonium are known for their anti-microbial behavior. The four long alkyl groups (C_6 and C_{14}) of the [$P_{6,6,6,14}$] cation further penetrates the cell membrane and disrupts the cells.

3.4.4. Longer-Term Response of *E. coli* after Exposure to IL

The mechanism of inhibited growth of microorganisms by certain chemical compounds may be bacteriostat or bacteriocide depending extent of alteration of outer membrane, cytoplasmic membrane or within the cytoplasm. A bacteriostat causes a temporary inhibition to cell growth but the inhibition can be reversible. A bactericide causes cell death where an irreversible breakdown of cell activities occurs.From the inhibition studies, the model ionic liquid

[HMIm][Tf_2N] was found to be unsuitable for *in situ* fermentation due to its low EC_{50} value. However, in order to understand the longer-term growth rate of the cells that survive exposure to the IL, a series of experiments were performed. The cells were incubated in a 3.3 mM IL solution for 5hours. The cells were centrifuged and the supernatant removed and the cells were washed 3 times with DI water. The cells were returned to fresh broth and the cell growth with time was measured and compared with controls that underwent a similar washing procedure. Figure 3.13 illustrates that growth inhibition of cells exposed to IL can be overturned by washing the cells. The growth rate of washed cells in the control was 0.57 hr^{-1} and those exposed to IL concentrations of 3.3 mM was 0.43 hr^{-1}. This suggests that some cells either directly survived the interaction with [HMIm][Tf_2N] or were able to re-grow after expelling the [HMIm][Tf_2N]. In the literature, repeated washings and exposing to higher concentrations of the growth inhibiting substance can improve the resistance of microorganisms to the toxic substance.[25,26]

Figure 3.13**:** Growth rate after incubation with [HMIm][Tf_2N] for 5 hours and cell washing.

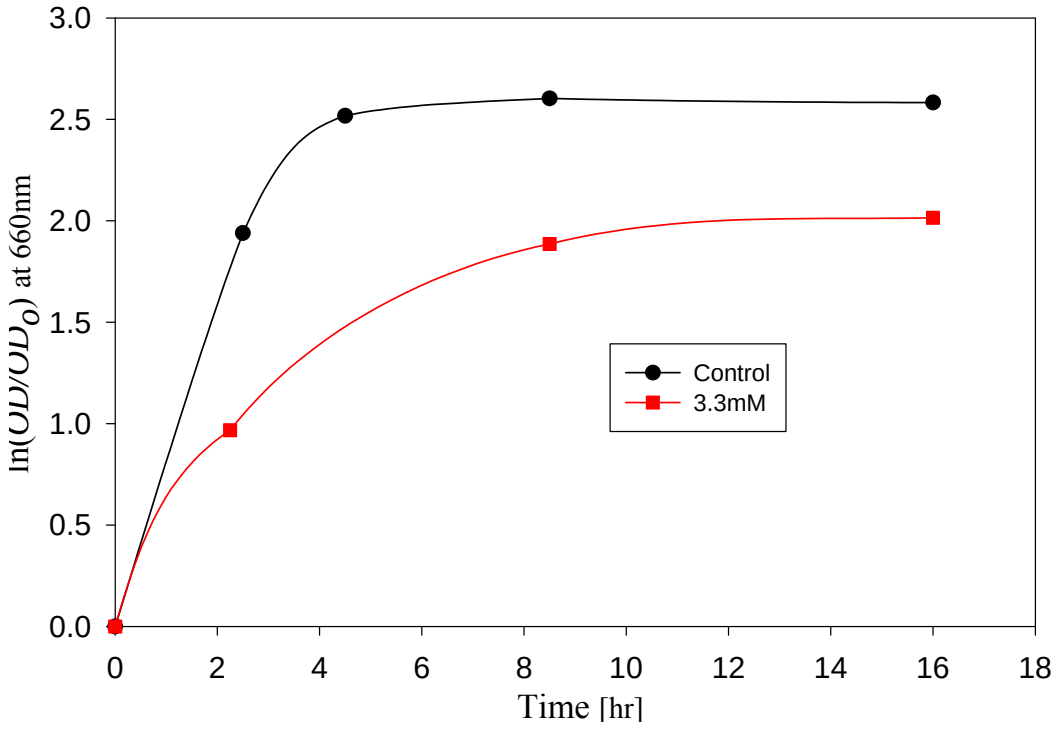

3.5. Discussion on how the structure of the ions affects toxicity and partitioning in unison.

As shown in Table 3.4 below, while some ionic liquids are suitable for fermentation and some have molecular toxicity greater than aqueous solubility. Based on the criteria that the partition coefficients must be > 1 for process economics, an optimal ionic liquid that is suitable for *in situ* extractive fermentation was not identified.

Table 3.4: Suitability of ionic liquids for *in situ* or *ex situ* extractive fermentation

Ionic Liquid	***Partition Coefficient (K_c)***	***Molecular Toxicity (EC_{50})***	***Fermentation Suitability***	***Extractive Suitability***	***In Situ Suitability***
[HMIm][Tf_2N]	≥1	< Aq. Sol.	No	*Ex situ* only	No
[HMIm][FAP]	<1	≥Aq. Sol.	Yes	No	No
[DMIm][TCB]	≥1	< Aq. Sol.	No	*Ex situ* only	No
[TBMAm][Tf_2N]	<1	≥Aq. Sol.	Yes	No	No
[THMAm][Tf_2N]	<1	≥Aq. Sol.	Yes	No	No
[TOMAm][Tf_2N]	<1	≥Aq. Sol.	Yes	No	No
[$P_{6,6,6,14}$][Tf_2N]	<1	≥Aq. Sol.	No	No	No
[$P_{6,6,6,14}$][FAP]	<1	≥Aq. Sol.	No	No	No
[DOM(5Bu-CN)][Tf_2N]	≥1	<Aq. Sol.	Yes	*Ex situ* only	No
[DOM(5-HxOne][Tf_2N]	≥1	<Aq. Sol.	Yes	*Ex situ* only	No

Table 3.5 below, compares the suitability of ionic liquids for extractive fermentation based on various combinations of the cation and anion structures. We classified the ionic liquids based on cation and anion structures. Imidazolium cations, which are aromatic, were classified as polar

along with ammonium cations with nitrile and ketone groups in the side chain which can be considered as mildly polar. Aliphatic quaternary ammonium and phosphonium cations were classified as non-polar. Non-planar [FAP] anion was classified as bulky due to the presence of three fluoro-ethyl side chains and the planar [Tf_2N] was classified relatively as non-bulky. We observe that, all non-polar cations - irrespective of anion size - and polar cations with bulky anions, are non-toxic but have low extractability. However, polar cations with non-bulky anions have the opposite behavior, i.e., they are toxic but have high extractability. Looking closely at the non-polar quaternary ammonium side chains, the non-polarity decreases relatively with decrease in the chain length. But EC_{50} increases and so does the aqueous solubility. We hypothesize that if we start with an ionic liquid with polar cations and bulky anions and reduce the toxicity by reducing the polarity or start with non-polar cation and non-bulky anion and then increase the partition coefficient by increasing the polarity, an optimal ionic liquid could be found.

Table 3.5. Dependency of ionic liquid extractive fermentation suitability on cation and anion structures

Cation side chain polarity	**Anion size**	***Partition Coefficient (K_c)***	***Molecular Toxicity (EC_{50})***	***Fermentation Suitability***	***Extractive Suitability***	***In Situ Suitability***
Polar	Bulky	<1	≥Aq. Sol.	Yes	No	No
Polar	Non-Bulky	≥1	<Aq. Sol.	No	Yes	No
Non-Polar	Bulky	<1	≥Aq. Sol.	Yes	No	No
Non-Polar	Non-Bulky	<1	≥Aq. Sol.	Yes	No	No

3.6. Conclusions

In this chapter, applicability of ionic liquids was studied by measuring toxicity and partition coefficients for the model system of NDHD production. It was observed that while the ILs that

had high partitioning for the solute were toxic to the cells. None of the ILs investigated were both non-toxic and had high extractability but ILs like [HMIm][Tf_2N], [DOM(5-BuCN)][Tf_2N] and [DOM(5-HxOne)][Tf_2N] are suitable for *ex situ* extraction while aliphatic quaternary ammonium ILs could potentially improve product yields in *In situ* fermentation. From the structure-property (toxicity and partitioning) relationships developed, future work should aim at synthesis of ILs that are moderately polar than imidazolium cation and less bulkier than [FAP] anion to identify optimal ionic liquids for *in situ* extraction.

3.7. References

(1) Harrop, A. J.; Woodley, J. M.; Lilly, M. D. Production of Naphthalene cis-Glycol by Pseudomonas Putida in the Presence of Organic Solvents. *Enzyme and Microbial Technology* **1992**, *14*, 725.

(2) McIver, A. M.; Garikipati, S. V. B. J.; Bankole, K. S.; Gyamerah, M.; Peeples, T. L. Microbial Oxidation of Naphthalene to cis-1,2-Naphthalene Dihydrodiol Using Naphthalene Dioxygenase in Biphasic Media. *Biotechnol. Prog.* **2008**, *24*, 593.

(3) Lye, G. J.; Woodley, J. M. Application of in situ product removal techniques to biocatalytic processes. *Trends in Biotechnology* **1999**, *17*, 395.

(4) Kanazawa, A.; Ikeda, T.; Endo, T. Synthesis and Antimicrobial Activity of Dimethyl- and Trimethyl-Substituted Phosphonium Salts with Alkyl Chains of Various Lengths. *Antimicrobial Agents and Chemotherapy* **1994**, *38*, 945.

(5) Anderson, K.; Rodriguez, H.; Seddon, K. R. Phase behaviour of trihexyl(tetradecyl)phosphonium chloride, nonane and water. *Green Chem.* **2009**, *11*, 780.

(6) Shaw, G. D.; Maczynski, A.; Goral, M.; Wisniewska-Goclowska, B.; Skrzecz, A.; Owczarek, I.; Blazej, K.; Haulait-Pirson, M.; Hefter, T. G.; Huyskens, P. L.; Kapuku, F.; Maczynska, Z.; Szafranski, A. IUPAC-NIST Solubility Data Series. 81. Hydrocarbons with Water and Seawater—Revised and Updated. Part 9. C10 Hydrocarbons with Water. *J Phys Chem Ref Data* **2006**, *35*, 93.

(7) Docherty, K. M.; Kulpa, C. F. Toxicity and antimicrobial activity of imidazolium and pyridinium ionic liquids. *Green Chem.* **2005**, *7*, 185.

(8) Lee, S.-M.; Chang, W.-J.; Choi, A.-R.; Koo, Y.-M. Influence of ionic liquids on the growth of Escherichia coli. *Korean J. Chem. Eng.* **2005**, *22*, 687.

(9) Pfruender, H.; Jones, R.; Weuster-Botz, D. Water immiscible ionic liquids as solvents for whole cell biocatalysis. *J. Biotech.* **2006**, *124*, 182.

(10) Brautigam, S.; Bringer-Meyerb, S.; Weuster-Botz, D. Asymmetric whole cell biotransformations in biphasic ionic liquid/water-systems by use of recombinant Escherichia coli with intracellular cofactor regeneration. *Tetrahedron: Asymmetry* **2007**, *18*, 1883.

(11) Cornmell, R. J.; Winder, C. L.; Schuler, S.; Goodacre, R.; Stephens, G. Using a Biphasic Ionic Liquid/Water Reaction System To Improve Oxygenase-Catalysed Biotransformation With Whole Cells. *Green Chemistry* **2008**, *10*, 685.
(12) Cornmell, R. J.; Winder, C. L.; Tiddy, G. J. T.; Goodacre, R.; Stephens, G. Accumulation of Ionic Liquids in Escherichia coli cells. *Green Chemistry* **2008**, *10*, 836
(13) Gilbert, P.; Moore, L. E. Cationic Antiseptics: Diversity of Action under a Common Epithet. *Journal of Applied Microbiology* **2005**, *99*, 703.
(14) Ishikawa, S.; Matsumara, Y.; Yoshizako, F.; Tsuchido, T. Characterization of a cationic surfactant-resistant mutant isolated spontaneously from *Escherichia coli*. **2002**, *92*, 261.
(15) Salton, M. R. J. The adsorption of Cetyltrimethylammonium bromide by bacteria, its action in releasing cellular constituents and its bactericidal effects. *J. Gen. Microbiol.* **1951**, *5*, 391.
(16) Yoshimatsu, T.; Hiyama, K. Mechanism of the action of Didecyldimethylammonium chloride (DDAC) against *Escherichia coli* and morphological changes of the cells. *Biocontrol Science* **2007**, *12*, 93.
(17) Walsh, S. E.; Mallard, J.-Y.; Russell, A. D.; Catrenich, C. E.; Charbonneau, D. L.; Bartolo, R. G. Activity and mechanisms fof action of selected biocidal agemts on gram-positive and -negative bacteria. *Journal of Applied Microbiology* **2003**, *94*, 240.
(18) Blois, D. W.; Swarbrick, J. Interaction of Quaternary ammonoium bactericides with biological materials 1: Conductance studies with Cephalin. *Journal of Pharmaceutical Sciences* **1971**, *61*, 390.
(19) Midgley, M. The phosphonium ion efflux system of Escherichia coli: Relationship to the ethidium efflux system and energetic studies. *Journal of General Microbiology* **1986**, *132*, 3187.
(20) Maillard, J.-Y. Bacterial target sites for biocide action. *Journal of Applied Microbiology Symposium Supplement* **2002**, *92*, 16S.
(21) Silhavy, T. J.; Kahne, D.; Walker, S. The Bacterial Cell Envelope. *Cold Spring Harb Perspect Biol* **2010**, *2*, 1.
(22) Meroueh, S. O.; Bencze, K. Z.; Hesek, D.; Lee, M.; Fisher, J. D.; Stemmler, T. L.; Mobashery, S. Three-dimensional structure of the bacterial cell wall peptidoglycan. *Proceedings of the National Academy of Sciences of United States of America* **2006**, *103*, 4404.
(23) Benz, R.; Bauer, K. Permeation of hydrophilic molecules through the outer membrane of gram-negative bacteria. *European Journal of Biochemistry* **1988**, *176*, 1.
(24) Schrimer, T. General and specific porins from bacterial outer membranes. *Journal of Structural Biology* **1998**, *121*, 101.
(25) Joynson, J. A.; Forbes, B.; Lambert, R. J. W. Adaptive resistance to benzalkonium chloride, amikacin and tobramycin: the effect on susceptibility to other antimicrobials. *Journal of Applied Microbiology* **2002**, *93*, 96.
(26) Ishikawa, S.; Matsumura, Y.; Yoshizako, F.; Tsuchido, T. Characterization of a cationic surfactant-resistant mutant isolated spontaneously from *Escherichia coli*. *Journal of Applied Microbiology* **2002**, *92*, 261.
(27) Bosetti, A.; Bianchi, D.; Andriollo, N.; Cidaria, D.; Cesti, P.; Sello, G.; Gennaro, P. D. Microbial Oxidation of Naphthalene to cis-1,2-Dihydroxy-1,2-dihydronaphthalene in a Membrane Bioreactor. *J. Chem. Tech. Biotechnol.* **1996**, *66*, 375.
(28) Chapeaux, A.; Simoni, L. D.; Stadtherr, M. A.; Brennecke, J. F. Liquid Phase Behavior of Ionic Liquids with Water and 1-Octanol and Modeling of 1-Octanol/Water Partition Coefficients. *J. Chem. Eng. Data* **2007**, *52*, 2462.

(29) Freire, M. G.; Carvalho, P. J.; Gardas, R. L.; Marrucho, I. M.; Santos, L. M. N. B. F.; Coutinho, J. A. P. Mutual Solubilities of Water and the [Cnmim][Tf2N] Hydrophobic Ionic Liquids. *J. Phys. Chem. B* **2008**, *112*, 1604.
(30) Mellein, B. R.; Aki, S. N. V. K.; Ladewski, R. L.; Brennecke, J. F. Solvatochromic studies of Ionic Liquid/Organic mixtures. *J. Phys. Chem. B* **2007**, *111*, 131.
(31) Kempter, V.; Kirchner, B. The role of hydrogen atoms in interactions involving imidazolium-based ionic liquids. *Journal of Molecular Structure* **2010**, *972*.
(32) Dong, K.; Zhang, S.; Wang, D.; Yao, X. Hydrogen bonds in Imidazolium ionic liquids. *J. Phys. Chem. A* **2006**, *110*, 9775.
(33) Hardacre, C.; Holbrey, J. D.; Nieuwenhuyzen, M.; Youngs, T. G. A. Structure and Solvation in Ionic Liquids. *Acc. Chem. Res.* **2007**, *40*, 1146.

4. TOWARDS IN SITU EXTRACTION OF BIORENEWABLE FUELS USING IONIC LIQUIDS

In this section, the extractability of acetone-butanol-ethanol (ABE) solutes, produced from the fermentation of sugars by *Clostridia*, from aqueous media using ionic liquid as an extractant were studied. Ternary diagrams were developed and the partition coefficients & selectivities were used to evaluate the performance of ionic liquids. Further, energy and preliminary cost analysis were conducted to compare the ionic liquid based extraction process with conventional distillation and organic solvent extraction processes.

Extraction of ABE solutes using ionic liquids has been reported by various authors in the literature. In the pure systems area, some authors have worked on binary systems (i.e., IL + ABE) to obtain the temperature composition data; while a few others have worked on ternary systems and developed pure systems overall ternary diagrams. Additionally, very few authors have investigated the extraction of 1-butanol from fermentation broths by measuring the partition coefficients and selectivities.

Domanska *et al.,*[1] developed a temperature composition phase diagram for 1-butanol - IL binary system using N-octylisoquinolinium [Tf_2N] as ionic liquid and modeled the vapor-liquid equilibrium (VLE) using NRTL activity coefficient method. Vale *et al.,*[2] studied binary systems consisting of [EMIm][Tf_2N] & n-alcohols and estimated phase behavior of these systems. Doker *et al.,*[3], Kato *et al.,*[4] and Nebig *et al.,*[5] measured the VLE as a function of temperature for binary systems of acetone-IL, ethanol/acetone-IL and ethanol-IL respectively. Revelli *et al.,*[6] and Bahadur *et al.,*[7] studied non-water based pure ternary systems for the extraction of n-alcohols from heptane and ethylacetate respectively.

4.1. Experimental Ternary LLE data: Overall concentration ranges

Extraction of ABE solutes from aqueous solutions was carried using model ionic liquid [HMIm][Tf_2N]. Overall phase equilibrium curves for the three ternary systems of ionic liquid/ (A, B & E) /Water were developed at ambient temperature and pressure. Ternary diagrams with the phase equilibrium curves and tie-lines for extraction of 1-butanol, acetone and ethanol are shown in Figures 4.1, 4.2 and 4.3 respectively. Phase equilibrium curves for all three ternary systems are similar forming two regions. The region inside the curve, termed as binodal curve, results in phase split forming two phases (Extract and Raffinate) and outside this region no phase splitting occurs, single phase is observed. IL-water binary system forms an immiscible mixture. Their mutual solubility increases upon the addition of a third component, either of A or B or E and the two phase interface disappears leading to miscible, single phase system.

[HMIm][Tf_2N]/1-butanol/Water: Water and [HMIm][Tf_2N] have a large immiscibility gap,[8] water and 1-butanol have limited solubility, while this ionic liquid and 1-butanol are completely miscible.[8,9] The resulting ternary system of [HMIm][Tf_2N]/1-butanol/water forms a type 2 ternary diagram extending between the two immiscible binaries.[10] It was reported that presence of butyl side chain instead of hexyl on the cation led to immiscibility between [BMIm][Tf_2N] and 1-butanol, and the resulting ternary diagram was a type 3B where there are 3 distinct two-phase regions.[11,12] Incorporating a hydroxyl group in hexyl chain ([HOHMim]) did not change mutual solubility between ionic liquid and 1-butanol and resulted in a type 2 LLE system, though because of increased water solubility of the ionic liquid, the 2-phase region was shrunk. While with [HMIm][FAP][13], enhanced water-IL immiscibility lead to an extended 2-phase region. Selectivities were in the order of [HMIm][FAP] > [HMIm][Tf_2N] > [HOHMim][Tf_2N].

Figure 4.1: Overall phase equilibrium curves for the ternary systems of [HMIm][Tf_2N], 1-butanol and Water

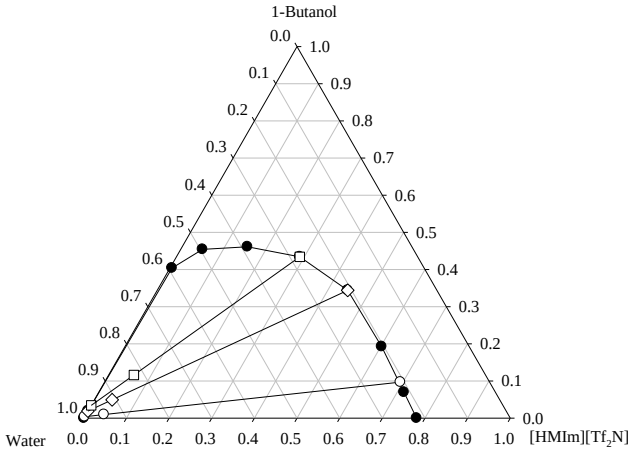

[HMIm][Tf_2N]/Acetone/Water: In this system, apart from the IL-water binary, the other two binaries are completely miscible. The ternary diagram, Figure 4.3b, forms a type 1 LLE[10] which occurs because of immiscibility of one binary system (IL-water).

Figure 4.2: Overall phase equilibrium curves for the ternary systems of [HMIm][Tf_2N], Acetone and Water

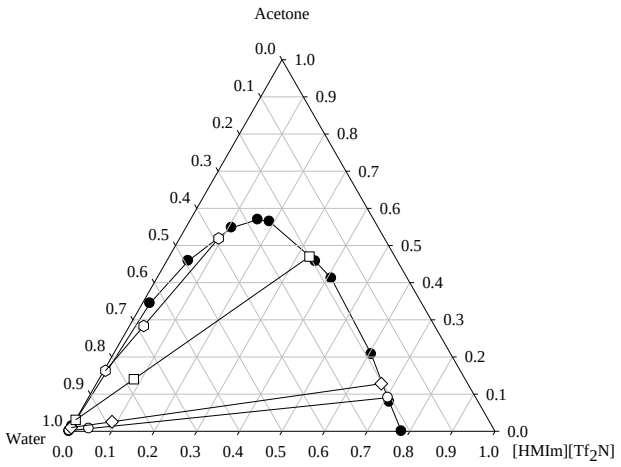

[HMIm][Tf_2N]/Ethanol/Water: Apart from IL-water immiscibility and ethanol-IL miscibility, the ethanol-water system is completely miscible at ambient temperatures.[8] The ternary diagram is type 1 LLE[10] because of the immiscibility gap between IL-water. This is similar to the acetone ternary. The tielines at lower concentrations are flat and at higher concentrations the slopes are less steeper than either of the cases of 1-butanol or acetone. So, going from ethanol to 1-butanol, reduces water solubility but does not affect their ionic liquid solubility, and the resulting ternaries shift from type 1 for ethanol to type 2 for 1-butanol. Ternary diagrams with [BMIm][PF_6], [HMIm][PF_6], [HOHMIm][Tf_2N] and [HMIm][FAP] as extractants have been published.[11,13,14] and they form type 2a or type 1 LLE. The hydrophobicity of anions is in the order [FAP]>[Tf_2N]>[PF_6]. This is attributed to better performance of [HMIm][FAP] over the other two solvents in extracting ethanol, while [HMIm][Tf_2N] is better than [HMIm][PF_6], though all three ionic liquids are unsuitable as extractants because of low K_x values. From this, a suitable ionic liquid for ethanol extraction should have a lower affinity for water as observed with 1-butanol or it should have high affinity for ionic liquid as observed with acetone.

Figure 4.3: Overall phase equilibrium curves for the ternary systems of [HMIm][Tf_2N], Ethanol and Water

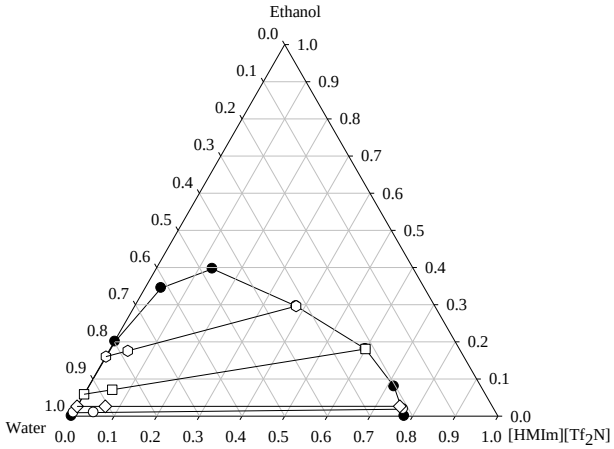

Since the focus of the present work is on the extraction of ABE solutes from fermentation broth, where the solutes are produced at lower concentrations,[15] the ternary diagram at lower concentrations were studied in detail.

4.2. Experimental Ternary LLE data: Low concentration ranges

Extraction of ABE solutes from aqueous solutions was carried using model ionic liquid [HMIm][Tf_2N] at low solute concentrations in the range of 0 – 2 mol %, at a temperature of 295±1 K and pressure of 1 atm. For each solute, 6-7 tie lines were obtained. The 0 – 2 mol% concentration ranges were selected as this range is typically observed in ABE fermentation systems (as discussed in section 1.2.2.1). The experimental process is described in section 2.3.

4.2.1. Othmer-Tobias plots

The reliability of the experimentally measured tie line data can be ascertained using well-established Othmer-Tobias plots.[16] Linearity of the plot indicates consistency of the data. The Othmer-Tobias plots are based on the weight fractions of components and plotted using the following equation.

$$\ln\left(\frac{1-w_{33}}{w_{33}}\right) = b + a\ln\left(\frac{1-w_{11}}{w_{11}}\right)$$

Where,

w_{33} – Weight fraction of Ionic liquid in the bulk Ionic liquid phase

w_{11} – Weight fraction of Water in the bulk aqueous phase

Figure 4.4a, b, c shows the plots and Table 4.1 lists the constants and R^2 values obtained. From these plots and R^2 values, it can be ascertained that the experimental data are reliable.

Figure 4.4: Othmer-Tobias plots for the ternary systems of [HMIm][Tf_2N], Water and A.) 1-butanol, B.) Acetone & C.) Ethanol

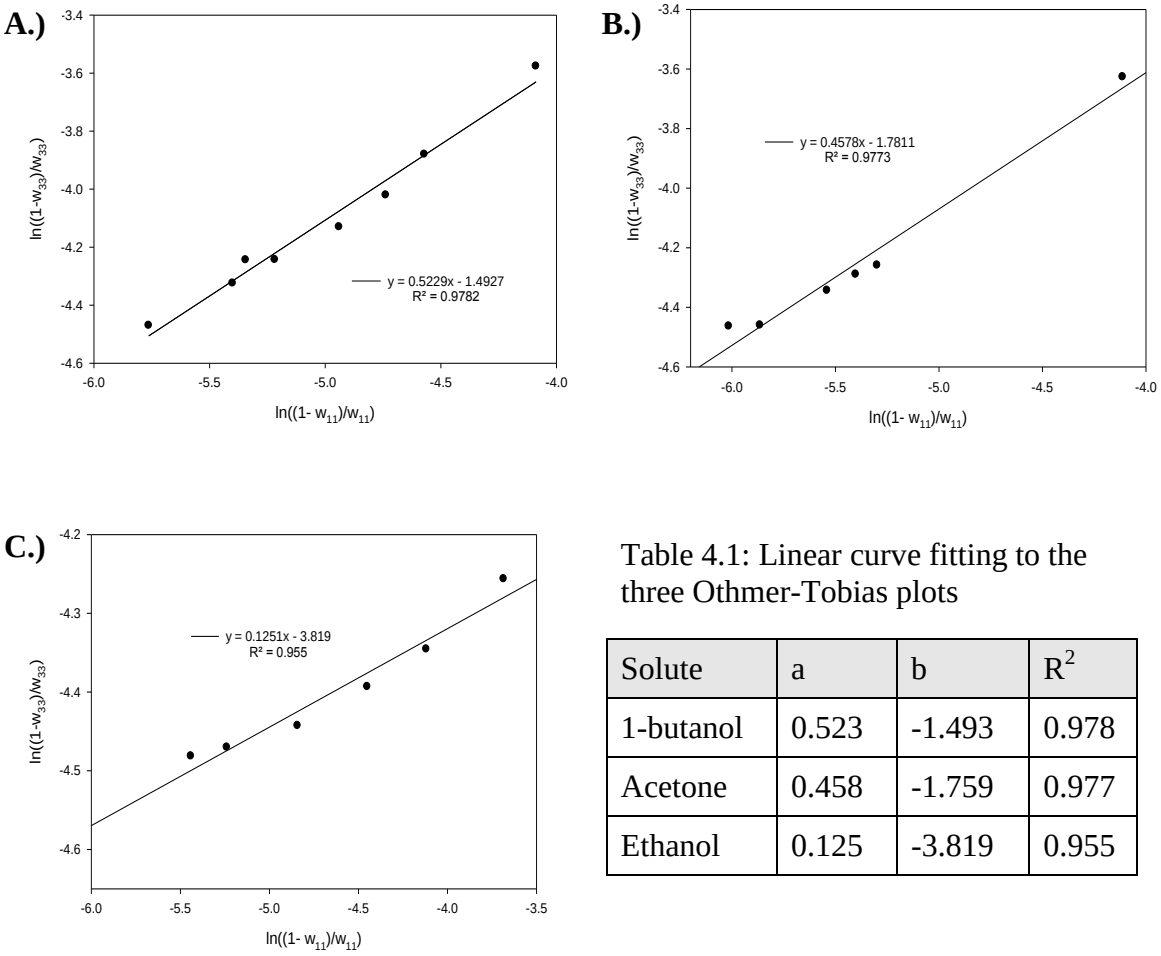

Table 4.1: Linear curve fitting to the three Othmer-Tobias plots

Solute	a	b	R^2
1-butanol	0.523	-1.493	0.978
Acetone	0.458	-1.759	0.977
Ethanol	0.125	-3.819	0.955

4.2.2. Ternary LLE for IL/1-butanol/Water system

The data were collected in the lower initial feed concentration of 0 – 1 mol% in water (0 – 5% by vol. and 0 – 6% by wt.). The partition coefficients and selectivities for IL/1-butanol/water system are shown in Figure 4.6 and

Table 4.2. Slopes of tie-lines for 1-butanol are greater than zero which suggests that at equilibrium the solutes partitions higher into the extractant ionic liquid phase than the aqueous

phase. This is confirmed by the partition coefficients > 1 (mole fraction based). The water – 1-butanol system is partially miscible, solubility of 1-butanol in water is 7.4% by wt. and 1.9% by mole,[10] while IL − 1-butanol are completely miscible at 295 K. This suggests that 1-butanol partitions less into water and more into ionic liquid. The high partition coefficients obtained here confirm that 1:1 solvent phase ratio (i.e., water to ionic liquid ratio) is sufficient to extract 1-butanol from water over an extraction train (multiple extractions).

In this range, the partition coefficients are relatively constant, varying from 19 to 21. The selectivities are relatively invariant below 0.2% but decrease continuously from 127 to 104 as the 1-butanol concentration is increased from 0.2 to 1%. Selectivities (S_x) of 100 were reported by Chapeaux *et al.,*[8] when the wt.% of 1-butanol in water was around 2. Using [HMIm][FAP], the K_x and S_x at 5% by wt. of 1-butanol were 6 and 300 respectively.[13] For extraction of 5% by wt. of 1-butanol, Hu *et al.,*[17] reported K_x of around 6 for both 1-(2-hydroxyethyl)-2,3-dimethylimidazolium tetrafluoroborate [HOEMMIm][BF_4] and 1-(2-hydroxyethyl)-3-methylimidazolium tetrafluoroborate [HOEMIm][BF_4] and corresponding S_x were 50 and 250 respectively. K_x for the extraction of 5% by wt. of 1-butanol from water using [BMIm][BF_4] and [OMIm][BF_4] were 0.8 and 0.9 respectively while corresponding S_x were 21.5 and 36.7 respectively.[18]

Garcia-Chavez *et al.,*[19] studied recovery of 1% by wt. of 1-butanol from water using non-flourinated ionic liquids. Tetraoctylammonium 2-methly-1-naphthoate was reported to be the most promising ionic liquid tested with K_w = 3.42 and S_w = 192, while for [HMIm][Tf_2N] was 1.1 and 120 respectively. They compared the ionic liquid extraction with conventional distillation and reported that the former has 73% less energy requirement than the later. The energy demand

per kg of 1-butanol for ionic liquid based process, Oleyl alcohol based extraction, and conventional distillation was 5.65 MJ, 6.1 MJ and 21.3 MJ respectively.

Cascon *et al.*,[20] studied 1-butanol extraction from water using Phosphonium and Ammonium based ionic liquids. They further evaluated the effect of anions and cations on the partition coefficients. They measured toxicity to *Clostridium Acetobutylicum* and *Clostridium Beijerinckii.* It was reported that anion moieties controlled the 1-butanol extraction with dihexylsulfosuccinate [DHSS] better than dicynamide [DCN] better than [Tf_2N]. Further, akylammonium cations performed better than aklyphosphonium cations. It was also reported that in a ABE fermentation with [$P_{6,6,6,14}$] as cation and [DHSS] & [DCN] as cations, acetone and ethanol were co-extracted.

Table 4.2: Partitioning Coefficients & Selectivities for 1-butanol

K_x	S_x	K_w	S_w	K_C	S_C
18.7±0.7	87.0±7.5	1±0.1	87.0±6.5	1.3±0.02	87.0±6.5

Figure 4.6: Selectivities and partition coefficients for the extraction of 1-butanol from water using model ionic liquid [HMIm][Tf_2N]

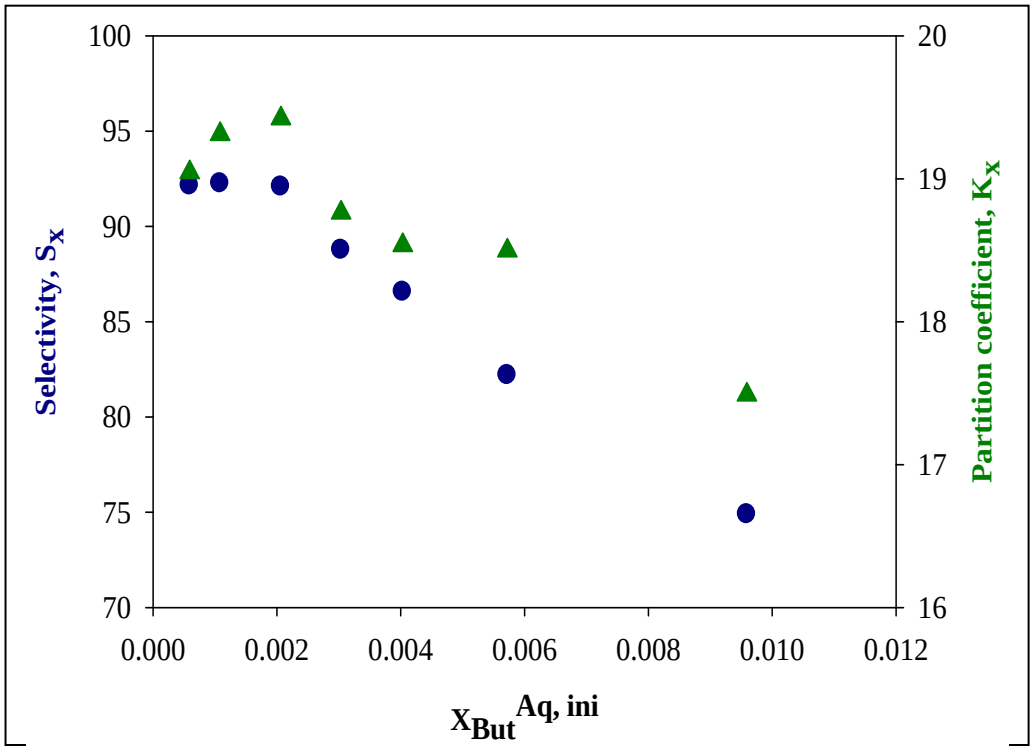

Figure 4.5: Tie-lines for the /[HMIm][Tf_2N]/1-butanol/water system

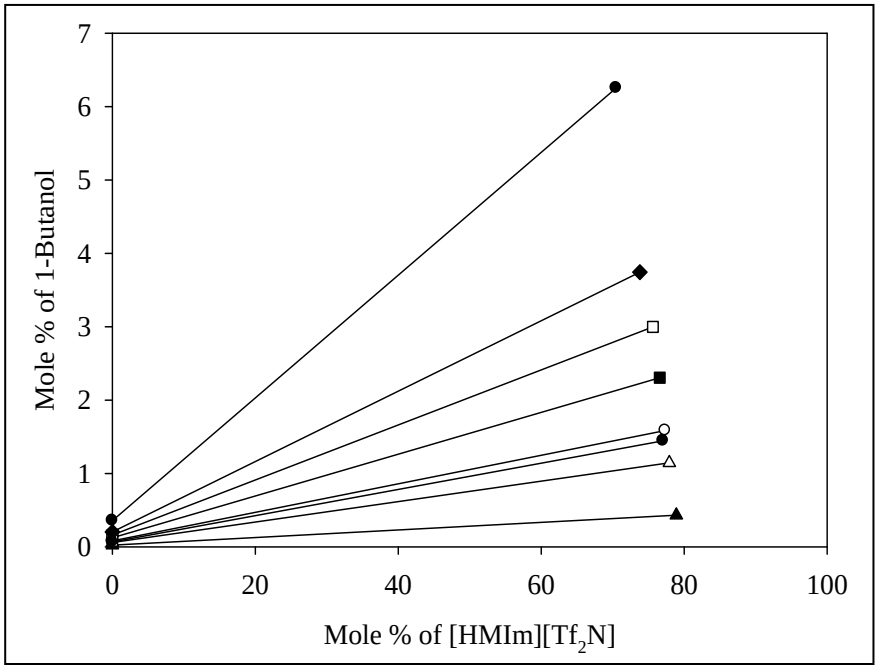

4.2.3. Ternary LLE for IL/Acetone/Water system

The partition coefficients and selectivities for water/acetone/IL system are shown in Figure 4.7 and Table 4.3. As the partition coefficients are greater than 1, it can be inferred that ionic liquid is successful in extracting acetone from water, i.e., tie lines have a positive slope. High partition coefficients obtained here confirm that a 1:1 solvent-phase ratio (i.e., water to ionic liquid ratio) is sufficient for extraction of acetone from water over a series of extraction stages. Though, acetone is completely miscible with ionic liquid and water, the high partition coefficients could be attributed to higher affinity of acetone towards ionic liquid.

The data were collected in the lower initial solute concentration range of 0 – 1.6 mol% in water (0 – 6.2% by vol. and 0 – 5% by wt.). Below 0.5%, the partition coefficients are relatively constant. However, they decrease by approx. 10% as the acetone concentration is increased from 0.5% to 1.6%. The selectivities decrease from 137 to 110 as the acetone concentration is increased from 0 to 1.5%.

Table 4.3: Partitioning Coefficients & Selectivities for Acetone in mole fractions, weights and concentration units

K_x	S_x	K_w	S_w	K_C	S_C
20.1±1.1	94.6±7.4	1.04±0.03	94.6±7.4	1.43±0.05	94.6±7.4

Figure 4.7: Selectivities and partition coefficients for the extraction of acetone from water using model ionic liquid, [HMIm][Tf_2N]

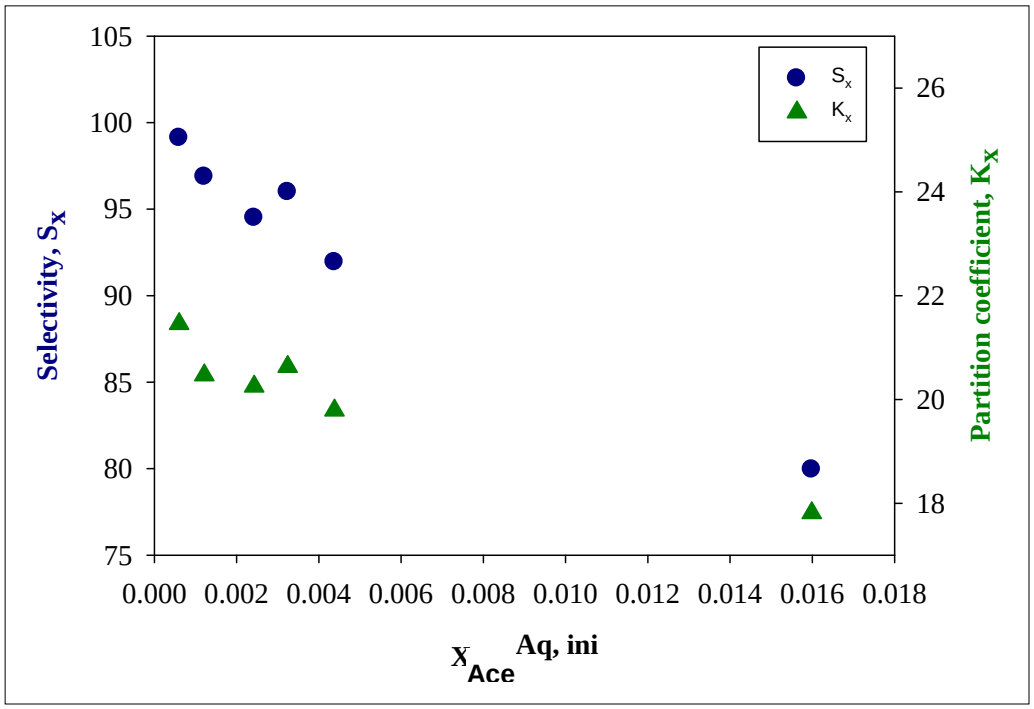

Figure 4.8: Tie-lines for the [HMIm][Tf_2N]/Acetone/Water system

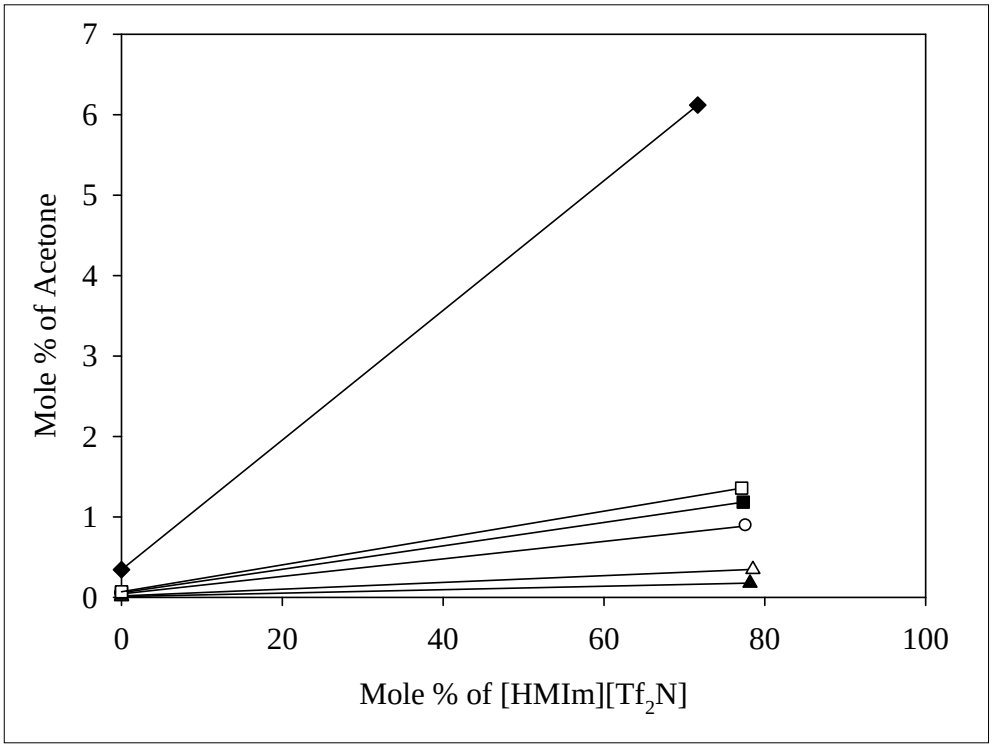

4.2.4. Ternary LLE for IL/Ethanol/Water system

The partition coefficients and selectivities for the IL/ethanol/water system are shown in Figure 4.10 and Table 4.4. At equilibrium, ethanol partitions more into water phase. Average partition coefficient (K_x) for this system is 2.1 which is much lower than those obtained with either acetone or 1-butanol ternary systems. Also, average partition coefficient based on weight fractions is 0.11 which is much less than 1, and it can be inferred that ionic liquid is less successful in extracting ethanol from water. The extraction process would require higher amount of ionic liquid to extract ethanol from water compared to acetone or 1-butanol. IL-water ratio much higher than 1:1, e.g., 10:1 and/or more contact stages could be required to extract useful quantities of ethanol from water; the resulting process might not be economically feasible.

The data was collected in the lower initial solute concentrations of 0 – 1.5 mol% (0 – 3.7% by vol. and 0 – 6% by wt.). In this range, the partition coefficients and selectivities are relatively constant, at approximately 2.3 and 13.6 respectively. Similar partition coefficient values for extraction of ethanol from water with [HMIm][Tf_2N] are reported in the literature.[13]

Table 4.4: Partitioning Coefficients & Selectivities for Ethanol

K_x	S_x	K_w	S_w	K_C	S_C
2.1±0.08	9.8±0.4	0.11±0.004	9.8±0.4	0.152±0.006	9.8±0.4

Figure 4.10: Selectivities and partition coefficients for the extraction of ethanol from water using model ionic liquid [HMIm][Tf_2N]

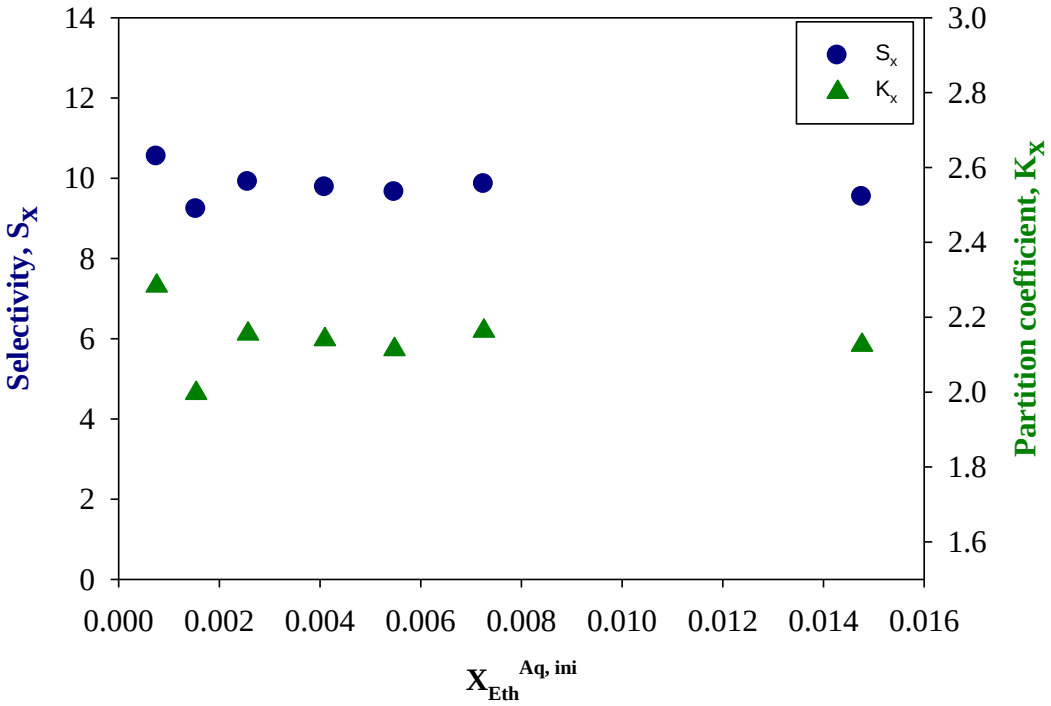

Figure 4.10: Tie-lines for ternary system of [HMIm][Tf_2N]/ Ethanol/

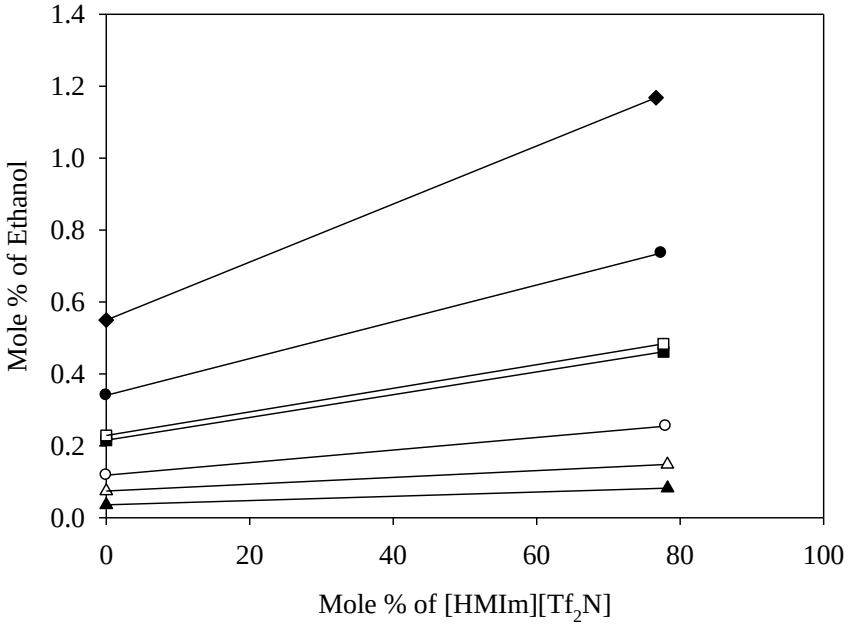

4.2. Modeling of ternary Liquid-Liquid Equilibrium

4.2.1. G^{EX}/Activity coefficient modeling using NRTL

As described in the introduction chapter, NRTL and UNIQUAC are the frequently employed parameter models for modeling Gibbs free energy of multicomponent liquid systems using activity coefficients when experimental phase equilibrium data is available. NRTL and UNIQUAC provide the best fit for the experimental data.[21,22] Though NRTL is a 3 parameter model, it is simpler to implement than UNIQUAC method which requires estimation of structural parameters.[22] Modeling of ternary LLE from binary systems is in itself not well established and modeling of ternary LLE involving ionic liquids is still infancy as the capabilities of the activity coefficients models is not well studied.[23] Further, the literature for binary data involving ionic liquids is in its nascent stage. Simoni *et al.*,[11] did extensive work on the modeling of ternary LLE systems involving ionic liquids and dilute aqueous solutions using minimization of Gibbs free energy approach and employing interval-newton technique. They observed that either of NRTL or UNIQUAC or eNRTL (electrolyte NRTL) models did not satisfactorily predict phase diagrams especially for type 3b systems. For modeling [HMIm][Tf_2N]/1-butanol or Ethanol /Water systems, UNIQUAC and eNRTL were better models for type 2 systems while NRTL was more accurate for type 1 system.[12] When using only binary data or component data, asymmetric NRTL/eNRTL model provided better predictions than symmetric models such as NRTL, UNIQUAC. Here, ionic liquid dissociation in water was incorporated in the model.

Santiago *et al.*,[24] correlated [HOEMMIm][BF_4]/1-butanol/water based ternary systems using UNIQAUC model where new area and volume parameters were obtained from quantum chemistry calculations. Simplex method for function minimization was used and the objective

function consisted of sum of squares of error between experimental and calculated mole fractions. Maximum deviations of up to 1.5% were reported.

Group contributing methods such as UNIFAC, where the ionic liquid parameters are estimated, have also been commonly used for predicting thermodynamic behavior of ionic liquid systems.[25] Unavailability of all the ionic liquid parameters is a disadvantage with using UNIFAC method. Alternate to UNIFAC, a novel method, based on unimolecular quantum calculations, the Conductor-like Screening Model for Real Solvents (COSMO-RS) has been used for prediction of thermodynamic behavior of a few non-water systems and water-IL systems.[23]

NRTL (Non-Random two liquid) activity coefficient model is used in this work to predict the phase equilibrium and the model is described in Equation 4.1 below.[22] A reduced form of this model for three components was used in the modeling.

Equation 4.1: Non-Random two liquid activity coefficient model used for modeling liquid-liquid equilibrium for system consisting of 'n' components

$$G_i^{EX} = RT \ln \gamma_i$$

$$\ln \gamma_i = \frac{\sum_j x_j \tau_{ji} G_{ji}}{\sum_k x_k G_{ki}} + \sum_j \frac{x_j G_{ij}}{\sum_k x_k G_{kj}} \left(\tau_{ij} - \frac{\sum_m x_m \tau_{mj} G_{mj}}{\sum_k x_k G_{kj}} \right)$$

$$G_{ij} = \exp(-\alpha_{ij} \tau_{ij})$$

$$\tau_{ij} = a_{ij} + b_{ij}/T + e_{ij} \ln T + f_{ij} T$$

where,

G_i^{Ex} – Excess Gibbs free energy

i, j, k, m – Total components in the mixture

R – Universal gas coefficient

T – Temperature of the system in K

γ_i – Activity coefficient

x_i – Mole fraction

$G_{ii} = 1$

$\tau_{ii} = 0$

a_{ij}, b_{ij}, e_{ij}, f_{ij} are the BIPs between components i and j; these are asymmetric (i.e., $a_{ij} \neq a_{ji}$)

α_{ij} is the randomness factor defined as $\alpha_{ij} = c_{ij} + d_{ij}\,(T - 273.15K)$

c_{ij}, d_{ij} are chosen based on the binary components

The key inputs for the NRTL model are the binary interaction parameters (BIPs) and randomness factor (α_{ij}). These inputs are required for the simulation of separation equipment like LLE extractor, distillation column, etc., using the NRTL model. The randomness factor values found in literature are shown in Table 4.5 below.[8,10,11,22]

Table 4.5: Randomness factor (α_{ij}) from literature

System	α_{ij}
IL – 1-butanol	0.3
IL – Water	0.2
1-butanol –Water	0.2

4.2.2. Regression of BIPs from LLE data

For implementing the NRTL activity coefficient model in process simulation, binary interaction parameters (BIPs) have to be regressed from the experimental data. Least squares minimization technique for the regression was employed. Since the experimental data was collected at one temperature, the temperature dependency of the BIPs is not considered in this work.

4.2.2.1. Least squares minimization technique

The calculation of the activity coefficient using NRTL model results in a non-linear equation as the model involves exponential terms and ratios. When the number of data points used to fit to a given model is more than the number of unknown parameters, which is the case here, least squares minimization technique is typically used. For regression of BIPs for ternary system using NRTL model, a non-linear least squares minimization is used.

In this non-linear least squares minimization technique, the sum of the square of the error between estimated and experimental mole fractions of one or both phases is minimized by varying the BIPs and the estimated mole fractions of either one or both phases. This sum of squares is considered as the objective function for the regression. To obtain the BIPs for this non-linear problem, initialization of the parameters is required and the equations have to be solved iteratively. The iterative process is stopped when a convergence criterion is met. For the present problem dealing with ternary LLE system, there would be 3 binary systems and a total of six parameters need to be regressed as the temperature dependence of BIPs is not being considered.

4.2.2.2. Software selection

Commercial process simulation packages like ASPEN Plus and CHEMCAD, which have in-built data regression modules, can be used to regress BIPs from experimental data. For the low ranges studied here, the two software packages encountered convergence issues and generated high least squares minimization output. Hence, a program code was written and implemented in MATLAB.

4.2.2.3. Regression algorithm

Reliable and precise phase equilibrium calculations are important design considerations for simulation of chemical processes. The usual approaches,[27,28,29] which are similar to single-stage flash calculations, for solving phase equilibrium problems to predict the phase compositions and number of phases present are:

1. Equation solving approach: This method is based on isofugacity (equality of fugacity at equilibrium) that involves mass balances and equilibrium constants such as *K*-values (thermodynamic equations). The approach requires solving these simultaneous mass balance and equilibrium equations and hence is a fast converging algorithm. Here, the number of phases at equilibrium is assumed as the method fails to correctly calculate the number of phases. As it involves using *K*-values, it is also referred to as *K*-value method. The underlying thermodynamics of this model is accurate though the computational method used, the initial guesses and sensitivity to objective function may lead to trivial solutions or multiple solutions that are not global minima which satisfy isofugacity criteria. Two subclasses are commonly used to solve the equations which differ in how equations are solved. One is the simultaneous equation solving, where all equations are solved at a time and other is equation decoupling, where equations are solved in inner loop and the *K*-values updated in the outer. While the former suffers from ill-conditioning and convergence, the latter is slow to converge but can be accelerated using various methods. In a review by Teh, *et al.*,[28] it was reported that the equation-solving method is reliable and efficient for LLE problems.

2. Minimization of Gibbs free energy approach: This is based on the fact that at equilibrium the Gibbs free energy of the system (both liquid phases) is the lowest and there is only one global minimum. This is based on the stability criterion that is sufficient condition, while equilibrium is

the necessary condition. Both Deterministic and Stochastic methods have been used which are based on local optimization and global optimization. A stochastic Genetic algorithm was found to be most reliable one. A detailed review can be found elsewhere.[28,30,31] But for simple regressions of two phase ternary systems, the Gibbs energy is itself a highly non-linear and complex, while Genetic Algorithm requires large computational effort.

For the present regression modeling, an initial equation solving algorithm for ternary LLE phase equilibrium calculations developed by Ohanomah, *et al.*,[32] was used. This is based on the second subclass, equation decoupling, which uses an acceleration method, RMW method - a combination of Rachford-Rice formulation, Mean value theorem and Wegstein's projection. Though this equation solving method has its drawbacks, it is the most efficient and reliable method listed in the literature. Further to avoid trivial solutions, low tolerances in the order of 10^{-12} were used, sensitivity of the BIPs to heat duty (discussed later) was done. Figure 4.11 shows single stage LLE flash and notation used.

A modified algorithm was used in the current simulation to regress the data and to estimate BIPs along with predicting phase compositions is described below:

a. Assume number of phases at equilibrium to be 2.
b. Select initial BIPs value (use binary system BIPs, if available). Set lower/upper bounds.
c. Determine feed points (mid-points of experimental end-points)
d. Outer loop: Parameter optimization
    i. For particular value of BIPs, initialize $\{K_i\}$, θ^{L2}.
    ii. Calculate $\{x_i^{L\alpha}\}$ and $\{x_i^{L\beta}\}$ using Eqn 4.2.5 and 4.2.6.

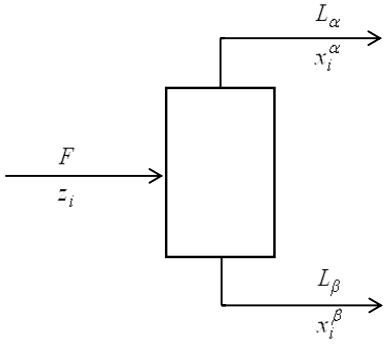

Figure 4.11: LLE extractor with initial feed (F) and equilibrated phases (α and β)

iii. Calculate γ_i^{α} and γ_i^{β}, from the NRTL thermodynamic model, using $\{x_i^{L\alpha}\}$ and $\{x_i^{L\beta}\}$. Update $\{K_i\}$ using Eqn. (4.2.2). Using Rachford-Rich (RR) formulation in Eqn. (4.2.7) and applying mean value theorem below, update $\theta^{L\beta}$. Here, mean value theorem is used to accelerate the search. Note the RR formulation is not solved for $\theta^{L\beta}$ but the convergence criterion is checked for.

iv. Calculate corresponding $\{x_i^{\alpha}\}$ and $\{x_i^{\beta}\}$ using final $\theta^{L\beta}$

v. Check for fugacity equality using latest $\{x_i^{\alpha}\}$ and $\{x_i^{\beta}\}$

vi. If Fugacity equality error < tolerance, go to step vii, else, modify $\{x_i^{\alpha}\}$ and/or $\{x_i^{\beta}\}$ such that fugacity equality is met. Go to step vii

vii. Calculate objective function (Obj. fun = Absolute average error between calculated and experimental data). If error is less than tolerance, use the BIPs to calculate *K* and *S*. Else go to step d.

e. Vary BIPs to minimize objective function, go to step c

Equation 4.2: Mass balance equations, equilibrium conditions, K-values, Rachford-Rice formulation and mean value theorem

Mass balance equations

$$F = L_\alpha + L_\beta$$

$$z_i F = x_i^{L_\alpha} L_\alpha + x_i^{L_\beta} L_\beta; \qquad i = 1,2,3$$

$$Let,\ \theta^{L_\beta} = \frac{L_\beta}{F};\ 1-\theta^{L_\beta} = \frac{L_\alpha}{F}$$

$$Hence,\ z_i = x_i^{L_\alpha}\left(1-\theta^{L_\beta}\right) + x_i^{L_\beta}\theta^{L_\beta};\ i = 1,2,3 \quad ----------Eqn(4.2.1)$$

Equilibriu m conditions

$$\gamma_i^{L_\alpha} x_i^{L_\alpha} = \gamma_i^{L_\beta} x_i^{L_\beta}; \qquad i = 1,2,3 \qquad ----------Eqn(4.2.2)$$

K – values

$$x_i^{L_\beta} = K_i\, x_i^{L_\alpha}; \qquad i = 1,2,3 \qquad ----------Eqn(4.2.3)$$

$$From\ the\ fugacity\ equality\ eqn(4.2.2),$$

$$\gamma_i^{L_\alpha} = K_i\, \gamma_i^{L_\beta}; \qquad i = 1,2,3 \qquad ----------Eqn(4.2.4)$$

$$Substituting\ for\ x_i^{L_\beta}\ from\ Eqn(4.2.3)\ in\ Eqn(4.2.1),$$

$$x_i^{L_\alpha} = \frac{z_i}{1+\theta^{L_\beta}\left(K_i-1\right)}; \qquad i = 1,2,3 \qquad ----------Eqn(4.2.5)$$

$$x_i^{L_\beta} = \frac{K_i\, z_i}{1+\theta^{L_\beta}\left(K_i-1\right)}; \qquad i = 1,2,3 \qquad ----------Eqn(4.2.6)$$

Rachford – Rice Formulation (Convergence Criterion)

$$\sum_{i=1}^{C}\left(x_i^{L_\beta} - x_i^{L_\alpha}\right) = \sum_{i=1}^{C}\left[\frac{z_i\left(K_i-1\right)}{1+\theta^{L_\beta}\left(K_i-1\right)}\right] = 0 \quad ----------Eqn(4.2.7)$$

α, β = Equilibriu m phases

z_i = Initial concentration of the component *'i'* in the Feed

F, L_α, L_β = Total moles in the feed, α and β phases

$\theta^{L_\beta} = \frac{L_\beta}{F}$ = Fraction of overall moles in the β – phase

Mean value theorem

After n^{th} iteration, θ^{L_β} is updated as

$$\left(\theta^{L_\beta}\right)^{n+1} = \left(\theta^{L_\beta}\right)^{n} - \frac{f\left(\left(\theta^{L_\beta}\right)^{n+1}\right)}{f'\left(\left(\theta^{L_\beta}\right)^{m}\right)}$$

where

$$\left(\theta^{L_\beta}\right)^{m} = \left(\theta^{L_\beta}\right)^{m} - \alpha.\frac{f\left(\left(\theta^{L_\beta}\right)^{n}\right)}{f'\left(\left(\theta^{L_\beta}\right)^{n}\right)}$$

and $f\left(\theta^{L_\beta}\right)^{n} = \sum_{i=1}^{NC}\left[\frac{z_i\left(K_i-1\right)}{1+\left(\theta^{L_\beta}\right)^{n}\left(K_i-1\right)}\right]$; $f'\left(\theta^{L_\beta}\right)^{n} = -\sum_{i=1}^{NC}\left[\frac{z_i\left(K_i-1\right)^2}{\left(1+\left(\theta^{L_\beta}\right)^{n}\left(K_i-1\right)\right)^2}\right]$

The BIPs are obtained from the experimental data by minimizing a suitable objective function. Here, the following objective function (O.F.) in Equation 4.3 was used. The O.F. is based on the sum of absolute average deviation between the experimental and calculated mole fractions for each component in each phase in each tie line. Further, a root mean square difference (RMSD) is calculated from the O.F. This number is an indicator of how calculated and experimental mole fractions compare to one another and is commonly reported as the output of the regression.

Equation 4.3: Objective function and RMSD

$$O.F. = \sum_{k=1}^{ND}\sum_{j=1}^{NP}\sum_{i=1}^{NC}\left|x_{ijk}^{\exp} - x_{ijk}^{calc}\right|$$

$$RMSD = \left[\frac{O.F.}{2(ND)(NC)}\right]^{-0.5}$$

ND – No. of experimental tie lines

NP – No. of phases at equilibrium in each tie line

NC – No. of components in each phase

4.2.2.4. Implementing regression algorithm in MATLAB

MATLAB has many in-built functions to implement the least squares minimization of an objective function for constrained and unconstrained nonlinear optimization problems. Of these, Genetic Algorithm and 'Fminsearchbnd' were evaluated. Genetic algorithm finds solution by creating a random initial population and this population is updated in the next iteration based on the scores obtained from fitness values. This function does not require an initial guess but requires bounds of the parameter. But the function takes a lot of computation time and it has reportedly given different final outputs using the same initial bounds.[28,33,34]

'Fminsearchbnd' is a multidimensional nonlinear minimization routine. This function uses the Nelder-Mead simplex algorithm to minimum of a function with bound constraints. However, this function requires careful selection of an initial guess for the binary interaction parameter and bounds for the parameter. Of these two functions, 'Fminsearchbnd' was used for regressing the BIPs.[28,33]

To determine the initial guesses, the BIPs were regressed using the binary data from literature for the IL (1) – water (3) and 1-butanol (2) – water (3) systems (see section 4.2.3.2). Binary data for IL-alcohols system are published but they are mostly for the immiscible systems.[9,35] Doker *et al.,*[3], Kato *et al.,*[4] and Nebig *et al.,*[5] measured the VLE with [HMIm][Tf_2N] as the ionic liquid and calculated the binary interaction parameters primarily using UNIFAC method (UNIQUAC and NRTL were also used). However the [HMIm][Tf_2N] (1) – 1-butanol (2) the binary system is completely miscible at room temperature and only excess volume properties are published.[9] So, a separate search of their binary interaction parameters (B_{12} and B_{21}) for all values between -1000 and +1000 was done and the set of parameters that provide the lowest RMSD was identified and as initial estimates was done, while the other four parameters

were obtained from literature as shown in Table 4.7. Here, lower and upper limits on all the six parameters were chosen as -3000 and 3000 respectively. From this overall search, the initial estimates of B_{12} and B_{21} that resulted in larger fugacity and RMSD values were eliminated. As the Fminsearch uses simplex method, four starting values (1000 & -100, 1 & 1, -100 & 1000 and -100 & -1000) were used. These converged to around the same point and were used in process modeling. The MATLAB code used is included in the Appendix A.

4.2.3. Regression results for IL/1-butanol/Water system

4.2.3.1. Results from MATLAB for low concentration range (0 - 1 mol %)

The binary interaction parameters determined from the MATLAB simulation using Fminsearchbnd function are shown in Table 4.6.

Table 4.6: BIPs for low concentration range

Binary system		BIPs		RMSD
i	j	B_{ij}	B_{ji}	
[HMIm][Tf_2N]	1-butanol	-164.71	980.95	$6.89x10^{-4}$
[HMIm][Tf_2N]	Water	99.65	2619.2	
1-butanol	Water	-549.63	1745.02	

Average absolute relative deviation (%AARD) were calculated between the mutual solubilities obtained from the literature and those calculated obtained from the above regressed binary interaction parameters (from the ternary data) for the two binary systems (IL – water and water – 1-butanol). The %AARD values for IL-water binary system and for the water – 1-butanol binary systems are: 0.1% and 10% resepectively.

4.2.3.2. Results from constituent binary systems that make up the ternary system

The BIPs for the three binary systems that makeup the ternary system was obtained from literature as shown in Table 4.7.

Table 4.7: BIPs for binary systems obtained from Literature

Binary system		BIPs		Temperature (K)	α	% AARD for the binary data obtained from literature	Source
I	J	B_{ij}	B_{ji}				
[HMIm][Tf_2N]	1-butanol	n/a	n/a	295.15	0.3	-	Completely miscible at this temperature and VLE data not available
[HMIm][Tf_2N]	Water	83.67	2616.49	296.65	0.2	< 0.1%	Regressed from literature data [36] using ASPEN
1-butanol	Water	-321.78	1530.1	298	0.2	< 0.1%	Regressed from literature data[37],[38] using ASPEN

4.2.3.3. Comparison of BIPS

In Table 4.8 below, the BIPS obtained from the low concentration range and the BIPs for [HMIm][Tf_2N]/1-butanol/Water ternary system from literature were compared with the BIPs for the three binary systems.

Table 4.8: Comparison of BIPS from various methods

	B_{ij} (K)	Present work (low conc. range)	Literature (binary systems)	Literature[8]
IL – 1-butanol (1,2)	B_{12}	-164.71	n/a	-628.1694
	B_{21}	980.95	n/a	1107.794
IL - Water (1,3)	B_{13}	99.65	83.67	84.4451
	B_{31}	2619.20	2616.49	2624.489
1-butanol – Water (2,3)	B_{23}	-549.63	-321.78	-308.733
	B_{32}	1745.02	1530.1	1504.089

4.2.3.4. Comparison of regression modeling results with experimental data

Table 4.10 below compare the partition coefficients and selectivities obtained from the regression modeling with experimental data. Both the calculated K_x and S_x values deviated 1.97 and 2.05% from the experimental results.

$$\%\,AARD = \frac{1}{ND}\left(\sum_{j=1}^{ND}\sum_{i=1}^{NC}\frac{\left|x_{ij}^{\exp} - x_{ij}^{calc}\right|}{x_{ij}^{\exp}}\right).100$$

ND – No. of experimental tie lines

NC – No. of components in each phase

Table 4.9: Absolute average relative deviations (AARD) for all components in both phases

	% AARD	
	Aqueous-rich Phase	IL-rich Phase
Water	0.002	0.95
1-Butanol	2.29	0.19
IL	4.48	0.26

Table 4.10: Experimental and simulated partition coefficients and selectivities

Experimental Partition coefficients	Calculated Partition coefficients
19.04	19.56
19.31	19.31
19.42	19.16
18.76	18.90
18.53	18.66
18.50	18.38
17.49	17.49

Experimental Selectivities	Calculated Selectivities
92.14	94.97
92.26	92.25
92.09	90.63
88.77	88.04
86.57	85.61
82.20	82.96
74.89	74.89

Experimental Partition coefficients	Calculated Partition coefficients
92.14	94.97
92.26	92.25
92.09	90.63
88.77	88.04
86.57	85.61
82.20	82.96
74.89	74.89

Experimental Selectivities	Calculated Selectivities
92.14	94.97
92.26	92.25
92.09	90.63
88.77	88.04
86.57	85.61
82.20	82.96
74.89	74.89

4.3. Simulation of 1-butanol separation at pilot plant scale using ionic liquid

The experiments were conducted at the lab scale, i.e., approx. 2 ml. To really understand if the ionic liquid based extraction process can be implemented at larger volumes, simulation of 1-butanol separation at pilot plant scale level is described in this section. For this process simulation, simulation package, ASPEN Plus was used. Here, the separation of 1-butanol from water is achieved using the ionic liquid. Though theoretically, water can be extracted from the ternary mixture, it is obvious that this route would be energy intensive because of amount of water present compared to 1-butanol. The following sections describe the input parameters, equations, methodology and results.

4.3.1. Input parameters for flowsheets

To begin developing the flowsheet in Aspen Plus, first the components are identified in the database and selected. Water and 1-butanol are available as built-in components in the databank. Unlike other two compounds, 1-butanol and water, used in the simulation, Ionic liquids that have been used recently are not present as default option in the Aspen databank. Hence for developing the flowsheet, [HMIm][Tf_2N] is created as a new component by prescribing its properties. Using the model ionic liquid for the simulation as many of its properties are available in literature unlike many ionic liquid's whose properties are evaluated as required. These include general physical properties and heat capacities, viscosity, density, vapor pressure at various temperatures. The table with the property data for [HMIm][Tf_2N] are included in the Appendix D.

4.3.2. Equations for calculating enthalpy change for ionic liquid

Along with creating the database for the model ionic liquid, appropriate equations in Aspen Plus need to be identified for calculating ionic liquid enthalpy change. This is required for heat

duty calculations of different equipment. Since ionic liquids are salts made up of cations and anions and is a liquid at the temperatures encountered in the process flowsheet (with negligible vapor pressure), built-in equations in Aspen Plus cannot be used directly for the calculation of enthalpy changes and need to be modified. Total mixture enthalpy is calculated as the sum of component enthalpy and excess mixture enthalpy as shown in Equation 4.4 below.

Equation 4.4: Total mixture molar enthalpy of the liquid phase.

$$H_m^{\ l} = \sum x_i H_i^{*,l} + H_m^{E,l}$$

where,

$H_m^{\ l}$ - Mixture molar liquid enthalpy

x_i - Component mole fractions

$H_i^{*,l}$ - Pure component liquid enthalpy

$H_m^{E,l}$ - Mixture molar excess enthalpy

Pure component enthalpies can be calculated using heat capacities as shown in Equation 4.5. Though ionic liquid heat capacity data is available, for calculation of mixture enthalpy, the mixture C_p is required which are not readily available; hence, this is not a suitable option.

Equation 4.5: Pure component liquid molar enthalpy using liquid heat capacity data

$$H_i^{*,l}(T) = H_i^{*,l}(T^{ref}) + \int_{T^{ref}}^{T} C_{p,i}^{*,l}(T)\,dT$$

$$H_i^{*,l}(T^{ref}) = H_i^{*,ig} + \left(H_i^{*,v} - H_i^{*,ig}\right) - \Delta_{vap}H_i^{*,l}$$

$$C_{p,i}^{*,l} = C_{1i} + C_{2i}T + C_{3i}T^2 + C_{4i}T^3 + C_{5i}T^4$$

$\Delta_{vap}H_i^{*,l}$ – Heat of vaporization from Watson/DIPRR model

Another route for calculation of enthalpy is using equation of state (EoS). Though EoS is more suitable for components in vapor state, it was used in calculation of mixture enthalpy as there was no better option available. However, the equations could be rewritten such that part of mixture enthalpy is calculated from activity coefficient models. Equation 4.6 and 4.7 shows two slightly different calculations methods to calculate mixture enthalpy using EoS. Peng-Robinson

/ Redlich-Kwong-Soave were tried as the EoS model for calculating liquid and vapor pure component molar enthalpy departure function $(H_m^{*,l} - H_m^{*,ig})$ or $(H_m^{*,v} - H_m^{*,ig})$, while for calculating excess molar enthalpy, the NRTL activity coefficient model was used. These equations for calculating mixture enthalpy are validated from the excess enthalpy experimental data.

Equation 4.6: Mixture enthalpy calculations based on equation of state involving liquid departure functions and activity coefficient models (1)

$$H_m^l = (H_m^l - H_m^{ig}) + H_m^{ig}$$

$$DH_m^l = H_m^l - H_m^{ig}$$

$$(H_m^l - H_m^{ig}) = \sum_i x_i (H_i^{*,l} - H_i^{*,ig}) + H_m^{E,l}$$

$$(H_i^{*,l} - H_i^{*,ig}) = -RT^2 \frac{\partial \ln \phi_i^{*,l}}{\partial T} \quad \text{(calculated from Peng – Robinson EOS)}$$

$$H_m^{E,l} = -RT^2 \sum_i x_i \left(\frac{\partial \ln \gamma_i}{\partial T} \right) \quad \text{(calculated from activity coefficient models)}$$

$$H_m^{ig} = \sum_i y_i H_i^{*,ig} = \sum_i y_i (\Delta_{form} H_i + \int_{T_{ref}}^{T} C_{p,i}^{ig} \, dT)$$

$$C_{p,i}^{*,ig} = C_{1i} + C_{2i} T + C_{3i} T^2 + C_{4i} T^3 + C_{5i} T^4$$

T^{ref} – Reference temperature = 298.15 K

$\Delta_{form} H_i^{ig}$ – Standard enthalpy of formation for ideal gas at 298.15 K and 1 atm

Equation 4.7: Mixture enthalpy calculations based on Equation of state involving vapor departure functions and activity coefficient models

$$H_m^l = H_m^l - H_m^{ig} + H_m^{ig}$$

$$H_m^l = \sum_i x_i (H_i^{*,l} - H_i^{*,ig}) + H_m^{Ex}$$

$$H_m^{Ex} = -RT^2 \sum_i x_i \left(\frac{\partial \ln \gamma_i}{\partial T} \right)$$

$$(H_i^{*,l} - H_i^{*,ig}) = DH_i^{*,l} = \left(H_i^{*,v}(T,p_i^{*,l}) - H_i^{*,ig}(T)\right) - \Delta_{vap} H_i^*(T) + \left(H_i^{*,l}(T,p) - H_i^{*,l}(T,p_i^{*,l})\right)$$

$p_i^{*,l}$ = Liquid pure component vapor pressure

$$\left(H_i^{*,v}(T,p_i^{*,l}) - H_i^{*,ig}(T)\right) = DH_i^{*,v} = -RT^2 \frac{\partial \ln \phi_i^v}{\partial T}$$

$\Delta_{vap} H_i^*(T)$ = Pure component enthalpy of vaporization at 'T'

$$DHLPC = \left(H_i^{*,l}(T,p) - H_i^{*,l}(T,p_i^{*,l})\right)$$

$$= \left(H_i^{*,l}(T,p) - H_i^{*,ig}(T)\right) - \left(H_i^{*,l}(T,p_i^{*,l}) - H_i^{*,ig}(T)\right)$$

(Liq. pure component molar enthalpy departure pressure correction)

Departure of mixture molar enthalpy using EoS

$$H_m^v - H_m^{ig} = \sum_i x_i \left(H_i^{*,v} - H_i^{*,ig}\right)$$

$$= -\int_\infty^V \left(p - \frac{RT}{V} \right) dV - RT \ln \left(\frac{V}{V^{ig}} \right) + T\left(S_m^v - S_m^{ig}\right) + RT(Z_m - 1)$$

4.3.2.1. Validation of ASPEN enthalpy calculations using literature data

While the published pure component enthalpy data for this [HMIm][Tf_2N] is scarce, infinite dilution and partial molar excess enthalpy for 1-butanol in [HMIm][Tf_2N] are reported in the literature.[39] Since it is difficult to calculate partial enthalpies with Aspen, the mixture enthalpies (HLXS) values calculated using excel were used. To ensure validation of the equations chosen for mixture liquid enthalpy, excess enthalpy back-calculated from Aspen should compare well

with the excess enthalpy calculated using the BIPs regressed from the modeling. Equations for calculating the molar excess enthalpy for binary systems using NRTL activity coefficient model is shown in Equation 4.8 below. These were evaluated in excel using the regressed BIPs.

Equation 4.8: Reduced Excess enthalpy equation based on NRTL activity coefficient model for a binary mixture[22]

$$H^{EX} = -x_1 x_2 \left[\left(\frac{\tau_{21}\left(\frac{B_{21}}{RT}\right) G_{21} N_1 - B_{21} G_{21} N_1 - \tau_{21} x_2 \frac{B_{21}}{RT} G_{21}^2}{N_1^2} \right) + \left(\frac{\tau_{12}\left(\frac{B_{12}}{RT}\right) G_{12} N_2 - B_{12} G_{12} N_2 - \tau_{12} x_1 \frac{B_{12}}{RT} G_{12}^2}{N_2^2} \right) \right]$$

where

$\tau_{12} = \alpha_{12} B_{12}$; $\tau_{21} = \alpha_{21} B_{21}$ *and* $\alpha_{12} = \alpha_{21}$

$G_{12} = \exp\left(-\frac{\tau_{12}}{RT}\right)$; $G_{21} = \exp\left(-\frac{\tau_{21}}{RT}\right)$

$N_1 = x_1 + x_2 G_{21}$; $N_2 = x_2 + x_1 G_{12}$

1-butanol – [HMIm][Tf_2N] system: To verify the BIPs regressed from the ternary data for 1-butanol and ionic liquid binary system, excess enthalpy (HLXS) of the mixture calculated from excel were used. Estimated HLXS values from Aspen were back calculated from the values of HLMX, DHL and HIGMX obtained at particular conditions from Aspen as shown in equation 4.9. Aspen does not calculate the excess enthalpies of mixture separately. For a particular temperature, pressure and composition of 1-butanol & ionic liquid, HLMX, DHL and HIGMX are obtained from Aspen. HLXS is then calculated based on the above equation.

Table 4.11 below shows the data was obtained from Excel with a particular set of BIPs.

Equation 4.9: Excess enthalpy calculations from Aspen

$HLMX = HLMX + HIGMX$

$DHLMX = HLXS + DHL$

Eliminating $DHLMX$,

$HLXS = HLMX - DHL - HIGMX$

where

$HLMX$ – Enthalpy of the liquid mixture

$DHLMX = \sum_i (H_i^{*,l} - H_i^{*,ig})$ – Departure of liquid mixture molar enthalpy

$HIGMX$ – Ideal gas mixture enthalpy

$DHL = DH_i^{*,l} = (H_i^{*,l} - H_i^{*,ig})$ – Departure of pure liquid molar enthalpy

$HLXS$ – Excess molar enthalpy of liquid mixture

Table 4.11: Comparison of IL – 1-butanol excess enthalpy: Aspen vs. experimental data

X_{but}	HLXS (cal/mol)	
	Excel calculations	Aspen Equation 4.7
0.05	-14.6	-14.64
0.2	-44.2	-42.65
0.5	-59.2	-16.32
0.9	34.6	79.07

*BIPS: B_{12} = -164.71 K, B_{21} = 980.95 K, T = 298.15 K

Comparing the HLXS values calculated from excel and Aspen, the order and sign are the same. HLXS value was sensitive to changes in B_{21} value as shown in table below.

Table 4.12: Effect of Comparison of changes in B_{12}

		Calculated HLXS (cal/mol)	
B_{12} (1-butanol/ionic liquid)	X_{but}	Excel calculations	Aspen Equation 4.7
-164.71	0.05	-14.6	-24.1
300	0.05	28.4	-74.1
-500	0.05	-47.8	15.9

Heat duties: The following table shows the equation used to calculate the enthalpy change of the components, especially for the Ionic liquid, and the heat duties along with the product recovery. Heat duty for the flash unit was verified by hand calculations where in mole-fractions of inlet and outlet streams were used to calculate enthalpy change.

Table 4.13: Comparison of heat duties obtained using different enthalpy functions

Equation used	*Distillation (MW)*	*Flash (MW)*	*Product recovery*
4.6	1.22	1.22	91.4%
4.7	1.33	1.10	90.0%

4.3.3. Creating a flowsheet in ASPEN Plus

Simulation of the separation of 1-butanol using model ionic liquid was performed in Aspen Plus version 7.1. The creation of the flowsheet is started from the setup stage where the global settings of the run type: Flowsheet, units of measurement: Metric, and input mode: steady state are selected. For this simulation, the flow basis was chosen as mole. As described in earlier section, the three components: water, ionic liquid and 1-butanol from the component database are added to the flowsheet after the ionic liquid database is created. The different sections of the flowsheet include an extractor unit, distillation tower and vacuum flash or a stripper.

1. Liquid- Liquid Extractor

For extracting the solute from the aqueous phase using ionic liquid, a rigorous counter-current liquid-liquid extractor is selected from the list of available separators in the Aspen Plus database. In Aspen Plus, each equipment unit added as a block. Input and output streams are created for the extractor. There are two input streams: pure ionic liquid (heavier phase) enters

the unit as the top stream while the bottom stream is the aqueous 1-butanol stream. Selected components are further assigned to the input streams along with the operating conditions of 22°C and 1 atm. Component mole fractions & flow rates of the two streams are entered into the Aspen Plus as state variables. The aqueous phase flowrate is fixed and the ionic liquid phase flowrate is varied to obtain optimum solute extraction. These streams were fed to the extractor. As mentioned, the unit operates in a counter current mode which allows maximum mixing between the top and bottom streams. Two centrifugal pumps are used to pump the inlet streams into the extractor unit at a constant flow rate.

Main input parameters for the extractor are the number of stages and stage efficiency. Further, the extractor is assumed to be operated under adiabatic conditions. For correct identification of the output streams, the heavier ionic liquid phase is chosen as the 1^{st} liquid phase and lighter aqueous phase as the 2^{nd}. Here ideal stage efficiency of 1 was used. However, the effect of stage efficiency on the simulation is studied below as in real systems this would be <1. Initially a random stage number is chosen and optimum number of stages is obtained iteratively by looking at the extracted 1-butanol concentration. Once the optimum number of stages is determined, corresponding concentration of the two outlet streams are noted. This data used to determine the next step in the process.

2. Distillation Column

The bottom ionic liquid stream, containing the extracted 1-butanol and water, coming from the extractor, is sent to the distillation column to remove either water or 1-butanol. It is easier to separate the water from ionic liquid stream because of its low boiling point compared to 1-butanol. Here, the distillation column is operated below atmospheric pressure so a compressor is used to reduce the pressure of the stream entering the distillation column. The distillation

column chosen was the rigorous 2 or 3 phase for single columns. Setup of the distillation column includes the calculation type chosen as equilibrium and convergence chosen as custom. Specifications for the distillation column are maximum separation of water from the ionic liquid stream along with minimum 1-butanol entrainment into the top phase. To achieve this, the following parameters for the distillation column are optimized: number of stages, stage efficiency, feed stage, feed temperature, condenser recycle rate and reboiler specification. Except for the number of stages and condenser recycle rate, other parameters are optimized iteratively. The remaining parameters are optimized using design specification available in Aspen plus in the flowsheeting options. The condenser recycle rate and number of stages are optimized to ensure that the product yield is high and the heat duties are low. Ionic liquid rich stream from the distillation unit containing mainly ionic liquid and 1-butanol (and trace amount of water) can be passed either to a flash unit or stripper column to separate 1-butanol and ionic liquid. Both unit operations were simulated. 1-butanol can be separated from the ionic liquid stream either using a flash unit or a stripper column.

3. Flash Unit

The 1-butanol in the ionic liquid rich stream from the distillation unit can be separated in a single stage process, flash unit, as shown in the Figure 4.12. As 1-butanol can be readily evaporated from ionic liquid rich stream, the temperature and operating pressure of the unit are varied to obtain the high 1-butanol product yield. The heater and compressor are included to heat and compress the stream before it enters the unit as required. Here, the 1-butanol rich stream from the top phase and the pure ionic liquid from the bottom phase are at a very high temperature and needs to be condensed. Ionic liquid rich stream can be recycled back. Co-generation options are evaluated to conserve the energy.

Ionic liquid-rich stream, the bottoms from the distillation unit, is compressed from 0.5 to 0.1 atm using a compressor. This compressed stream enters the flash unit, which is under vacuum and at 225°C. Iteratively, it was found that very low pressures (< 0.1 atm) and high temperatures (> 200°C) were required to achieve separation and good product yields (> 80%). This could be because infinite dilution activity coefficient of 1-butanol in this ionic liquid are much greater than 1 (around 2 at 50°C) and decrease to 1 as the temperature is increased (1.14 at 110°C).[39] 99.85% pure 1-butanol coming out as vapor from the flash unit is condensed and the heat released can be used for co-generation. One of the disadvantages of using flash unit is that high temperatures and low pressures required are not desired for process safety. Other disadvantage is that at these temperatures, the thermal stability of [HMIm][Tf_2N] needs to be carefully considered as the onset of decomposition is around 400°C.[40] Additionally, the low operating pressures, can add to equipment costs.[21]

Figure 4.12: Simulated flowsheet of Ionic liquid based extraction of 1-butanol from water in Aspen Plus using Flash unit

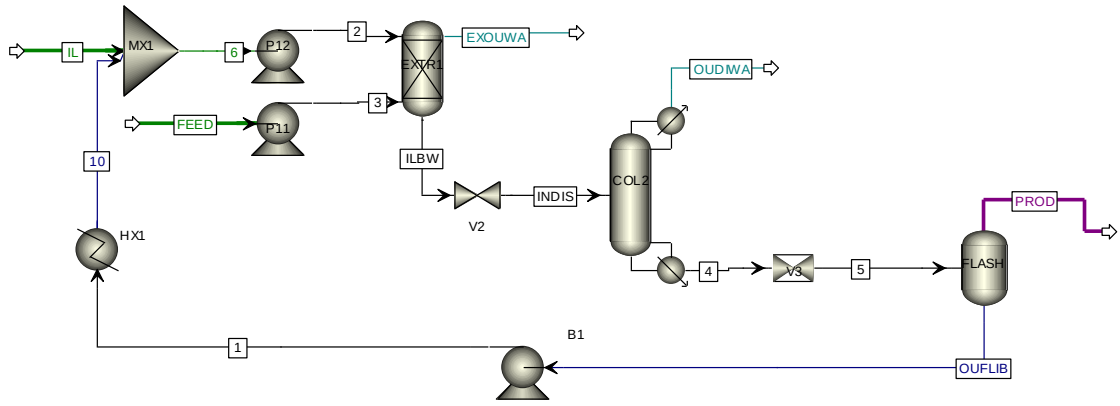

4. Stripper

Instead of using a flash unit, since the ionic liquid-rich stream from the distillation column is at a higher temperature this can be passed to stripping unit. This is due to the fact that 1-butanol is closer to its boiling point. Here, either N_2 or air is used to strip 1-butanol from ionic liquid phase and the effects of their cost on production and safety are evaluated. Steam is another commonly used stripping agent but in this case the purity of 1-butanol would be affected. The number of stages, flow rate of the stripping agent along with the temperatures of the unit and inlet feed are optimized for higher product yields similar to those obtained in traditional distillation process below (section 4.4.1). The feed to the unit is at the top stage while the stripping agent is pumped into the bottom stage and so that the stripping occurs in a counter-current manner. The mixture of air/N_2 and the stripped 1-butanol are obtained from the top outlet stream and this mixture is further separated in the decanter where the temperature is reduced to collect liquid 1-butanol as bottoms, while the top phase of air/N_2 is mixed with the inlet stream and pumped to the unit. The setup options for this unit include: Calculation type – equilibrium and convergence – Custom. Anticipated outlet stream phases are also inputted to this unit. For this unit, neither a condenser nor a reboiler is required. Temperatures of the outlet streams from this unit are much lower than from using a flash unit. Pumps are used as required to pump different streams.

Figure 4.13: Simulated flowsheet of Ionic liquid based extraction of 1-butanol from water in Aspen Plus using Stripper.

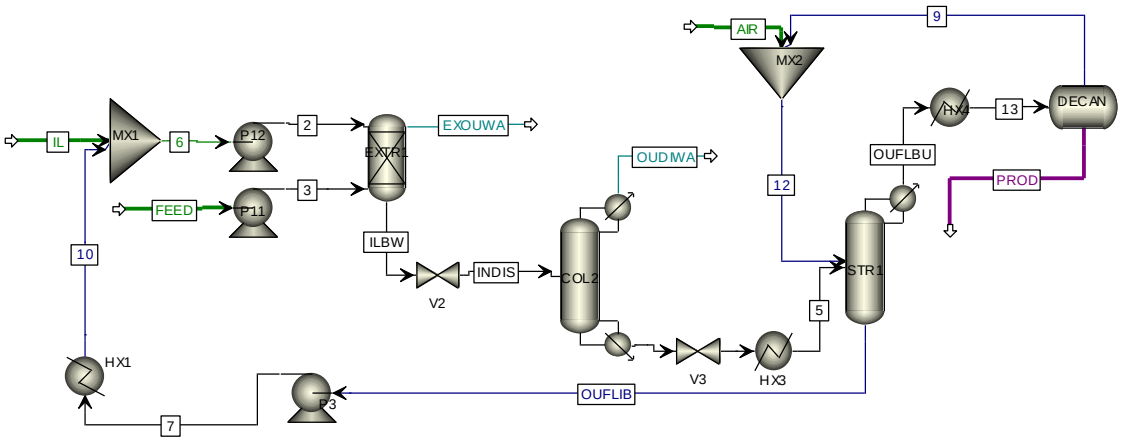

The process flowsheet in Figure 4.13 shows the 1-butanol separation from the ionic liquid after the 1-butanol is extracted from the aqueous phase. Initially the ionic liquid is when contacted with 2% by mole of 1-butanol in water in the extractor at an IL: water phase ratio of 1.37 : 1. The extractor is operated at room temperature and 10 equilibrium stages are required for complete extraction of 1-butanol into the ionic liquid at tray efficiency of 1. The upper stream leaving the extractor contains 99.97 mol% of water indicating that neither 1-butanol or [HMIm][Tf_2N] is not lost to the aqueous stream, probably due to the tray efficiency of 1. However, around 27.6 mol% of the aqueous phase is present in the ionic liquid phase.

Chapeaux *et al.*,[8] performed multistage liquid-liquid extraction calculations using the Hunter-Nash method to extract 2% by wt. of 1-butanol from water using [HMIm][Tf_2N]. They reported that 4 stages were required to completely remove water at 1:1 IL to water mass flow ratio.

The ionic liquid stream (containing 15.4 mol% of 1-butanol) from the bottom of the extractor is compressed in a compressor by reducing the pressure from 1atm to 0.5 atm. The compressed stream is then sent to a distillation column operated under vacuum at 0.5 atm. Here, the goal is to separate the aqueous phase in the ionic liquid stream such that the ionic liquid stream leaving the distillation contains just the 1-butanol and the ionic liquid phase. In this case 1-butanol can

also be removed first instead of water, but since 1-butanol forms a heteroazeotrope mixture with water at lower concentrations, the heat duties can be reduced by removing water first. The residual water content in the ionic liquid stream leaving the distillation column is 0.03 mol% and the amount of 1-butanol lost with the aqueous phase is 1.85 kmol/hr. 10 stages are required to efficiently remove water from the bulk ionic liquid phase with the feed stream entering the column at the top stage. The ionic liquid stream leaving the distillation column is further heated to 416.6 K using a heater and then passed to a stripping column with 10 stages. Total flow rate of the air entering the column is 100 kmol/hr. The top stream leaving the stripping column contains 84.1 mol% of air and 15.6 mol% of 1-butanol. This stream is cooled to room temperature and the final product obtained. Air is recycled back to the stripping column. The bottom stream from the stripping column, containing ionic liquid-rich phase, is cooled to room temperature and sent back to the extractor. Here, air was used to strip 1-butanol from ionic liquid as it is readily available compared to nitrogen which needs to be generated onsite and hence additional cost for these generators would be incurred. The disadvantage with air is that the mixtures of air and 1-butanol can be flammable at room temperatures with electrostatics being a main source of ignition. The lower and upper flammability limits of 1-butanol in air[41,42] (by vol.) are 1.4% and 11.2%, further 1-butanol is flammability rating of 3. Here, Nitrogen being inert gas does not result in flammable mixture with 1-butanol. The flow rate of air entering the stripper is 100 kmol/hr while that of 1-butanol is 20 kmol/hr which is the maximum. At these flowrates, the volume % of 1-butanol is < 0.1%, so possibility of flammable mixture is low however it cannot be ruled out inside the stripper.

4.3.4. Flowsheet optimization

Various parameters in the distillation column may be optimized with the objective of extracting greater than 99% pure 1-butanol while incurring minimum heat duties. These include, operating pressure, number of stages, feed stage.

Table 4.14: Flowsheet optimization: Impact of parameter change

Parameter change	1-butanol purity	Heat duty	Optimal parameter
1. Lowering operating pressure	Improves recovery	Lowers heat duty	0.5 atm pressure
2. Increasing number of stages	≤ 8 stages: increases purity > 8 stages: minimal impact	≤ 8 stages: lowers heat duty > 8 stages: minimal impact	10 stages
3. Higher feed stage	Improves recovery	No impact	Top stage

* Capital costs will be higher for vacuum operation.[21]

4.3.5. Flowsheet results: Product yield / purity and energy analysis

Flowsheet version 1: using stripping column: A volumetric flow rate ratio of IL: water of 1.4:1 was used to obtain the final product, 1-butanol, with a yield of 90.0% at a purity of 99.85%. Heat duties for the reboiler in the distillation column and the heater are 1.33 MW and 0.16 MW respectively. Hence, the total duty for an *ex situ* extraction of 1-butanol from aqueous solution is 1.50 MW. The heat duties for the two cooling heat exchangers are -0.56 MW and -0.43 MW respectively, i.e., -0.99 MW can potentially be used in cogeneration. In current simulation, cogeneration potential refers to utilization of heat captured in a hot stream. A heat exchanger can be integrated in the flowsheet such that the hot stream and cold stream can be contacted to

eliminate the extra heat required for raising the temperature of cold stream. In this flowsheet, the 1-butanol stream or the ionic liquid stream leaving the stripper at higher temperatures can be used to heat the steam used in the boiler of distillation unit.

Flowsheet version 2: using flash unit: A volumetric flow rate ratio of IL: water of 1.4:1 was used to obtain the final product, 1-butanol, with a yield of 90.0% at a purity of 99.85%. Heat duties for the reboiler in the distillation column and the flash unit are 1.33 MW and 1.10 MW respectively. Hence, the total duty for an ex situ extraction of 1-butanol from aqueous solution is 2.43 MW. The heat duties for the cooling ionic liquid recycle and 1-butanol stream from flash are -1.51 MW and -0.41 MW, i.e., -1.92 MW can potentially be used in cogeneration.

Table 4.15: Comparison of results for flowsheet with stripping column vs. flash unit

Flowsheet version	Yield (%)	Purity (%)	Heat duty (MW)	Heat required per Kg of product (MJ/Kg)	Cogeneration potential (MW)
1. using stripping column	90.0	99.85	1.49	3.6	-0.99
2. using flash unit	90.0	99.85	2.43	6.6	-1.92

From the energy analysis, the stripping unit operation requires low energy input heat to achieve the same separation as the flash unit. But the stripper requires air, the processing of which requires adds to pump and compressor costs which need to be evaluated. The total costs for both the flowsheets need to be compared before making final comment.

4.3.6. Flowsheet sensitivity analysis

4.3.6.1. Changing the six BIPs one at a time

A sensitivity analysis was conducted on the flowsheet to study changes in BIPs (to indirectly study of the impact of temperature). The sensitivity analysis was done in particular to understand the effect of changes in the binary interaction parameter on the energy requirements,

product purity and, water content. For the ternary system of IL/1-butanol/water, there would be six BIPs used. Out of the 6 BIPs, data for the IL + 1-butanol and IL + water system, the phase equilibrium data are limited to LLE data at room temperature. BIPs have been regressed from the experiment LLE data measured at the room temperature. But in the actual simulation of different unit operations, elevated temperatures would be encountered, for e.g. in the distillation column, the column temperature varies from 298 K to 373 K. At elevated temperatures, the vapor-liquid equilibrium would be attained. Since there is no experimental or literature data available at these higher temperatures especially for the ionic liquids, the binary interaction parameters as a function of temperature cannot be calculated and incorporated in the simulation. This study would provide an insight into whether or not any of the of the six BIPS effects the final heat duties on whether any one or more than one of the six BIPS affects the final heat duties. Table 4.17 summarizes the effect of variation of BIPs on the heat duty, product yield and purity. The BIPs were varied between +50% to -50%. This does not result in significant changes in the three variables studied, the change observed is < ±10% in most of the cases. However, for certain BIPs, B_{21}, B_{23} and B_{32}, when they are varied by ±50%, heat duties change by > 10% with highest change in heat duty observed to be 26% when B_{32} is reduced by -50%. The product yield is reduced by > 40% when B_{23} and B_{32} are increased by 30% and 50%; the largest reduction being by 93% when B_{32} is increased by 50%. These values could be reduced if the product purity specification on the distillation is relaxed. The product purity however is largely unaffected by the variation in BIPs, one exception was that purity was reduced by 18% when B_{21} was reduced by 50%.

Table 4.16: Effect of variation of BIPs on heat duty, product yield and product purity

Heat duty

	50%	30%	15%	0%	-15%	-30%	-50%
B_{12}	4%	2%	1%	0%	-1%	-2%	-4%
B_{21}	-5%	-7%	-5%	0%	7%	16%	18%
B_{13}	3%	2%	1%	0%	-1%	-2%	-3%
B_{31}	8%	4%	2%	0%	-2%	-3%	-4%
B_{23}	3%	0%	3%	0%	-4%	-7%	-10%
B_{32}	26%	10%	-1%	0%	0%	0%	0%

Product yield

	50%	30%	15%	0%	-15%	-30%	-50%
B_{12}	-1%	-1%	0%	0%	0%	1%	1%
B_{21}	-6%	0%	1%	0%	-1%	-4%	-6%
B_{13}	2%	1%	1%	0%	-1%	-2%	-3%
B_{31}	3%	2%	1%	0%	-1%	-1%	-1%
B_{23}	-72%	-41%	-5%	0%	0%	-1%	-1%
B_{32}	-93%	-85%	-66%	0%	0%	0%	1%

Product purity

	50%	30%	15%	0%	-15%	-30%	-50%
B_{12}	0%	0%	0%	0%	0%	0%	0%
B_{21}	0%	0%	0%	0%	0%	0%	-18%
B_{13}	0%	0%	0%	0%	0%	0%	0%
B_{31}	0%	0%	0%	0%	0%	0%	0%
B_{23}	0%	0%	0%	0%	0%	0%	0%
B_{32}	-2%	0%	0%	0%	0%	0%	0%

4.3.6.2. Changing temperature while keeping BIPs constant

The effect of temperature of the feed streams: aqueous 1-butanol stream and ionic liquid stream entering the extractor on the extractability needs to be understood. This is important when the context is about fermentation systems as the ABE fermentation is conducted mostly at 37°C.[15] Table 4.18 summarizes the effect of temperature on the process flow sheet. Increasing

the temperature reduces the heat duty and product yield when the product purity is maintained constant at 99.85%. The decrease in heat duty could be attributed to the increase in temperature of the feed entering the distillation unit. The decrease in the product purity could be related to increase the mutual solubilities of the water – 1-butanol and water – IL binary systems at higher temperatures.

Table 4.17: Effect of feed temperature on the heat duty, product yields and purity

Feed temperature (K)	Heat duty (MW)	Product yield (%)	Product purity (%)
295.15	1.33	90.0	99.85
303.15	1.25	89.4	99.85
310.15	1.18	88.7	99.85

4.3.6.3. Effect of distillation column efficiency

The effect of efficiency of distillation column on the heat duties was studied as the stage efficiencies in an actual distillation column are much less than 1.[21] Table 4.20 summarizes this effect. As the stage efficiency is changed from 100% to 50%, the heat duty and the product yield do not vary but the number of stages to achieve same yield and purity increase from 10 to 20.

Table 4.18: Effect of distillation column efficiency on heat duty, product purity

Distillation column			*Product*	
Stage Efficiency (%)	Optimal No. of Stages	Heat duty (MW)	Yield (%)	Purity (%)
100	10	1.33	90.0	99.85
90	10	1.33	90.1	99.85
70	14	1.33	89.9	99.85
50	20	1.33	89.9	99.74

4.3.6.4. Multiple stage separations: energy

The effect of number of stages on the effectiveness of the distillation column was studied. The number of stages is varied from 5 to 15 and the corresponding change in column heat duty, product yield and product purity was tabulated in Table 4.21. As the number of stages is doubled from 5 to 10, the product yield doubles and the column heat duty reduces too. However, increasing stages beyond 10, there is minimal change in the product yield and heat duty, while the product purity reduces to 97.4%. 10 stages seem to be an optimal number of stages. Number of stages has direct effect on the costing of the column.[21]

Table 4.19: Effect of stages in distillation on energy and cost based on product quantity, energy and cost

No. of stages in distillation column	Heat duty (MW)	Product yield (%)	Product purity (%)
5 stages	1.56	45.3	99.72
10 stages	1.33	90.0	99.85
15 stages	1.30	90.3	97.36

4.4. Simulation of 1-butanol separation at pilot plant scale using conventional methods

The goal here was to analyze the performance for ionic liquid, 1-butanol separation from the aqueous phase using two conventional methods namely distillation and extraction using organic solvent. The heat duties or energy requirements for these flowsheets are compared. Then the equipment costs for each of these methods with the ionic liquid based flowsheet are compared to better evaluate ionic liquid benefits over competing methods.

4.4.1. Distillation

4.4.1.1. Flowsheet Description

Distillation, an age-old conventional method, used frequently to distill low boiling points compounds was studied by Luyben[43] to separate the heteroazeotrope mixture of 1-butanol and water. Luyben developed a flowsheet as shown in Figure 4.14 to achieve a final 99.9% purity of 1-butanol the separation. A brief description of the flowsheet is included here as it is used as basis for present calculations. The total feed flowrate used was 1000 kmol/hr and the initial solute mole % in the feed was varied from 2 – 40%. For this study, only 2 mol% of 1-butanol in the aqueous feed was used to evaluate the process as the focus is on the concentrations encountered in the fermentation broths. Two distillations, one for treating water rich phase and the other for 1-butanol rich phase were used to achieve the separation. In both the columns, the mixture was distilled until the azeotrope is encountered. To handle the azeotrope, a 3-phase decanter was used and the temperature was reduced to obtain phase separation. The bottom water rich layer is recycled to the 1st distillation column while the top organic 1-butanol rich layer is sent to the 2nd column. Both the columns were operated under vacuum at pressure of 0.5 atm as this reduces the operating temperatures.

Figure 4.14: Conventional distillation column for separation of 1-butanol from water based on 1000 kmol/hr (19,122 kg/hr) using two 10–staged columns developed by Luyben (2008)[43]

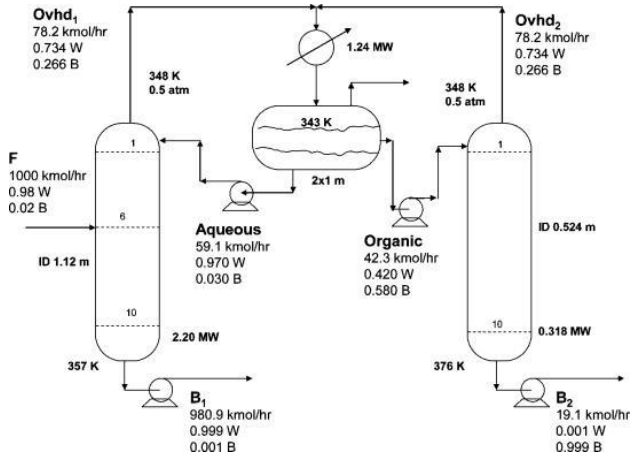

Luyben further simulated the flowsheet in the Aspen Plus to obtain column operating conditions, column sizes and the heat duty for each unit. This simulation was replicated according to the procedure described by the author. The simulated Aspen flowsheet is shown in Figure 4.15. The UNIQUAC activity coefficient model was used to model water – 1-butanol binary system. The reason for repeating this work was to perform economic analysis on the flowsheet and compare it with the ionic liquid based extraction.

Figure 4.15: Replicated simulation flowsheet of conventional distillation of 1-butanol from water in Aspen Plus

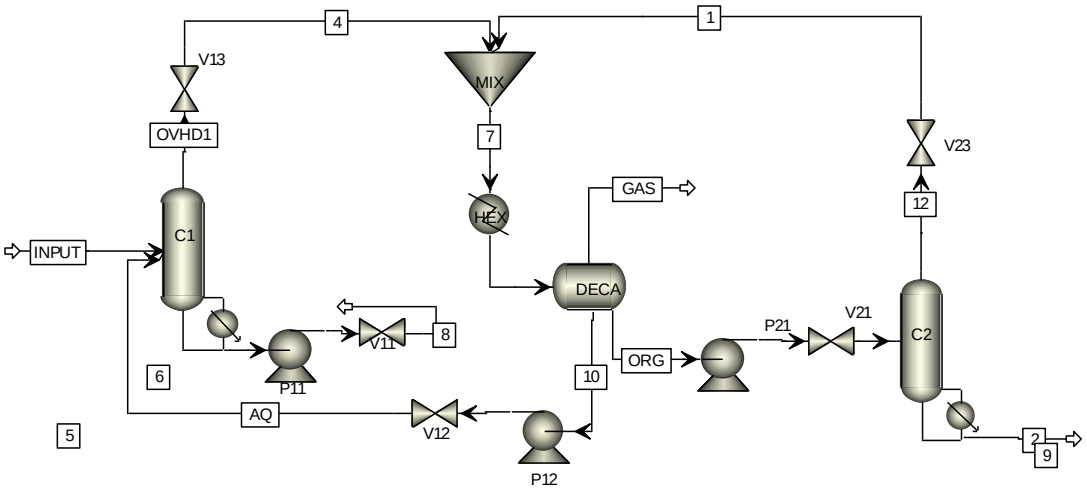

4.4.1.2. Describe energy analysis to calculate heat duty of each component

The design specification created by the Luyben was used to evaluate heat duties for the two distillation towers. Duties of 2.2 MW and 0.318 MW respectively were calculated. Further, a heat duty of -1.24 MW is released from the cooling the streams to the decanter. Hence, the total duty for an *ex situ* extraction of 1-butanol from aqueous solution is 2.52 MW with final yield of 95.6% and 99.89% product purity.

4.4.2. Organic solvent

4.4.2.1. Flowsheet Description

Organic solvents have been traditionally used as an alternate to the direct distillation as they can potentially reduce the need to process a lot of water in the distillation column. Like ionic liquid, they can extract 1-butanol from the aqueous phase. Applying similar criteria used in identification of optimal ionic liquids for extraction, a suitable organic solvent has been identified and a process flowsheet developed. In the literature, Mesitylene and Oleyl alcohol have been reported to be the solvents with high partitioning coefficient and selectivities over water.[44,45,46,47] In this study, Oleyl alcohol was chosen as the organic solvent for extraction of 1-butanol. A process flowsheet was developed in Aspen Plus to simulate the separation of 1-butanol from water via Oleyl alcohol extraction as shown in the Figure 4.16. As this component is not available in the ionic liquid database, it was created. For simulation of the flowsheet, UNIFAC activity coefficient model was used to model the ternary mixture. Corresponding BIPs were calculated from Aspen Plus as UNIFAC does not require experimental data. Flowsheet consists of an extractor to extract 1-butanol into the organic solvent phase. Then to separate 1-butanol from the organic rich phase, two columns are used, first to remove excess water and second to separate 1-butanol. Here, flash or blower cannot be used as the organic solvent has measurable vapor pressure and final product purity of 99.9% cannot be reached. The parameters are optimized following the same procedure described for the ionic liquid flowsheet simulation. In the extractor, the initial aqueous to solvent ratio was varied between 1 & 2 and an optimized ratio was calculated as 1.75:1. A rigorous distillation column was used for one distillation. The number of equilibrium stages was found to be 20. A total condenser was used to recirculate the condensed liquid and a kettle reboiler, which is simple in operation compared to thermosyphon

reboiler, was used to vaporize the bottoms and the vapor is returned to the column. The reflux ratio for the condenser was used as the operating specification and upon iteration it was set to 0.05. Simulating the column at this specification separated water from 1-butanol and Oleyl alcohol mixture. So, using a flash did not separate the mixture very well because the Oleyl alcohol has measurable vapor pressures at boiling point of 1-butanol. Using the flash unit, the final product purity was 99.6% but the yield was <50%. Using a second rigorous distillation column that uses more rigorous calculation method resulted in a better separation of the mixture. Here, the reflux ratio used was 0.5 while a total condenser and kettle reboiler are used.

Figure 4.16: Simulated flowsheet of liquid-liquid extraction of 1-butanol from water in Aspen Plus using Oleyl alcohol as the extractant.

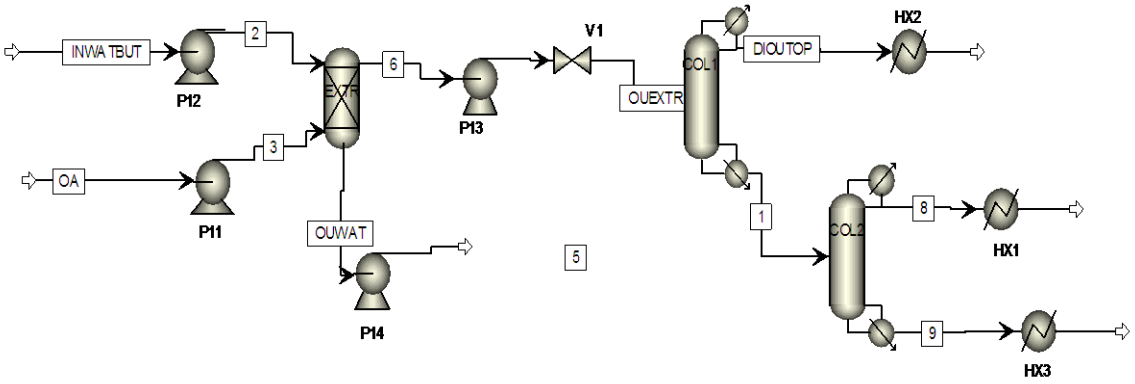

4.4.2.2. Describe energy analysis to calculate energy duty of each component

For the first distillation unit, the heat duty was 2.45 MW. The bottoms composition: 0.001 mol% water and 15.6 mol% 1-butanol. This stream is separated further in the second distillation column. The heat duty for 2nd column is 0.84 MW and the top stream composition is 99.71 mol% 1-butanol and a yield of 74.8%. Higher reboiler duty increased the 1-butanol yields but the bottoms solvent temperature was >500 K. The number of stages is 10 and the column is operated at a reduced pressure of 0.5 atm.

4.5. Discussion

In this work, model ionic liquid, [HMIm][Tf_2N] was evaluated as a potential candidate for the extraction of solutes such as acetone, 1-butanol and ethanol from pure aqueous phase. Entire solubility range of solute and water was investigated in these phase equilibrium studies. Lower concentration ranges, of up to 2 mol%, which are commonly encountered in fermentation broths, were studied in greater detail. Ternary diagrams were created for higher solute concentrations. Selectivity and partition coefficients calculated in the phase equilibrium studies show that 1-butanol and acetone are extracted with high selectivities whereas ethanol is not. Hence, this ionic liquid shows potential as a solvent for downstream processing of fermentation broths. The data from the phase equilibrium studies was used to develop an NRTL model which was subsequently used in the simulation of solute extraction from water using ionic liquid.

4.5.1. Advantages of ionic liquid over other methods

Energy and preliminary cost analyses were conducted on the flow sheet developed. Heat duties for separation based on the ionic liquid based extraction were significantly lower than for traditional distillation indicating that presence of high boiling ionic liquids leads to reduced heat duties.

Table 4.20: Simulation of separation of 1-butanol from dilute aqueous feed (1-butanol in the Feed = 2 mol%, flow rate of aqueous feed stream = 1,000 kmol/hr)

Category	Ionic liquid based extraction	Conventional distillation	Organic solvent extraction
Equipment used	LLE extractor, distillation column and Stripping unit	2 distillation columns and a decanter	LLE extractor, 2 distillation columns
Operating conditions	1. LLE extraction (10 stages) 2. Distillation column at 0.5 atm (10 stages) 3. Stripping unit	0.5 atm (10 stages)	1. LLE extraction (10 stages) 2. Distillation column at 0.5 atm (20 stages) 3. 2nd distillation

Category	Ionic liquid based extraction	Conventional distillation	Organic solvent extraction
			column at 0.5 atm (10 stages)
Final product purity	99.84%	99.9%	99.71%
Final product recovery	90.9%	95.4%	74.8%
Heat duty (in MW)	1.33	2.52	3.29

4.5.2. Comparison of equipment costing for techniques

Based on the energy requirement from the flowsheet analysis, it was observed that the ionic liquid based extraction requires less energy than conventional distillation while organic solvent based extraction requires higher energy than both of these combined. To obtain a better understanding of the suitability of ionic liquid based process for the 1-butanol separation, cost analysis on these three flowsheets was performed. The focus of the cost analysis for this report was to compare equipment cost. Integrated costing available with Aspen Plus was used. The flowsheet was simulated and the results were then loaded into the costing section. Then the equipment was mapped and subsequently sized. Sizing results were used to evaluate the flowsheet. In the current evaluation, major equipment such as Extractor and minor equipment like mixer and valves were not sized by simulator. Major equipment costs without extractor are summarized in Table 4.21. Cost analysis shows that equipment for separation of 1-butanol in the ionic liquid based extraction is close to the traditional distillation while the equipment cost for the organic solvent based process is much higher. The cost of distillation column for oleyl alcohol based extraction is much higher than either of ionic liquid based or traditional processes.

Table 4.21: Flowsheet costing summary for distillation and stripper only.

	Ionic liquid based extraction	Direct distillation	Oleyl Alcohol based extraction
Distillation Column	198,700 $	Column 1: 121,900 $	Column 1: 358,800 $
		Column 2: 114,000 $	Column 2: 129,900 $
Decanter	15,000 $	15,000 $	-
Stripper	60,700 $	-	-
Total	286,540 $	250,900 $	480,700$

4.5.3. Discussion of practical considerations

As the model ionic liquid was shown to be a good extractant of solutes, 1-butanol and acetone, it has potential for application in an *in situ* system. But unlike the pure systems used in this work, an actual fermentation broth consists of cells, extra-cellular constituents like salts, proteins, surfactants, etc in addition to the aqueous medium. The effect of these impurities on the extraction and phase separation processes needs to be evaluated. From the literature, common inorganic salts like K_3PO_4, NaCl, etc., have little solubility in the ionic liquid phase. Further, the ionic liquids have little partitioning for glucose, which is generally the substrate for ABE fermentation. Amino acids, including aliphatic and aromatic ones, have little partitioning into ionic liquids except at low pH (<~3) which are not generally not encountered in a ABE fermentation, while proteins are known to have lower partitioning than amino acids.

In fermentation broth, if the model ionic liquid is used as an *in situ* solvent, then the broth can be recycled and losses would be minimized. However, in a post-fermentation or *ex situ* scenario, losses would accumulate if ionic liquid is not recovered from water (Ionic liquid solubility in water is about 2 mg/ml which is very low). Preliminary studies have shown that 90+% of ionic liquid saturated in water can be removed using simple adsorbent resins such as Amberlite XAD16 at a resin to aqueous concentration of 1:4 by weight.[48]

4.6. References

(1) Domańska, U.; Zawadzki, M.; Królikowski, M.; Lewandrowska, A. Phase equilibria study of binary and ternary mixtures of {N-octylisoquinolinium bis{(trifluoromethyl)sulfonyl}imide + hydrocarbon, or an alcohol, or water}. *Chemical Engineering Journal* **2012**, *181–182*, 63.

(2) Vale, V. R.; Will, S.; Schroer, W.; Rathke, B. The general phase behavior of mixtures of 1-alkyl-3-methylimidazolium bis[(trifluoromethyl)sulfonyl]amide ionic liquids with n-alkyl alcohols. *Chemphyschem : a European journal of chemical physics and physical chemistry* **2012**, *13*, 1860.

(3) Döker, M.; Gmehling, J. Measurement and prediction of vapor–liquid equilibria of ternary systems containing ionic liquids. *Fluid Phase Equilibria* **2005**, *227*, 255.

(4) Kato, R.; Gmehling, J. Systems with ionic liquids: Measurement of VLE and $\gamma\infty$ data and prediction of their thermodynamic behavior using original UNIFAX, mod. UNIFAC(Do) and COSMO-RS(O1). *Jorunal of Chemical Thermodynamics* **2005**, *37*, 603.

(5) Nebig, S.; Bölts, R.; Gmehling, J. Measurement of vapor–liquid equilibria (VLE) and excess enthalpies (HE) of binary systems with 1-alkyl-3-methylimidazolium bis(trifluoromethylsulfonyl)imide and prediction of these properties and $\gamma\infty$ using modified UNIFAC (Dortmund). *Fluid Phase Equilibria* **2007**, *258*, 168.

(6) Revelli, A.-L.; Mutelet, F.; Jaubert, J.-N. Extraction of n-Alcohols from n-Heptane Using Ionic Liquids. *Journal of Chemical and Engineering Data* **2011**, *56*, 3873.

(7) Bahadur, I.; Deenadayalu, N.; Tywabi, Z.; Sen, S.; Hofman, T. Volumetric properties of ternary (IL + 2-propanol or 1-butanol or 2-butanol + ethyl acetate) systems and binary (IL + 2-propanol or 1-butanol or 2-butanol) and (1-butanol or 2-butanol + ethyl acetate) systems. *The Journal of Chemical Thermodynamics* **2012**, *49*, 24.

(8) Chapeaux, A.; Simoni, L. D.; Ronan, T. S.; Stadtherr, M. A.; Brennecke, J. F. Extraction of alcohols from water with 1-hexyl-3-methylimidazolium bis(trifluoromethylsulfonyl)imide. *Green Chemistry* **2008**, *10*, 1301.

(9) Lachwa, J.; Morgado, P.; Esperanca, J. M. S. S.; Guedes, H. J. R.; Lopes, J. N. C.; Rebelo, L. P. N. Fluid-Phase Behavior of {1-Hexyl-3-methylimidazolium Bis(trifluoromethylsulfonyl) Imide, [C6mim][NTf2], + C2−C8 n-Alcohol} Mixtures: Liquid−Liquid Equilibrium and Excess Volumes. *Journal of Chemical and Engineering Data* **2006**, *51*, 2215.

(10) Arlt, W.; Macedo, M. E. A.; Rasmussen, P.; Sorensen, J. M. *Liquid-Liquid Equilibrium Data Collection*; DECHEMA, 1980; Vol. V.

(11) Simoni, L. D.; Chapeaux, A.; Brennecke, J. F.; Stadtherr, M. A. Asymmetric Framework for Predicting Liquid-Liquid equilibrium of Ionic Liquid-Mixed-Solvent Systems. 2. Prediction of Ternary Systems. *Industrial & Engineering Chemistry Research* **2009**, *48*, 7257.

(12) Simoni, L. D.; Lin, Y.; Brennecke, J. F.; Stadtherr, M. A. Modeling Liquid-Liquid Equilibrium of Ionic Liquid Systems with NRTL, Electrolyte-NRTL and UNIQUAC. *Industrial & Engineering Chemistry Research* **2008**, *47*, 256.

(13) Simoni, L. D.; Chapeaux, A.; Brennecke, J. F.; Stadtherr, M. A. Extraction of Biofuels and Biofeedstocks from Aqueous Solutions Using Ionic Liquids. *Computers & Chemical Engineering* **2010**, *34*, 1406.

(14) Swatloski, R. P.; Visser, A. E.; Reichert, W. M.; Broker, G. A.; Farina, L. M.; Holbrey, J. D.; Rogers, R. D. On the solubilization of water with ethanol in hydrophobic hexafluorophosphate ionic liquids. *Green Chemistry* **2002**, *4*, 81.
(15) Qureshi, N.; Blaschek, H. P. Evaluation of recent advances in butanol fermentation, upstream, and downstream processing *Bioprocess and Biosystems Engineering* **2001**, *24*, 219.
(16) Othmer, D.; Tobias, P. Tie Line Correlation. *Industrial and Engineering Chemistry* **1942**, *34*, 693.
(17) Hu, X.; Yu, J.; Liu, H. Liquid-Liquid Equilibria of the system of 1-(2-hydroxyethyl)-3-methylimidazolium tetrafluoroborate or 1-(2-hydroxyethyl)-2,3-dimethylimidazolium tetrafluoroborate + water + 1-butanol at 293. 15 K. *Journal of Chemical and Engineering Data* **2006**, *51*, 691.
(18) Fadeev, A. G.; Meagher, M. M. Opportunities for ionic liquids in recovery of biofuels. *Chemical Communications* **2001**, *3*, 295.
(19) Garcia-Chavez, L. Y.; Garsia, C. M.; Schuur, B.; de Haan, A. B. Biobutanol Recovery Using Nonfluorinated Task-Specific Ionic Liquids. *Industrial & Engineering Chemistry Research* **2012**, *51*, 8293.
(20) Cascon, H. R.; Choudhari, S. K.; Nisola, G. M.; Vivas, E. L.; Lee, D.-J.; Chung, W.-J. Partitioning of butanol and other fermentation broth components in phosphonium and ammonium-based ionic liquids and their toxicity to solventogenic clostridia. *Separation and Purification Technology* **2011**, *78*, 164.
(21) Seader, J. D.; Henley, E. J.; Roper, D. K. *Separation Process Principles*; 3rd Edition ed.; John Wiley & Sons, Inc., 2011.
(22) Walas, S. M. *Phase Equilibria in Chemical Engineering*; Butterworth-Heinemann: USA, 1985.
(23) Freiré, M. G.; Santos, L. M. N. B. F.; Marrucho, I. M.; Coutinho, J. A. P. In *Molten Salts and Ionic Liquids*; John Wiley & Sons, Inc.: 2010, p 101.
(24) Santiago, R. S.; Santos, R. G.; Aznar, M. UNIQUAC correlation of liquid–liquid equilibrium in systems involving ionic liquids: The DFT–PCM approach. *Fluid Phase Equilibria* **2009**, *278*, 54.
(25) Lei, Z.; Dai, C.; Liu, X.; Xiao, L.; Chen, B. Extension of the UNIFAC Model for Ionic Liquids. *Industrial & Engineering Chemistry Research* **2012**.
(26) *Aspen Plus: Steady State Simulation - Version 10*

Physical Property Methods and Models: Reference Manual.
(27) Iglesias-Silva, G. A.; Bonilla-Petriciolet, A.; Eubank, P. T.; Holste, J. C.; Hall, K. R. An algebraic method that includes Gibbs minimization for performing phase equilibrium calculations for any number of components or phases. *Fluid Phase Equilibria* **2003**, *210*, 229.
(28) Teh, Y. S.; Rangaiah, G. P. A Study of Equation-Solving and Gibbs Free Energy Minimization Methods For Phase Equilibrium Calculations. *Trans IchemE* **2002**, *80*, 745.
(29) Olaya, M. M.; I.;, I.; Reyes-Labarta, J. A.; Serrano, M. D.; Marcilla, A. Computing Liquid-Liquid phase Equilibria. *Chemical Engineering Education* **2007**.
(30) Michelsen, M. L. The isothermal flash problem. Part I. Stability. *Fluid Phase Equilibria* **1982**, *9*, 1.
(31) Tessier, S. R.; Brennecke, J. F.; Stadtherr, M. A. *Chemical Engineering Science* **2000**, *55*, 1785.

(32) Ohanomah, M. O.; Thompson, D. W. Computation of Multicomponent Phase Equilibria-Part-II. Liquid-Liquid and Solid-Liquid Equilibria. *Computers & Chemical Engineering* **1984**, *8*, 157.
(33) 7.9 ed.; The Mathworks, Inc.: Natick, Massachusetts, 2009, p R2009b.
(34) Houck, R. C.; Joines, J. A.; Kay, M. G. A Genetic Algorithm for Function Optimization: A Matlab Implementation
(35) Simoni, L. D.; Lin, Y.; Brennecke, J. F.; Stadtherr, M. A. Reliable computation of binary parametrs in activity coefficient models for liquid-liquid equilibrium. *Fluid Phase Equilibria* **2007**, *255*, 138.
(36) Chapeaux, A.; Simoni, L. D.; Stadtherr, M. A.; Brennecke, J. F. Liquid Phase Behavior of Ionic Liquids with Water and 1-Octanol and Modeling of 1-Octanol/Water partition Coefficients. *Journal of Chemical and Engineering Data* **2007**, *52*, 2462.
(37) H.;, F. *BER. DTSCH.CHEM.GES.* **1924**, *57*, 510.
(38) A.E.;, H.; W.M.;, M. *Journal of American Chemical Society* **1926**, *48* 91.
(39) Heintz , A.; Verevkin, S. P.; Lehmann, J. K.; Vasiltsova, T. V.; Ondo, D. Activity coefficients at infinite dilution and enthalpies of solution of methanol, 1-butanol, and 1-hexanol in 1-hexyl-3-methyl-imidazolium bis(trifluoromethyl-sulfonyl) imide. *Journal of Chemical Thermodynamics* **2007**, *37*, 1327.
(40) Zhang, S.; Sun, N.; He, X.; Lu, X.; Zhang, X. Physical Properties of Ionic Liquids: Database and Evaluation. *Jorunal of Physical and Chemical Reference Data* **2006**, *35*, 1475.
(41) Suzuki, T.; Koide, K. Short Communication: Correlation between Upper Flammability Limits and Thermochemical Properties of Organic Compounds. *Fire and Materials* **1994**, *18*, 393.
(42) Liaw, H.-J.; Chen, C.-T.; Gerbaud, V. Flash-point prediction for binary partially miscible aqueous–organic mixtures. *Chemical Engineering Science* **2008**, *63*, 4543.
(43) Luyben, W. L. Control of the Heterogeneous Azeotropic n-Butanol/Water Distillation System. *Energy Fuels* **2008**, *22*, 4249.
(44) Kraemer, K.; Harwardt, A.; Bronneberg, B.; Marquardt, W. In *20th European Symposium on Computer Aided Process Engineering – ESCAPE20*

Pierucci, S., Ferraris, G. B., Eds.; Elsevier: 2010.
(45) Shukla, R.; Kang, W.; Sirkar, K. K. Acetone-Butanol-Ethanol (ABE) production in a hollow fiber fermentor-extractor. *Biotechnology and Bioengineering* **1989**, *34*, 1158.
(46) Dadgar, A. M.; Foutch, G. L. Improving the Acetone-Butonol Fermentation Process With Liquid-Liquid Extraction. *Biotechnology progress* **1988**, *4*, 36.
(47) Roffler, S.; Blanch, H. W.; Wilke, C. R. In situ extractive fermentation of Acetone and Butanol. *Biotechnology and Bioengineering* **1988**, *31*, 135.
(48) Scurto, A. M., Preliminary Adsorption studies for extraction of ionic liquids from aqueous phase with XAD 16 adsorbents.

5. TRAJECTORY OF CHARGED DROPLETS DISPERSED INTO NON-NEWTONIAN LIQUID-LIQUID SYSTEMS IN PRESENCE OF APPLIED DC ELECTRIC FIELD

5.1. Introduction

5.1.1. Relevance of intensification of contacting of non-Newtonian systems

Solvent extraction processes, in this context, extraction of metabolites/chemicals from biological processes[1-3], and in other cases, like, production of chemicals through chemical reaction like biodiesel from raw feedstocks[4] and phase separations of immiscible phases[5-9] are potential industrial processes suitable for intensification by DC electric fields. The necessity for intensification arises in biological extractions as the solutes are produced in dilute concentrations as biochemical reactions are inherently mass transfer limited and the resulting solutions can be more viscous and exhibit non-Newtonian behavior.[10] Further, solvent extraction of these dilute solutes from fermentation systems can also be mass transfer limited due to the nature of the fermentation broth medium.[10] Intensification of this extraction is important. As identified in chapter 3 and 4, ionic liquids are suitable for extraction of solutes and are compatible to micro-organisms. However, contact between ionic liquids known for their relatively high viscosities (> 40 cP at room temperature) and fermentation broths needs to be intensified to achieve higher mass transfer rates. Also, viscous continuous phases are encountered in cases where the extracted solute from the dispersed phase increases the viscosity of the continuous phase. For example, this situation is encountered in the extraction of biopolymers like Poly hydroxyalkanoates[11] from cell broth medium. Further, non-Newtonian fluids are encountered in multiphase processes such as interfacial polymerizations, microencapsulations, phase transfer catalysis, ionic liquids, etc where enhancement of

contacting is important.[12,13] Application of electric fields causes increase in interfacial area leading to enhanced mass transfer rates and hence improving both the product yields.[1,4,8,14] Here, intensification can be defined as the reduction in droplet size that leads to increased interfacial area for contacting; intensification does not necessarily imply an increase in droplet velocities. Simulated design of possible configurations of electrically enhanced reactors would be important in this context.

5.1.2. Problem Statement

The aim of this work was to investigate the effectiveness of electric fields to intensify liquid-liquid contacting of non-Newtonian fluids. In the literature, research in this area was primarily focused on low viscosity systems in the range 1-30 cP. Maximum viscosity of continuous phase used was around 100 cP. While for the dispersed phase, apart from water, water-glycerol solutions were also used as dispersed phase.[15-17] In the present study, application of electric fields was extended to study the spraying of non-Newtonian liquid into non-Newtonian liquids and explore the possibility of intensifying the contacting of very viscous solutions. The trajectories of electrically charged non-Newtonian droplets dispersed into a non-Newtonian immiscible continuous phase in an electrically enhanced rectangular glass column were evaluated. Physical parameters including, interfacial tension, viscosity, the density of both phases, and electrical conductivity of the dispersed phases, were measured to physically explain the droplet behavior and also to model the system accurately. The effects of the applied DC electric field, the polarity of the electric field, the nozzle dimensions, the dispersed phase flow rate, the nozzle insertion depth, and inter electrode distance upon the trajectories were investigated. Also, some interesting phenomena associated with falling drops in the

presence of electric fields including droplet breakup, coalescence, oscillation and jet formation were studied. Further, the potential for extending a novel finite element algorithm, developed for predicting three-dimensional drop trajectories for electrically charged drops in Newtonian fluids to non-Newtonian fluids was evaluated.

5.2. Physical properties of dispersed and continuous phases

5.2.1. Selection of continuous and dispersed phases

n-Decanol, used by Hume *et al.,*[15] as the Newtonian continuous phase to produce electrostatic spray regime with aqueous dispersed phase, was initially used as continuous phase. Initial attempts focused on modifying the rheology of n-Decanol using paraffin wax, and isobutylene. However, despite numerous attempts, a suitable modifier soluble in n-Decanol was not found. Subsequently, mineral oil, which was successfully used by He *et al.,*[18] was tried. A suitable modifier, Polyisobutylene (PIB), commercially available as Oppanol, was identified.[19] PIB not only modified the rheology to non-Newtonian (Shear-thinning) but made the resulting mineral oil / PIB mixture viscous. In the present study, pure mineral oil and 1% & 3% PIB (by wt.) in mineral oil were used. The procedure for preparing this solution is described in the experimental section 2.4.1.

In real world applications for electric fields, water is the main constituent of the dispersed phase. The rheology of water may be changed to non-Newtonian by addition of a cellulose derivative, carboxymethylcellulose (CMC). CMC is commonly used as a thickener in food science. In the present study, pure aqueous phase and 3%, 5% & 7% Aq. CMC solutions were used. Various physical properties of dispersed phase and continuous phase were measured and analyzed to better understand system behavior in the presence of an applied electric field.

5.2.2. Electrical conductivity (*EC*)

Electrical conductivities of the dispersed and continuous phase influences droplet charge accumulation and droplet charge loss respectively. As a droplet is formed from the nozzle, excess charge accumulates on the droplet and destabilizes to form smaller drops as shown in Figure 5.1.

Figure 5.1: Charge accumulation on the droplet [20]

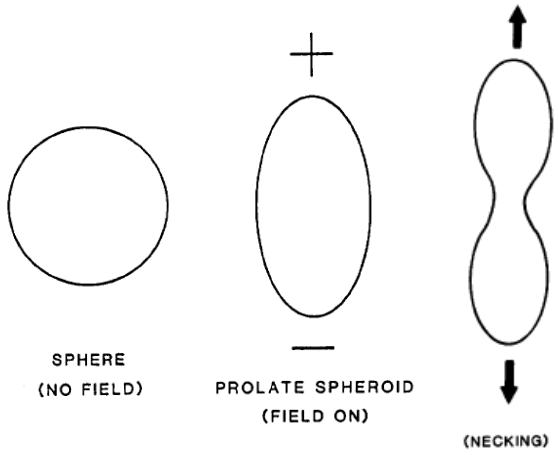

In the literature, this behavior is theoretically explained but not much experimental work has been to explain how electrical conductivity of the phases affects charge accumulation and subsequently droplet diameter and the role they play in reaching the electrostatic spray regime. In this work, the effect of electrical conductivity on the droplet diameter was studied for droplets of controlled rheology. The rheology of the droplet phase was adjusted by addition of CMC to water.

Figure 5.2: Droplet formation at a charged nozzle at different field strengths for furfural dispersed in n-heptane. (A) 0kV/cm, (B) 0.5kV/cm, (C) 1.0kV/cm, (D) 1.5kV/cm. [21]

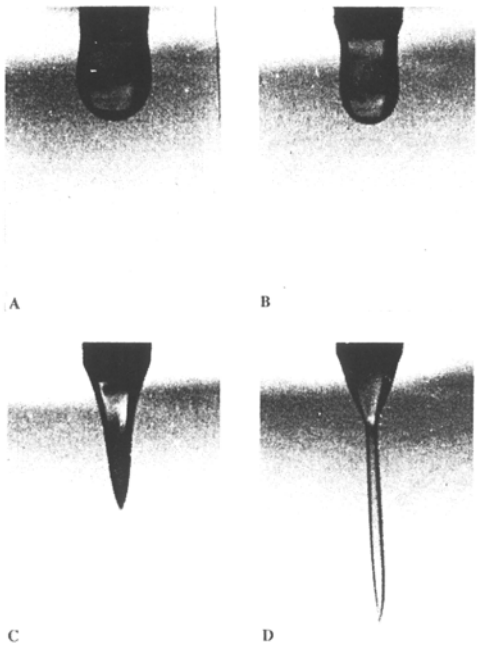

5.2.2.1. Electrical conductivity of the dispersed phase (EC_d)

Addition of CMC increased the electrical conductivity of the resulting solutions along with increasing the viscosity of the solution (refer to section 2.4.3.4 for more details). The addition of CMC modifier (3%, 5%, 7% were studied) increases EC_d by a factor of 1000. EC_d of Aq. CMC solutions are positively correlated to increase in CMC content; EC_d value doubles when CMC is increased from 3% to 7%. According to conventional wisdom, higher conductivity reduces relaxation time, thus forming drops acquire surface charge easily and destabilize quickly. This would suggest that the reduction in droplet size, as it is formed in presence of electric fields would be significant. Hence, for same E, it can be expected to lower droplet sizes with Aq. CMC solutions compared with pure

aqueous phase. Further, increase in electrical conductivity could also result in significant movement in the x-direction.

5.2.2.2. Electrical conductivity of continuous phase (EC_C)

The dielectric constants and electrical conductivities of pure Mineral oil and pure PIB are low, being in the range of 2.1 – 2.2[18,22] and of the order of 10^{-12} – 10^{-14} S/cm respectively. As the droplet acquires charge at the nozzle and detaches, it loses charge to the continuous phase[15,23-25] and the rate at which this decay happens is given by the equation below. 1st order time constant for this decay is termed as relaxation time which depends on the properties of the liquid and is the product of electrical resistivity and permittivity of the medium.

$$q = q_o \, e^{-t/\tau}$$

$$\tau = \frac{\varepsilon \, \varepsilon_o}{K}$$

q – Charge on the droplet at time 't'

q_o – Charge on the droplet at time $t = 0$

τ – Relaxation time or time constant

ε – Dielectric constant of continuous phase

ε_o – Permittivity of free space = $8.854 * 10^{-12} \; m^{-3} kg^{-1} A^2 \; s^4$

K – Electrical conductivity of continuous phase

Relaxation time can be defined as the rate at which charge relaxes from bulk to its surface. Relaxation time can be calculated for both the dispersed and the continuous phases. Relaxation time of the continuous phase, for the range of dielectric constant and electrical conductivity expected, is calculated to be in the range of 0.2 – 20 seconds. From the equation above, it can be inferred that the higher the relaxation time, slower is the droplet discharge to the continuous phase and vice versa. In an electrically enhanced

contactor, higher relaxation times are useful because the droplet in motion would be under the influence of electric field as it reaches the bottom electrode which increases the possibility of back-mixing. Further, droplet discharge at the formation stage to the continuous phase could impact droplet formation and onset of electrostatic spray from discrete droplet regime.

5.2.3. Density

The difference in densities of the phases determines the net gravitational force acting on the droplet at formation and significantly influences velocity during the fall. The density of mineral oil does not change significantly with addition of PIB ((refer to section 2.4.3.1 for more details). Addition of CMC marginally increases the density of the aqueous dispersed phase. The density of water increases by only 2.5% when 7% CMC is added. Density of both phases was found to be independent of temperature in the temperature range pertinent to this study which is 20 – 35°C. So, in the current study, the density difference is taken to be a constant at 0.14 g/cm^3. This density difference is expected to enable good phase separation.[26]

5.2.4. Rheology

5.2.4.1. Continuous phase Rheology

Shear thinning behavior of mineral oil increases with increase in PIB concentration (refer to section 2.4.3.3 for more details). The apparent viscosity of 3% PIB in mineral oil is 100 times the viscosity of mineral oil. As the viscosity of the continuous phase increases, the resisting drag force on the droplet increases, resulting in an increase in the droplet formation time and decrease in its terminal velocity.

5.2.4.2. Dispersed phase Rheology

Rheology of dispersed phase also changes to shear thinning behavior with increasing amount of CMC in the aqueous phase as described in the experimental section 2.4.3.3. The apparent viscosity increases almost 500 fold with the addition of 7% CMC. For Newtonian liquids, the rate of deformation (fluid flow) is linear to applied stress. But for fluids with non-Newtonian rheology, especially for those with shear thinning behavior exhibited by Aq. CMC solutions, the relation is non-linear. Here, the fluid flow (rate of deformation) is slow initially and but at higher applied stress, the relation becomes linear. This non-Newtonian behavior of the dispersed phase, could affect how a drop responds to various forces acting as it is formed.

5.2.5. Interfacial Tension (IFT)

IFT of water and mineral oil decreases with increase in concentration of continuous phase rheology modifier PIB. Lowering IFT makes it easier for drops to break up. Hence it is expected that dispersions will be easier to form with increase in PIB concentration.

IFT of water and mineral oil also decreases with increase in the concentration of dispersed phase modifier CMC (refer to section 2.4.3.2 for more details). This trend is similar to the electrical conductivity. For system of 3% PIB in Mineral oil and water, the average interfacial tension value is 23 mN/m. For systems of n-Decanol and water, sunflower oil and water, the IFT values are 9 and 33 mN/m; both of them form electrostatic sprays. These observations are quite contrary to the fact that the onset of electrostatic spray occurs at lower values of IFT between phases involved.

Interfacial tension and conductivity are not the only factors affecting drop size – for discrete drops – viscosity and density difference, nozzle size and fluid velocity through

the nozzle are also major factors. There could be a dimensionless number that would involve these properties along with applied voltage, drop size or drop volume that can be used to predict onset of electrostatic spray. In the literature, empirical correlations based on dimensional analysis were developed in 1980's and earlier for drop size – for both charged and uncharged drops by identifying forces acting on the droplet during formation.[18,25,27]

5.3. Droplet diameter

5.3.1. Droplet diameter measurement

In the present work, droplet diameter was calculated from high resolution still photographs taken as the drop was in motion using image analysis and assuming spherical droplets. In the literature, the droplet volume as it detaches at the nozzle and hence droplet diameter has been calculated mainly from knowing the dispersed phase flowrate and the drop formation time together with property data. Here, the drop formation time was an average time taken to form one drop by counting the time taken for formation of 'n' drops. Takamatsu *et al.,*[25] used videos to get a better handle on the formation times when the frequency of the formation was high and manual measurement was not reliable. In cases where the droplet size is observed to be non-uniform, image analysis software like Optimus were used.[15,28] However, these were found to be inadequate as the quality of the video was blurred.[18,25,27]

Table 5.1 below gives a summary of the droplet diameters obtained with various parameters studied. Droplet diameters ranged from 3.5 mm to 11.1 mm for various continuous and dispersed phases used. The image analysis technique used here to calculate the droplet diameter was found to have statistical error up to 7%. This mainly

includes human error, non-spherical droplets being formed, and calculation of scaling factor during the image analysis.

From the table, further observations were made on the droplet diameters calculated. Here, for 1% and 3% PIB in Mineral oil irrespective of dispersed phases or other parameters used, an average diameter could be calculated indicating the effect of electric field is not as predominant.

a) For the less viscous mineral oil system, the maximum reduction in the droplet diameter was from 7.9 mm to 3.5 mm. There was a reduction of 56% upon the application of DC fields up to -11 kV.

b) For the other two more viscous continuous phases, 1% PIB in Mineral oil and 3% PIB in Mineral oil, standard deviation on an average diameter was around 15%. Highest and lowest droplet diameters with 1% PIB in Mineral oil were 5.5 mm and 3.5 mm respectively. There was a reduction in droplet size of 35% at a maximum applied E of -10 kV with small sized nozzle (OD = 2.12 mm) with higher thickness (t = 0.47 mm). With other nozzles sizes even at higher values of applied voltage, the droplet size was higher than 3.5 mm.

c) With 3% PIB in Mineral oil, highest and lowest droplet diameters observed were 11.2 mm and 6.6 mm respectively. There was a reduction in droplet size of 40% at a maximum applied E of -20 kV with big sized nozzle with 7% Aq. CMC solution as the dispersed phase. There was a reduction in droplet size by 35% at a maximum applied E of -10 kV with small sized nozzle with higher thickness.

d) For the two continuous phases, irrespective of other parameters used, the average drop diameters were 4.5±0.7 mm (15.5%) and 8.6±1.3 mm (15%) respectively.

From these averaged diameters, it can be observed that the viscosity of the continuous phase plays an important role in determining the diameters that can be produced. Increasing the viscosity from 1% to 3% PIB in Mineral oil, the averaged droplet diameter obtained almost doubled.

Table 5.1: Droplet diameters for a given system, applied voltages, nozzle diameter

Cont. phase	*Mineral Oil*	
Disp. Phase	*Pure water*	
Appl. Volt nozzle type	*Knob setting*	*Drop size (mm)*
-5kV_MN	8	7.9
-10kV_MN	8	3.5
-10kV_MN	10	6.4
-22kV_MN	10	3.6

Cont. phase	*Mineral Oil*	
Disp. phase	*3% Aq. CMC*	
Appl. Volt _nozzle type	*Knob setting*	*Drop size (mm)*
-11kV_MN	8	4.5
-11kV_MN	10	6.23

Cont. phase	*1% PIB in MO*	
Disp. Phase	*Pure water*	
Appl. Volt _nozzle type	*Knob setting*	*Drop size (mm)*
-13.5kV_BN	8	5.5
-17.5kV_BN	10	5.2
-24kV_BN	10	4.6

Cont. phase	*1% PIB in MO*	
Disp. phase	*3% Aq. CMC*	
Appl. Volt _nozzle type	*Knob setting*	*Drop size (mm)*
-10kV_SN	8	3.9
-15kV_SN	9	3.9
-12.5kV_SN	10	5.2
-10kV_SNThic	8	3.5
-10kV_SNThic	9	4.5
-12.5kV_SNThic	9	4.0
-12.5kV_MNIns	8	3.9
-17.5kV_MNIns	10	5.3

Cont. phase	*3% PIB in MO*	
Disp. Phase	*Pure water*	
Appl. Volt nozzle type	*Knob setting*	*Drop size (mm)*
-13.5kV_BN	8	8.4
-13.5kV_BN	10	11.2
-15kV_BN	8	8.2
-15kV_BN	10	10.6
-17.5kV_BN	10	11.0

Cont. phase	*3% PIB in MO*	
Disp. phase	*3% Aq. CMC*	
Appl. Volt _nozzle type	*Knob setting*	*Drop size (mm)*
-15kV_BN	9	9.1
+15kV_BN	9	8.3
-20kV_BN	9	8.4
-20kV_BNInsul	9	8.5

-20kV_MN	9	8.3
-20kV_MN	10	9.8

-20kV_MN	9	7.6
-20kV_SN	9	8.3
-20kV_SNThic	9	7.7

Cont. phase	*3% PIB in MO*	
Disp. Phase	*5% Aq. CMC*	
Appl. Volt _nozzle type	*Knob setting*	*Drop size (mm)*
-20kV_BN	10	9.4
-20kV_BNIns	10	10.1
-20kV_MN	9	7.8
+20kV_MN	9	7.7
-20kV_SN	9	6.6

Cont. phase	*3% PIB in MO*	
Disp. phase	*7% Aq. CMC*	
Appl. Volt _nozzle type	*Knob setting*	*Drop size (mm)*
-20kV_BN	8	6.6
-20kV_BN	9	7.6
-15kV_MN	9	8.4
-20kV_MN	9	7.8
-20kV_SN	9	7.9

DIMENSIONS OF NOZZLE TYPE USED
BN – Big nozzle with OD – 6.6 mm, thickness = 0.32 mm, E =5.95 mm
BNIns – Big nozzle with longer insulation of nozzle OD = 6.6 mm, thickness = 0.32 mm, E = 0
MN – Medium nozzle with OD – 4.18 mm, t = 0.28 mm, E =5.95 mm
SN – Small nozzle with OD – 2.12 mm, t = 0.27 mm, E =5.95 mm
SNThic – Small nozzle with bigger thickness OD – 2.12 mm, t = 0.47mm, E =5.95 mm

Note: Knob setting 8, 9, 10 refer to dispersed volumetric flow rate through the nozzle of 71.4, 180.2 and 360.4 ml/hr

5.3.2. Drop formation images

The following section looks at the drop formation through images take using a "stills" camera using continuous release mode. The four images in each figure were taken in continuous mode and within 2-3 second duration. When there is no applied E, the drop grows until dynamic equilibrium of forces is reached and droplet detaches by necking process. The drop formation is similar at applied voltages of 0, -5 kV and -12 kV as

shown in the Figure 5.3, Figure 5.4 and Figure 5.5 respectively. However, as the applied voltage is increased from 0 to -12 kV, the neck of the droplet prior to detachment becomes progressively thinner. We postulate that this is due to greater charge accumulation. Further, satellite droplets were observed at 0, -5 kV and -12 kV. At -12 kV, the effect of electric field is more evident as the detaching droplet pulls the residual liquid near the nozzle and stretches the neck.

Figure 5.3: Drop formation at the nozzle when 3% Aq. CMC dispersed into pure mineral oil with no applied voltage

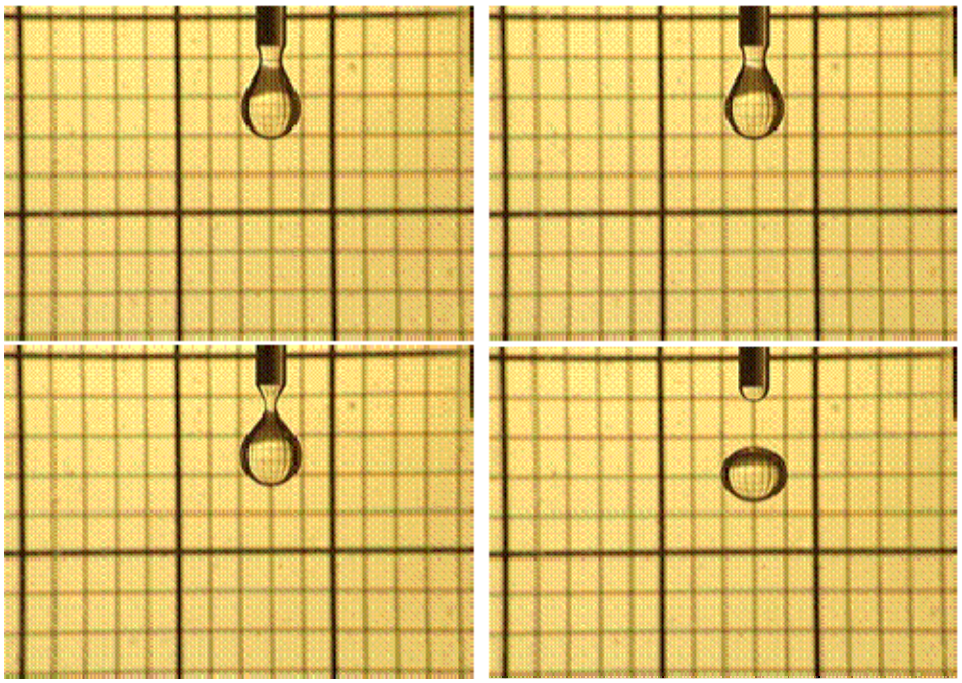

Figure 5.4: Drop formation at the nozzle with 3% Aq. CMC dispersed into pure mineral oil at -5 kV

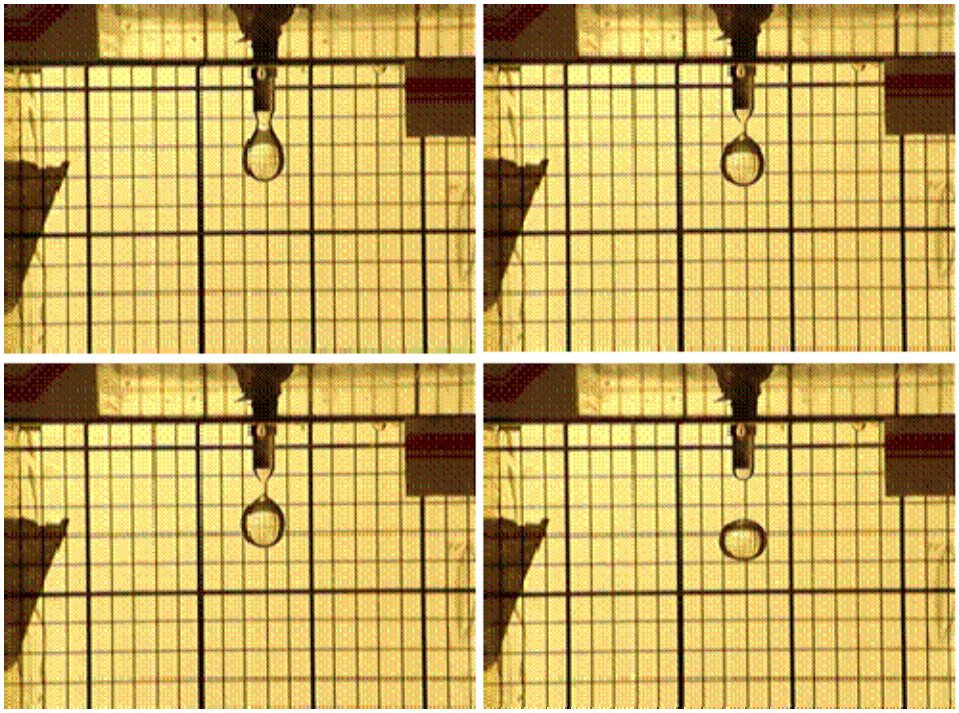

Figure 5.5: Drop formation at the nozzle with 3% Aq. CMC dispersed into pure mineral oil at -12 kV

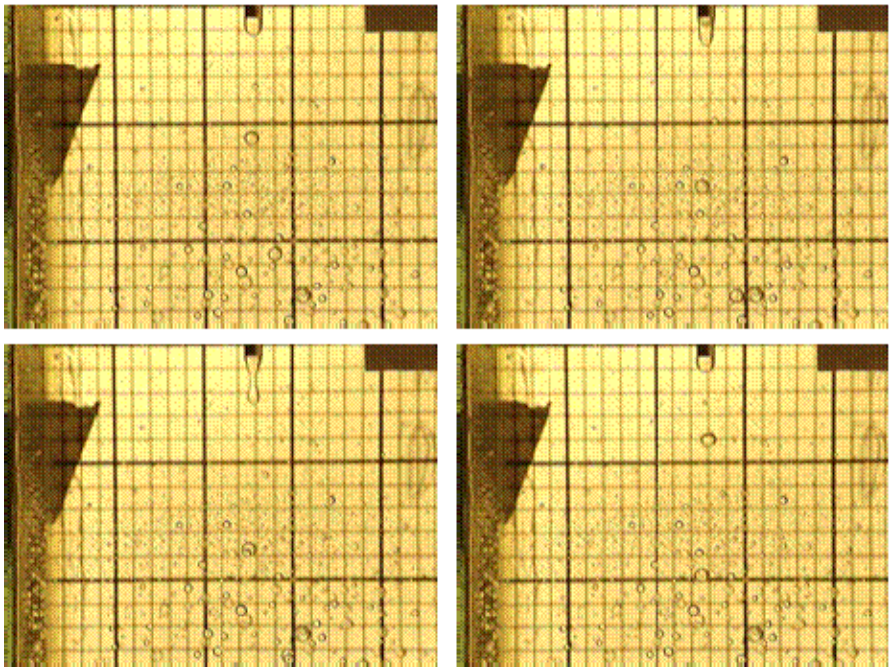

5.3.3. Droplet formation

Average droplet formation time, for each system, was measured from the droplet trajectory videos. During the droplet formation at the nozzle, the various forces[29,30] acting on the droplet are:

1. Buoyancy force acting in the downward direction
2. Inertial/Kinetic force in the downward direction
3. Electrical force in the downward direction (as described in the experimental section 2.4.2, electric field is applied to bottom electrode and earthed at the nozzle)
4. Interfacial tension force in the upward direction
5. Drag force in the upward direction

Droplet formation times give an indication of the extent of these forces. When the viscosity of the continuous phase is changed, the magnitude of the drag forces acting on the droplet is changed. Further, the diameter of a droplet, as it is detached from the nozzle is related to the droplet formation time as shown in the equations below. The droplet volume and hence the diameter are directly proportional to the formation time, i.e. longer droplet formation time results in bigger droplet volume and hence, bigger mean droplet diameter.

$$V_d = Q.t, \qquad i.e.,\ V_d \ \alpha\ t$$

$$Further,\ V_d = \frac{\pi}{6}d^3, \quad i.e.,\ d\ \alpha\ t^{1/3}$$

$$\frac{d_1}{d_2} = \left(\frac{t_1}{t_2}\right)^{1/3}$$

$$v_d = \frac{Q}{A_N}$$

where,

$d \rightarrow$ Droplet diameter

$V_d \rightarrow$ Droplet volume

$v_d \rightarrow$ Droplet velocity as it is detached from the nozzle

$Q \rightarrow$ Dispersed phase volumetric flow rate

$t \rightarrow$ Average droplet formation time

$A_N \rightarrow$ Nozzle surface area based on outside diameter

To understand primarily the effect of viscosity of the continuous phase on the formation time and hence on the droplet diameter, an average droplet formation time was measured for different systems. Here, the following parameters were held constant: applied electric field at -11 kV, volumetric flow rate at a 71.4 ml/hr and a medium sized nozzle (OD = 4.18 mm). Table 5.2 below shows the formation times for different continuous and dispersed systems studied. With water as the dispersed phase, the viscosity of the continuous phase is increased by adding 1% w/w of PIB to mineral oil. The formation time increases by a factor of 3.5. Increasing the wt% of PIB from 1% to 3%, further increases the formation time by a factor of 3.6. Additionally, the formation time for 3% PIB in Mineral oil compared to that of pure mineral oil is reduced by a factor of 12.7.

Table 5.2: Average droplet formation time at the nozzle for different continuous and dispersed phases. Knob setting: 8 (dispersed phase flow rate to 71.4 ml/hr) and Nozzle type: Medium (OD – 4.18 mm).

Continuous phase	Dispersed phase	Applied Electric field (kV)	Time taken for 1 drop to form (seconds)
Mineral oil	Water	-10	0.48
Mineral oil	3% Aq. CMC	-11	0.95
1% PIB in Mineral oil	Water	-10	1.67
3% PIB in Mineral oil	Water	-10	6.1
3% PIB in Mineral oil	3% Aq. CMC	-10	6.6

Apart from increase in magnitude of the drag force from the addition of rheology modifier, its effect on other forces is looked at here. With the addition of PIB, the interfacial tension of these continuous phases with water decreases. This should result in lower droplet formation times instead of higher as obtained above as the upward acting interfacial force on the droplet is reduced. As the wt. % of PIB increases, the change in density of the continuous phase is insignificant and the role of buoyancy force would be similar to that with no PIB added. l Inertial/Kinetic forces are dependent on the droplet velocity as it is formed. Droplet velocity as it is formed can be calculated from the equation given above. Further, higher viscosity of the continuous phase could negatively affect the inertial force as the droplet velocity as it is detached is affected due to higher drag force. From analyzing various forces acting on the droplet, it can be mentioned that

higher viscosity of the continuous phase results in significantly higher drag force on the droplet which has a direct effect on the formation time and results in higher formation time.

Now, the effect of applying external electric field was determined to understand droplet formation dynamics. The electrical force acts as an opposing force to the drag force, the net force in downward direction increases and the droplet detachment time decreases.[15,18,31] As the applied electric field is increased from 0 to ±25 kV, the droplet formation process can transition from a discrete droplet regime to an electrostatic droplet (dispersion) regime where the droplet formation time would be in milliseconds. But in the present study with mineral oil, even at an applied voltage of -10 kV, the droplet formation is in the discrete droplet regime. The transition to the electrostatic regime is not observed when the voltage is increased to -22 kV though there is a corresponding decrease in droplet formation times and diameters. When mineral oil is used as the continuous phase, which has moderate viscosity, applying the electric field decreases droplet diameters but the electrostatic regime is not reached. Further, addition of the rheological modifiers to mineral oil, which increases drag force, obtaining drop diameters similar to pure mineral oil system with the application of electric field was found to be difficult.

The same cannot be implied by increasing the viscosity of the dispersed phase while the continuous phase is the same. Neither droplet diameter nor droplet volume is directly dependent on the viscosity of the dispersed phase; it would be difficult to qualitatively understand the effect of dispersed phase viscosity on the formation times. From the table below, the formation time with 3% Aq. CMC increases by 0.5 seconds approximately

compared to water when they are used with either Mineral oil or the 3% PIB in Mineral oil. Unlike the continuous phase where the addition of PIB does not increase the density, the density of the 3% Aq. CMC increases by 1.6% compared to water which leads to slightly higher buoyancy force. Further, addition of CMC reduces the interfacial tension of 3% Aq. CMC by 8 to 15% compared to water for all the three continuous phases. This results in lower upward acting interfacial tension force acting on the droplet. Both these forces should slightly reduce formation time as the drag force is the same and inertial forces are not affected by change in dispersed phase properties but the observations suggest otherwise. Additionally, along with the increase in the viscosity of the aqueous phase, the electrical conductivity increases significantly. As discussed in section 5.2.2.3, increase in electrical conductivity should result in easier destabilization of the droplet and hence reduced droplet diameter, lower formation time and higher initial droplet velocities at nozzle. This effect was not observed in the experiments. This could be related to the non-Newtonian behavior of aqueous CMC solutions and the rheological behavior here.

5.3.4. Jet formation

Formation of long jets while dispersing one fluid into a second has been reported in the literature.[32-34] Similar observations were made with 7% Aq. CMC as the dispersed phase and 1% PIB in Mineral oil as the continuous phase at -12.5 kV as shown in the images below Figure 5.6. We observe that the droplet formation is different from other systems as the droplet elongates without separating from the nozzle, forming a "jet" (equivalent to an elongated neck). The elongated dispersed phase almost reaches the middle of the column (i.e. the length of the jet was about half of the distance between the electrodes.

As the applied voltage was increased, the length of the jet decreased and the jet broke up into droplets which eventually hit the side walls of the column. We postulate that at E=0, the viscous forces are much stronger than gravitational force prolonging droplet formation. The effect of the electric field can be seen from the fact that with increased applied E, the length of the jet decreases.

Figure 5.6: Jet formation at higher concentrations

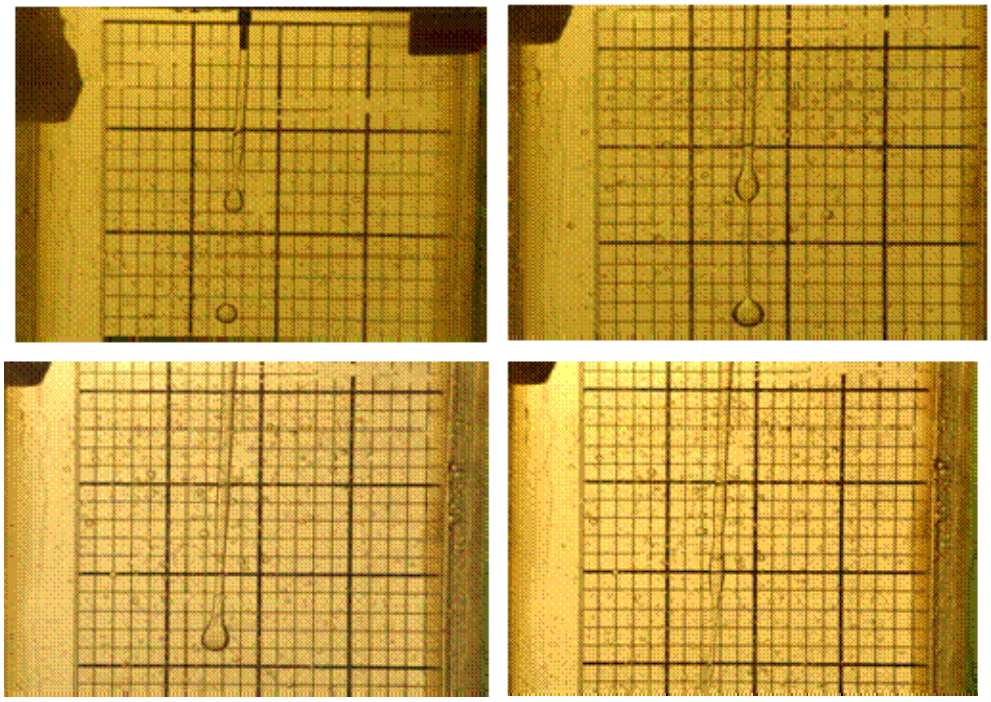

5.4. Effect of various parameters on droplet trajectory

As described in the experimental section, the droplet trajectories were digitized from the videos. The shapes of the droplet trajectories varied depending on the intensity of the electric field. When both the dispersed phase and continuous phase are in motion, the resulting droplet trajectories would be random.

5.4.1. Trajectories for the Mineral oil – Water system

In a system where a droplet falls vertically into a second phase (with no electric field), as can be expected, the droplets followed a vertical trajectory downwards influenced only by gravitational force. The electric field was increased by a magnitude of 2.5 kV up to a maximum of -25 kV. Between 0 to ~ -10 kV, the droplets continued to follow a vertical trajectory, but some horizontal movement and oscillatory movements were observed. Between -10 kV to -20 kV, an "S" shaped trajectory was observed – the droplet trajectory relative to the vertical axis varied between 0 to 45 degrees. The droplets alternated to either side of the center – if one droplet started the S-motion towards the right, the next droplet would start the S towards the left. This effect could be explained by the mutual repulsive forces acting between adjacent drops as they detach from the same nozzle. However, the S-shaped motion of the droplets was unstable with the acute angles varying between 0 and 60 degrees even in the steady state. Between -20 kV and -25 kV, the acute angles increased resulting in the droplets directly hitting the sidewalls. The droplet follows a swirling trajectory because of the increase in frequency of droplet detachment as E is increased which leads to charge repulsions between detaching droplets and with the nozzle. Further droplets during their immediate motion lose charge which leaves a wake which could also affect the trajectory.[18] The unstable

droplet trajectory could also be due to non-linearity of E around the nozzle due to the above reasons and due to presence of impurities.[31] Table 5.3 below summarizes trajectory pattern observed with different continuous phase and dispersed phases.

In addition, "satellite" droplet formation was observed mainly with Mineral oil and Water/Aq. CMC systems. Satellite drop forms at the same instance when a fully grown droplet detaches from the nozzle, it is a much smaller droplet (in the order of micrometers) is formed at the point of detachment. Though the satellite drop size is very small, they are not much of importance in liquid-liquid contacting because they do not settles to bottom of the contactor easily. Further, at higher voltages it was observed that they stick to column side walls very easily and hindering the quality of droplet imaging.

Table 5.3: Trajectory patterns of all systems studied

Continuous phase	Dispersed phase	Electric field (0 – 10 kV)	Electric field (10 – 20 kV)	Electric field (20 – 25 kV)	Satellite droplet (Y/N)
Mineral oil	Water	Small oscillations	S-shape	Hit side wall	Y
Mineral oil	3% Aq. CMC	Small oscillations	S-shape	Hit side wall	Y
1% PIB in Mineral oil	Water	Small oscillations	S-shape	Hit side wall	N
1% PIB in Mineral oil	3% Aq. CMC	Small oscillations	S-shape	Hit side wall	N
3% PIB in Mineral oil	Water	*Small oscillations*	*S-shape*	*Hit side wall*	*N*
3% PIB in Mineral oil	3% Aq. CMC	*Small oscillations*	*S-shape*	*Hit side wall*	*N*
3% PIB in Mineral oil	5% Aq. CMC	*Small oscillations*	*S-shape*	*Hit side wall*	*N*

A summary on how various parameters could affect the droplet sizes, droplet trajectories, and droplet velocities for a given liquid-liquid system is presented here. The parameters studied include: applied electric field voltages, rheologies of continuous and dispersed phases, electrical conductivity of the dispersed phase, nozzle diameter, polarity of the applied E and dispersed phase flow rate. The effect of each parameter is described in more detail below by choosing a suitable system.

5.4.2. Applied Electric field voltage

In an electrically enhanced liquid-liquid contactor, the shortest droplet residence times are obtained when E = 0 as the droplet diameter is the largest and the droplet falls vertically downwards with zero x- and z-directional velocities. Increasing applied E results in finite velocities in x & z-directions and leads to longer residence time. As the applied E increases, droplet diameter decreases and the charge accumulated on the droplet and its residual charge increases as it reaches bottom electrode; this could result in reduced residence times. With 1% PIB in Mineral oil and water as dispersed phase, increasing the applied electric field from -17.5 to -24 kV decreases the average residence time from 4.5 to 4 seconds. Also, initial droplet velocities in the x- and y-directions are higher at higher E. This is a result of increased electrical force acting on the droplet both due to increased charge and E. Further, at both -17.5 and -24 kV, V_x is finite and varied between 0.5 cm/sec to 3 cm/sec. Terminal velocities of the droplets appear to be the same though the droplet velocities as it near the bottom electrode increases again (Figures 5.9 and 5.13).

As the electric field is increased from -17.5 kV to -24 kV, the droplet size decreases from 5.2 mm to 4.6 mm, i.e., an 11% reduction. Since gravitational force is proportional

to cube of droplet diameter and the opposing drag force is proportional diameter, the droplet sees a 30% decrease in gravitational force and an 11% decrease in drag, i.e., a net decrease of 19% in downward force. The 37% increase in electric potential (from -17.5 kV to -24 kV) should translate into an increased downward electric force. At the moment of release of the droplet, one can assume that the net increase in downward force is 18% (37% - 19%). This can be observed in the higher spike in vertical velocity at -24 kV. However, the droplet quickly loses accumulated charge, reducing the impact of the higher electric potential and dropping the vertical velocity of the -24 kV droplet to the same level as the -17.5 kV droplet.

The effect of E on the droplet trajectories for 3% Aq. CMC dispersed into 3% PIB in mineral oil at a flowrate of 360.4 ml/hr are shown in Figures 5.2a and 5.2b. Here, the electric field is varied from -15 kV to -20 kV. The residence time for this 3% PIB system is around 25 seconds, which is significantly higher than the residence time of 5 seconds for 1% PIB system described in Figure 5.1a-b.

Data presented in Figures 5.7, 5.10 and 5.11, indicate the residences time at -15 kV of ~22.5 seconds and at -20 kV of ~27 seconds. The droplet diameter at -15 kV is 9.1 mm and at -20 kV is 8.4 mm. It can be inferred that the larger droplet at lower applied E falls faster due to higher gravitational force. One would expect that the terminal velocity of the droplet would increase with an increase in applied voltage. However, the actual observations indicate otherwise - the terminal velocity at -15 kV is around 0.58 cm/sec and at -20 kV is around 0.45 cm/sec.

The x-direction velocities (*Vx*) are low and as a result, the drop falls vertically without a significant s-shaped trajectory as can be seen from Figure 5.8 and Figure 5.12.

At -15 kV, *Vx* is zero, while at -20 kV, *Vx* is around 0.05 cm/sec. The initial velocities in the y-direction does not change significantly between -15 kV and -20 kV.

Figure 5.7: Effect of applied voltage on the droplet trajectory

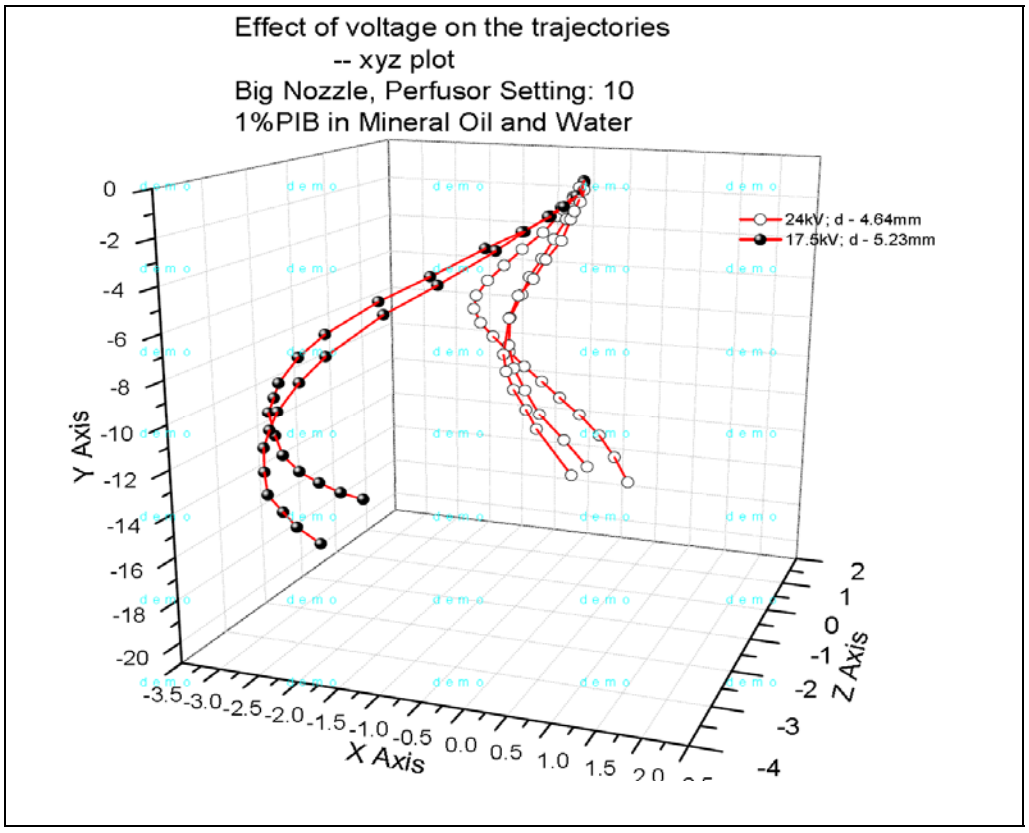

Figure 5.8: Effect of applied voltage on the x-directional droplet velocities

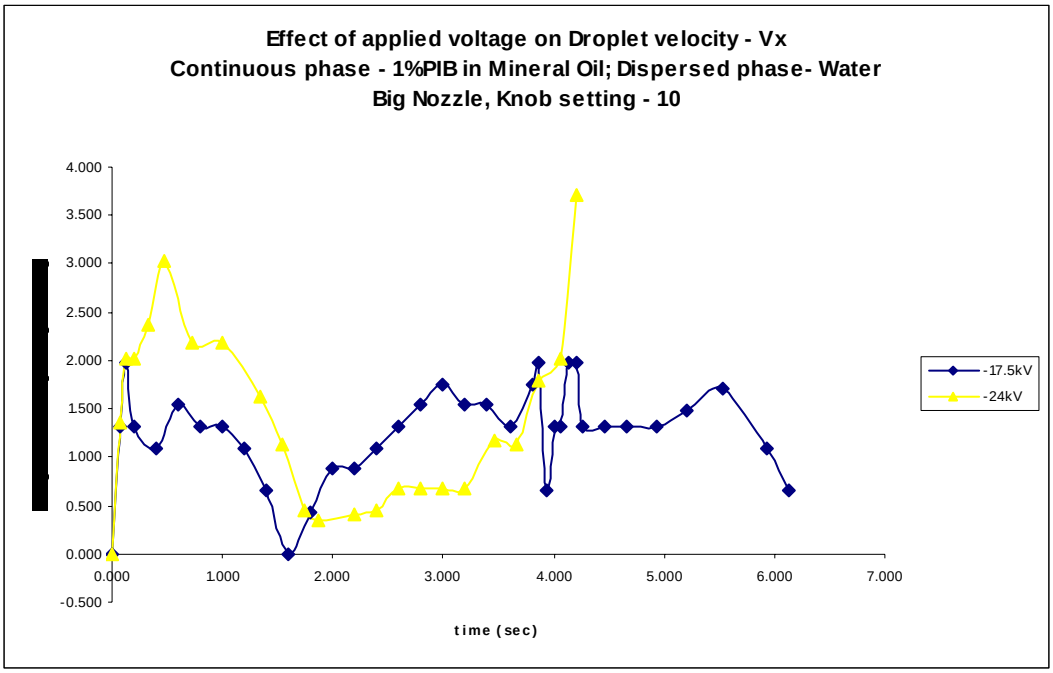

Figure 5.9: Effect of applied voltage on the y-directional droplet velocities

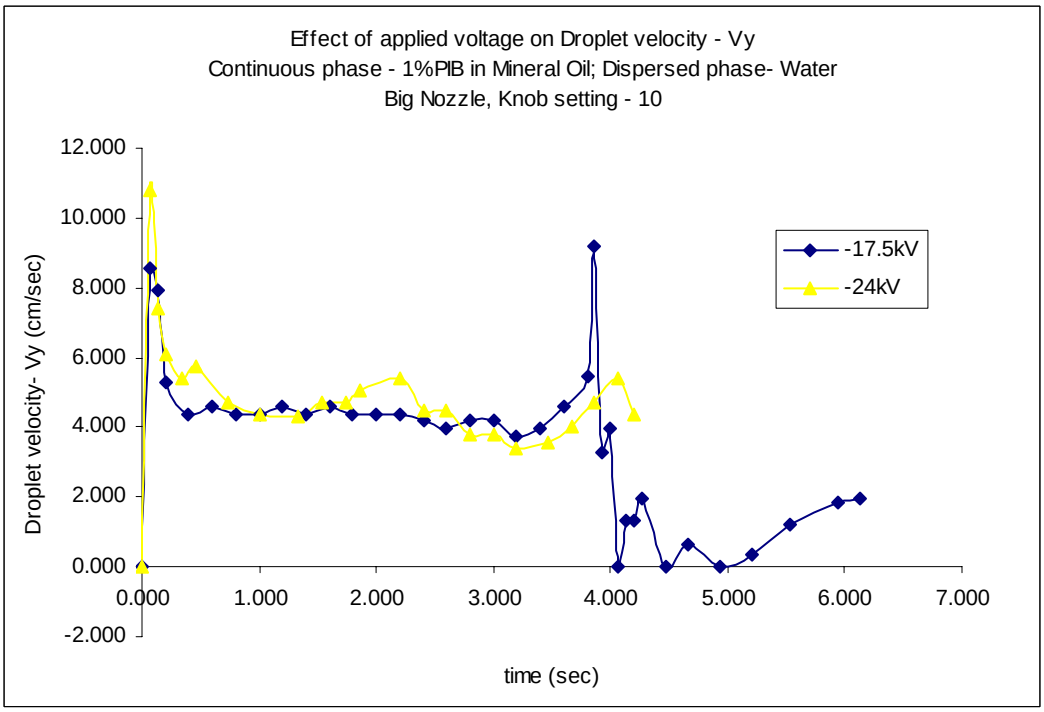

Figure 5.10: Effect of applied voltage on the droplet trajectory

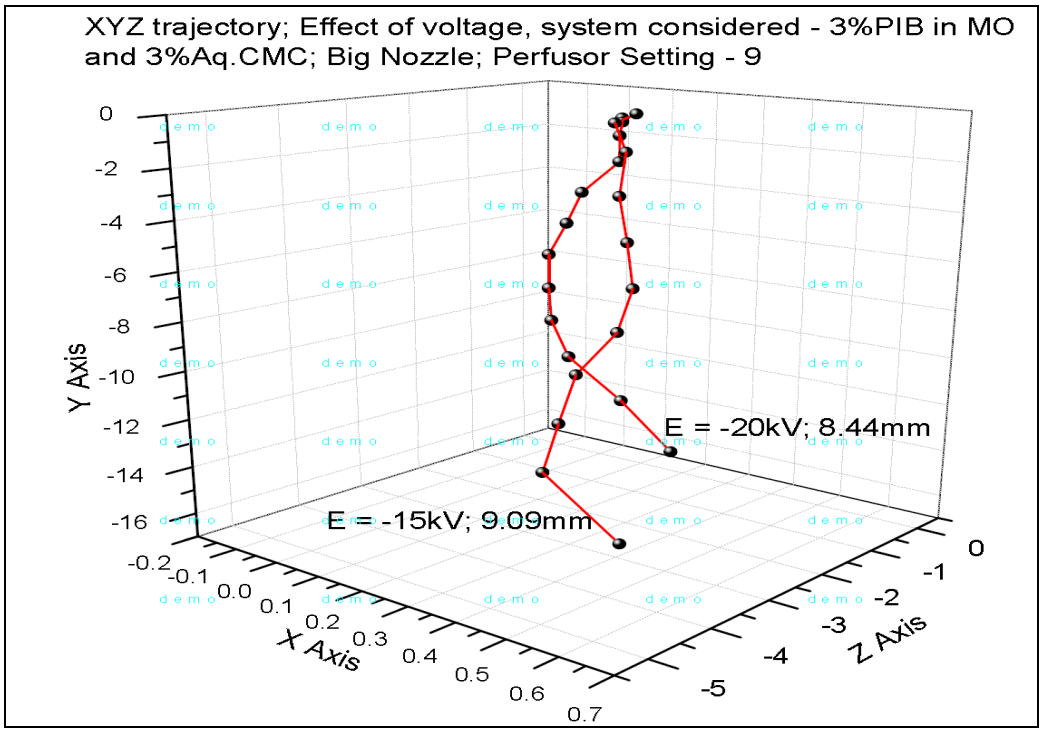

Figure 5.11: Effect of applied voltage on the droplet trajectory as a function of time

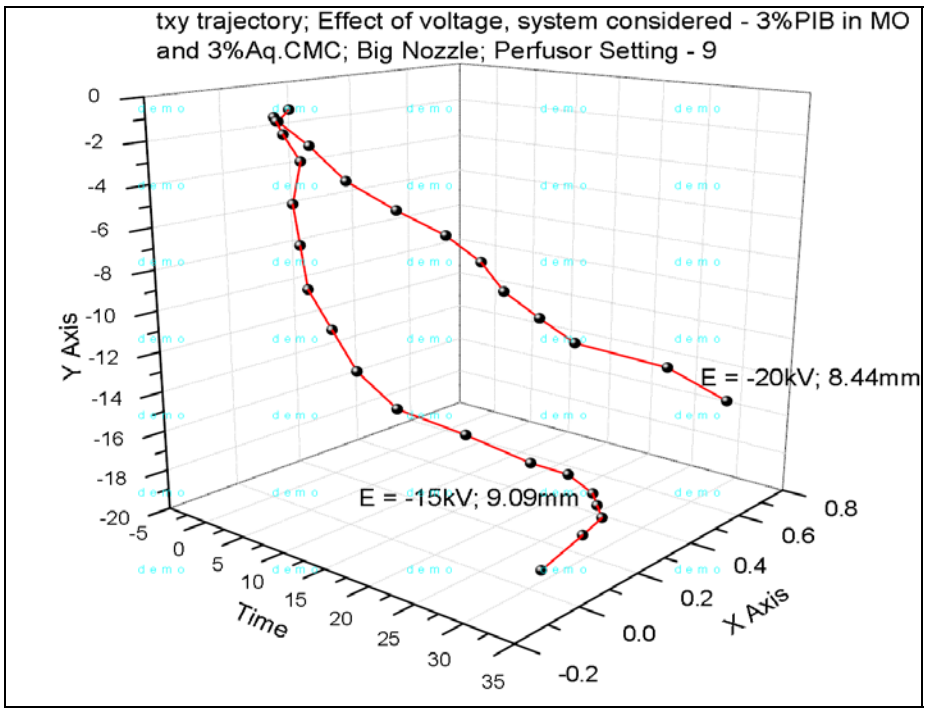

Figure 5.12: Effect of applied voltage on the x-directional droplet velocities

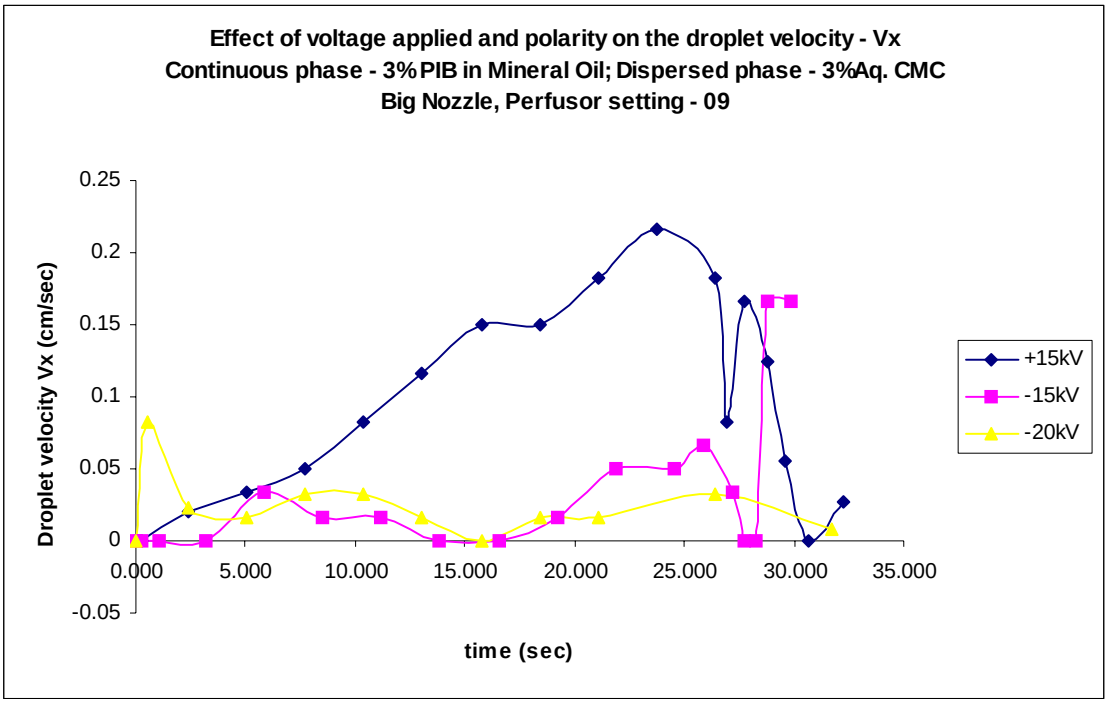

Figure 5.13: Effect of applied voltage on the y-directional droplet velocities

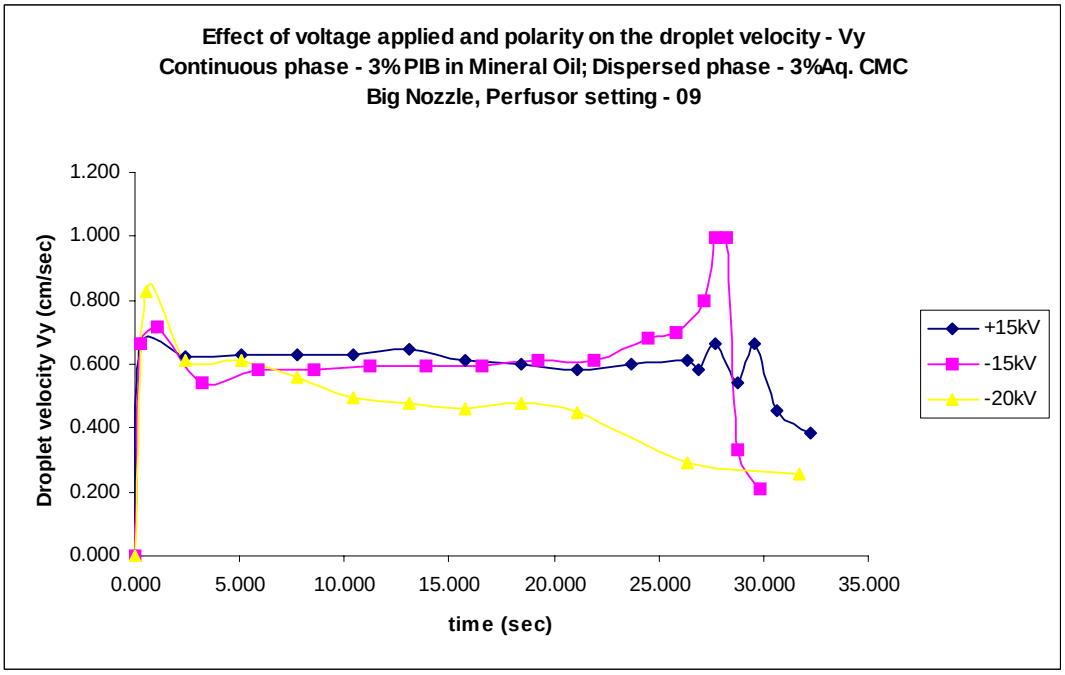

5.4.3. Dispersed phase

As mentioned above, both the rheology and electrical conductivity of the dispersed phase increase by increasing CMC concentration in the aqueous phase. In this section, these aspects are looked at closely both individually and in unison on how they droplet formation and droplet trajectory.

Increase in the electrical conductivity of the droplet results in greater charge accumulation on the droplets at the nozzle. Due to greater interaction between these charged droplets after they are detached, the droplet trajectory deviates towards the x- and z- directions of the column as seen from the figures Figure 5.14 and Figure 5.15. However, the droplet velocity in the y-direction is not impacted, indicating that the drops maintain their integrity despite higher charge acquisition. Further, the residence times of the droplet with different concentrations of the CMC cannot be compared directly because as the concentration of CMC increases the droplet trajectory is towards to the walls. But it can be expected that the residence times would be smaller for Aq. CMC droplets compared to that pure aqueous phase. Hence, the overall motion of the drops is enhanced at higher CMC concentrations.

There is a step decrease in drop size as the dispersed phase rheology changes from Newtonian to non-Newtonian. However the degree of non-Newtonian behavior (% of CMC in water) does not seem to have any impact on the drop size, i.e., 3%, 5% and 7% Aq. CMC solutions all have similar drop sizes. The aqueous drop diameter is 7% larger than non-Newtonian; therefore, the gravitational force is 19% higher, while the opposing drag force is only 7% higher. Velocity data of the droplets in the x and y- directions are shown in the figures Figure 5.16 and Figure 5.17. At the time of detachment, the

Newtonian aqueous drop has a higher initial vertical velocity. But as the drop falls down, the Newtonian aqueous phase loses it charge and reaches a terminal velocity. The non-Newtonian drops start with a lower initial vertical velocity, but due to higher charge retention, see a lower loss of vertical velocity. So, after an initial a few seconds, the vertical velocities of Newtonian and non-Newtonian phases are similar. As the degree of non-Newtonian behavior of the droplet increases, the electrical conductivity also increases and hence the initial vertical velocity is expected to increase – however, it is noticed that the initial vertical velocity decreases. The x-direction velocities behave in a different way – with the increase in non-Newtonianness – the x-direction velocities increase, as expected due to increase in electrical conductivity. Also, the velocity profiles of the Aq. CMC droplets are much more erratic compared to that of water.

As discussed at 7% CMC in the aqueous phase, jet formation was observed. This jet formation can be characterized by the length of the jet. Application of voltage decreased the length of the jet but the droplet motion was directed towards the walls of the column.

It can be concluded that, viscosity and electrical conductivity of dispersed phase both effect droplet. Electrical conductivity affects the drop size and the velocity acquired by the droplet while the viscosity seems to affect drop formation at very high apparent viscosities for example 7% Aq. CMC solutions.

Figure 5.14: Effect of dispersed phase rheology on the droplet trajectory

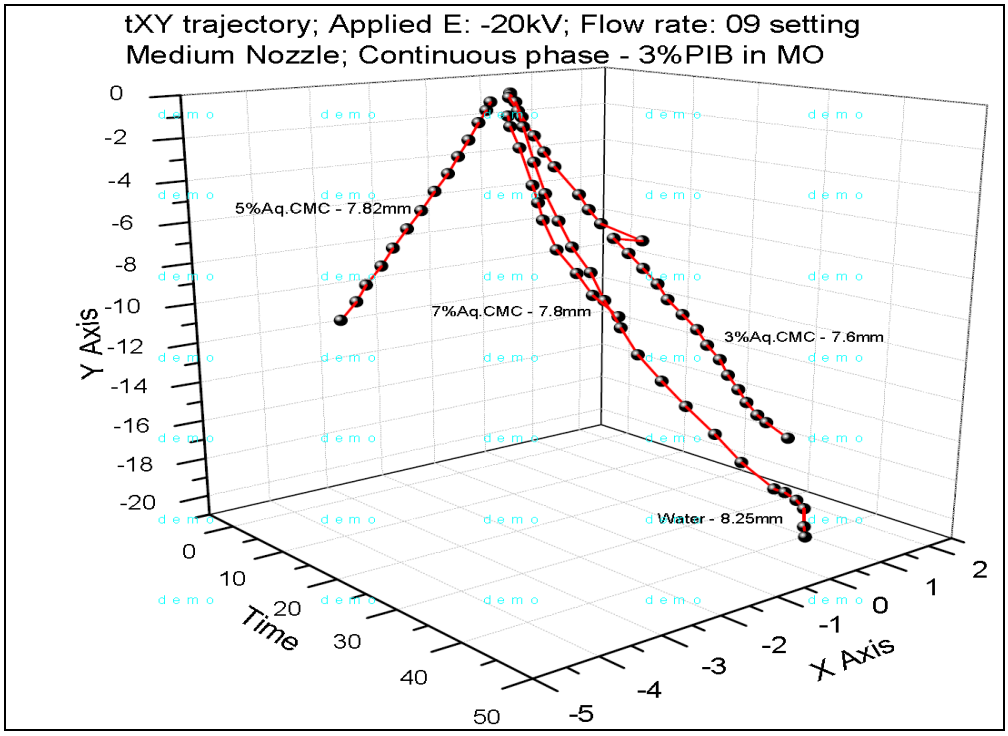

Figure 5.15: Effect of dispersed phase rheology on the droplet trajectory as function of time

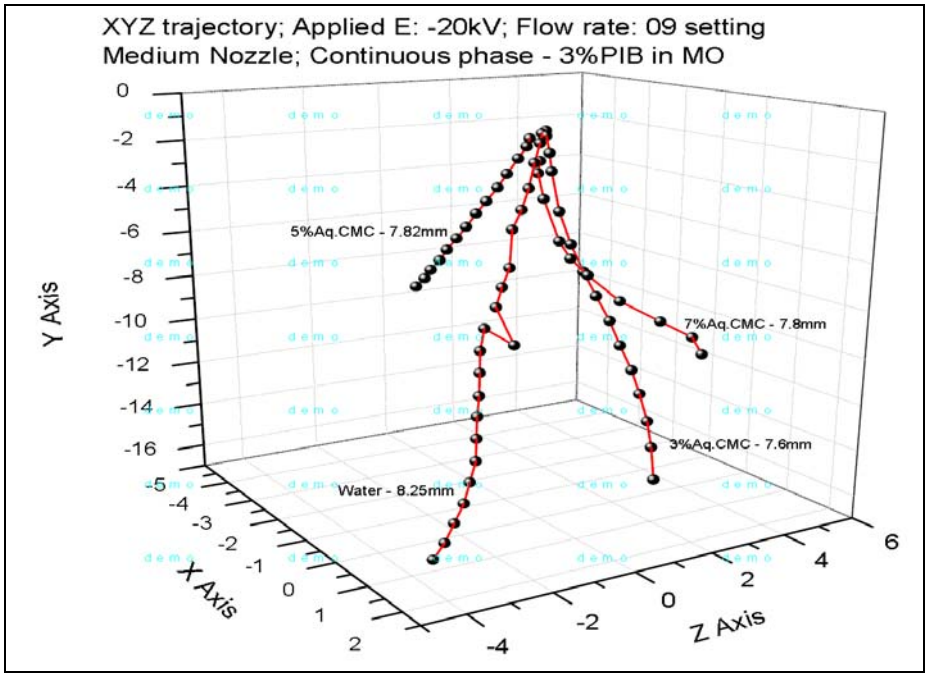

Figure 5.16: Effect of dispersed phase rheology on the x-directional droplet velocities

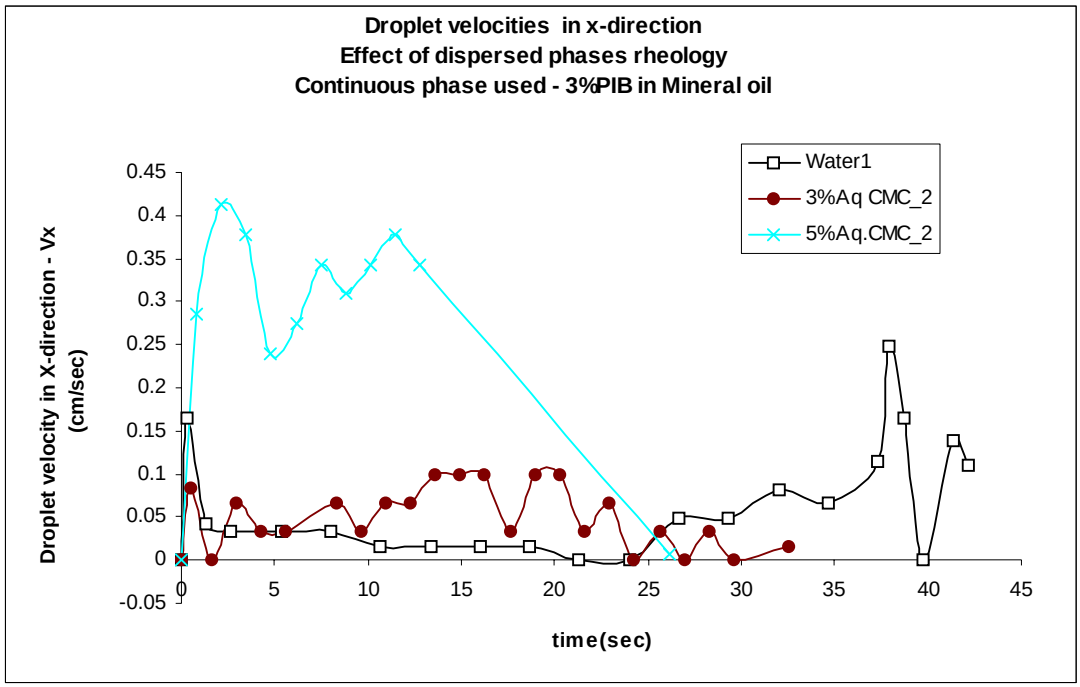

Figure 5.17: Effect of dispersed phase rheology on the y-directional droplet velocities

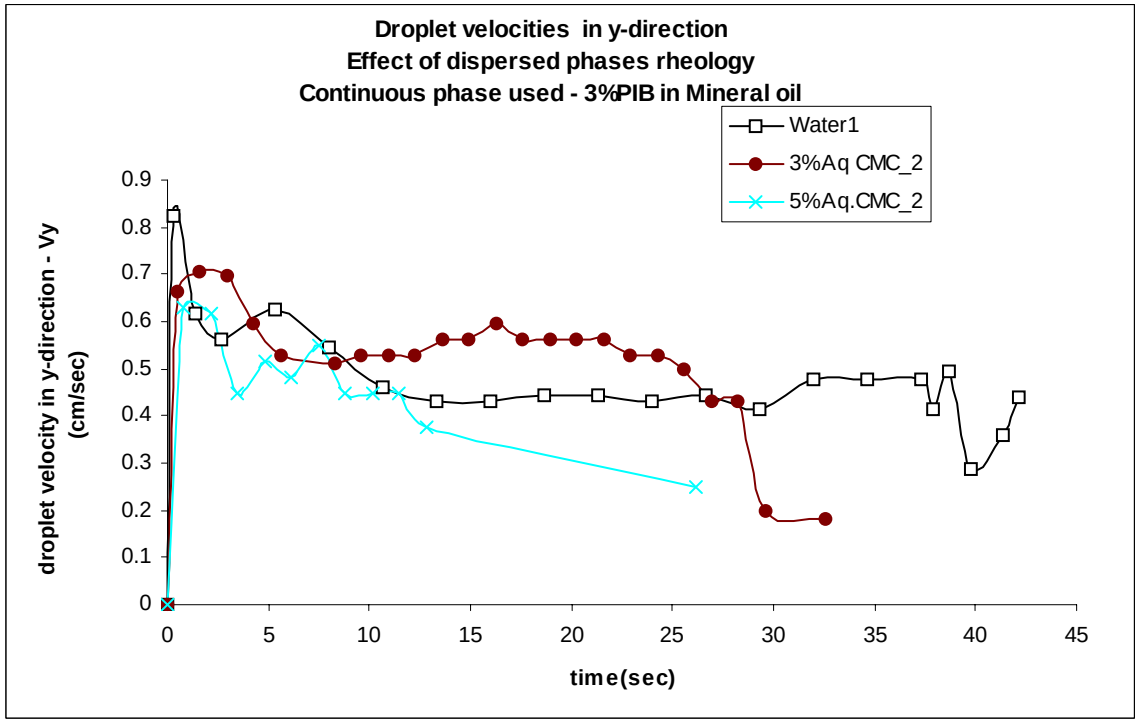

5.4.4. Continuous phase Rheology

As the rheology of the continuous mineral oil phase, changes from Newtonian to non-Newtonian (shear thinning rheology) by the addition of PIB, there is a significant jump in droplet size (~300%). Figure Figure 5.18 and Figure 5.19 show the droplet trajectories for these systems. Further, an increase in the % of PIB (from 1% to 3%) results in additional increase in the droplet size, by ~200%. Addition of the rheology modifier to mineral oil, results in lower interfacial tensions when water is used as the dispersed phase (IFT: MO: 50 mN/m, 1% PIB/MO: 38.7 mN/m, 3% PIB/MO: 23 nN/m).

As the size of the droplet increases, the droplet experiences significantly higher gravitational force ($F_g \alpha D^3$). At the same time, the droplet sees a much higher drag force arising from the higher viscosity of the continuous phase and lower Reynolds number (Re - MO: ~9, 1% PIB / MO: 2.4, 3% PIB / MO: 0.02). As a result, the droplet can sustain higher size at lower IFT.

It is noted that the increase in viscosity, i.e., with 3% PIB in Mineral oil, results in minimal flow in the x-direction and a steady flow in the y-direction, reaching a terminal velocity in the initial few seconds (Figure 5.20 and Figure 5.22). The effect of drop size is quite evident as large droplets move faster along the y-axis. As the viscosity of the continuous phase increases, the residence time of the droplet increases from 5 seconds to 38 seconds at a volumetric flow rate of 71.4 ml/hr. With 1% PIB, irrespective of the applied E and the flow rate, the droplets have a pronounced s-shape motion, with initial trajectory at a high angle to the vertical axis. 3% PIB gives smoother/minimal flow in the x-direction. Also, there is substantial effect of continuous phase rheology on the terminal velocity (Figure 5.21 and Figure 5.23). At higher viscosity of the continuous phase, the

initial vertical velocity is almost equal to the terminal velocity and the velocity in the x-direction is almost zero at volumetric flow rates of 71.4 and 360.4 ml/hr. Further, with 1% PIB and 3% PIB in Mineral oil as continuous phases, the probability of back-mixing occurring would decrease appreciably as the viscosity of the continuous phase.

Figure 5.18: Effect of continuous phase rheology on the droplet trajectory

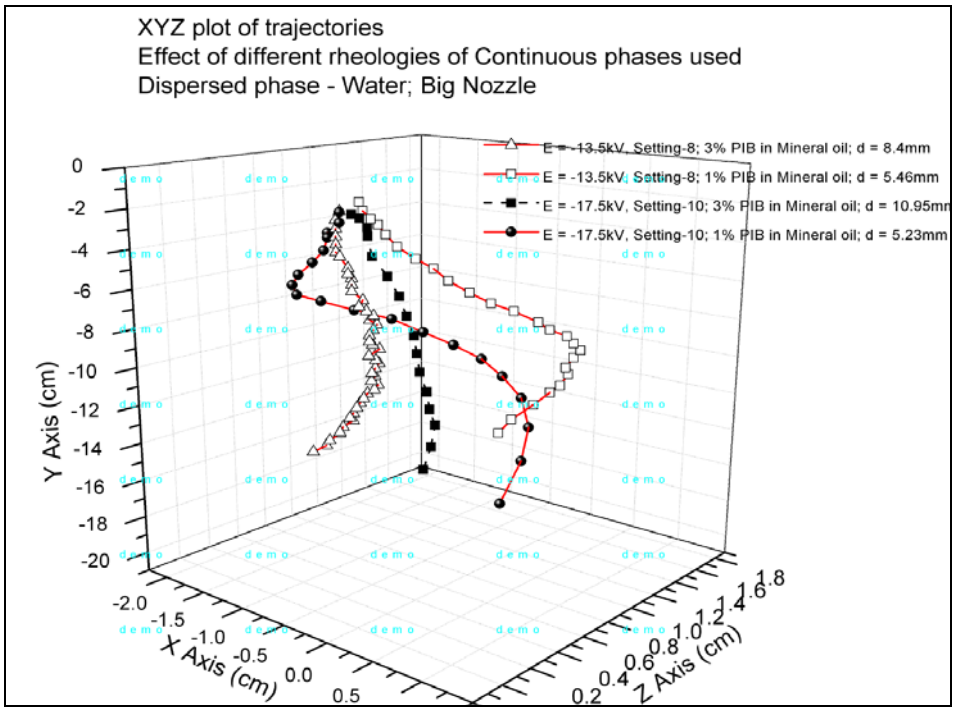

Figure 5.19: Effect of continuous phase rheology on the droplet trajectory as function of time

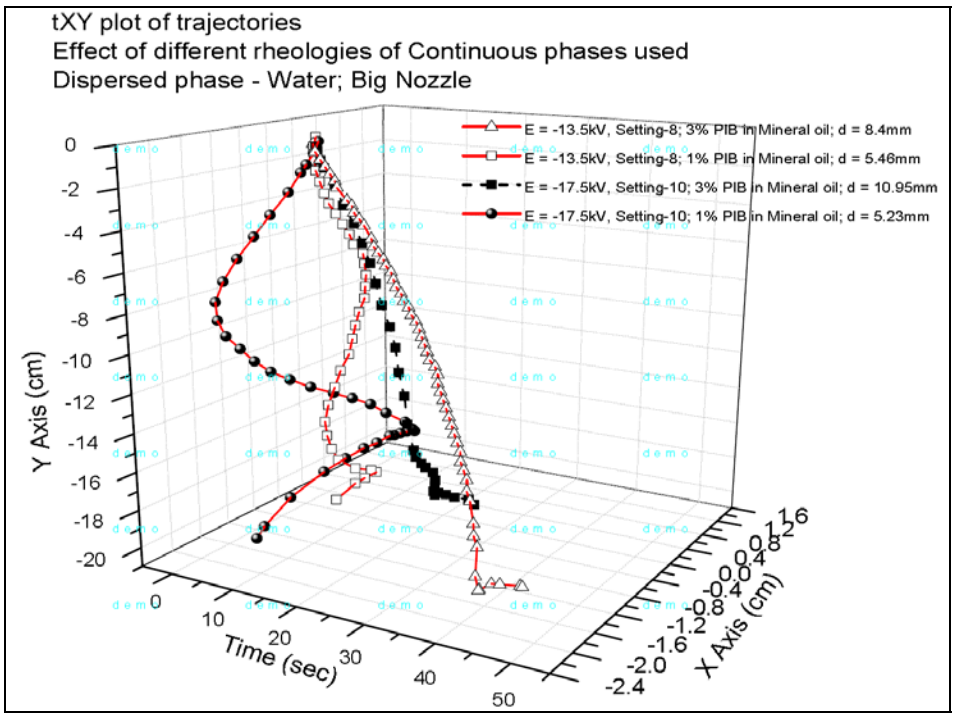

Figure 5.20: Effect of continuous phase rheology on the x-directional velocities

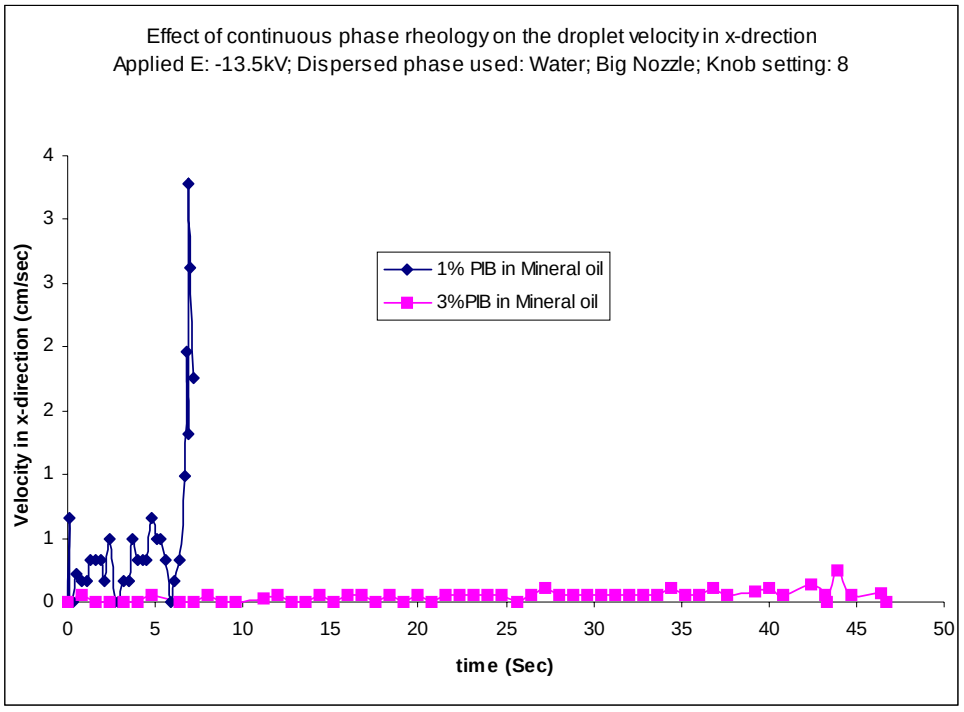

Figure 5.21: Effect of continuous phase rheology on the y-directional velocities

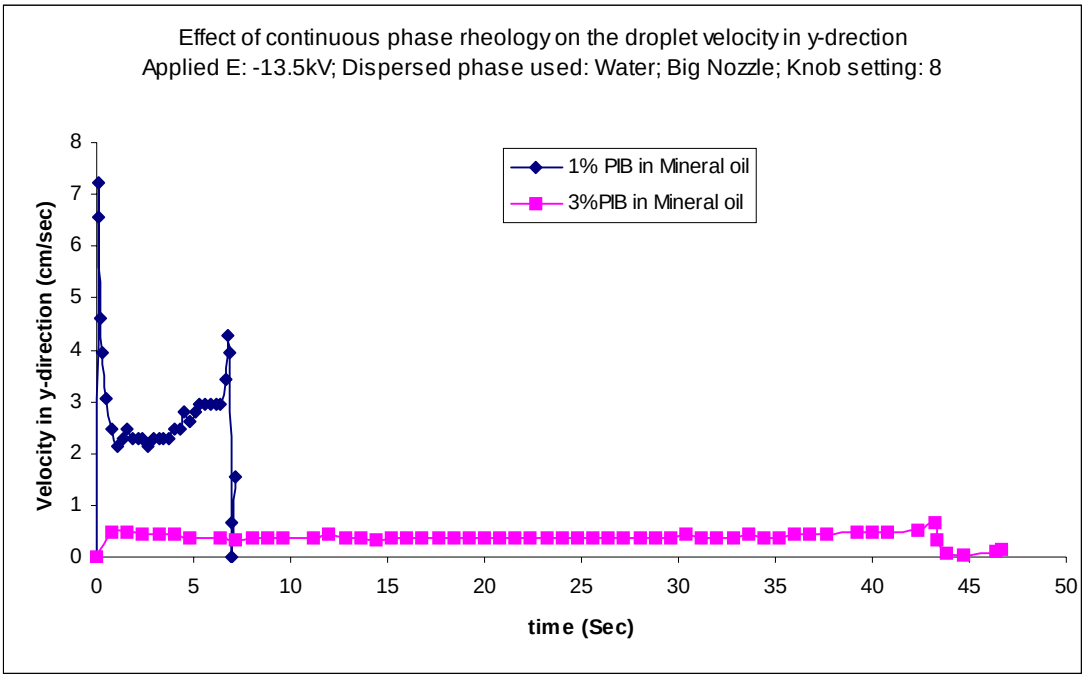

Figure 5.22: Effect of continuous phase rheology on the x-directional velocities

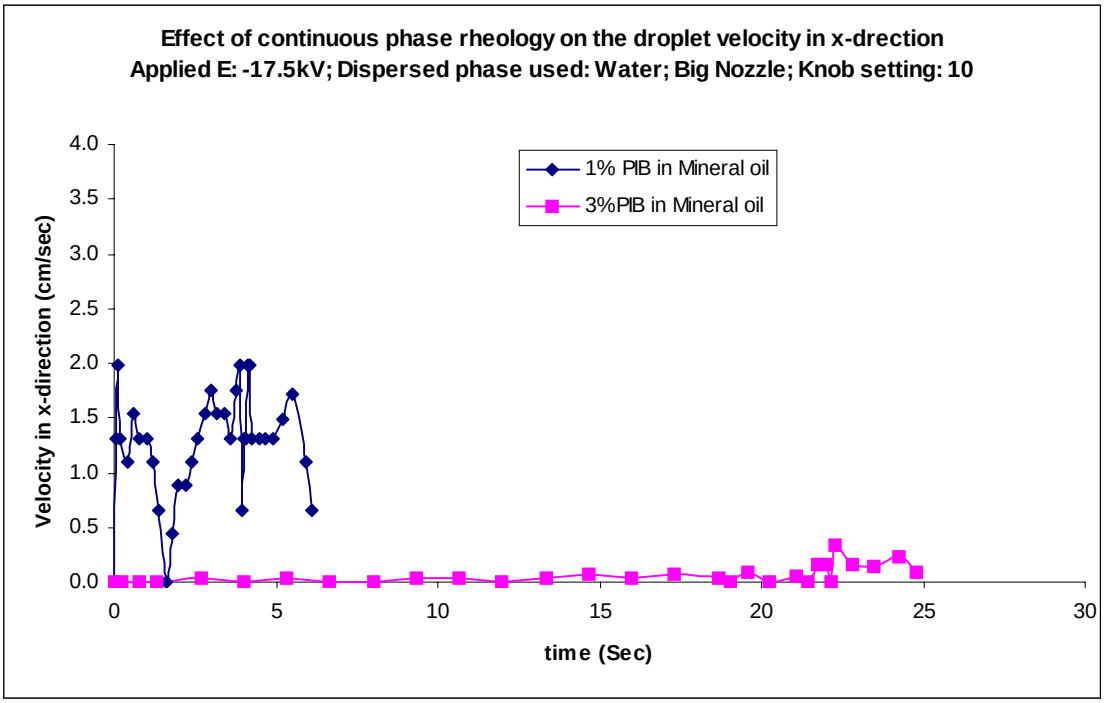

Figure 5.23: Effect of continuous phase rheology on the y-directional velocities

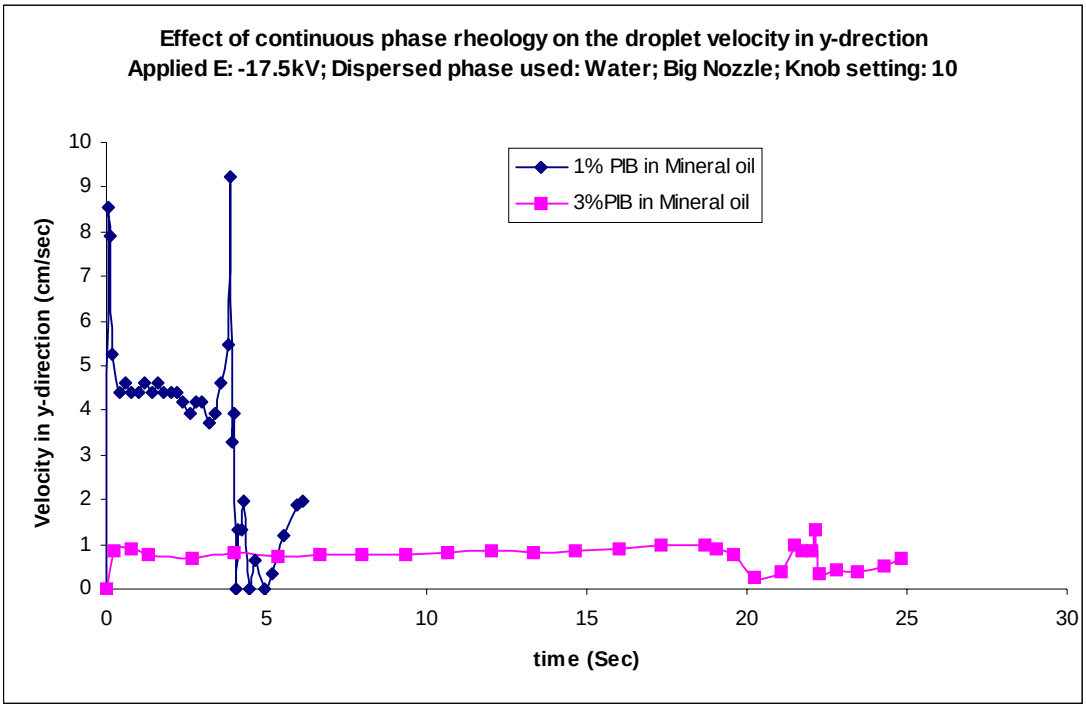

5.4.5. Nozzle dimensions

The effect of nozzle diameter on the droplet formation, specifically on the drop size at detachment, can be understood by observing the change in charge density in contact with forming drop and the local electric field strength near the nozzle tip. As the nozzle diameter decreases, the interfacial force acting on the droplet reduces, i.e. the droplet forms faster. Also, as the diameter of the nozzle reduces, velocity of the droplet through the nozzle increases (V_d α $1/(D_N)^2$). So, this reduces droplet residence time in the nozzle and hence charge acquired during formation though smaller diameter nozzle allows for greater charge accumulation. It was observed that there is no linear correlation between nozzle diameter and droplet size when viscous 3% Aq. CMC is dispersed into 3% PIB in Mineral oil. For the small nozzle diameter, the droplet size at formation is 8.3 mm. This

decreases to 7.6 mm for the medium nozzle. However, when the larger nozzle was used, the drop size increases to 8.4 mm. This contradiction could be attributed to the highly viscous nature of the continuous phase.

As the droplet diameters for small and large sized nozzle are similar, there is a strong possibility that the smaller nozzles are showing the effect alluded to above. From Figure 5.26, it can be observed that as the nozzle diameter is decreased, the x-directional velocity increases which indicates that the droplets do not fall vertically. Further, for the small and medium diameter nozzles, V_x is finite and reaches a terminal velocity whereas for the big nozzle, V_x is closer to zero. Higher charge acquisition is experienced by the drops forming at the smaller nozzles hence the increase in x-directional velocity, though the y-directional velocities do not give the entire picture. One would expect drops having higher electrical charge in the same field (i.e. with smaller nozzles) to behave more erratically and this is observed here.

As the thickness of the smaller nozzle is increased, i.e., the inside diameter is decreased by keeping the nozzle outside diameter constant, the droplet's initial x-directional velocity is much higher than the corresponding velocity of the nozzle with same outside diameter. It was observed that increasing thickness of the nozzle decreases the droplet size. When the thickness was higher, the droplet impacts the wall closer to the top. As a result, velocity in the x-direction increases. Further the initial vertical velocity and terminal velocity are lower for the nozzle with higher thickness.

During all the experimental runs, the nozzle was covered with an insulating tape and only a small area near the tip of the nozzle was left open. The charge accumulation occurs where the nozzle is exposed. The reason why the entire nozzle is insulated except

near the tip is for electrical safety and to ensure no discharge. The length exposed is kept constant with the different nozzles studied and the effect of length of nozzle exposed was studied with big nozzle. Using the big nozzle, the length of exposed area was reduced near the nozzle tip to understand how insulation plays a role in charge accumulation and hence diameter and trajectory. It was observed that decreasing the length of the exposed area does not have an effect on the droplet size, but results in an increase in x-directional velocity and the droplet impacts the wall closer to the top. As a result, velocity in the x-direction increases. This indicates higher charge acquisition. Further the initial vertical velocity and terminal velocity are lower for the nozzle with higher insulation/reduced exposed area.

Figure 5.24: Effect of nozzle diameter on the droplet trajectory

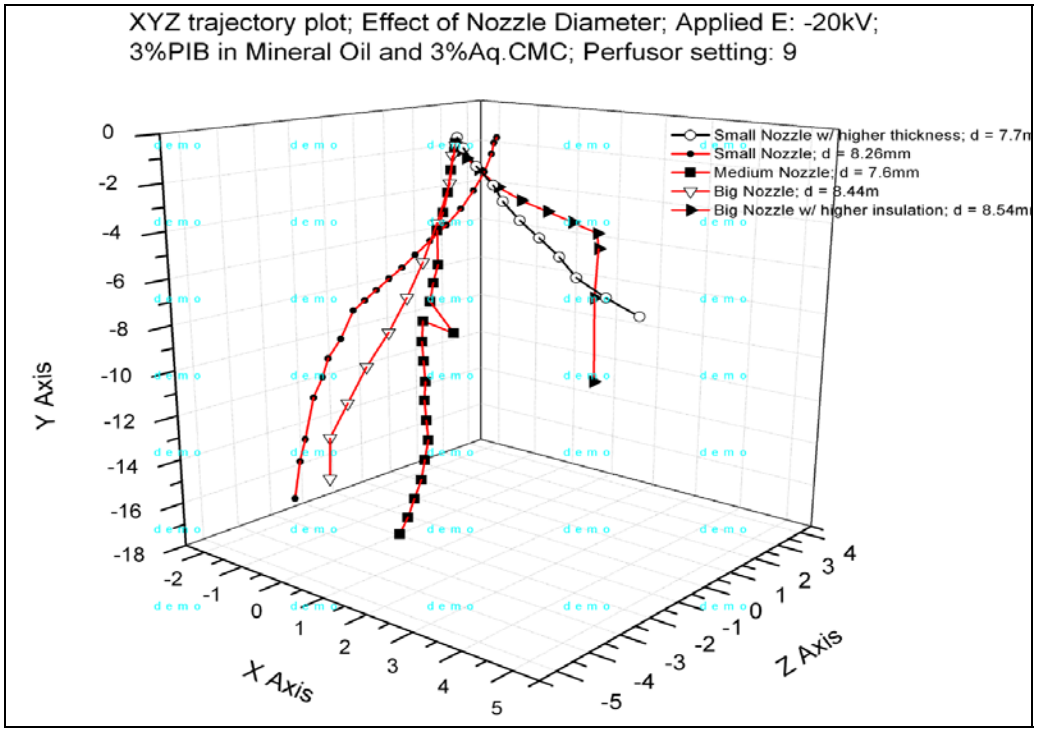

Figure 5.25: Effect of nozzle diameter on the droplet trajectory as function of time

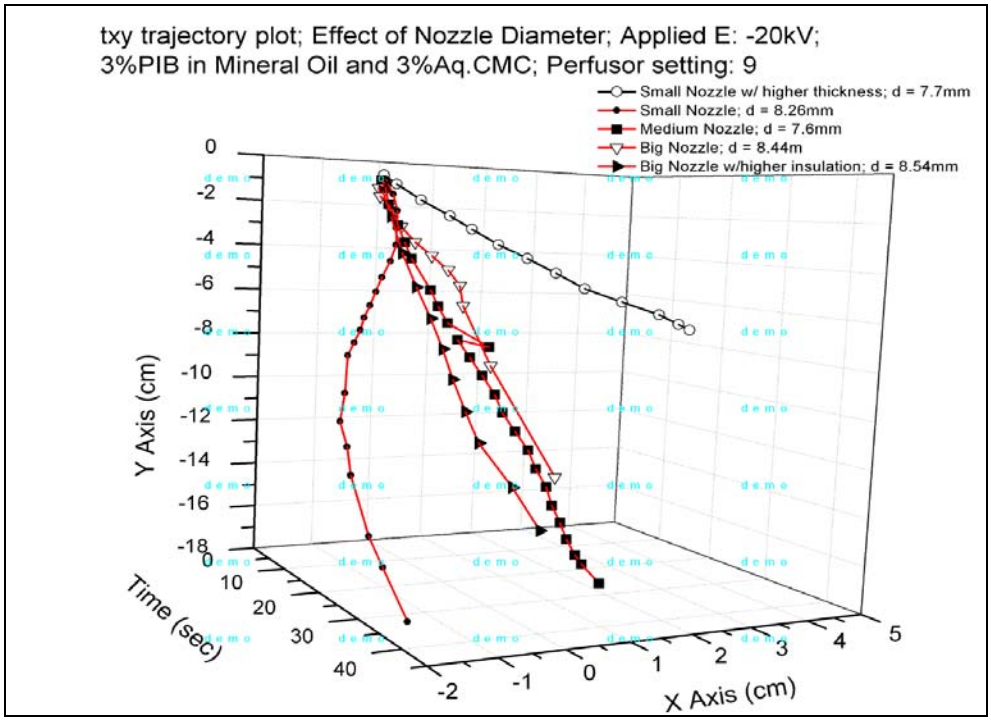

Figure 5.26: Effect of nozzle diameter on the x-directional droplet velocities

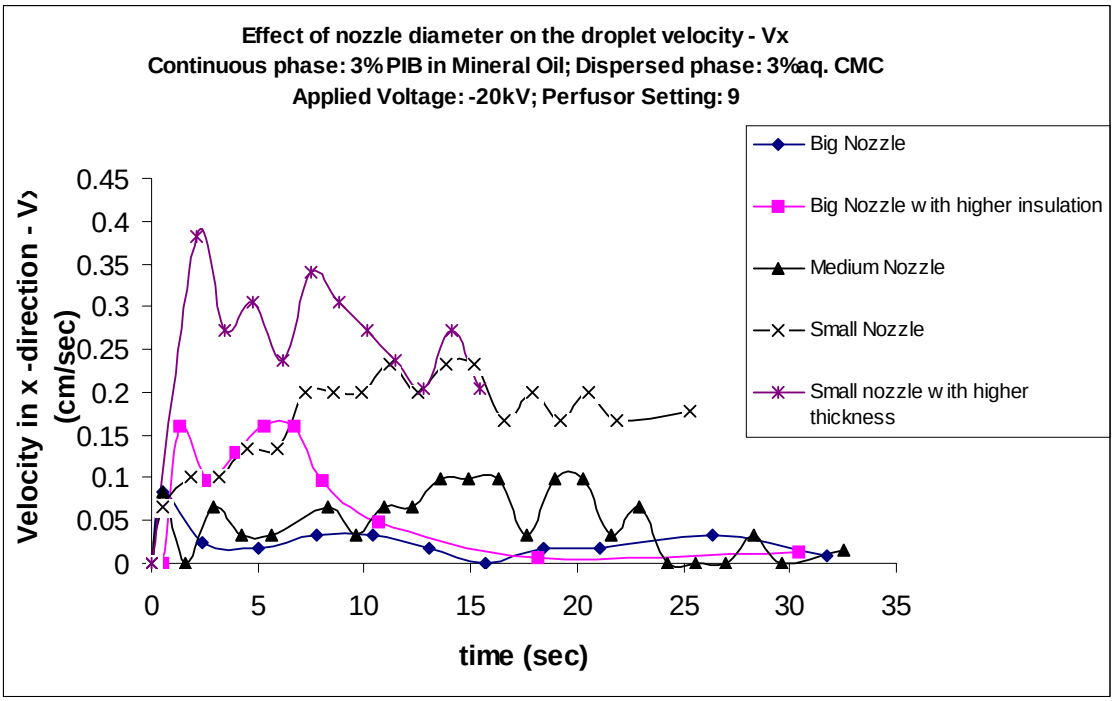

Figure 5.27: Effect of nozzle diameter on the y-directional velocities

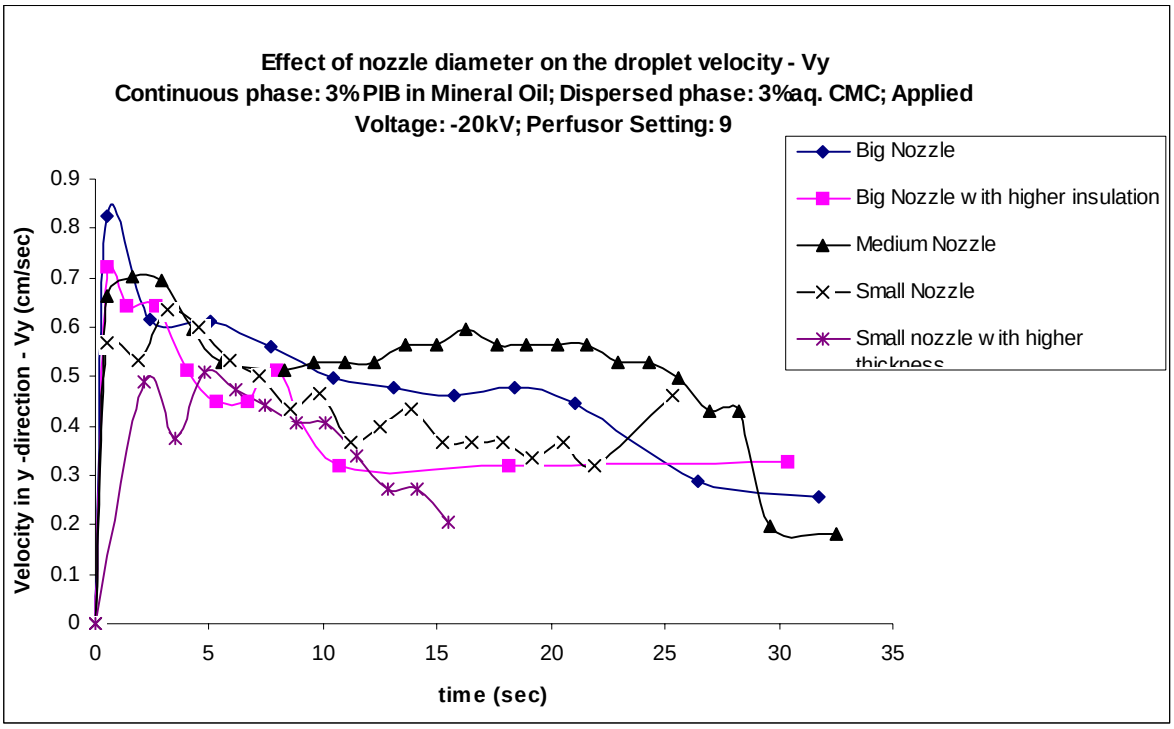

5.4.6. Dispersed phase flowrate

The effect of dispersed phase flow rate on the droplet diameter and subsequently on the droplet trajectory is studied by dispersing water into 3% PIB in mineral oil. The flow rate of the dispersed phase directly affects the droplet formation time as the velocity of the fluid in the nozzle is increased. When there is no applied E, droplet diameter should be lower at higher flow rates. In the presence of electric fields, when dispersed phase flow rate is changed, charge accumulation on the droplet could be affected and hence the droplet diameter. As the dispersed phase flow rate is increased from 71.4 to 360.4 ml/hr, the droplet diameter increases from 8.2 to 10.6 mm. Droplet diameter should have been lower at higher flow rate but because of the lower charge accumulation compared to the flow rate at 8, the droplet diameter was higher. So, with applied E, droplet diameters at

higher flow rate could be higher. Further, since the droplet diameter is higher at volumetric flow rate of 360.2 ml/hr, the residence time would be lower as can be seen from the trajectory plot (Figure 5.28 and 5.29).

Also, due to the lower charge accumulation on the droplet, the initial vertical velocities are lower at higher flow rate. At higher flow rate, the velocity in the x-direction is almost zero compared to that at lower flow rate varying between 0.05-0.2 cm/sec (Figure 5.30). The y-directional velocity at lower flow rate is higher than the velocity at higher flow rate until 20 seconds (Figure 5.31). However after 20 seconds, higher flow rate (resulting in larger drops) would produce higher velocities. The possibility of the smaller drops acquiring a higher charge density can only be answered by quantitative modeling which may partially explain the observed behavior prior to 20s with smaller drops moving faster.

Figure 5.28: Effect of dispersed phase flow rate on droplet trajectory

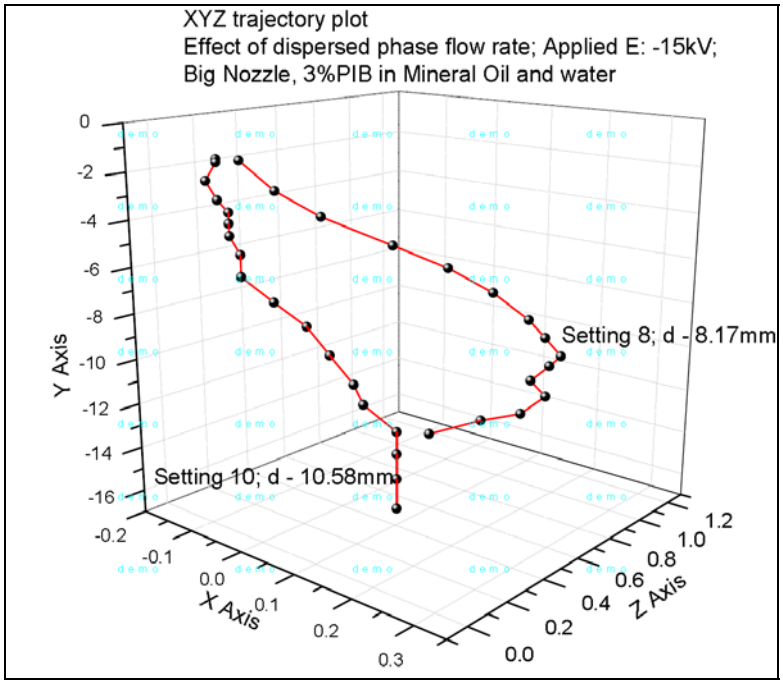

Figure 5.29: Effect of dispersed phase flow rate on the droplet trajectory as function of time

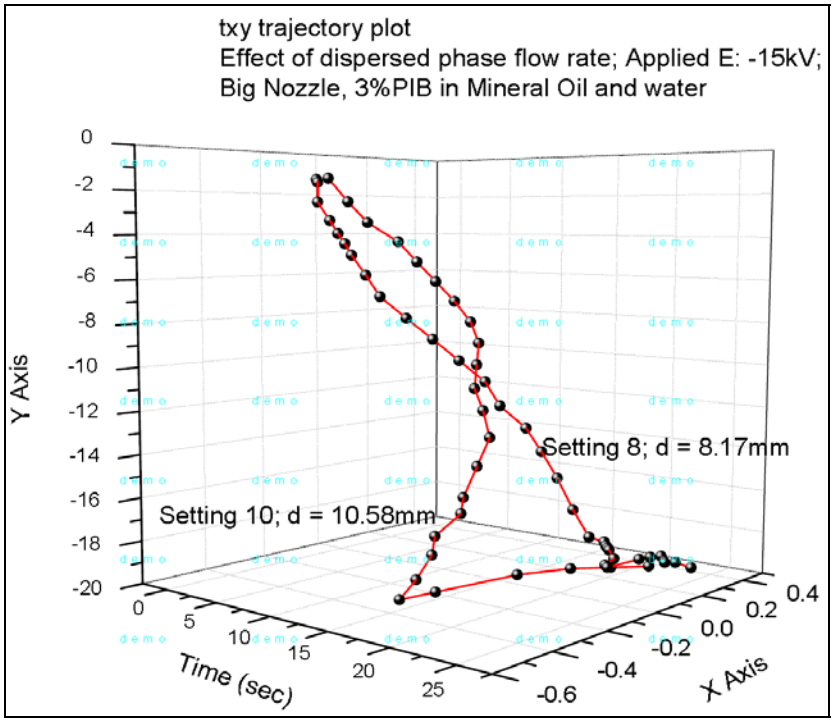

Figure 5.30: Effect of dispersed phase flow rate on the x-directional droplet velocities

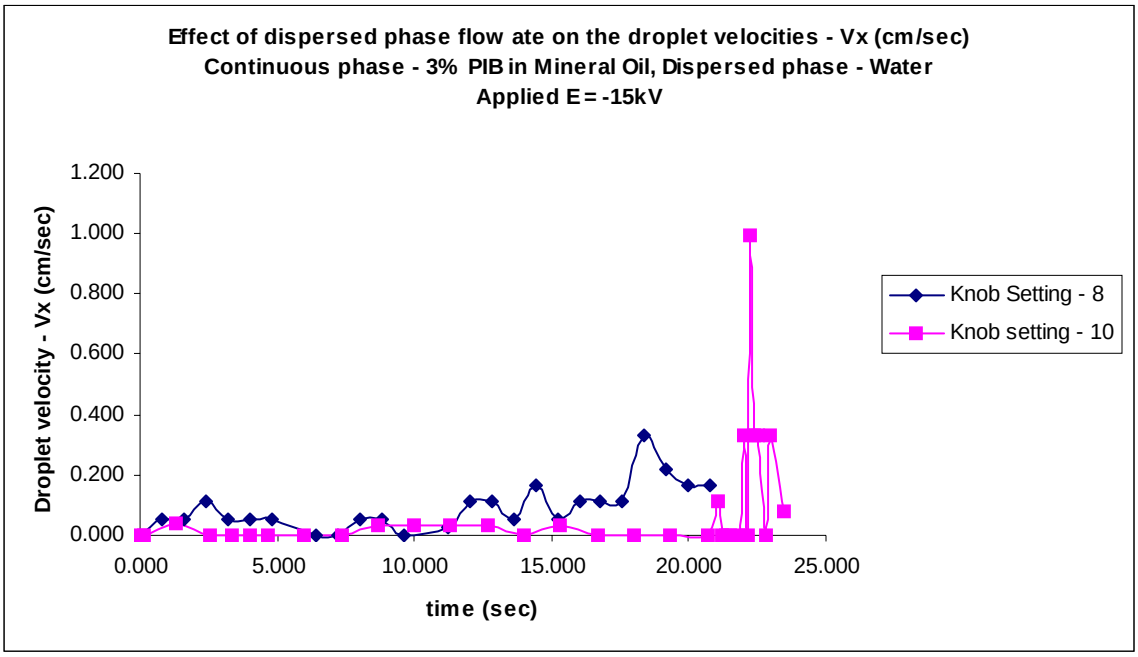

Figure 5.31: Effect of dispersed phase flow rate on the y-directional droplet velocities

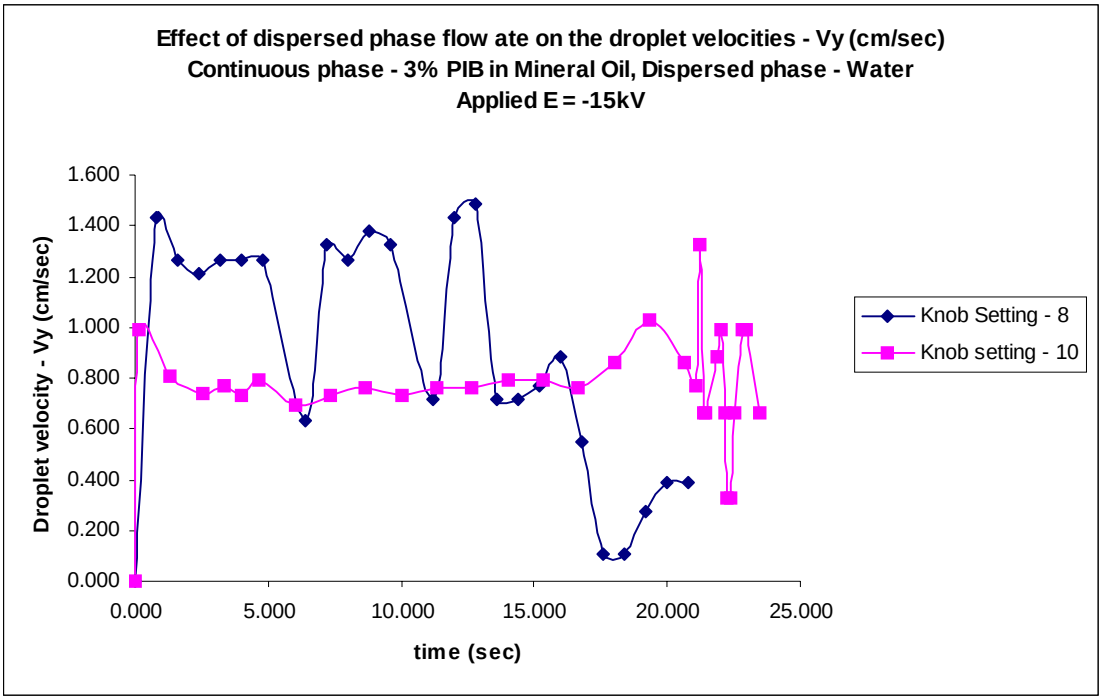

5.4.7. Polarity

In the experiments conducted, polarity of the electric field was switched from positive to negative in between runs. From the Table 5.4, the 3% PIB in MO continuous phase and 3% Aq. CMC disperse phase, when the polarity at 15 kV was switched, the drop size reduced from 9.1 to 8.3 (i.e., 9%). For the 3% PIB in MO continuous phase and 5% Aq. CMC disperse phase, when the polarity at 20 kV was switched, the drop size reduced from 7.8 to 7.7 (i.e., 2%). We observe that increasing the viscosity of the dispersed phase reduces the impact of polarity.

Table 5.4. Impact of change in Polarity

Cont. phase	*3% PIB in MO*	
Disp. phase	*3% Aq. CMC*	
Appl. Volt _nozzle type	*Knob setting*	*Drop size (mm)*
-15kV_BN	9	9.1
+15kV_BN	9	8.3

Cont. phase	*3% PIB in MO*	
Disp. Phase	*5% Aq. CMC*	
Appl. Volt _nozzle type	*Knob setting*	*Drop size (mm)*
-20kV_MN	9	7.8
+20kV_MN	9	7.7

Note: Knob setting of 9 refers to dispersed phase flow rate of 180.2 ml/hr; BN and MN refer to nozzle OD & thickness of 4.18 mm & 0.28 mm and 6.6 mm respectively and same wall thickness of 0.32mm.

Changing polarity has no influence on the charge accumulation at the nozzle. But, switching the polarity changes the direction of the electric field force lines acting on the charged droplet. When the applied voltage is negative, the electric force acts upwards, whereas when applied E voltage positive, the force lines point downwards. Downward electric field counteracts the viscosity more effectively than upward electric field. Hence, it makes sense that the positive applied E results in a smaller droplet than a negative applied E. Increasing the viscosity of the dispersed phase lowers the relative impact of

the electric field. Hence, switching polarity at higher viscosity has a smaller impact on the droplet size reduction.

5.5. Preliminary finite element modeling results

Preliminary modeling was performed with the experimental droplet trajectory data obtained with 3% Aq. CMC dispersed in pure Mineral oil at an applied voltage of -17.5 kV. This preliminary work was an extension to finite element modeling developed by Petera *et al.,*[31,35] for electrically enhanced contacting of Newtonian liquid-liquid systems.[15,28] The detailed model description was based on the force balances followed by the finite element model (See section 1.4.4).[31,35,36] A simulated droplet trajectory obtained from the finite element modeling is shown in the Figure 5.32.[37] The experimental trajectory shows a droplet that bounces off the bottom electrode, rises and then settles down. Simulated droplet trajectory predicts the shape of droplet motion and collision with the bottom electrode correctly. Further, in the x-direction (in x-z plot), the predicted droplet motion is lower than experimental; while in the y-direction (in y-z plot) the motion is very similar. Due to the unstable nature of the droplet trajectories discussed in the previous section, the prediction of droplet trajectory can be made robust if averaged droplet motion of different droplets instead of 1-2 droplets is used. This is an arduous task from image analysis standpoint due to amount of work involved though advanced knowledge of macro programming could be used to automate the task.

Figure 5.33 shows the electric potential contours along the length of the contactor along with overlay of the predicted and experimental droplet trajectory.[37] The electric potential increases from the nozzle to the bottom electrode. As discussed briefly, the electric field is non-linear near the electrodes due to presence of impurities which is

incorporated into the modeling as shown in the figure. Also, near the middle section of the contactor, the electric potential is constant and the contour is flat.

Figure 5.32: Finite element modeling of the droplet trajectory for the system of 3% Aq. CMC dispersed into Pure Mineral oil at an applied voltage of -17.5 kV (Green line – experimental; Orange line – simulated; z-axis represents vertical direction)

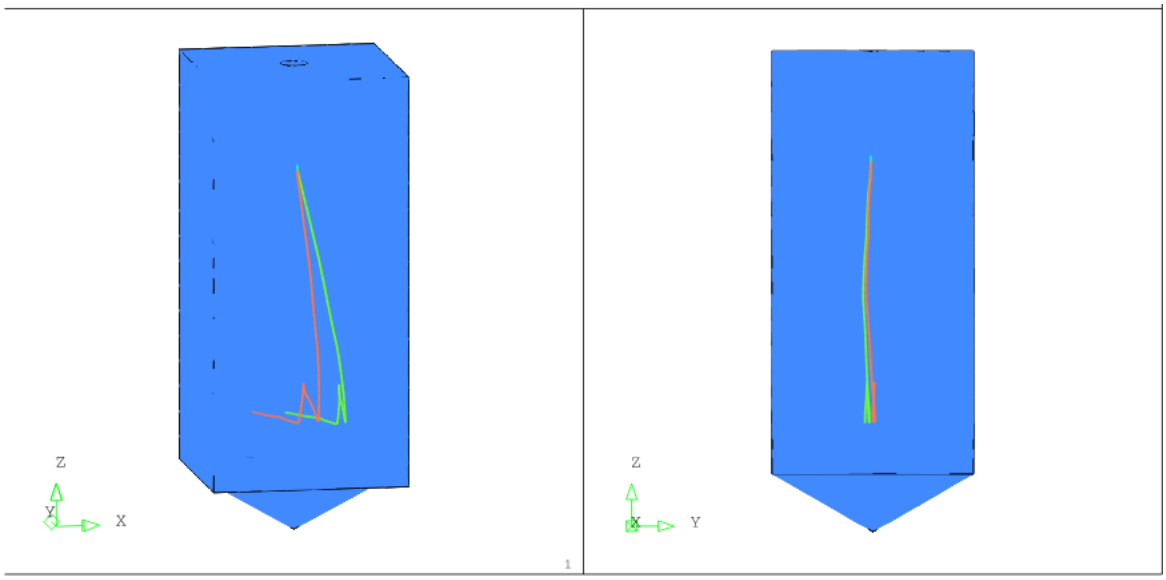

Figure 5.33: Electric potential contours along the length of contactor for the predicted droplet trajectories

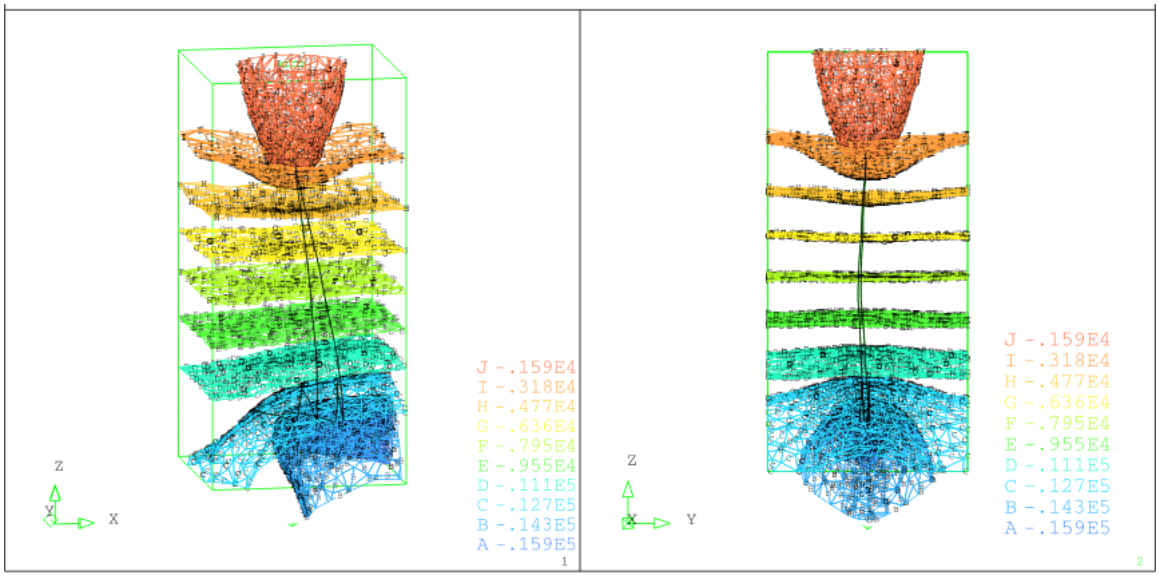

5.5.1. Electric field loss

As mentioned above, the non-linearity of electric fields at the top and bottom electrodes is incorporated into the modeling. But apart from these, loss of potential near the walls of the contactor is possible though the contactor is enclosed in glass which is a highly insulating material. This aspect was investigated experimentally by measuring losses through the front wall of the column using non-contact PCS-715 Static Locator. The losses were measured for a period of 2 hours at an interval of 30 minutes. At an applied voltage of -7.5 kV, the average field loss across the length of the front wall was almost unchanged, though it appeared the loss at the charged bottom electrode were marginally higher. The average field loss was -300 V (-0.3 kV). At higher applied voltages the losses increased. The losses decreased by moving from the charged bottom electrode to earthed electrode (nozzle). At an applied voltage of -10 kV, the average field loss was -375 V (-0.375 kV). These losses are minor in comparison with the actual applied voltage but they can change flatness of the contours.

5.6. Empirical correlations

5.6.1. Reynolds Number

Reynolds numbers for droplets were calculated by taking average of Reynolds number calculated at times through the droplet trajectory. From the Table 5.5, it can be seen that as the viscosity of the continuous phase increases, the Reynolds number falls drastically. Depending upon the Reynolds number of the droplet, they can be classified into solid spheres and droplets. Since $N_{Re} < 10$, the flow can be characterized as creeping flow based on Stokes law.[38,39] In this study, the formula for calculating the droplet Reynolds number is

$$N_{\mathrm{Re}} = \frac{D_d \; v_T \; \rho_c}{\mu_c}$$

ρ_c – Density of the continuous phase

μ_c – Viscosity of the continuous phase

D_d – Droplet diameter

v_T – Terminal velocity of the droplet

Table 5.5: Reynolds number for different systems

Continuous phase/ dispersed phased used	Applied Voltage and Nozzle used and knob setting	Droplet diameter (mm)	Reynolds number ($N_{Re,y}$)
Mineral Oil (MO) and Water	-10kV_MN_10	6.4	12.64
MO and Water	-24kV_MN_10	3.6	8.43
1% PIB in MO and Water	-13.5kV_BN_8	5.5	1.42
3% PIB in MO and Water	-13.5kV_BN_8	8.4	0.0147
1% PIB in MO and Water	-17.5kV_BN_10	5.2	2.3
3% PIB in MO and Water	-17.5kV_BN_10	11.0	0.038
3% PIB in MO and Water	-20kV_MN_9	8.3	0.0188
3% PIB in MO and Water	-20kV_MN_10	8.3	0.0188
3% PIB in MO and 3% Aq. CMC	-20kV_MN_9	7.6	0.022
3% PIB in MO and 5% Aq. CMC	-20kV_MN_9	7.8	0.0195

Note: Knob settings of 8, 9, and 10 refers to dispersed phase volumetric flow rates of 71.4, 180.2 and 360.4 (ml/hr) respectively; BN and MN refer to nozzle OD & thickness of 4.18 mm & 0.28 mm and 6.6 mm respectively and same wall thickness of 0.32mm

5.6.2. Dimensionless analysis

To understand the effect of the electric field and to predict the droplet diameter would involve solving complex equations. For the present systems, a finite element method was employed as discussed above. From the initial analysis it was observed that the finite element model was unable to model the system due to the unstable behavior exhibited by the droplets. However, prediction of the droplet diameter is important to better

understand the effect of various parameters. Here, the droplet diameter was related to the different physical parameters of the various systems studied to obtain an empirical correlation containing dimensionless number. As discussed in chapter 1.4, in the literature, droplet diameters have been either obtained from developing empirical correlations[27,40,41] or from semi-empirical force balances equations.[29]

In the present study, various parameters are identified that could affect the droplet diameter.[40] These parameters are those of the continuous phase, of the nozzle and of the two phase mixture. The droplet characteristics as it is formed from the nozzle are used. Mainly, the droplet velocity is calculated based on the flow rate of the dispersed phase and the nozzle dimensions. The dimensionless numbers used in the analysis are Reynolds number, electric Bond number and Taylor's number. The variations in dimensionless numbers with critical voltage were examined.

The physical parameters identified are tabulated along with the corresponding droplet diameters measured. The droplet diameter can be written as a function of various physical parameters as shown below:

$$\mathrm{D_d} = f(l,\ D_N,\ V_f,\ \rho_c,\ \mu_c,\ \varepsilon_c,\ V,\ \sigma)$$

Using dimensional analysis, the above function can be written as

$$D_d = \left\{(l)^a (D_N)^b (V_f)^d\right\}\left\{(\rho_c)^c (\mu_c)^e (\varepsilon_c)^f\right\}\left\{(V)^g (\sigma)^h\right\} \quad ----- \ Eqn\ (1)$$

Each of the physical parameters with their dimensions are given below:

Outside diameter of the nozzle (D_N) $= L$

Interelectrode distance (L) $= L$

Velocity of the droplet as it forms at the nozzle (V_f) $= \frac{L}{T}$

Density of the continuous phase (ρ_c) $= \frac{M}{L^3}$

Density of the continuous phase (μ_c) $= \frac{M}{LT}$

Interfacial tension between a dispersed and a continuous phase (σ) $= \frac{M}{T^2}$

Applied Voltage to the column (V) $= \frac{M L^2}{A T^3}$

Permittivity of the continuous phase (ε_c) $= \frac{T^4 A^2}{M L^3}$

where L, M, T, A are the fundamental entities for Length, Mass, Time and Amperes

$$L^1 = \left\{(L)^a (L)^b (LT^{-1})^d\right\}\left\{(ML^{-3})^c (ML^{-1}T^{-1})^e (T^4 A^2 M^{-1} L^{-2})^f\right\} \left\{(ML^2 A^{-1} T^{-3} V)^g (MT^{-2})^h\right\}$$

This can be reduced to

$$L^1 M^0 T^0 A^0 = L^{(a+b-3c+d-e-3f+2g)} M^{(c+e-f+g+h)} T^{(-d-e+4f-3g-2h)} A^{(2f-g)}$$

Exponents of L, M, T and A on the sides are equated and the resulting equations look like

L : $1 = a + b - 3c + d - e - 3f + 2g$ ---------- $Eqn\,(2)$

A : $0 = 2f - g$ ---------- $Eqn\,(3)$

M : $0 = c + e - f + g + h$ ---------- $Eqn\,(4)$

T : $0 = -d - e + 4f - 3g - 2h$ ---------- $Eqn\,(5)$

From $Eqn\,(2)$, $g = 2h$,

Substituti ng for g in $Eqn\,(4)$ and (5) and solving for c and d :

$c = -e - f - h$ ---------- $Eqn\,(6)$

$d = -e - 2f - 2h$ ---------- $Eqn\,(7)$

Substituti ng for c, d and g in $Eqn\,(2)$ and solving for b :

$b = 1 - a - 2e - 2f - h$ ---------- $Eqn\,(8)$

Substituti ng *b, c, d* and *g* in *Eqn* (1),

$$D_d = (l)^a (D_N)^{(1-a-2e-2f-h)} (\rho_c)^{-e-f-h} (V_f)^{-e-2f-2h} (\mu_c)^e (\varepsilon_c)^f (V)^{2f} (\sigma)^h \quad ----Eqn\,(10)$$

Rearrangin g *Eqn* (10),

$$\frac{D_d}{D_N} = \left(\frac{l}{D_N}\right)^a \left(\frac{\mu_c}{V_f D_N \rho_c}\right)^e \left(\frac{\varepsilon_c V^2}{V_f^2 D_N^2 \rho_c}\right)^f \left(\frac{\sigma}{V_f^2 D_N \rho_c}\right)^h \quad ----Eqn\,(11)$$

$$\frac{D_d}{D_N} = \left(\frac{l}{D_N}\right)^a \left(\frac{1}{\mathrm{Re}}\right)^e \left(\frac{Ta}{\mathrm{Re}}\right)^f \left(\frac{Ta}{\mathrm{Re}\,.\,Bo}\right)^h \quad ----Eqn\,(12)$$

$$\frac{D_d}{D_N} = \left(\frac{l}{D_N}\right)^a (\mathrm{Re})^b (Ta)^c (Bo)^d \quad ----Eqn\,(13)$$

Dimensionless numbers used in the study are the Taylor's number, Bonds number and Reynolds number as described here:

$$\mathrm{Re} = \frac{\text{Inertial forces}}{\text{Viscous force}} = \frac{D_N V_f \rho_c}{\mu_c}$$

$$Ta = \frac{\text{Electrostatic force}}{\text{Viscous force}} = \frac{\varepsilon_c V^2}{\mu_c V_f D_N}$$

$$Bo = \frac{\text{Electrostatic force}}{\text{Interfacial force}} = \frac{\varepsilon_c V^2}{\sigma D_N}$$

The various physical parameters are calculated at the average temperature of 27°C. All the data is populated in a table and the dimensionless numbers are calculated. The predicted dimensionless diameter is calculated from the correlation by initially guessing the values of the exponents (a, b, c, d) in Eqn(13). The effectiveness of the correlation to predict the droplet diameter is known by calculating the coefficient of determination (R^2) between the predicted and experimental data. Further, the error between experimental and predicted dimensionless diameters is calculated. A good correlation would have R^2 value > 0.9 and low %error values.

An in-built excel solver is used to obtain the exponents while maximizing the value of R^2. From here, the values of exponents are adjusted to obtain lower %errors and correspondingly higher R^2 value. In the present study, using the reduced the form of the correlation developed in Eqn(13), an R^2 value of 0.94 and corresponding average % error of 8.9% were obtained. Final exponent values obtained are a = 0.468; b = 0.014, c = -0.065, d = -0.18 as shown in Eqn 14.

$$\frac{D_d}{D_N} = \left(\frac{l}{D_N}\right)^{0.468} (\mathrm{Re})^{0.014} (Ta)^{0.065} (Bo)^{-0.18} \qquad ----Eqn\ (14)$$

R^2 value of 0.94 indicates a good correlation for prediction of droplet diameter as it is formed at the nozzle. Predicted and experimental droplet diameters along with the trendline are shown in the Figure 5.34.

Figure 5.34: Empirical correlations for droplet diameter

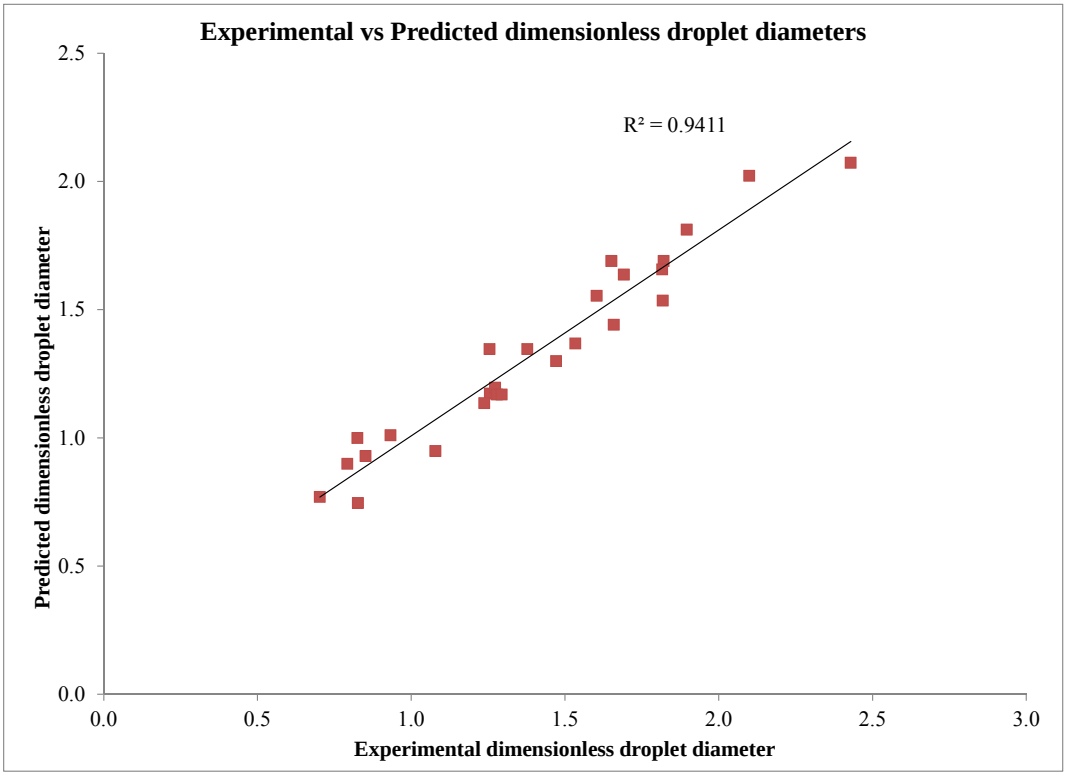

5.7. Conclusions

The ability of increased drop viscosity and non-Newtonian rheology to inhibit drop motion in electrically charged liquid-liquid systems was studied. There is potential for enhancing liquid-liquid contacting by imposing an electrical charge on a viscous dispersed phase that exhibits non-Newtonian behavior. The ability to create smaller droplets of viscous liquids is evident and mass transfer can be increased. The enhanced acceleration of charged drops following dispersion is not necessarily observed and the motion is influenced by a combination of factors including rheological properties, changes in oscillation behavior, electrical relaxation, and non-linearities in the local electrical field through which the drops are moving. Further experimentation is required to quantify the effect of a range of electrical field strengths upon drop motion in non-Newtonian system, including an examination of the effect of the properties of the continuous phase and a detailed comparison with uncharged drops of different sizes and rheological properties. In more complex systems like systems of swarming droplets, there is inter-dependency of local mixing in the continuous phase on the droplet trajectory and droplet size, which is not well understood. Little work has been done on the backmixing occurring in these systems. The experience from the above work can be used to predict the relationship between continuous phase residence time distributions, liquid properties, drop size and trajectory, velocity and electrical field for systems of swarming drops.

5.8. References

(1) Weatherley, L. R. Electrically Enhanced Mass Transfer. *Heat Recovery Systems & CHP* **1993**, *13*, 515.
(2) Weatherley, L. R. Relationship between Drop-size and Field Strength in Enhanced Whole-broth Liquid Liquid Extraction. *Speculations in Science and Technology* **1991**, *15*, 91.
(3) Laughland, G. J.; Miller, M. K.; Weatherley, L. R. In *Extraction '87 IChem E Symposium Series No 103* 1987, p 263.
(4) Qiu, Z.; Zhao, L.; Weatherley, L. R. Process intensification technologies in continuous biodiesel production. *Chemical Engineering and Processing: Process Intensification* **2010**, *49*, 323.
(5) Eow, J. S.; Ghadiri, M.; Sharif, A. O. Electrostatic and hydrodyamic separation of aqueous drops in a flowing viscous oil. *Chemical Engineering and Processing* **2002**, *41*, 649.
(6) Eow, J. S.; Ghadiri, M. Motion, deformation and break-up of aqueous drops in oils under high electric fields. *Chemical Engineering and Processing* **2003**, *42*, 259.
(7) Bailes, P. J.; Larkai, S. K. L. Liquid Phase Separation in Pulsed D.C. Fields. *Trans IChemE* **1982**, *60*, 115.
(8) Bailes, P. J. Solvent Extraction in an Electrostatic Field. *Ind. Eng. Chem. Process Des. Dev.* **1981**, *20*, 564.
(9) Ristenpart, W. D.; Bird, J. C.; Belmonte, A.; Dollar, F.; Stone, H. A. Non-coalescence of oppositely charged drops. *Nature* **2009**, *461*.
(10) Debus, D.; Reuss, N. Rheological properties of fermentation fluids. *The Chemical Engineer* **1982**, *381*.
(11) Weatherley, L. R.
(12) Weatherley, L. R.; Etuk, B.; Murray, K. R. Formation of nylon 610 capsules by interfacial polymerization in a high-voltage electric field. *Powder Technology* **1991**, *65*, 227.
(13) Berkland, C.; Packa, D. W.; Kimb, K. Controlling surface nano-structure using flow-limited field-injection electrostatic spraying (FFESS) of poly(d,l-lactide-co-glycolide). *Biomaterials* **2004**, *25*, 5649.
(14) Petera, J.; Weatherley, L. R. Modeling of mass transfer from falling droplets. . *Chemical Engineering Science* **2001**, *56*.
(15) Hume, A. P.; Weatherley, L. R.; Petera, J. Trajectories of charged drops in a liquid-liquid system. *Chemical Engineering Journal* **2003**, *95*.
(16) Takamatsu, T.; Hashimoto, Y.; Yamaguchi, M.; KAtayamna, T. Theoretical and experimental studies of charge drop formation in a uniform electric field. *Journal of Chemical Engineering of Japan* **1981**, *14*, 172.
(17) Ghadiri, M.; Eow, J. S. The behaviour of liquid-liquid interface and drop-interface coalescence under the influence of an electric field. *Colloids and Surfaces A: Physicochem. Eng. Aspects* **2003**, *215*, 101.
(18) He, W.; Baird, M. H. I.; S.;, C. J. The effect of electric field on droplet formation and motion in a viscous liquid. *The Canadian Journal of Chemical Engineering* **1991**, *69*.

(19) Derdouri, A.; Ait-kadi, A.; Carreau, P. J. Rheological properties of Polymer-added lubricating oils. *Canadian Journal of Chemical Engineering* **1988**, *66*, 709.
(20) Scott, T. C. Use of Electric Fields in Sovlent Extraction: A Review and Prospectus. *Seperation and Purification Methods* **1989**, *18*, 65.
(21) Thornton, J. D. Electrically Enhanced Liquid-Liquid Extraction. *Birmingham University Chemical Engineer Journal* **1976**, *27*, 6.
(22) *Oppanol B Types*, 2005.
(23) Stewart, G.; Thornton, J. D. In *IChemE Symposium series* 1967; Vol. 26, p 29.
(24) Stewart, G.; Thornton, J. D. In *IChemE Symposium series* 1967; Vol. 26, p 37.
(25) Takamatsu, T.; Yamaguchi, M.; Katayama, T. Formation of single charged drops in liquid media under a uniform electric field. *Journal of Chemical Engineering of Japan* **1982**, *15*, 349.
(26) Seader, J. D.; Henley, E. J.; Roper, D. K. *Separation Process Principles: Chemical and Biochemical Operations*; 3rd ed.; John Wiley & Sons, Inc., 2011.
(27) Vu, N.; Carleson, T. E. Electric Field Effects on Drop Size and Terminal Velocity in Liquid-Liquid Systems. *AIChE* **1986**, *32*, 1739.
(28) Hume, A. P.; Petera, J.; Weatherley, L. R. Trajectories of Charged Drops in a Liquid-Liquid System: The Effect of Geometrical Scale-Up. *American Chemical Society* **2004**.
(29) Scheele, G. F.; Mesiter, B. J. Drop formation at low velocities in Liquid-Liquid Systems: Part 1: Prediction of drop volume. *AIChE* **1968**, *14*, 9.
(30) Mochizuki, T.; Mori, Y.; Kaji, N. Drop Interactions in Electrostatic Liquid-Liquid Contactors. *AIChE* **1992**, *38*, 311.
(31) Petera, J.; Rooney, D.; Weatherley, L. R. Particle and droplet trajectories in a non-linear electrical field. *Chemical Engineering Science* **1998**, *53*.
(32) Scheele, G. F.; Mesiter, B. J. Drop formation at low velocities in Liquid-Liquid systems: Part 2. Prediction of Jetting velocity. *AIChE* **1968**, *14*, 15.
(33) Webster, D. R.; Longmire, E. K. Jet pinch-off and drop formation in immiscible liquid-liquid systems. *Experiments in Fluids* **2001**, *30*, 47.
(34) Richards, J. R.; Lenhoff, A. M.; Beris, A. N. Dynamic breakup of liquid-liquid jets. *Physics of Fluids* **1994**, *6*, 2640
(35) Petera, J.; Strzelecki, W.; Agrawal, D.; Weatherley, L. R. Charged Droplet and Particle-mixing Studies in Liquid-liquid systems in the presence of Non-linear Eletrical Fields. *Chemical Engineering Science* **2005**, *60*, 135.
(36) Petera, J.; Weatherley, L. R.; Hume, A. P.; Gawrysiak, T. A finite element algorithm for particle/droplet trajectory tracking, tested in a liquid–liquid system in the presence of an external electric field. *Computers & Chemical Engineering* **2007**, *31*, 1369.
(37) Petera, J.
(38) Clift, R.; Grace, J. R.; Weber, M. E. *Bubbles, Drops and Particles*; Academic Press. INC., 1978.
(39) Grace, J. R.; Wairegi, T. In *Transport Processes in Bubbles, Drops, and Particles*; 1st ed.; Chhabra, R. P., Kee, D. D., Eds.; Taylor & Francis: 1991, p 133.

(40) Scott, T. C. Dimensional analysis of continuous high-capacity electrodispersion of aqueous based liquids in an organic continuous phase. *Separation Science and Technology* **1990**, *25*, 1709.
(41) Weatherley, L. R.; Turmel, C. Terminal Velocity Studies of Whole Broth Single Drops in a Liquid-Liquid System. *Ind. Eng. Chem. Res.* **1992**, *31*, 1739.

6. CONCLUSIONS AND FUTURE WORK

6.1. Conclusions

Application of ionic liquids to the whole cell biocatalysis/*in situ* extraction may have great potential for the production of a large variety of chemical products. In order to realize this opportunity, for systems, simultaneous optimization of the biocompatibility/microbial toxicology and phase equilibrium thermodynamics (product partitioning) is required. The focus of this work was to evaluate the suitability of ionic liquids for whole-cell fermentation both from biological and thermodynamics perspective. Further, another important aspect that arises in a biphasic system is the liquid-liquid contacting of Ionic liquid-aqueous broth; this aspect was studied through the application of electric fields.

The biological perspective was developed by measuring the toxicity of ionic liquids to the micro-organisms used as the biocatalyst in the fermentation for achieving the required synthesis. This approach has been demonstrated through the example of the biotransformation of naphthalene to (1*R*,2*S*)-cis-1,2-dihydro-1,2-naphthalenediol (NDHD) by a mutant strain of *E. coli* in the presence of ionic liquids. Toxicity of the ionic liquids for a particular strain of *Escherichia coli* was investigated by measuring the molecular toxicity through EC_{50}. Aliphatic ammonium and phosphonium cations with [Tf_2N] and [FAP] anions were found to be biocompatible with the cells, while their corresponding halides were very toxic. Imidazolium cations were biocompatible only in the [FAP] anion. Incorporation of polar functional groups in the cation of the quaternary ammonium cation resulted in the hydrophobic ammonium ionic liquid being more toxic to the cells. Pyrrolidinium ionic liquids with [Tf_2N] inhibited the cells. As is widely known, the toxicity increased with increasing alkyl chain length. As demonstrated

here, several trends in toxicology do exist, but a large number of exceptions temper this structure-property understanding.

Thermodynamics perspective was developed by measuring the partitioning ability of the ionic liquid of the model solute and also its selectivity for aqueous phase. Hydrophobic ionic liquids were tested as potential solvents for the *in situ* extraction of NDHD, acetone, 1-butanol and ethanol solutes by measuring the partition coefficients from pure aqueous phase. The model ionic liquid, [HMIm][Tf_2N], demonstrated the highest affinity for NDHD among the ionic liquids, while phosphonium and ammonium ionic liquids with bulkier alkyl side chains like [$P_{6,6,6,14}$][Tf_2N] and [TOMAm][Tf_2N] had lowest extractability for NDHD. Incorporating polar functional groups like carbonyl and cyano in the non-polar side chains of the cation increased the partition coefficients (2.3-2.5). Replacing the anion with [FAP] further reduces the partition coefficient irrespective of the cation used.

For the extraction of ABE solutes from aqueous phase, the suitability of model ionic liquid [HMIm][Tf_2N] as an extractant was studied by developing ternary diagrams for entire concentration range; lower concentrations, commonly observed with ABE fermentation, were studied in greater detail. Model ionic liquid was found to be suitable extractant for acetone and 1-butanol (concentration based partition coefficients greater than 1) and not suitable for ethanol (concentration based partition coefficients were much less than 1, around 0.2). High selectivity (concentration based) for 1-butanol/acetone relative to water, > 85, were obtained which suggests easier phase separation. This favorable partition data for the extraction of 1-butanol using [HMIm][Tf_2N] was used to scale-up the process in process simulator. Binary interaction parameters were regressed from the experimental data. An optimized flowsheet for the separation of 1-butanol from water using the model ionic liquid was developed. From this, the

effects of ionic liquid on the energy and cost analysis were evaluated. This aided in understanding how the energy requirements and cost analysis compare to standard processes like conventional distillation process and extraction using organic solvents. The ionic liquid based extraction requires 57% energy than conventional distillation while organic solvent based extraction requires higher energy than both of these combined. The distillation equipment cost for ionic liquid based did not change considerably when compared with traditional distillation equipment costs; these equipment costs were significantly lower than the distillation cost used in organic solvent extraction process.

Ionic liquids are viscous, with the viscosity of the ionic liquids used in this study, ranging from tens to hundreds centipoise. Extraction of solutes from viscous fermentation broth using viscous ionic liquid is an important aspect. Intensification of contacting viscous fluids, which is an integral part of liquid-liquid contacting, was studied by the application of DC electric fields. The ability of increased drop viscosity and non-Newtonian rheology to inhibit drop motion in electrically charged liquid-liquid systems was studied. There is potential for enhancing liquid-liquid contacting by imposing an electrical charge on a viscous dispersed phase that exhibits non-Newtonian behavior. The ability to create smaller droplets of viscous liquids is evident. The enhanced acceleration of charged drops following dispersion is not necessarily observed and the motion is influenced by a combination of factors including rheological properties, changes in oscillation behavior, electrical relaxation, and non-linearities in the local electrical field through which the drops are moving. The experience from the above work can be used to predict the relationship between continuous phase residence time distributions, liquid properties, drop size and trajectory, velocity and electrical field for systems of swarming drops.

6.2. Recommendations for Future work

- Progress is needed in two different fields of research: (i) physical/solution chemistry of ionic liquids and (ii) microbiology/toxicology of ionic liquids. Solution chemistry of ionic liquids would require knowledge of aspects such as the dissociation of different ionic liquids in aqueous and non-aqueous systems – correlations with dielectric constant might be a good starting point.
- Biocompatibility of ionic liquids to other micro-organisms mainly, *Clostridia*, would greatly speed-up research in this field. Process of identifying new ionic liquids for a given fermentation process can be streamlined in two ways: high-throughput screening of ionic liquids for their biocompatibility to different micro-organisms by identifying dyes that help in differentiating between viable and non-viable cells; rapid synthesis of small quantities of new ionic liquids.
- New quantum mechanical tools, such as the COSMO-RS, COSMO-SAS, etc. may play significant future roles in understanding and screening these ionic liquid systems for extraction.
- Finding a cost-effective approach for synthesis of ionic liquids would enable large-scale use as current ionic liquid synthesis is uneconomical. Here, organic solvents gain a lot of raw material cost advantage over ionic liquids. A life cycle analysis of the process for producing ionic liquids from raw materials would enable better understanding of the overall environmental impact – Non-availability of relevant information in literature could be a key hurdle.
- Another aspect to be analyzed as a part of cost-effective study is the recovery of ionic liquid lost to the aqueous phase after contacting. Ionic liquids are known for their low water

solubilities, *e.g.*, the model ionic liquid solubility in water is around 2.1 mg/ml. At a large scale, this translates to kilos of unrecovered ionic liquid. Because of the ionic nature of these ionic liquids, Adsorption could be a technique to separate ionic liquids efficiently from the aqueous stream; further study in this area could lead to development of a better recovery process. Another study could look at the effect of some primary cell broth constituents on the adsorption.

- While the current study on 1-butanol is the focus of ABE fermentation, future work to study the profitability of extraction of acetone and ethanol can be conducted.
- The performance of optimized or un-optimized ionic liquids in an actual fermentation in terms of improving product yields and phase separation is necessary for suitability studies. Experimental work on studying the effect of some primary cell broth constituents on the partitioning is important.
- The ability to obtain solute, with maximum purity, from the IL-solute mixture post extraction needs to be analyzed; as ionic liquids are non-volatile, evaporation of solutes is a possibility. Spraying IL-solute mixture into air in presence of applied electric fields can result in sizeable reduction in drop size and increase interfacial area due to high electrical conductivity of ionic liquids. This could result in faster evaporation of volatile solutes from the mixture. This process can be optimized by controlling the temperature in the spraying unit.
- The effect of electric fields on the intensification of extraction from fermentation broth can be understood by studying the mass transfer rate between non-Newtonian phases. In more complex systems such as swarms of droplets, inter-dependency between local mixing in the continuous phase and the droplet trajectory / size is not well understood; further, back-mixing in these systems has received little attention.

APPENDIX A - MATLAB program to regress binary interaction parameters for ternary system

A MATLAB program to regress binary interactions for ternary system

```
%--------------------------------------------------------------------------
 Program to obtain binary interaction parameters for LLE ternary system
%--------------------------------------------------------------------------
clear all
clc
format long G
disp('NRTL Binary interaction parameters - Regression modeling for IL/Butanol/Water')
disp(blanks(2)')
% Global variables declaration
% global ND_start ND_end NDmarker
global T alpha NC ND BCOUNTER
global alp_exp_x beta_exp_x
global feed_exp_z n_feed
global alp_calc_x beta_calc_x

NC = 3; % number of components
T  = 295.15; % in Kelvin
ND_ini = input('enter data points - total (4(1-4) or 6(1-6)) or data pt. row ([1 3..] in a maxtrix \n');
BCOUNTER =0;
%ND = 8;

% 1-IL  2-Butanol  3-Water
%**************************************
alpha = [ 0     0.3     0.2
        0.3   0       0.2
        0.2   0.2     0   ];

B12    =  1;
B21    =  1;
B13    =   83.67;
B31    =   2616.49;
B23    =   -321.78;
B32    =   1530.1;

BIP_bds =   [-3000         3000
          -3000          3000
          -3000          3000
          -3000          3000
          -3000          3000
          -3000          3000];

LB = BIP_bds(:,1);
UB = BIP_bds(:,2);

%Experimental molefractions
```

```
%ALPHA phase          IL          Butanol        Water
alp_exp_x_ini =     [ 8.89982E-05   0.000226134   0.999684867
                      8.3417E-05    0.000593413   0.99932317
                      8.27894E-05   0.00081628    0.99910093
                      8.42893E-05   0.001228492   0.998687219
                      8.42324E-05   0.001616794   0.998298973
                      8.03833E-05   0.000675157   0.999244459
                      8.0559E-05    0.00202317    0.997896271
                      8.05099E-05   0.003575494   0.996343996];

%BETA phase           IL          Butanol        Water
beta_exp_x_ini =    [ 0.789083721   0.004306477   0.206609802
                      0.779352655   0.011459943   0.209187402
                      0.773432136   0.01585319    0.210714674
                      0.765877004   0.023048913   0.211074083
                      0.756287707   0.029966737   0.213745556
                      0.770407927   0.014442835   0.215149238
                      0.738020765   0.037421682   0.224557553
                      0.704814243   0.062528663   0.232657094];

% Feed moles (F)
n_feed_ini     =     [0.117046421
                      0.116999299
                      0.117210541
                      0.117663437
                      0.117221239
                      0.119508564
                      0.120870235
                      0.120304335];

% FEED Phase calculated as mid-point of ALPHA and BETA phases

for i = 1:8
   for j = 1:3
      feed_exp_z_ini(i,j) =  (alp_exp_x_ini(i,j) + beta_exp_x_ini(i,j))*0.5;
   end
end

%Allows to choose experimental points-----------------------------------
if length(ND_ini) == 1
   ND = ND_ini;
   for i = 1 : ND
      ND_ini(i)      = i;
      alp_exp_x(i,:)  = alp_exp_x_ini(i,:);
      beta_exp_x(i,:) = beta_exp_x_ini(i,:);
      feed_exp_z(i,:) = feed_exp_z_ini(i,:);
      n_feed(i,:)     = n_feed_ini(i,:);
   end
else
   ND = length(ND_ini);
   for i = 1 : ND
```

```
        alp_exp_x(i,:)  = alp_exp_x_ini(ND_ini(i),:);
        beta_exp_x(i,:) = beta_exp_x_ini(ND_ini(i),:);
        feed_exp_z(i,:) = feed_exp_z_ini(ND_ini(i),:);
        n_feed(i,:)     = n_feed_ini(ND_ini(i),:);
    end
end

BIPcounter = 0;
for B12 = 1: 20: 201
    for B21 = 1:20:201
        BIPcounter = BIPcounter + 1;

BIP_ini = [ B12
            B21
            B13
            B31
            B23
            B32 ];

% %--------------------FMINSEARCH ALGORITHM-----------------------------------------
% display('the binary interaction parameters are obtained using FMINSEARCHBND algorithm');
options = optimset('MaxFunEvals',600000, 'MaxIter', 600000, 'TolFun', 0.000000000001,
'DiffMinChange', 0.000005);
[B, FVAL,exitflag,output] = fminsearchbnd(@(B) O_F_X_Jul29_5pm(B), BIP_ini, LB, UB, options);
% ---------------------------------------------------------------

RMSD_temp = 0;
for i = 1:ND
    for j = 1:NC
        RMSD_temp = RMSD_temp + abs(alp_exp_x(i,j) - alp_calc_x(i,j)) + abs(beta_exp_x(i,j) -
beta_calc_x(i,j));
    end
end
RMSD = (abs(RMSD_temp)/(2*ND*NC));

Error_K_temp = 0;
Error_S_temp = 0;

j = 2;
for i = 1: ND
   K_exp(i)     = beta_exp_x(i,j)/alp_exp_x(i,j);
   K_calc(i)    = beta_calc_x(i,j)/alp_calc_x(i,j);
   Error_K_temp = Error_K_temp + abs(1 - (K_calc(i)/K_exp(i)));
end

Error_perc_K = (Error_K_temp/ND)*100;

j = 3;
for i = 1: ND
   K_exp_aq(i)   = beta_exp_x(i,j)/alp_exp_x(i,j);
   K_calc_aq(i)  = beta_calc_x(i,j)/alp_calc_x(i,j);
```

```
end

for i = 1:ND
  S_exp(i) = K_exp(i)/K_exp_aq(i);
  S_calc(i) = K_calc(i)/K_calc_aq(i);
  Error_S_temp = Error_S_temp + abs(1 - S_calc(i)/S_exp(i));
end

K_calc
S_calc
K_exp
S_exp
pause
Error_perc_S = (Error_S_temp/ND)*100;

for i = 1: ND
  temp_alp_calc_x (1,:) = alp_calc_x(i,:);
  temp_beta_calc_x (1,:) = beta_calc_x(i,:);
  gam_alp(i,:) = gam_nrtl_Jul21(temp_alp_calc_x,B);
  gam_beta(i,:) = gam_nrtl_Jul21(temp_beta_calc_x,B);
end

fugacitysum_sq = 0;
for j = 1:NC
   for i = 1:ND
   fugacitydiff(i,j) = alp_calc_x(i,j)*gam_alp(i,j) - beta_calc_x(i,j)*gam_beta(i,j);
   fugacitysum_sq = fugacitysum_sq + fugacitydiff(i,j)^2;
   end
end
fugacitysum = sqrt(fugacitysum_sq);

%AARD calculations
for i = 1:ND
   for j = 1:NC
      alp_AARD(i,j)  = abs(alp_exp_x(i,j)  - alp_calc_x(i,j))/alp_exp_x(i,j);
      beta_AARD(i,j) = abs(beta_exp_x(i,j) - beta_calc_x(i,j))/beta_exp_x(i,j);
   end
end

for j = 1:NC
   Error_alp_AARD(j) = 0;
   Error_beta_AARD(j) = 0;
   for i = 1:ND
      Error_alp_AARD(j)  = Error_alp_AARD(j)  + alp_AARD(i,j);
      Error_beta_AARD(j) = Error_beta_AARD(j) + beta_AARD(i,j);
   end
end

disp([BIP_ini])
disp([B])
disp([fugacitysum RMSD Error_perc_K Error_perc_S]')
```

```
disp([Error_alp_AARD*100/ND]')
disp([Error_beta_AARD*100/ND]')

BIPstore(:, BIPcounter)= [BIP_ini
                    B];
RMSDstore(BIPcounter) = RMSD;
fugacitysumstore(BIPcounter) = fugacitysum;
Error_alp_AARDstore(:, BIPcounter) = [Error_alp_AARD*100/ND]';
Error_beta_AARDstore(:, BIPcounter) = [Error_beta_AARD*100/ND]';

ErrorK_S_store(:, BIPcounter) = [Error_perc_K
                        Error_perc_S];
   end
end


-------------------------------------------------

function O_F_X = O_F_X_Jul29_5pm(B_temp)

global NC ND  BCOUNTER
global alp_exp_x beta_exp_x
global alp_calc_x beta_calc_x theta_arr

B_temp
% B_temp =       [-116.72
%          1629
%       -1469.3
%        3083.8
%        196.18
%          2043];

%------------ Initial guesses ------------------------
theta_ini = 0.1;    % theta = L2/F i.e., Moles(IL Phase)/Moles(Feed)
K_ini = [11000, 20, 0.14];
%  K_ini = [1000, 100, 1];
%-----------------------------------------

O_F_X = 0;
BCOUNTER = BCOUNTER + 1;

% for i = 1:ND
%     theta_temp(i) = theta_ini;
%     K_temp(i,:)= K_ini;
% end
for i = 1:ND
   ND_marker = i;
   theta = Flashsolver_Jul28_7pm(theta_ini, B_temp, K_ini, ND_marker);
%     theta_temp(i) = theta;
%     K_temp(i,:) = K;
```

```
%     if theta >9999
%         RMSD = theta
%         break
%     end

    for j = 1 : NC
        O_F_X = O_F_X + abs(alp_exp_x(i,j) - alp_calc_x(i,j)) + abs(beta_exp_x(i,j) - beta_calc_x(i,j));
    end
end

RMSD  = (O_F_X/(2*ND*NC));

BCOUNTER
RMSD
% if RMSD > 1000
%     disp('high RMSD')
%     pause
% end


----------------------

function [F, K] = Flashsolver_Jul28_7pm(theta, B_temp, K, ND_marker)

global NC COUNTER
global alp_calc_x beta_calc_x feed_exp_z

alp_est_temp = zeros(1,NC);
beta_est_temp = zeros(1,NC);
alp_est_tempN = zeros(1,NC);
beta_est_tempN = zeros(1,NC);
F = 0;

for COUNTER = 1:10000

    for j = 1 : NC
        alp_est_temp(1,j)  = feed_exp_z(ND_marker,j) / (1 + theta * (K(1,j) - 1));
        beta_est_temp(1,j) = K(1,j) * feed_exp_z(ND_marker,j) / (1 + theta * (K(1,j) - 1));
    end

%NORMALIZATION OF MOLE FRACTIONS

    for j = 1 : NC
        alp_est_tempN(1,j)  = alp_est_temp(1,j)/ (alp_est_temp(1,1) + alp_est_temp(1,2) +
alp_est_temp(1,3));
        beta_est_tempN(1,j) = beta_est_temp(1,j)/ (beta_est_temp(1,1) + beta_est_temp(1,2) +
beta_est_temp(1,3));
    end

    %------------GAMMA calculation-----------------------
    %------------   ALPHA Phase ------------
```

```
   gam_alp    = gam_nrtl_Jul21(alp_est_tempN,B_temp);

   %------------   BETA Phase ------------
   gam_beta   = gam_nrtl_Jul21(beta_est_tempN,B_temp);
   %-----------------------------------------------------

%K calculation from Gammas
   for j = 1 : NC
      Kprev(1,j) = K(1,j);
      K(1,j) = gam_alp(1,j)/gam_beta(1,j);
   end

%Rachford-Rice formulation
   F_theta = 0;
   Fdash_theta = 0;
   Fdash_thetam = 0;
   Kerror = 0;
   Fugerror = 0;

   for j = 1 : NC
      F_theta = F_theta + feed_exp_z(ND_marker,j)*(K(1,j) - 1) / (1 + theta * (K(1,j) - 1));
      Fdash_theta = Fdash_theta - feed_exp_z(ND_marker,j)*(K(1,j) - 1)^2 / (1 + theta * (K(1,j) - 1))^2;
      Kerror = Kerror + (Kprev(1,j)-K(1,j))^2;
      Fugerror = Fugerror + (alp_est_tempN(1,j)*gam_alp(1,j) - beta_est_tempN(1,j)*gam_beta(1,j))^2;
   end
   Kerror = sqrt(Kerror);
   Fugerror = sqrt(Fugerror);
   F_theta;

% exit if F_theta is small
   if abs(F_theta) <0.000000001
%        F_theta
%        ND_marker
%        COUNTER
%       disp('exit if F_theta is small')
      break
   end

   thetam = theta - 0.6*F_theta/Fdash_theta;

   for j = 1 : NC
      Fdash_thetam = Fdash_thetam - feed_exp_z(ND_marker,j)*(K(1,j) - 1)^2 / (1 + thetam * (K(1,j) -
1))^2;
   end

   theta = theta - F_theta/Fdash_thetam;
%    theta
%    F_theta
%
end
```

```
F = theta;
% COUNTER
% Display error message if convergence not achieved in 10,000 iterations
if abs(F_theta) >= 0.000000001
   display  ('Flashsolver convergence not achieved in 10,000 iterations')
   theta
   F_theta
   Fugerror
   F=1000
%    pause
end


alp_calc_x(ND_marker,:)    = alp_est_tempN(1,:);
beta_calc_x(ND_marker,:)    = beta_est_tempN(1,:);

Fugerror;
%-------------completed calculation of alpha and beta using flashsolver

if(Fugerror > 0.0000001)
   %--------Revise alp_x_calc using Fugacity matching with FMINSEARCH--------
   % display('Fugacity matching using FMINSEARCHBND algorithm');
   options = optimset('MaxFunEvals',600000, 'MaxIter', 600000, 'TolFun', 0.000000000001,
'DiffMinChange', 0.000005);


   INI                  =  [alp_est_tempN(1,1)
                            alp_est_tempN(1,2)];
   LB                   =  [alp_est_tempN(1,1)*0.8
                            alp_est_tempN(1,2)*0.7];
   UB                   =  [alp_est_tempN(1,1)*1.2
                            alp_est_tempN(1,2)*1.4];

   [alp_calc_tempv_x, FVAL]    =   fminsearchbnd(@(alp_calc_tempv_x)
O_Fug_X_Jul28_7pm(alp_calc_tempv_x, beta_est_tempN, B_temp), INI, LB, UB, options);

   alp_calc_x(ND_marker,1)    =   alp_calc_tempv_x(1,1);
   alp_calc_x(ND_marker,2)    =   alp_calc_tempv_x(2,1);
   alp_calc_x(ND_marker,3)    =   1 - alp_calc_x(ND_marker,1) - alp_calc_x(ND_marker,2);

   beta_calc_x(ND_marker,:)    = beta_est_tempN(1,:);

   %fugacity matching error for NDmarker'th datapoint
   % ND_marker
   % FVAL
end

% ---------------------------------------------------------------------

function gam_est = gam_nrtl_Jul21(x_est,B_temp)
```

```
global NC alpha T
%*************************************************************************
% Rearranging the 1x6 BIP input into 3x3 matrix for calculation of Gamma
%*************************************************************************
%Initializing the new 3x3 matrix (B) to zeros
B = zeros(NC, NC);

B(1,2) = B_temp(1);
B(2,1) = B_temp(2);
B(1,3) = B_temp(3);
B(3,1) = B_temp(4);
B(2,3) = B_temp(5);
B(3,2) = B_temp(6);

%*****************************************
% Initialization and calculation of G and Tau
%*****************************************
G   = zeros(NC,NC);
Tau = zeros(NC,NC);

for i = 1 : NC
   for j = 1 : NC
      Tau(i,j) = B(i,j)/T;
      G(i,j)   = exp(-alpha(i,j)*Tau(i,j));
   end
end
gam_est = zeros(1,NC);
x_temp(1,2) = x_est(1,2);
x_temp(1,3) = x_est(1,3);
x_temp(1,1) = 1 - x_est(1,2) - x_est(1,3);

for ii = 1 : NC
   gam_1 =  0;
   gam_5 =  0;
   for jj = 1 : NC
      gam_2 =  0;
      gam_3 =  0;
      gam_4 =  0;
      for kk = 1 : NC
         gam_2 = gam_2 + G(kk,ii) * x_temp(1,kk);  %sum(Gki.Xk)
         gam_3 = gam_3 + G(kk,jj) * x_temp(1,kk);  %sum(Gkj.Xk)
         gam_4 = gam_4 + G(kk,jj) * Tau(kk,jj)* x_temp(1,kk); %sum(Gki.Tkj.Xk)
      end
      gam_1 = gam_1 + (Tau(jj,ii)*G(jj,ii)*x_temp(1,jj));   %sum(Gji.Tji.Xj)
      gam_5 = gam_5 + (((x_temp(1,jj)*G(ii,jj))/gam_3)*(Tau(ii,jj) - (gam_4/gam_3)));
%sum(Gji.Xj)/sum
   end
   gam_est(1,ii) = exp((gam_1/gam_2) + gam_5);
end
```

APPENDIX B – LLE Data and error analysis for NDHD extraction

Supplementary Data File for NDHD partition measurements with various ionic liquids

	Feed Fractions (V^{IL}:V^{Aq}=1)			IL - Phase							Aqueous Phase						
	z_{NDHD}	z_{IL}	z_{H2O}	x^{IL}_{NDHD}	x^{IL}_{H2O}	w^{IL}_{NDHD}	w^{IL}_{H2O}	ρ [g/cm^3]	C^{IL}_{NDHD} (mg/ml)	C^{IL}_{H2O} (mg/ml)	x^{Aq}_{NDHD}	x^{Aq}_{H2O}	w^{Aq}_{NDHD}	w^{Aq}_{H2O}	ρ [g/cm^3]	C^{Aq}_{NDHD} (mg/ml)	C^{Aq}_{H2O} (mg/ml)
[HMIm][Tf_2N]	6.5E-05	0.05	0.95	7.7E-04	0.207	3.5E-04	0.010	1.37	0.5	14.2	2.4E-05	0.9999	2.2E-04	0.9977	0.9983	0.2	996.0
	2.4E-04	0.05	0.95	3.0E-03	0.206	1.4E-03	0.010	1.37	1.9	14.2	8.8E-05	0.9998	7.9E-04	0.9971	0.9983	0.8	995.5
	4.9E-04	0.05	0.95	6.5E-03	0.206	3.0E-03	0.010	1.37	4.1	14.2	1.7E-04	0.9997	1.6E-03	0.9963	0.9983	1.5	994.7
	6.5E-04	0.05	0.95	1.3E-02	0.205	5.7E-03	0.010	1.37	7.8	14.2	2.9E-04	0.9996	2.6E-03	0.9953	0.9983	2.6	993.7
	8.3E-04	0.05	0.95	8.8E-03	0.206	4.0E-03	0.010	1.37	5.5	14.2	2.1E-04	0.9997	1.9E-03	0.9960	0.9983	1.9	994.3
	2.4E-04	0.04	0.96	1.5E-03	0.094	4.3E-04	0.003	1.56	0.7	4.7	1.9E-04	0.9998	1.7E-03	0.9966	0.9984	1.7	995.0
[HMIm][FAP]	3.4E-04	0.04	0.96	2.1E-03	0.094	6.2E-04	0.003	1.56	1.0	4.7	2.9E-04	0.9997	2.6E-03	0.9957	0.9984	2.6	994.1
	6.3E-04	0.04	0.96	3.4E-03	0.094	9.9E-04	0.003	1.56	1.5	4.7	5.3E-04	0.9994	4.7E-03	0.9935	0.9984	4.7	991.9
	3.2E-04	0.05	0.95	3.7E-03	0.369	2.7E-03	0.030	0.97	2.6	29.4	3.8E-05	0.9999	3.4E-04	0.9991	0.9978	0.3	996.8
[DMIm][TCB]	5.2E-04	0.05	0.95	5.8E-03	0.369	4.3E-03	0.030	0.97	4.1	29.4	5.1E-05	0.9999	4.6E-04	0.9990	0.9978	0.5	996.7
	7.6E-04	0.05	0.95	9.1E-03	0.368	6.8E-03	0.030	0.97	6.6	29.4	7.7E-05	0.9999	6.9E-04	0.9987	0.9978	0.7	996.5
	3.5E-04	0.05	0.95	3.2E-03	0.121	1.2E-03	0.005	1.26	1.5	6.5	2.3E-04	0.9997	2.1E-03	0.9971	0.9979	2.1	995.1
[TBMAm][Tf_2N]	9.3E-04	0.05	0.95	8.0E-03	0.120	3.1E-03	0.005	1.26	3.9	6.5	6.2E-04	0.9994	5.5E-03	0.9937	0.9979	5.5	991.7
	7.2E-04	0.04	0.96	7.9E-03	0.105	2.5E-03	0.004	1.19	3.0	4.4	4.5E-04	0.9995	4.0E-03	0.9955	0.9978	4.0	993.4
[THMAm][Tf_2N]	1.3E-03	0.04	0.96	1.5E-02	0.104	4.8E-03	0.004	1.19	5.7	4.4	8.2E-04	0.9992	7.3E-03	0.9922	0.9978	7.3	990.1
	5.0E-04	0.03	0.97	5.3E-03	0.092	1.5E-03	0.003	1.11	1.6	3.1	3.3E-04	0.9997	3.0E-03	0.9970	0.9978	3.0	994.8
[TOMAm][Tf_2N]	1.1E-03	0.03	0.97	1.1E-02	0.092	2.9E-03	0.003	1.11	3.3	3.1	7.9E-04	0.9992	7.1E-03	0.9929	0.9978	7.1	990.7
	8.6E-04	0.02	0.97	6.8E-03	0.193	1.8E-03	0.006	1.06	1.9	6.0	6.5E-04	0.9993	5.8E-03	0.9940	0.9978	5.8	991.8
[$P_{6,6,6,14}$][Tf_2N]	1.2E-03	0.02	0.97	1.2E-02	0.192	3.3E-03	0.006	1.06	3.5	6.0	8.2E-04	0.9992	7.3E-03	0.9925	0.9978	7.3	990.3
	6.5E-04	0.02	0.98	1.8E-03	0.040	3.2E-04	0.001	1.18	0.4	1.0	6.1E-04	0.9994	5.5E-03	0.9943	0.9978	5.5	992.1
[$P_{6,6,6,14}$][FAP]	8.1E-04	0.02	0.98	2.7E-03	0.040	5.0E-04	0.001	1.18	0.6	1.0	7.5E-04	0.9992	6.7E-03	0.9931	0.9978	6.7	990.9
	1.3E-04	0.03	0.97	2.4E-03	0.274	8.2E-04	0.010	1.16	1.0	12.1	4.5E-05	0.9999	4.1E-04	0.9987	0.9979	0.4	996.6
[DOM(5-BuCN)][Tf_2N]	5.9E-04	0.03	0.97	1.0E-02	0.272	3.5E-03	0.010	1.16	4.1	12.0	2.0E-04	0.9998	1.8E-03	0.9974	0.9979	1.8	995.3
	1.2E-04	0.03	0.97	2.0E-03	0.296	7.3E-04	0.012	1.12	0.8	13.3	3.7E-05	0.99996	3.3E-04	0.9996	0.9978	0.3	997.4
[DOM(5-HxOne)][Tf_2N]	5.9E-04	0.03	0.97	1.0E-02	0.294	3.7E-03	0.012	1.12	4.2	13.3	1.8E-04	0.9998	1.6E-03	0.9983	0.9978	1.6	996.1
	6.5E-05	0.05	0.95	7.7E-04	0.207	3.5E-04	0.010	1.37	0.5	14.2	2.4E-05	0.9999	2.2E-04	0.9977	0.9983	0.2	996.0

Notes:

1. Mutual solubilities of ionic liquid and water were used in the LLE calculations as the effect of NDHD on the solubilities at very low concentrations was considered minimal.
2. Since NDHD is a solid at room temperature, the change in density of either of the solvent phases was assumed to be minimal due to dilute NDHD concentrations.

1. Error analysis for [HMIm][Tf2N]/NDHD/Water system

1. Aqueous Phase

ca	cn	ci	dca	dcn	dci	rho_t	d(rho_t)	%d(rho_t/rho_t calc)
996	0.22	2.105	0.05	0.01	0.063	998.35	0.078568	0.008%
995	0.79	2.105	0.05	0.02	0.063	998.35	0.084850	0.008%
995	1.55	2.105	0.07	0.05	0.063	998.35	0.102041	0.010%
994	2.59	2.105	0.09	0.08	0.063	998.35	0.134709	0.013%
994	1.91	2.105	0.07	0.06	0.063	998.35	0.112348	0.011%
			0.01%	3%	3%	error%		

2. [HMIm][Tf2N]

C'a	rho_T	Ca	Cn	Ci	dCa	dCn	dCi	rho_calc	d(RHO_calc)	%d(RHO_calc/RHO_calc)
10.383	1368.7	14.2	0.48	1354	0.71	0.01	0.979	1368.7	1.209705	0.088%
10.383	1368.2	14.2	1.85	1352	0.71	0.06	0.981	1368.2	1.212697	0.089%
10.383	1367.4	14.2	4.06	1349	0.71	0.12	0.982	1367.4	1.22594	0.090%
10.383	1366	14.2	7.85	1344	0.71	0.24	1.029	1366	1.271797	0.093%
10.383	1366.9	14.2	5.47	1347	0.71	0.16	1.003	1366.9	1.23963	0.091%

rho_pure					
rho_pure	998	998	1374		
	5%	3%	0.07%	%error	

Mw	18.013	162	447.4

wa	wn	wi	dwa	dwn	dwi	%dwa	%dwn	%dwi
0.9977	0	0.002	9E-05	0	6E-05	0.01%	3.0%	3.0%
0.9971	0	0.002	1E-04	0	6E-05	0.01%	3.0%	3.0%
0.9963	0	0.002	1E-04	0	6E-05	0.01%	3.0%	3.0%
0.9953	0	0.002	2E-04	0	6E-05	0.02%	3.0%	3.0%
0.996	0	0.002	1E-04	0	6E-05	0.01%	3.0%	3.0%

Wa	Wn	Wi	dWa	dWn	dWi	%dWa	%dWn	%dWi
0.0104	0	0.989	5E-04	0	0.001	5.00%	3.0%	0.1%
0.0104	0	0.988	5E-04	0	0.001	5.00%	3.0%	0.1%
0.0104	0	0.987	5E-04	0	0.001	5.00%	3.0%	0.1%
0.0104	0.01	0.984	5E-04	0	0.001	5.00%	3.0%	0.1%
0.0104	0	0.986	5E-04	0	0.001	5.00%	3.0%	0.1%

Xa	Xn	Xi	dXa	%dXa	dXn	%dXn	dXi	%dXi
0.207	0	0.793	0.0082	3.97%	0	3.17%	0.01	1.03%
0.206	0	0.791	0.0082	3.97%	0	3.17%	0.01	1.03%
0.206	0.01	0.788	0.0082	3.97%	0	3.16%	0.01	1.03%
0.205	0.01	0.782	0.0082	3.98%	0	3.14%	0.01	1.03%
0.206	0.01	0.786	0.0082	3.97%	0	3.15%	0.01	1.03%

3. Partition Coefficients

KCa	dKCa	%dKCa
0.01	0	5.00%
0.01	0	5.00%
0.01	0	5.00%
0.01	0	5.00%
0.01	0	5.00%

KCn	dKCn	%dKCn
2.18	0.09	4.24%
2.36	0.1	4.24%
2.62	0.11	4.24%
3.03	0.13	4.24%
2.87	0.12	4.24%
2.61	0.11	
0.35		

KCi	dKCi	%dKCi
7.86E-05		
0.001		

KWa	dKWa	%dKWa
0.01041	0	5.00%
0.0104	0	5.00%
0.0104	0	5.00%
0.0104	0	5.00%
0.0104	0	5.00%

KWn	dKWn	%dKWn
1.598	0.07	4.24%
1.72	0.07	4.24%
1.913	0.08	4.24%
2.216	0.09	4.24%
2.095	0.09	4.24%
1.908	0.08	
0.256		

KXa	dKXa	%dKXa
0.207	0	0.01%
0.206	0	0.05%
0.206	0	0.10%
0.205	0	0.13%
0.206	0	0.13%

KXn	dKXn	%dKXn
31.725	1.385	4.37%
34.088	1.487	4.36%
37.807	1.646	4.35%
43.581	1.892	4.34%
41.332	1.797	4.35%
37.706	1.641	
4.9128		

4. Selectivities

SC_n	dSC_n	%dSC_n
154	6.51	4.2%
165	7.01	4.2%
184	7.79	4.2%
212	9.01	4.2%
201	8.53	4.2%
183	7.77	
24.4		

SW_n	dSW_n	%dSW_n
153.51	6.51	4.2%
165.17	7.01	4.2%
183.6	7.79	4.2%
212.43	9.02	4.2%
201	8.53	4.2%
183.14	7.77	
24.381		

SX_n	dSX_n	%dSX_n
153.5	6.7	4.4%
165.2	7.2	4.4%
183.6	7.99	4.4%
212.4	9.22	4.3%
201	8.74	4.3%
183.1	7.97	
24.38		

2. Error analysis for [HMIm][FAP]/NDHD/Water system

1. Aqueous Phase

ca	cn	ci
995	1.69	1.745
994	2.56	1.745
992	4.71	1.745

dca	dcn	dci	rho_t	d(rho_t)	%d(rho_t calc)
0.06	1.05	0.052	993.4	0.09487	0.010%
0.06	1.06	0.052	993.4	0.125229	0.013%
0.5	0.14	0.052	993.4	0.209463	0.021%
0.01%	3%	3%	error%		

w_a	w_n	w_i
0.997	0.002	0.0017
0.996	0.003	0.0017
0.994	0.005	0.0017

dw_a	dw_n	dw_i
1E-04	5E-05	5E-05
2E-04	9E-05	5E-05
3E-04	1E-04	5E-05

%dw_a	%dw_n	%dw_i
0.01%	3.0%	3.0%
0.02%	3.0%	3.0%
0.03%	3.0%	3.0%

xa	xn	xi
1	2E-04	5E-05
1	3E-04	5E-05
0.999	5E-04	5E-05

dx_a	%dx_a
0.002	0.00%
0.003	0.03%
0.003	0.03%

dx_n	%dx_n
6E-06	3.00%
3E-06	3.00%
2E-05	3.00%

dx_i	%dx_i
2E-06	3.00%
2E-06	3.00%
2E-06	3.00%

2. [HMIm][FAP]

C*a	rho_T	Ca	Cn	Ci
3.040	1556.0	4.7E	0.07	1552
3.048	1556.8	4.7E	0.96	1551
3.048	1556.5	4.74	1.55	1553

dCa	dCn	dCi	rho_calc	d(RHO_t_calc)	%d(RHO_t_calc)
0.24	1.02	0.372	1556.0	0.447047	0.029%
0.24	1.03	0.374	1556.8	0.44357	0.028%
0.24	1.05	0.378	1556.5	0.448563	0.029%

w_a	w_n	w
0.000	4E-04	0.9995
0.000	6E-04	0.9993
0.000	1E-03	0.996

dw_a	dw_n	dw
2E-04	1E-05	4E-04
2E-04	2E-05	4E-04
2E-04	3E-05	4E-04

%dw_a	%dw_n	%dw_i
5.00%	3.0%	0.0%
5.00%	3.0%	0.0%
5.00%	3.0%	0.0%

Xa	Xn	Xi
0.004	0.001	0.994
0.004	0.002	0.994
0.004	0.002	0.993

dx_a	%dx_a
0.43%	4.53%
0.43%	4.53%
0.43%	4.53%

dx_n	%dx_n
4E-05	3.00%
6E-05	3.03%
1E-04	3.03%

dx_i	%dx_i
0.004	0.47%
0.004	0.47%
0.004	0.47%

rho_pure

rho_pure	998	998	1563
	5%	3%	0.02%

%error

MW

	18.01	162.2	612.29

3. Partition Coefficients

KCa	dKCa	%dKCa
0	)	5.00%
0	)	5.00%
0	)	5.00%

KCn	dKCn	%dKCn
0.4	1.02	4.24%
0.38	1.02	4.24%
0.33	0.01	4.24%
0.37	1.02	
0.03		

KWa	dKWa	%dKWa
0.003	2E-04	5.00%
0.003	2E 04	5.00%
0.003	2E-04	5.00%

KWn	dKWn	%dKWr
0.254	0.011	4.24%
0.241	0.01	4.24%
0.211	0.009	4.24%
0.235	0.01	
0.022		

KXa	dKXa	%dKXa
0.054	4E-05	0.15%
0.054	EE 05	0.07%
0.054	1E-04	0.1%

KXn	dKXn	%dKXn
7.314	0.333	4.27%
7.393	0.315	4.26%
6.448	0.275	4.26%
7.218	0.308	
C.7		

4. Selectivities

SC_n	dSC_n	%dSC_n
83.1	3.52	1.2%
78.6	3.34	4.2%
68.6	2.91	4.2%
76.6	3.26	
7.41		

SW_r	dSW_r	%dSW_n
83.08	3.525	1.2%
78.63	3.336	4.2%
68.62	2.911	4.2%
76.78	3.258	
7.41		

SX_n	dSX_n	%dSX_r
83.08	3.5141	1.3%
78.63	3.355	4.3%
68.62	2.924	4.3%
76.78	3.275	
7.41		

3. Error analysis for [HMIm][FAP]/NDHD/Water system

1. Aqueous Phase

ca	cn	ci
997	0.34	0.587
997	0.45	0.587
995	0.69	0.587

da-a	da-n	da-i	rho_t	d(rho_t	%d(rho_t calc)
0.021	0.01	0.008	997.75	0.02510383	0.003%
0.023	0.01	0.008	997.75	0.03177033	0.003%
0.027	0.02	0.008	997.75	0.03861231	0.004%
0.00%	3%	3%	error%		

wa	wn	wi	dwa	dwn	dwi	%dwa	%dwn	%dw	xa	xn	xi	dx-a	%dx-a
1	J	6E-04	4E-05	1E-05	2E-05	0.00%	3.0%	3.0%	1	4E-05	3E-05	0.00%	0.00%
1	J	6E-04	4E-05	1E-05	2E-05	0.00%	3.0%	3.0%	1	5E-05	3E-05	0.16%	0.16%
1	J	6E-04	5E-05	2E-05	2E-05	0.00%	3.0%	3.0%	1	8E-05	3E-05	0.16%	0.16%

dwi	%dwi
3E-07	3.00%
3E-07	3.00%
3E-07	3.00%

2. [DMIm] [TCB]

C*a	rho_T	Ca	Cn	Ci
3C328	970.89	294	2.64	588.8
3C328	970.93	294	4.14	887.3
3C328	971	294	6.56	935

dCa	dCn	dCi	?HO_ca	d(RHC_ca	%d(RHO_ca
1472	0.18	1463	970.89	2.0562924	0.212%
1472	0.12	1.196	970.93	2.0666994	0.212%
1472	0.2	1464	971	2.0783013	0.213%
5%	3%	1.762%	%error		

rho_pure	rho_pure
393	398
398	970

wa	wn	wi	dwa	dwn	dwi	%dwa	%dwn	%dw	xa	xn	xi	dx-a	%dx-a
0.03	J	0.967	0.002	8E-05	0.003	5.00%	3.0%	1.3%	0.369	0.004	0.627	1.17%	3.16%
0.03	J	0.965	0.002	7E-05	0.003	5.00%	3.0%	0.3%	0.369	0.005	0.626	1.17%	3.16%
0.03	0.01	0.963	0.002	2E-04	0.003	5.00%	3.0%	0.3%	0.368	0.009	0.623	1.17%	3.17%

dXi	%dXi
0.012	1.85%
0.012	1.85%
0.011	1.85%

3. Partition Coefficients

KCa	dKCa	%dKCa
0.03	0	5.00%
0.03	0	5.00%
0.03	0	5.00%

KCn	dKCn	%dKCn
7.942	0.33	4.24%
9.138	0.39	4.24%
9.532	0.4	4.24%
8.794	0.37	
0.935		

KWa	dKWa	%dKWa
0.03	J	5.00%
0.03	J	5.00%
0.03	J	5.00%

KWn	dKWn	%dKWn
7.956	0.338	4.25%
8.359	0.398	4.25%
8.794	0.416	4.25%
8.037	0.384	
0.961		

KXa	dKXa	%dKXa
0.369	1E-04	0.04%
0.369	2E-04	0.05%
0.368	3E-04	0.09%

KXn	dKXn	%dKXn
96.8	4.48	4.63%
112.7	5.238	4.62%
116.8	5.433	4.62%
108.8	5.074	
11.52		

4. Selectivities

SC_n	dSC_n	%dSC_n
262	11.1	4.2%
303	13.1	4.2%
323	13.7	4.2%
293	12.6	
31.6		

SW_n	dSW_n	%dSW_n
262	11.1	4.2%
308	13.1	4.2%
323	13.7	4.2%
298	12.6	
31.6		

SX_n	dSX_n	%dSX_n
262.1	12.13	4.6%
308.3	14.25	4.6%
322.5	14.89	4.6%
297.6	13.76	
31.59		

4. Error analysis for [DMIm][TCB]/NDHD/Water system

1. Aqueous Phase

ca	cn	ci
937	0.34	0.587
937	0.45	0.587
936	0.69	0.587

dca	dcn	dci	rho_t	d(rho_t)	%d(rho_t/calc)
0.021	0.01	0.018	997.75	0.02910363	0.003%
0.023	0.01	0.018	997.75	0.03177033	0.003%
0.027	0.02	0.018	997.75	0.03861281	0.004%
0.00%	3%	3%	error%		

2. [DMIm] [TCB]

C*a	rho_T	Ca	Cn	Ci
30.328	970.89	29.4	2.64	938.8
30.328	970.93	29.4	4.14	937.3
30.328	971	29.4	6.56	935

dCa	dCn	dCi	rho_t_ca	d(RHO_t_ca)	%d(RHO_t/calc)
1.472	0.08	1.433	970.89	2.0562924	0.212%
1.472	0.12	1.436	970.93	2.06068914	0.212%
1.472	0.2	1.444	971	2.07183013	0.213%
5%	3%	0.75%	%error		

rho_pure	
rho_pure	938
	970

w/a	w/n	w/i	dw/a	dw/n	dw/i	%dw/a	%dw/n	%dw/i
1	0	6E-04	4E-05	1E-05	2E-05	0.00%	3.0%	3.0%
1	0	6E-04	4E-05	1E-05	2E-05	0.00%	3.0%	3.0%
1	0	6E-04	5E-05	2E-05	2E-05	0.00%	3.0%	3.0%

w/a	w/n	w/i	dw/a	dw/n	dw/i	%dw/a	%dw/n	%dw/i
0.03	0	0.967	0.002	8E-05	0.003	5.00%	3.0%	0.3%
0.03	0	0.965	0.002	1E-04	0.003	5.00%	3.0%	0.3%
0.03	0.01	0.963	0.002	2E-04	0.003	5.00%	3.0%	0.3%

MW

18	162	338.3

3. Partition Coefficients

KCa	dKCa	%dKCa
0.03	0	5.00%
0.03	0	5.00%
0.03	0	5.00%

KCn	dKCn	%dKCn
7.742	0.33	4.24%
3.109	0.39	4.24%
3.532	0.4	4.24%
8.794	0.37	
0.935		

KWa	dKWa	%dKWa
0.03	0	5.00%
0.03	0	5.00%
0.03	0	5.00%

KWn	dKWn	%dKWn
7.956	0.338	4.25%
3.359	0.338	4.25%
3.794	0.416	4.25%
9.037	0.384	
0.961		

KXa	dKXa	%dKXa
0.369	1E-04	0.04%
0.369	2E-04	0.05%
0.368	3E-04	0.09%

KXn	dKXn	%dKXn
96.8	4.48	4.63%
113.7	5.258	4.62%
118.8	5.483	4.62%
109.8	5.074	
11.52		

4. Selectivities

SC_n	dSC_n	%dSC_n
262	11.1	4.2%
308	13.1	4.2%
323	13.7	4.2%
298	12.6	
316		

SW_n	dSW_n	%dSW_n
262	11.1	4.2%
308	13.1	4.2%
323	13.7	4.2%
298	12.6	
316		

SX_n	dSX_n	%dSX_n
262.1	12.13	4.6%
308.3	14.25	4.6%
322.5	14.89	4.6%
297.6	13.76	
31.59		

5. Error analysis for [TBMAm][Tf_2N]/NDHD/Water system

1. Aqueous Phase

	ca	cn	ci
	985	2.0E	0.778
	992	5.5	0.778

	dca	dcn	dci	rho_t	drho_t) %:dfr=o_t=alc)
	0.07	0.0E	0.123	997.93	0.0932862 0.009%
	0.17	0.16	0.123	997.93	0.2351926 0.024%
	n mr%	3%	3%	error%	

	xa	xn	xi	dxa	%:dxa
	0.997	0.002	8E-04	0.0E%	0.00%
	0.994	0.006	8E-04	0.1%	0.11%

	dxn	%:dxn
	0	3.02%
	0	3.02%

	cxi	%:dxi
	0	3.00%
	0	3.00%

2. [TBMAm][Tf2N]

Ca	rho_T	Ca	Cn	Ci
5.1246	1263.8	6.48	1.52	1256
5.1246	1263.2	6.47	3.9	1253

	dCa	dCn	dCi	%HD_t_cal	d(RHD_t_cal)	d(RHD_t_calc
	0.32	0.0E	0.415	1263.8	0.5283403	0.042%
	0.32	0.12	0.137	1263.2	0.5559749	0.044%
	5%	3%	0.03%	%:error		

rho_pure	rho_pure	998	998	1265

	xa	xn	xi	dxa	dxn	dxi
	1.005	0.001	0.994	3E-04	4E-05	5E-04
	1.005	0.003	0.992	3E-04	9E-05	6E-04

	%:dxa	%:dxn	%:dxi
	5.00%	3.0%	0.1%
	5.00%	3.0%	0.1%

ylw	18.01	162.2	480.5

	xa	xn	xi	dxa	%:dxa
	1	2E-04	3E-05	0.0E%	0.00%
	1	6E-04	3E-05	0.1%	0.11%

	dxn	%:dxn
	0	3.02%
	0	3.02%

	cxi	%:dxi
	0	3.00%
	0	3.00%

3. Partition Coefficients

KCa	dKCa	%:dKCa
0.01	0	5.00%
0.01	0	5.00%

KCn	dKCn	%:dKCn
0.73	0.03	4.24%
0.71	0.03	4.24%
0.72	0.03	
0.02		

KWa	dKWa	%:dKWa
1.005	3E-04	5.0C%
1.005	3E-04	5.0C%

KWn	dKWn	%:dKWn
0.578	0.025	4.2C%
0.56	0.024	4.2C%
0.569	0.024	
0.013		

KXa	dKXa	%:dKXa
0.12	1E-04	0.0E%
0.12	2E-04	0.2C%

KXn	dKXn	%:dKXn
13.56	0.58	4.23%
13.06	C.557	4.27%
13.31	C.569	
0.353		

4. Selectivities

SC_n	dSC_n	%:dSC_n
112	4.77	4.2%
109	4.61	4.2%
110	4.65	
2.01		

SW_n	dSW_n	%:dSW_n
112.6	4.77	4.2%
108.6	4.607	4.2%
110.5	4.688	
2.01		

SX_n	dSX_n	%:dSX_n
112	4.81	4.3%
109	4.634	4.3%
110	4.688	
2.01		

6. Error analysis for [TBMAm][Tf_2N]/NDHD/Water system

1. Aqueous Phase

ca	cn	ci	dca	dcn	dci	rho_t	d(rho_t)	%d(rho_t/calc)
993.4	4.014	0.452	0.121	0.12	0.014	997.842	0.171234	0.017%
990.1	7.331	0.452	0.22	0.22	0.014	997.842	0.311527	0.031%
			0.02%	3%	3%	error%		

xa	xn	xi	dxa	%dxa	dxn	%dxn	dxi	%dxi
0.996	0.004	5E-04	2E-04	1E-04	1E-05	0.00%	0.00%	1E-05	3.00%	4E-07	3.00%
0.992	0.007	5E-04	4E-04	2E-04	1E-05	0.10%	0.10%	2E-05	3.00%	4E-07	3.00%

2. [TBMAm][Tf2N] Phase

C*a	rho_T	Ca	Cn	Ci
3.7456	1186.58	4.444	2.997	1179
3.7456	1186.06	4.442	5.75	1176

dCa	dCn	dCi	RHO_t_ca	d(RHO_t_ca)	%d(RHO_t_ca/calc)
0.222	0.09	0.285	1186.58	0.372235	0.031%
0.222	0.172	0.335	1186.06	0.437283	0.037%
5%	3%	0.03%	%error		

Wa	Wn	Wi
0.004	0.003	0.994
0.004	0.005	0.991

dWa	dWn	dWi
2E-04	8E-05	4E-04
2E-04	1E-04	5E-04

%dWa	%dWn	%dWi
5.00%	3.0%	0.0%
5.00%	3.0%	0.0%

Xa	Xn	Xi
0.105	0.008	0.887
0.104	0.015	0.881

dXa	%dXa
0.47%	4.48%
0.47%	4.48%

dXn	%dXn
2E-04	3.02%
4E-04	3.00%

dXi	%dXi
0.005	0.52%
0.005	0.52%

rho_pure

rho_pure			
997.8	997.8	1188	

MW

18.01	162.2	564.7

3. Partition Coefficients

KCa	dKCa	%dKCa
0.004	2E-04	5.00%
0.004	2E-04	5.00%

KCn	dKCn	%dKCn
0.746	0.032	4.24%
0.784	0.033	4.24%
0.765	0.032	
0.027		

KWa	dKWa	%dKWa
0.004	2E-04	5.00%
0.004	2E-04	5.00%

KWn	dKWn	%dKWn
0.628	0.027	4.24%
0.66	0.028	4.24%
0.644	0.027	
0.023		

KXa	dKXa	%dKXa
0.105	2E-04	0.23%
0.104	5E-04	0.43%

KXn	dKXn	%dKXn
17.5	0.745	4.26%
18.25	0.774	4.24%
17.87	0.76	
0.528		

4. Selectivities

SC_n	dSC_n	%dSC_n
166.8	7.079	4.2%
174.8	7.416	4.2%
170.8	7.247	
5.616		

SW_n	dSW_n	%dSW_n
166.8	7.079	4.2%
174.8	7.416	4.2%
170.8	7.248	
5.616		

SX_n	dSX_n	%dSX_n
166.8	7.104	4.3%
174.8	7.415	4.2%
170.8	7.259	
5.616		

7. Error analysis for [TBMAm][Tf_2N]/NDHD/Water system

1. Aqueous Phase

ca	cn	ci
994.8	2.965	0.039
990.7	7.065	0.039

dca	dcn	dci	rho_t	d(rho_t)	%d(rho_t)
0.089	0.089	0.001	997.774	0.12579	0.013%
0.212	0.212	0.001	997.774	0.29977	0.030%
0.02%	3%	3%	error%		

2. [TOMAm][Tf2N] Phase

C°a	rho_I	Ca	Cn	Ci
2.8371	1109.46	3.137	1.633	1105
2.8371	1109.28	3.136	3.255	1103

rho_pure

rho_pure	997.8	997.8	1110

dCa	dCn	dCi	KH2O_t_calc	KH2O_t_calc	%d(KH2O_tcalc)
0.157	0.049	0.183	1109.46	0.24578	0.022%
0.157	0.098	0.206	1109.28	0.27632	0.025%
5%	3%	0.02%	%error		

Wa	Wn	Wi	MW	18.01	162.2	648.8
0.003	0.001	0.996				
0.003	0.003	0.994				

va	vn	vi
0.997	0.003	4E-05
0.993	0.007	4E-05

dva	dvn	dvi
2E-04	9E-05	1E-06
4E-04	2E-04	1E-06

%dva	%dvn	%dvi
0.02%	3.0%	3.0%
0.04%	3.0%	3.0%

xa	xn	xi
1	3E-04	1E-06
0.999	8E-04	1E-06

dxa	%dxa
0.00%	0.00%
0.08%	0.08%

dxn	%dxn
1E-05	3.00%
2E-03	3.00%

dxi	%dxi
3E-08	3.00%
3E-08	3.00%

3. Partition Coefficients

KCa	dKCa	%dKCa
0.003	2E-04	5.00%
0.003	2E-04	5.00%

KCn	dKCn	%dKCn
0.551	0.023	4.24%
0.461	0.02	4.24%
0.506	0.021	
0.064		

KCWa	dKCWa	%dKCWa
0.003	1E-04	5.00%
0.003	1E-04	5.00%

KCWn	dKCWn	%dKCWn
0.495	0.021	4.24%
0.414	0.018	4.24%
0.455	0.019	
0.057		

KCXa	dKCXa	%dKCXa
0.092	2E-04	0.17%
0.092	3E-04	0.35%
		14.76
		1.939

KCXn	dKCXn	%dKCXn
16.13	0.687	4.26%
13.39	0.568	4.24%
14.76	0.627	
1.939		

4. Selectivities

SC_r	dSC_r	%dSC_r
174.7	7.413	4.2%
145.5	6.175	4.2%
160.1	6.794	
20.64		

SW_n	dSW_n	%dSW_n
174.7	7.413	4.2%
145.5	6.175	4.2%
160.1	6.794	
20.64		

SX_n	dSX_n	%dSX_n
174.7	7.436	4.3%
145.5	6.177	4.2%
160.1	6.806	
20.64		

8. Error analysis for [DOM(5-BuCN)Am][Tf_2N]/NDHD/Water system

1. Aqueous Phase

	ca	cn	ci	dca	dcn	dci	rho_t	d(rho_t)	%d(rho_t/calc)
	906.6	0.408	0.85	0.025	0.012	0.025	997.8888	0.03781	0.004%
	995.3	1.78	0.85	0.058	0.053	0.025	997.8888	0.08265	0.008%
				2.00%	3%	3%	error%		

	wa	wn	wi
	0.999	4E-04	9E-04
	0.997	0.002	9E-04

	dwa	dwn	dwi	%dwa	%dwn	%dwi
	5E-05	1E-05	3E-05	0.00%	3.0%	3.0%
	1E-04	5E-05	3E-05	0.01%	3.0%	3.0%

	xa	xn	xi	dxa	%dxa	dxn	%dxn
	1	5E-05	2E-05	0.00%	0.00%	1E-06	3.00%
	1	2E-04	2E-05	0.08%	0.08%	6E-06	3.00%

2. [DO(CN)MAm][Tf2N] Phase

C°a	rho_T	Ca	Cn	Ci	dCa	dCn	dCi	RHO_t_ca	RHO_t_ca	%d(RHO_tcalc)
10.41	1157.79	12.05	0.953	1145	0.603	0.029	0.701	1157.787	0.92512	0.080%
10.41	1157.28	12.05	4.077	1141	0.602	0.122	0.715	1157.28	0.91252	0.081%
rho_pure		rho_pure			5%	3%	0.06%	%error		

	Wa	Wn	Wi
	0.01	8E-04	0.989
	0.01	0.001	0.985

	dWa	dWn	dWi	%dWa	%dWn	%cWi
	5E-04	2E-05	1E-03	5.00%	3.0%	0.1%
	5E 01	1E 01	0.001	5.00%	3.0%	0.1%

	Xa	Xn	Xi	dXa	%dXa	dXn	%dXn
MW	18.01	162.2	647.3	0.99%	3.63%	8E-05	3.29%
	0.274	0.002	0.724	0.99%	3.64%	3E 01	3.27%
	0.272	0.01	0.717				

3. Partition Coefficients

KCa	dKCa	%dKCa
0.012	6E-04	5.00%
0.012	6E-04	5.00%

KCn	dKCn	%dKCn
2.337	0.099	4.24%
2.291	0.097	4.24%
2.314	0.098	
0.033		

KWa	dKWa	%dKWa
0.01	5E-04	5.00%
0.01	5E-04	5.00%

KWn	dKWn	%dKWn
2.014	0.085	4.24%
1.975	0.084	4.24%
1.995	0.085	
0.028		

KXa	dKXa	%dKXa
0.274	8E-05	0.03%
0.272	3E-04	0.12%

KXn	dKXn	%dKXn
52.95	2.359	4.45%
51.55	2.287	4.44%
52.25	2.323	
0.987		

4. Selectivities

SC_n	dSC_n	%dSC_n
193.2	8.109	4.2%
189.2	8.029	4.2%
191.2	8.114	
2.835		

SW_n	dSW_n	%dSW_n
193.2	8.7	4.5%
189.2	8.03	4.2%
191.2	8.115	
2.835		

SX_n	dSX_n	%dSX_n
193.2	8.608	4.5%
189.2	8.395	4.4%
191.2	8.502	
2.835		

9. Error analysis for [DOM(5-HxOne)Am][Tf_2N]/NDHD/Water system

1. Aqueous Phase

ca	cn	ci
997.4	0.334	0.09
996.1	1.64	0.09

dca	dcn	dci	rho_t	d(rho_t)	%d(rho_t calc)
0.01	0.01	0.003	997.7802	0.014624	0.001%
0.049	0.049	0.003	997.7802	0.069673	0.007%
0.00%	3%	3%	error%		

wa	wn	wi
1	3E-04	9E-05
0.998	0.002	9E-05

dwa	dwn	dwi
2E-05	1E-05	3E-06
9E-05	5E-05	3E-06

%dwa	%dwn	%dwi
0.00%	3.0%	3.0%
0.01%	3.0%	3.0%

xa	xn	xi	dxa	%dxa
1	4E-05	3E-06	0.00%	0.00%
1	2E-04	3E-06	0.09%	0.09%

dxn	%dxn
1E-05	3.00%
5E-05	3.00%

2. [DO(one)MAm][Tf2N] Phase

C°a	rho_T	Ca	Cn	Ci
11.826	1123.89	13.29	0.824	1110
11.826	1123.46	13.29	4.203	1106

dCa	dCn	dCi	RHO_t ca	(RHO_t ca)/d(RHO_t calc)	%error
0.665	0.025	0.75	1123.89	1.002581	0.089%
0.664	0.126	0.763	1123.458	1.019379	0.091%
3%	3%	0.07%			

rho_pure

rho_pure
99.8
99.8
1126

Wa	Wn	Wi
0.012	7E-04	0.987
0.012	0.004	0.984

MW

18.01	162.2	634.8

Xa	Xn	Xi
0.266	0.002	0.702
0.264	0.01	0.695

dXa	%dXa
1.04%	3.52%
1.04%	3.53%

dXn	%dXn
7E-05	3.34%
3E-04	3.32%

3. Partition Coefficients

KCa	dKCa	%dKCa
0.013	7E-04	5.00%
0.013	7E-04	5.00%

KCn	dKCn	%dKCn
2.467	0.105	4.24%
2.563	0.109	4.24%
2.515	0.107	
0.067		

KWa	dKWa	%dKWa
0.012	6E-04	5.00%
0.012	6E-04	5.00%

KWn	dKWn	%dKWn
2.19	0.093	4.24%
2.276	0.097	4.24%
2.233	0.095	
0.061		

KXa	dKXa	%dKXa
0.266	7E-05	0.02%
0.264	3E-04	0.12%

KXn	dKXn	%dKXn
54.83	2.463	4.49%
56.56	2.529	4.47%
55.7	2.496	
1.219		

4. Selectivities

SC_n	dSC_n	%dSC_n
185.1	7.855	4.2%
192.1	8.151	4.2%
188.6	8.003	
4.938		

SW_n	dSW_n	%dSW_n
185.1	7.856	4.2%
192.1	8.153	4.2%
188.6	8.005	
4.938		

SX_n	dSX_n	%dSX_n
185.1	8.314	4.5%
192.1	8.59	4.5%
188.6	8.452	
4.938		

10. Error analysis for $[P_{6,6,6,14}][Tf_2N]$/NDHD/Water system

1. Aqueous Phase

ca	cn	ci	dca	dcn	dci	rho_t	d(rho_t)	%d(rho_t/rho_t)
991.8	5.779	0.168	0.173	0.173	0.005	997.781	0.245275	0.025%
990.3	7.282	0.168	0.219	0.218	0.005	997.781	0.309039	0.031%
			0.02%	3%	3%	error%		

2. $[P_{6,6,6,14}][Tf_2N]$ Phase

Ca	Cn	Ci	dCa	dCn	dCi	RHO_t_ca	RHO_t_cn	%d(RHO_t_calc)
6.023	1.916	1057	0.301	0.057	0.527	1064.66	0.488439	0.042%
6.022	3.52	1055	0.301	0.106	0.341	1064.56	0.466736	0.044%
			5%	3%	0.03%	%error		

rho_pure: 997.8 | 997.8 | 1063

3. Partition Coefficients

KCa	dKCa	%dKCa	KCn	dKCn	%dKCn
0.006	3E-04	5.00%	0.332	0.014	4.24%
0.006	3E-04	5.00%	0.483	0.021	4.24%
			0.407	0.017	
			0.107		

4. Selectivities

SC_n	dSC_n	%dSC_n
54.6	2.317	4.2%
79.48	3.372	4.2%
67.04	2.844	
17.59		

wa	wn	wi	dwa	dwn	dwi	%dwa	%dwn	%dwi
0.994	0.006	2E-04	3E-04	2E-04	5E-06	0.03%	3.0%	3.0%
0.993	0.007	2E-04	4E-04	2E-04	5E-06	0.04%	3.0%	3.0%

Wa	Wn	Wi	dWa	dWn	dWi	%dWa	%dWn	%dWi
0.006	0.002	0.993	3E-04	2E-04	5E-04	5.00%	3.0%	0.1%
0.006	0.003	0.991	3E-04	1E-04	5E-04	5.00%	3.0%	0.1%

MW: 18.01 | 162.2 | 764

KWa	dKWa	%dKWa
0.006	3E-04	5.00%
0.006	3E-04	5.00%
0.006	3E-04	
6E-06		

KWn	dKWn	%dKWn
0.311	0.013	4.24%
0.453	0.019	4.24%
0.382	0.016	
0.101		

SW_n	dSW_n	%dSW_n
54.6	2.317	4.2%
79.48	3.372	4.2%
67.04	2.845	
17.59		

xa	xn	xi	dXa	%dXa
0.999	6E-04	4E-06	0.00%	0.00%
0.999	8E-04	4E-06	0.07%	0.07%

Xa	Xn	Xi	dXa	%dXa
0.193	0.807	0.8	0.78%	4.03%
0.192	0.812	0.795	0.78%	4.04%

KXa	dKXa	%dKXa
0.193	2E-04	0.11%
0.193	4E-04	0.20%
0.193	3E-04	
6E-04		

SX_n	dSX_n	%dSX_n
54.6	2.368	4.3%
79.48	3.436	4.3%
67.04	2.902	
17.59		

KXn	dKXn	%dKXn
10.56	0.458	4.34%
15.31	0.662	4.32%
12.94	0.56	
3.357		

dxa	%dxa
0.00%	0.00%
0.07%	0.07%

dXa	%dXa
0.78%	4.03%
0.78%	4.04%

dxn	%dxn
2E-05	3.00%
2E-05	3.00%

dXn	%dXn
2E-04	3.15%
4E-04	3.12%

dxi	%dxi
1E-07	3.00%
1E-07	3.00%

dXi	%dXi
0.008	0.97%
0.008	0.96%

11. Error analysis for $[P_{6,6,6,14}][FAP]$/NDHD/Water system

1. Aqueous Phase

	ca	cn	ci	dca	dcn	dci	rho_t	d(rho_t)	%d(rho_t calc)
	992.1	5.476	0.204	0.164	0.164	0.005	997.8019	0.23244	0.023%
	990.9	6.682	0.204	0.201	0.2	0.005	997.8019	0.28362	0.028%
				0.02%	3%	3%	error%		

	wa	wn	wi	dwa	dwn	dwi	%dwa	%dwn	%dwi	xa	xn	xi	dxa	%dxa	dxn	%dxn
	0.994	0.005	2E-04	3E-04	2E-04	6E-06	0.03%	3.0%	3.0%	0.999	6E-04	4E-06	0.00%	0.00%	2E-05	3.00%
	0.993	0.007	2E-04	3E-04	2E-04	6E-06	0.03%	3.0%	3.0%	0.999	7E-04	4E-06	0.06%	0.09%	2E-05	3.00%

2. $[P_{6,6,6,14}][FAP]$ Phase

C°a	rho_T	Ca	Cn	Ci	dCa	dCn	dCi	RHO_t	ca	RHO_t	c%	d(RHO_t calc)
0.81802	1181.72	0.967	0.382	1180	0.048	0.011	0.059	1181.721		0.07702		0.007%
0.81802	1181.71	0.967	0.387	1180	0.048	0.018	0.061	1181.713		0.07976		0.007%
rho_pure		rho_pure	997.8	997.8	1182	5%	3%	0.01%	%error			

	Wa	Wn	Wi	dWa	dWn	dWi	%dWa	%dWn	%dWi
	8E-04	3E-04	0.999	4E-05	1E-05	8E-05	5.00%	3.0%	0.0%
	8E-04	3E-04	0.999	4E-05	1E-05	8E-05	5.00%	3.0%	0.0%
MW	18.01	162.2	928.9						

	Xa	Xn	Xi	dXa	%dXa	dXn	%dXn
	0.04	0.002	0.958	0.19%	4.80%	2E-05	3.00%
	0.04	0.003	0.957	0.19%	4.80%	8E-05	3.00%

3. Partition Coefficients

KCa	dKCa	%dKCa
1E-03	5E-05	5.00%
1E-03	5E-05	5.00%

KCn	dKCn	%dKCn
0.07	0.003	4.24%
0.088	0.004	4.24%
0.079	0.003	
0.013		

KWa	dKWa	%dKWa
8E-04	4E-05	5.00%
8E-04	4E-05	5.00%

KWn	dKWn	%dKWn
0.059	0.003	4.24%
0.074	0.003	4.24%
0.067	0.003	
0.011		

KXa	dKXa	%dKXa
0.04	5E-05	0.13%
0.04	8E-05	0.20%

KXn	dKXn	%dKXn
2.991	0.123	4.24%
3.645	0.155	4.24%
3.273	0.139	
0.526		

4. Selectivities

SC_n	dSC_n	%dSC_n
71.67	3.041	4.2%
90.11	3.823	4.2%
80.89	3.432	
13.04		

SW_n	dSW_n	%dSW_n
71.67	3.041	4.2%
90.11	3.823	4.2%
80.89	3.432	
13.04		

SX_n	dSX_n	%dSX_n
71.67	3.041	4.2%
90.11	3.821	4.2%
80.89	3.431	
13.04		

APPENDIX C – LLE Data and error analysis for ABE solutes extraction using [HMIm][Tf2N]

1. Ternary data

1. Aqueous Phase

ca	c_ac	ci	dca	dc_ac	dci	rho_t	d(rho_t)	%d(rho_t)	wa	w_ac	wi	dwa	dw_ac	dwi	%dwa	%dw_ac	%dwi	xa	x_ac	xi	dxa	%dxa
995.8	0.238	2.0932	0.147	0.01	0.0628	998.28	0.079314	0.008%	0.99756	3E-04	0.0021	9E-05	1E-05	6E-05	0.01%	3.0%	3.0%	0.9988	1E-04	6E-05	0.0000	0.00%
995.4	0.393	2.1317	0.153	0.02	0.0664	998.22	0.085881	0.009%	0.99711	7E-04	0.0021	0.0001	2E-05	6E-05	0.01%	3.0%	3.0%	0.9987	2E-04	5E-05	0.0000	0.00%
994.1	1.792	2.1086	0.182	0.054	0.0633	997.99	0.116734	0.012%	0.99609	0.002	0.0021	0.0001	5E-05	6E-05	0.01%	3.0%	3.0%	0.9984	6E-04	5E-05	0.0000	0.00%
993.4	2.344	2.1313	0.1	0.07	0.0639	997.89	0.138183	0.014%	0.99562	0.002	0.0021	0.0002	7E-05	6E-05	0.02%	3.0%	3.0%	0.9982	7E-04	5E-05	0.0000	0.00%
992.8	2.302	2.161	0.16	0.084	0.0648	997.81	0.157432	0.016%	0.99503	0.003	0.0022	0.0002	8E-05	6E-05	0.02%	3.0%	3.0%	0.999	9E-04	5E-05	0.0000	0.00%
990.4	4.798	2.2639	0.189	0.144	0.0679	997.44	0.246981	0.025%	0.99292	0.005	0.0023	0.0003	1E-04	7E-05	0.03%	3.0%	3.0%	0.9984	0.002	5E-05	0.0000	0.00%
979.6	13.89	2.1427	0.529	0.417	0.0843	995.60	0.678765	0.068%	0.98388	0.014	0.0022	0.0009	4E-04	6E-05	0.09%	3.0%	3.0%	0.9965	0.004	5E-05	0.0001	0.01%
			0.02%	3%	3%	error%																

2. [HMIm][Tf2N]

Ca	C_ac	Ci	dCa	dC_ac	dCi	RHO_t_ca	RHO_t_ca	%d(RHO_t_calc)	Wa	W_ac	Wi	dWa	dW_ac	dWi	%dWa	%dW_ac	%dWi	Xa	X_ac	Xi	dXa	%dXa	dX_ac	%dX_ac	dXi	%dXi
15.08	0.307	1352.7	0.754	0.01E	1.0387	1368.25E	1.283525	0.094%	0.00110	4E-04	0.9888	0.0006	1E-05	0.0012	500%	3.0%	0.1%	0.2163	0.002	0.7834	0.0085	3.92%	7E-05	3.19%	0.008457	1.36%
14.65	0.388	1352.5	0.732	0.03	1.01	1368.104	1.247936	0.091%	0.0007	7E-04	0.9888	0.0005	2E-05	0.0012	500%	3.0%	0.1%	0.211	0.004	0.7845	0.0083	3.95%	1E-04	3.17%	0.008283	1.36%
14.98	2.352	1345.4	0.749	0.077	1.04	1366.961	1.23838	0.091%	0.00098	0.002	0.9872	0.0005	6E-05	0.0012	500%	3.0%	0.1%	0.2137	0.011	0.775	0.0084	3.93%	4E-04	3.16%	0.008288	1.37%
15.07	3.413	1341.9	0.753	0.102	1.0529	1366.365	1.238773	0.095%	0.00103	0.002	0.9865	0.0006	7E-05	0.0012	500%	3.0%	0.1%	0.2141	0.015	0.7709	0.0084	3.93%	5E-04	3.14%	0.008263	1.37%
15.12	3.323	1347	0.756	0.118	1.0612	1366.014	1.308235	0.096%	0.00107	0.003	0.9861	0.0006	9E-05	0.0012	500%	3.0%	0.1%	0.2143	0.017	0.7685	0.0084	3.93%	5E-04	3.14%	0.008247	1.37%
13.76	6.309	1343.9	0.688	0.207	1.014	1364.582	1.242786	0.091%	0.00108	0.005	0.9849	0.0005	2E-04	0.0012	500%	3.0%	0.1%	0.1985	0.031	0.7729	0.0079	4.02%	9E-04	3.07%	0.007632	0.99%
16.45	16.68	1322.8	0.823	0.56	1.4955	1355.894	1.73641	0.182%	0.00121	0.014	0.9741	0.0006	4E-04	0.0017	500%	3.0%	0.2%	0.2181	0.077	0.7061	0.0085	3.92%	0.002	2.98%	0.007871	1.12%
*ho_pure	997.8	788.8	13743									MW	18.0128	58.08	447.42											
			5%	3%	0.08%	%error																				

3. Partition Coefficients

KCa	dKC_ac	%dKCa	KC_ac	dKC_ac	%dKC_ac	KWa	dKWa	%dKWa	KW_ac	dKW_ac	%dKW_ac	KXa	dKXa	%dKXa	KX_ac	dKX_ac	%dKX_ac
0.015	8E-04	5.00%	1.501	0.084	4.24%	0.00110	6E-04	5.00%	1.0949	0.046	4.24%	0.2184	7E-05	0.03%	21.44775	0.9385	4.38%
0.015	7E-04	5.00%	1.425	0.06	4.24%	0.00074	5E-04	5.00%	1.0401	0.044	4.24%	0.2111	1E-04	0.07%	20.45044	0.8925	4.36%
0.015	8E-04	5.00%	1.424	0.06	4.24%	0.001	6E-04	5.00%	1.0395	0.044	4.24%	0.2108	4E-04	0.17%	20.20863	0.8798	4.35%
0.015	8E-04	5.00%	1.456	0.062	4.24%	0.00105	6E-04	5.00%	1.0636	0.045	4.24%	0.2142	5E-04	0.22%	20.56363	0.8936	4.34%
0.015	8E-04	5.00%	14	0.059	4.24%	0.00112	6E-04	5.00%	1.0229	0.043	4.24%	0.2145	5E-04	0.23%	19.72257	0.8569	4.34%
0.014	7E-04	5.00%	1.44	0.06	4.24%	0.00101	5E-04	5.00%	1.0526	0.045	4.24%	0.1969	9E-04	0.48%	20.40378	0.8786	4.28%
0.017	8E-04	5.00%	1.344	0.057	4.24%	0.00233	6E-04	5.00%	0.9871	0.042	4.25%	0.2191	0.002	1.05%	17.54031	0.7405	4.22%
			1.427	0.06					1.043	0.044					20.04871	0.868	
			0.148						0.0335						1.220613		

4. Selectivities

SC_ac	dSC_ac	%dSC_ac	SW_ac	SW_a	dSW_ac	%dSW_ac	SX_ac	SX_a	dSX_ac	%dSX_ac
99.12	4.206	4.2%	99.1177	4.207	4.2%		99.118	4.337	4.4%	
96.87	4.11	4.2%	96.8723	4.111	4.2%		96.872	4.228	4.4%	
94.51	4.01	4.2%	94.5128	4.011	4.2%		94.513	4.114	4.4%	
96.01	4.074	4.2%	96.0111	4.075	4.2%					
91.96	3.902	4.2%	91.9606	3.903	4.2%					
103.6	4.398	4.2%	103.649	4.399	4.2%		103.65	4.448	4.3%	
80.05	3.397	4.2%	80.0523	3.399	4.2%		80.053	3.38	4.2%	
94.6	4.014		94.5967	4.015			94.841	4.101		
7.394			7.39419				8.9274			

2. Ternary data and error analysis for [HMIm][Tf2N]/1-butanol/Water

1. Aqueous Phase

ca	cb	ci	dca	dcb	dci	rho_t	d(rho_t	%d(rho_tcalc)	wa	wb	wi	dwa	dwb	dwi	%dwa	%dwb	%dwi	xa	xb	xi	dxa	%dxa	dxb	%dxb	dxi	%dxi
9951	0.926	2.2001	0.059	0.028	0.066	998.19	0.092769	0.009%	0.9969	9E-04	0.0022	0.0001	3E-05	7E-05	0.01%	3.0%	3.0%	0.9997	2E-04	9E-05	7.3E-06	0.001%	7E-06	3.00%	2.7E-06	3.00%
9934	2.427	2.0694	0.101	0.073	0.0678	997.85	0.13878	0.014%	0.9965	0.002	0.0021	0.0002	7E-05	6E-05	0.02%	3.0%	3.0%	0.9993	6E-04	8E-05	1.8E-05	0.002%	2E-05	3.00%	2.5E-06	3.00%
9923	3.336	2.0421	0.132	0.1	0.0612	997.67	0.176266	0.018%	0.9946	0.003	0.002	0.0002	1E-04	6E-05	0.02%	3.0%	3.0%	0.9991	8E-04	8E-05	2.5E-05	0.003%	2E-05	3.00%	2.5E-06	3.00%
9903	5.012	2.0757	0.191	0.15	0.06227	997.35	1.251246	0.025%	0.9929	0.005	0.0021	0.0003	2E-04	6E-05	0.03%	3.0%	3.0%	0.9987	0.001	8E-05	3.7E-05	0.004%	4E-05	3.00%	2.5E-06	3.00%
9884	6.568	2.0712	0.249	0.198	0.06214	997.03	0.323538	0.032%	0.9913	0.007	0.0021	0.0004	2E-04	6E-05	0.04%	3.0%	3.0%	0.9983	0.002	8E-05	4.8E-05	0.005%	5E-05	3.00%	2.5E-06	3.00%
9865	8.229	1.9778	0.308	0.247	0.05934	996.68	0.399477	0.040%	0.9898	0.008	0.002	0.0005	2E-04	6E-05	0.05%	3.0%	3.0%	0.9979	0.002	8E-05	6.1E-05	0.007%	6E-05	2.99%	2.4E-06	3.00%
979	14.46	1.9648	0.538	0.434	0.05834	996.44	0.693657	0.070%	0.9835	0.015	0.002	0.0009	4E-04	6E-05	0.09%	3.0%	3.0%	0.9963	0.004	8E-05	1.1E-04	0.01%	1E-04	2.99%	2.4E-06	3.00%
			0.022%	3%	3%	error%																				

2. [HMIm][Tf2N]

Ca	Cb	Ci	dCa	dCb	dCi	RHO_t_cal	d(RHO_t_cal	%d(RHO_tcalc)	Wa	Wb	Wi	dWa	dWb	dWi	%dWa	%dWb	%dWi	Xa	Xb	Xi	dXa	%dXa	dXb	%dXb	dXi	%dXi
14.26	1.223	1352.6	0.713	0.037	0.984	1368.098	1.215707	0.089%	0.0104	9E-04	0.9887	0.0005	3E-05	0.0011	5.00%	3.0%	0.1%	0.2066	0.304	0.7891	0.0082	3.97%	1E-04	3.16%	0.00616	1.03%
14.58	3.226	1348.8	0.729	0.099	1.0177	1366.636	1.255568	0.092%	0.0107	0.002	0.9869	0.0005	7E-05	0.0012	5.00%	3.0%	0.1%	0.2092	0.011	0.7794	0.0083	3.96%	4E-04	3.15%	0.00616	1.05%
14.77	4.572	1346.4	0.738	0.137	1.04346	1365.726	1.285604	0.094%	0.0108	0.003	0.9858	0.0005	1E-04	0.0012	5.00%	3.0%	0.1%	0.2107	0.016	0.7734	0.0083	3.96%	5E-04	3.14%	0.00616	1.06%
14.9	6.654	1342.7	0.745	0.201	1.0814	1364.296	1.322834	0.097%	0.0109	0.005	0.9842	0.0005	1E-04	0.0012	5.00%	3.0%	0.1%	0.2111	0.023	0.7669	0.0083	3.96%	7E-04	3.12%	0.0031	1.06%
15.23	8.768	1338.8	0.761	0.264	1.14039	1362.807	1.396867	0.102%	0.0112	0.006	0.9824	0.0006	2E-04	0.0013	5.00%	3.0%	0.1%	0.2137	0.03	0.7563	0.0084	3.93%	9E-04	3.10%	0.00612	1.07%
16.33	11.2	1333.3	0.816	0.336	1.26177	1360.822	1.539946	0.113%	0.012	0.008	0.9798	0.0006	2E-04	0.0014	5.00%	3.0%	0.1%	0.2245	0.037	0.7381	0.0087	3.88%	0.001	3.10%	0.00633	1.13%
17.51	19.37	1318.2	0.875	0.581	1.56021	1356.054	1.88103	0.139%	0.0129	0.014	0.9728	0.0007	4E-04	0.0018	5.00%	3.0%	0.2%	0.2325	0.063	0.7049	0.0089	3.85%	0.002	3.05%	0.00631	1.13%

rho_pur	997.3	8066	1374.3
	5%	3%	0.09%

%error

MW 18.013 74.12 447.42

3. Partition Coefficients

KCa	dKCb	%dKCa	KCb	dKCb	%dKCb	KVa	dKVa	%dKVa	KVb	dKVb	%dKVb
0.014	7E-04	5.00%	1.321	0.056	4.24%				0.9635	0.041	4.24%
0.015	7E-04	5.00%	1.354	0.057	4.24%	3.28E-05			0.9885	0.042	4.24%
0.015	7E-04	5.00%	1.371	0.058	4.24%				1.0012	0.042	4.24%
0.015	8E-04	5.00%	1.336	0.057	4.24%				0.9764	0.041	4.24%
0.015	8E-04	5.00%	1.334	0.057	4.24%				0.9752	0.041	4.24%
0.017	8E-04	5.00%	1.361	0.058	4.24%	0.001			0.9968	0.042	4.24%
0.018	9E-04	5.00%	1.34	0.057	4.24%				0.9846	0.042	4.25%
			1.345	0.057					0.9839	0.042	
			0.017						0.3131		

KVa	dKVa	%dKVa	KVb	dKVb	%dKVb
1.01046	5E-04	5.00%	0.9635	0.041	4.24%
0.0107	5E-04	5.00%	0.9885	0.042	4.24%
0.0109	5E-04	5.00%	1.0012	0.042	4.24%
0.011	5E-04	5.00%	0.9764	0.041	4.24%
0.0113	6E-04	5.00%	0.9752	0.041	4.24%
0.0121	6E-04	5.00%	0.9968	0.042	4.24%
0.0131	7E-04	5.00%	0.9846	0.042	4.25%
			0.9839	0.042	
			0.3131		

KXa	dKXa	%dKXa	KXb	dKXb	%dKXb	%dKXb
0.2067	1E-04	0.07%	19.0462	0.8303	4.36%	
0.2093	4E-04	0.17%	19.3145	0.8396	4.35%	
0.2109	5E-04	0.24%	19.4241	0.8429	4.34%	
0.2113	7E-04	0.34%	18.7851	0.8113	4.32%	
0.2141	9E-04	0.43%	18.5361	0.7994	4.31%	
0.225	0.001	0.62%	18.5004	0.7977	4.31%	
0.2334	0.002	0.82%	17.4931	0.7472	4.27%	
			18.7269	0.8098		
			0.65117			

4. Selectivities

SC_b	dSC_b	%dSC_b
92.15	3.91	4.2%
92.27	3.915	4.2%
92.1	3.908	4.2%
88.73	3.768	4.2%
86.6	3.674	4.2%
82.23	3.489	4.2%
74.95	3.18	4.2%
87.01	3.692	
6.47%		

SW_b	dSW_b	%dSW_b
92.149	3.911	4.2%
92.268	3.916	4.2%
92.102	3.909	4.2%
88.795	3.769	4.2%
86.596	3.675	4.2%
82.232	3.491	4.2%
74.949	3.182	4.2%
87.013	3.693	
6.476		

SX_b	dSX_b	%dSX_b
92.149	4.017	4.4%
92.268	4.011	4.3%
92.102	3.997	4.3%
88.795	3.839	4.3%
86.596	3.734	4.3%
82.232	3.546	4.3%
74.949	3.202	4.3%
87.013	3.764	
6.476		

1. Aqueous Phase

ca	c_et	ci	dca	dc_et	dci	rho_t	d(rho_t)	%d(rho_tcalc)	wa	w_et	wi	dwa	dw_et	dwi	%dwa	%dw_et	%dwi	xa	x_et	xi	dxa	%dxa	dx_et	%dx_et	dxi	%dxi
993.9	1.472	2.8377	0.083	0.044	0.08513	998.26	0.127059	0.013%	0.99568	0.001	0.0028	0.00015	4E-05	9E-05	0.02%	3.0%	3.0%	0.9993	6E-04	0.0001	0.0000	0.00%	2E-05	3.00%	3.4E-06	3.00%
992.5	3.036	2.2307	0.125	0.091	0.06692	997.78	0.168662	0.017%	0.99472	0.003	0.0022	0.00021	9E-05	7E-05	0.02%	3.0%	3.0%	0.9987	0.001	9E-05	0.0000	0.00%	4E-05	3.00%	2.7E-06	3.00%
989.8	4.817	2.9964	0.194	0.145	0.08989	997.64	0.258322	0.026%	0.99217	0.005	0.003	0.00032	1E-04	9E-05	0.03%	3.0%	3.0%	0.998	0.002	0.0001	0.0001	0.01%	6E-05	2.99%	3.6E-06	3.00%
985	8.754	3.115	0.339	0.263	0.09345	996.89	0.439269	0.044%	0.98809	0.009	0.0031	0.00055	3E-04	9E-05	0.06%	3.0%	3.0%	0.9964	0.003	0.0001	0.0001	0.01%	1E-04	2.99%	3.8E-06	3.00%
985	9.232	2.2081	0.356	0.279	0.06624	996.53	0.457227	0.046%	0.98846	0.009	0.0022	0.00058	3E-04	7E-05	0.06%	3.0%	3.0%	0.9962	0.004	9E-05	0.0001	0.01%	1E-04	2.99%	2.7E-06	3.00%
979.7	13.76	2.1775	0.525	0.413	0.06533	995.64	0.670978	0.067%	0.98399	0.014	0.0022	0.00085	4E-04	7E-05	0.09%	3.0%	3.0%	0.9945	0.005	9E-05	0.0002	0.02%	2E-04	2.99%	2.7E-06	3.00%
969.7	22.35	2.2518	0.839	0.661	0.06875	994.03	1.070623	0.108%	0.97552	0.022	0.0023	0.00135	7E-04	7E-05	0.14%	3.0%	3.0%	0.9911	0.009	9E-05	0.0003	0.03%	3E-04	2.98%	2.8E-06	3.00%
			0.04%	3%	3%	error%																				

2. [HMIm][Tf2N]

Ca	C_et	C	dCa	dC_et	dCi	RHO_t_call	RHO_t_ca	%d(RHO_tcalc)	Wa	W_et	Wi	dWa	dW_et	dWi	%dWa	%dW_et	%dWi	Xa	X_et	Xi	dXa	%dXa	dX_et	%dX_et	dXi	%dXi
1508	0.235	1353.1	0.754	0.007	1.03854	1368.432	1.28338	0.094%	0.01102	2E-04	0.9888	0.00055	5E-06	0.0012	5.00%	3.0%	0.1%	0.2165	0.001	0.7822	0.0085	3.92%	4E-05	3.19%	0.00847	108%
1506	0.425	1352.8	0.753	0.013	1.03719	1368.316	1.28169	0.094%	0.011	3E-04	0.9887	0.00055	9E-06	0.0012	5.00%	3.0%	0.1%	0.2161	0.002	0.7815	0.0085	3.92%	8E-05	3.18%	0.00845	108%
1518	0.731	1352.2	0.759	0.022	1.04578	1368.072	1.292238	0.094%	0.01109	5E-04	0.9884	0.00055	2E-05	0.0012	5.00%	3.0%	0.1%	0.2171	0.004	0.7788	0.0085	3.92%	1E-04	3.18%	0.00846	109%
1513	1.329	1351	0.765	0.04	1.05616	1367.634	1.304795	0.095%	0.01119	1E-03	0.9878	0.00056	3E-05	0.0012	5.00%	3.0%	0.1%	0.218	0.007	0.7746	0.0085	3.91%	2E-04	3.17%	0.00845	109%
1513	1.393	1350.9	0.765	0.042	1.05652	1367.592	1.305215	0.095%	0.01119	0.001	0.9878	0.00056	3E-05	0.0012	5.00%	3.0%	0.1%	0.2179	0.008	0.7743	0.0085	3.91%	2E-04	3.17%	0.00844	109%
1537	2.126	1349.6	0.769	0.064	1.03435	1367.09	1.314357	0.096%	0.01124	0.002	0.9872	0.00056	5E-05	0.0012	5.00%	3.0%	0.1%	0.2179	0.012	0.7703	0.0085	3.91%	4E-04	3.16%	0.0084	109%
1569	3.4	1347	0.785	0.102	1.09517	1366.138	1.351054	0.099%	0.01149	0.002	0.986	0.00057	7E-05	0.0013	5.00%	3.0%	0.1%	0.2202	0.019	0.7611	0.0086	3.90%	6E-04	3.15%	0.0084	110%

rho_pure	997.8	787.8	1374.3	5%	3%	0.08%	%error	MW	18.0126	46.07	447.42

3. Partition Coefficients

KCa	dKC_et	%dKCa	KC_et	dKC_et	%dKC_et		KWa	dKWa	%dKWa	KW_et	dKW_et	%dKW_et		KXa	dKXa	%dKXa	KX_et	dKX_et	%dKX_et
0.015	8E-04	5.00%	0.16	0.007	4.24%		0.01107	6E-04	5.00%	0.11662	0.005	4.24%		0.2167	4E-05	0.02%	2.2830754	0.0999	4.38%
0.015	8E-04	5.00%	0.14	0.006	4.24%	0.000127	0.01106	6E-04	5.00%	0.10207	0.004	4.24%		0.2163	8E-05	0.04%	1.9960761	0.0873	4.37%
0.015	8E-04	5.00%	0.152	0.006	4.24%		0.01118	6E-04	5.00%	0.1107	0.005	4.24%		0.2175	1E-04	0.06%	2.1539634	0.0941	4.37%
0.016	8E-04	5.00%	0.152	0.006	4.24%		0.01132	6E-04	5.00%	0.11067	0.005	4.24%		0.2187	2E-04	0.11%	2.1376172	0.0932	4.36%
0.016	8E-04	5.00%	0.15	0.006	4.24%		0.01132	6E-04	5.00%	0.10926	0.005	4.24%		0.2187	2E-04	0.11%	2.1107696	0.092	4.36%
0.016	8E-04	5.00%	0.155	0.007	4.24%	0.001	0.01143	6E-04	5.00%	0.11254	0.005	4.24%		0.2191	4E-04	0.17%	2.1583222	0.0939	4.35%
0.016	8E-04	5.00%	0.154	0.007	4.24%		0.01177	6E-04	5.00%	0.11222	0.005	4.25%		0.2222	6E-04	0.27%	2.1178184	0.0918	4.33%
			0.152	0.006						0.11058	0.005						2.136806	0.0932	
			0.006							0.00442							0.0846523		

4. Selectivities

SC_et	dSC_et	%dSC_et		SW_et	dSW_et	%dSW_et		SX_et	dSX_et	%dSX_et
10.54	0.448	4.2%		10.5375	0.448	4.2%		10.538	0.461	4.4%
9.226	0.392	4.2%		9.22626	0.392	4.2%		9.2263	0.403	4.4%
9.901	0.421	4.2%		9.90118	0.421	4.2%		9.9012	0.433	4.4%
9.773	0.415	4.2%		9.77262	0.415	4.2%		9.7726	0.426	4.4%
9.65	0.41	4.2%		9.65003	0.41	4.2%		9.65	0.421	4.4%
9.85	0.418	4.2%		9.84961	0.418	4.2%		9.8496	0.428	4.3%
9.531	0.405	4.2%		9.53101	0.405	4.2%		9.531	0.413	4.3%
9.781	0.415			9.73118	0.415			9.7812	0.426	
0.404				0.40393				0.4039		

APPENDIX D - Physical property data for [HMIm][Tf_2N]

For creating model ionic liquid as a new component in the Aspen plus database, the following parameters were used. They were obtained from the literature primarily from the ILTHERMO database.

Parameter	Symbol	Units	Value
Normal boiling point	TB	K	635.05
Molecular weight	MW	-	447.42
Critical temperature	TC	C	1019.65
Critical pressure	PC	bar	23.9
Critical volume	VC	ml/mol	1104.4
Critical compressibility factor	ZC	-	0.2454
Std. enthalpy of formation for ideal gas at 25°C	DHFORM	kJ/kmol	195000
Std. free energy of formation for ideal gas at 25°C	DGFORM	kJ/kmol	0
Pfizer acentric factor	OMEGA		0.3839
Enthalpy of vaporization at bpoiling point	DHVLB	kJ/kmol	1.40E+05
Liquid molar volume at boiling point	VB	m^3/kmol	0.3035
Standard liquid molar volume at 60F	VLSTD	ml/mol	327
Radius of gyration	RGYR	ft	8.77E-10
Liquid thermal conductivity (between 273 – 400 K)	λ	W/m.K	0.122
Viscosity (between 273 – 400 K)	$ln\ \eta$	Pa.sec	3700-15.082/T
Surface tension (between 273 – 400 K)	σ	N/m	0.0348
Ideal gas heat capacity	$C_p^{*,ig}$	kJ/kmol.K	1000 + 0.6307 T
Density(between 273 – 400 K)	ρ	kg/m^3	1639.1 -0.8965 T
Vapor pressure (445 – 500 K)	$ln(P^{vap})$	Pascal	32.38 – 20137/T